The Dissertation Committee for Craig Nealon Dolder
certifies that this is the approved version of the following dissertation:

# Direct Measurement of Effective Medium Properties of Model Fish Schools

Committee:

_____
Preston S. Wilson, Supervisor

_____
Mark F. Hamilton

_____
Andrea Alù

_____
Todd A. Hay

_____
Ofodike A. Ezekoye

# Direct Measurement of Effective Medium Properties of Model Fish Schools

by

## Craig Nealon Dolder, B.S.E.; M.S.E.

**DISSERTATION**

Presented to the Faculty of the Graduate School of

The University of Texas at Austin

in Partial Fulfillment

of the Requirements

for the Degree of

**DOCTOR OF PHILOSOPHY**

THE UNIVERSITY OF TEXAS AT AUSTIN

May 2014

Dedicated to my family, friends and teachers.

# Acknowledgments

This work is truly a culmination of everything I have learned about the art and science of acoustics and everyone I have learned from deserves acknowledgment. I have been exposed to wonderful teachers throughout my career, all the way back to my middle school and high school music instructors Tom Erickson, Kris Lucander, and Kris Demoura and of course my physics instructor David Reponen. My secondary school experience is what launched me straight into my collegiate acoustics career under Dr. Robert Celmer (Dr. Bob to his students).

I gained a strong foundation in acoustics under Dr. Bob at the University of Hartford, which made my transition into graduate school an easy one. Under the tutelage of Dr. Charles Tinney I gained a strong foundation and understanding of spectral analysis. I had constant help from my fellow acoustic students from those who were there when I started at UT, including Matt Guild, Ted Argo, Steve Embleton and Kenny Nguyen, to those who are here as I finish, especially Mustafa Abbasi, Joelle Suits, Greg Enestein, and James Stephenson. I wish I could thank all the students I've worked with here, but neither space or my memory would allow it.

I would also like to thank all the UT professors and staff I have learned from, especially, Dr. Haberman, Dr. Hamilton, Dr. Blackstock, Dr. Hall, Dr Kevin Lee and most importantly my adviser Dr. Preston Wilson. I would also like to acknowledge and thank the Office of Naval Research for funding this research.

# Direct Measurement of Effective Medium Properties of Model Fish Schools

Craig Nealon Dolder, Ph.D.
The University of Texas at Austin, 2014

Supervisor: Preston S. Wilson

The scattering and attenuation caused by fish schools has been extensively studied for applications in fisheries management and naval sonar. The literature contains extensive *in situ* measurements of scattering by fish schools, however significant uncertainties exist with respect to characterizing the size, quantity, and distribution of fish within the schools, that confounds accurate measurement-model comparison. Hence there is a need for application of measurement techniques that can more precisely characterize the acoustic properties of fish schools and the variations intrinsic to live subjects in continual motion. To begin to address this deficiency, measurements of the sound speed through collections of live fish were conducted in a laboratory setting. The species chosen for measurement were zebrafish (*Danio rerio*). The sound speed was investigated using a resonator technique which yielded inferences of the phase speed within the fish school though measurements of the resonances of a one-dimensional waveguide. The waveguide was calibrated to compensate for finite wall impedance and for finite reflections from the ends of the waveguide. Fish

densities were investigated ranging from 8.6 to 1.7 fish lengths per mean free path. Measurements agree well with a predictive model that is based on shell-free spherical bubbles, which indicates that the phase speed is not significantly affected by the fish flesh or swimbladder morphology for the species studied. The variation in phase speed due to individual fish motion within the model school was measured to be up to ±5.6%. This indicates that precise knowledge of the fish position is required to achieve greater model accuracy.

To compliment the phase speed measurements, the attenuation through a cloud of encapsulated bubbles was evaluated through insertion loss measurements. Multiple arrangements of balloons of radius 4.68 cm were used to surround a projector. The insertion loss measurements indicated an amplification of around 10 dB at frequencies below the individual balloon resonance frequency and an insertion loss of around 40 dB above the individual balloon resonance frequency. Analytical modeling of the bubble collection predicted both the amplification and loss effect, but failed to accurately predict the level of amplification and insertion loss.

Effective medium models and full scattering models (requiring knowledge of bubble size and position) were evaluated for a model fish school. The two models agree for forward scattering for all frequencies except those immediately around the individual bubble resonance frequency. Back scattered results agree at low frequencies, however as soon as the wavelength becomes smaller than four mean free paths between fish the models diverge. Ramifications of these findings and potential future research directions are discussed.

# Table of Contents

# List of Tables

# List of Figures

xiv

xvi

# Chapter 1

# Introduction

The acoustics of fish schools has been studied since the Second World War. Initial interest was in understanding the origin of the phantom bottom of the sea floor known as the Deep Scattering Layer (DSL), which moved from great depth during the day to shallow depths during the night. It was quickly realized that this scattering layer was caused by biological organisms, however there was still great debate over the precise scatterer. Theories emerged relating the scattering to plankton, euphausiids, or squid[1], however the frequency response of the scattering hinted that small air bubbles played a role. While early investigations assumed that very few fish in the sea had swimbladders, later studies[2, 3, 4] showed that a majority of fish at the same depths as the DSL had swimbladders[1]. Ever since, there has been strong interest in understanding how sound propagates through, scatters from, and is attenuated by fish schools.

The purpose of this study is to perform laboratory measurements of the bulk acoustic properties of fish schools. Many models have been proposed in recent years [5, 6, 7, 8, 9, 10, 11, 12, 13, 14, 15] for determining the acoustic properties of fish schools, however most are based on *in situ* measurements, where the number of noise sources and variables cause considerable uncertainty. Also, many measure-

ments of fish attenuation and scattering made *in situ* lack detailed information about fish size and spacing, which are important factors in deriving a model. The laboratory measurements reported here involve interpreting the change in the resonance frequencies of one-dimensional resonators or in other words, a one-dimensional finite length waveguide. The resonances of this system are affected by the contents of the waveguide, from which the bulk properties of the medium can be calculated through appropriate models.

The fish of primary interest are the schooling fish in the ocean that live near the surface, or in the water column, but not on the bottom of the ocean. These are known as pelagic fish. The vast majority of pelagic fish are teleostei, which is a classification of ray-finned fish. These fish can also be divided into three subcategories: *a*) fish with a swimbladder that is connected to the digestive tract, physostomes; *b*) fish with a swimbladder that is sealed from the digestive tract, physoclists; and *c*) fish with either no swimbladder, or with a swimbladder that has evolved into a fat storage vessel.

Physostomes and physoclists are believed to be the primary scatterers involved in DSL since the presence of a swim bladder contributes 90% to 95% to the back-scattering cross-section of individual fish[16]. A physostome is a fish with pneumatic duct between its digestive system and its swim bladder, this allows the fish to modify its swim bladder volume while near the surface where tiny bubbles are present in the water. Physostomes typically do not have a means to modify the mass of air in the swim bladder while at depth. A physoclist is a fish whose only means of swim bladder regulation is a gland that secretes air into its swim bladder from the

blood stream. Physoclists modify the mass of air in its swim bladder at depth, and therefore the volume and pressure of the swim bladder is no longer solely a function of its size at the surface and depth. Additionally fish have the ability to control tension of the swim bladder, which affects prediction of the swim bladder resonance frequency.

## 1.1   Motivation

There are two primary motivations for having a better understanding of sound propagation and scattering associated with fish schools. The first is improved detemination of fish species and quantity via scattering measurements performed for fisheris management in the ocean. The second is in order to reduce the likelihood of sonar system false alarms due to scattering from fish schools, which is of interest for defense and security applications. In this second case, the signal that is reflected from the fish school is generally known as bio-clutter. Increased understanding of measurements and models of fish school scattering and propagation will have positive impacts on both fisheries management and defense applications.

### 1.1.1   Fishery Acoustics

Many fishery acoustics tools and techniques do not fully exploit frequency-domain information because narrow-band resonant transducers are more widely available than broadband transducers, and instead rely on back-scattering cross-section measurements from individual fish ($\sigma_{\text{bs, indivitual}}$) in order to approximate the scattering from entire schools of fish ($\sigma_{\text{bs, school}}$). One of the simplest assumptions made is

that the fish scatterers act incoherently, that is to say that the scattering scales as:

$$\sigma_{\text{bs, school}} = \sum_{i=1}^{N} \sigma_{\text{bs, individual}}, \tag{1.1}$$

where the scattering cross-section, $\sigma$, represents the ratio of the intensity of the scattered wave to the incident acoustic intensity on the scatterer, and back-scattering refers specifically to that ratio as observed from the direction of the source [17]. In reality, many of the scatterers are in phase and the resonance frequency of individual fish can be modified by the presence of other fish.

While models can be made to simulate the response from specific configurations of fish schools, for schools of a practical size this method becomes infeasible because it is difficult to obtain fish distribution information and the calculations generally involve the inversion of an $N \times N$ matrix, where $N$ is the number of fish in the school. For these reasons there is interest in finding an effective medium theory that can accurately describe the physics of acoustic propagation through fish schools in absence of precise knowledge of the relative position of every fish in the school. If the sound propagation through fish schools can be better understood, it will be easier to determine the properties and quantity of fish in ocean environments. This will be useful in both active fish finding and monitoring of populations in order to prevent over fishing.

### 1.1.2 Bio-Clutter

The second motivation is to reduce the number of false threats identified due to bio-clutter. Many times fish schools and marine mammals have a large enough

scattering strength to distract from real threats and make potential threats hard to identify. This can range from the scale of mines, to divers, to even submarines. In addition, a fish school can often appear as a single large threat. Better classification of fish school reflections will aid in the design of sonar and signal processing systems that can differentiate between a fish school and other targets. The measurements reported here validate acoustic models for fish schools and facilitate better understanding of the sound speed and attenuation through schools of fish, which will lead to better classification.

## 1.2 Fishery Acoustics Background

### 1.2.1 General Background

The acoustic properties of fish are usually represented by either a spectrum or a probability density function (PDF) of the scattered target strength (TS), which is defined as,

$$\text{TS} = 10 \log_{10}\left(\frac{\sigma_{\text{bs},x}}{4\pi R_{\text{ref}}^2}\right), \tag{1.2}$$

where $\sigma_{\text{bs}}$ is the back-scattering cross section, and $R_{\text{ref}}$ is generally 1 meter. For small spherical bubbles $\sigma_{\text{bs}}$ can be written in the form [18]:

$$\sigma_{\text{bs}} = \frac{4\pi R_0^2}{(\omega_0/\omega - 1)^2 + \delta^2}, \tag{1.3}$$

where $R_0$ is the equilibrium radius, $\omega_0$ is the resonance frequency, $\omega$ is the excitation frequency, and $\delta$ is the dimensionless frequency-dependent damping coefficient. Both

the resonance frequency and the damping coefficient are quantities that are important for the classification of fish schools. Since many authors have defined the term damping coefficient differently, here is an aside to link the damping coefficient to the well defined, and universally accepted quality factor for a mass-spring-damper system, $Q$. Consider the dynamic system characterized by:

$$m\ddot{x} + b\dot{x} + m\omega_0^2 x = 0, \tag{1.4}$$

where $m$ is a mass, $b$ is a damping tem, and $\omega_0$ is the resonance frequency. The damping coefficient $\delta$ for this system is related to $b$ and $Q$ and at resonance by the relations:

$$\delta = \frac{1}{Q} = \frac{b}{m\sqrt{\omega_0^2 - (\frac{b}{2m})^2}}. \tag{1.5}$$

Many studies approximate scattering from swimbladder fish as scattering from an air bubble. Often the swimbladder is simplified as a spherical bubble, while in reality swimbladders have complex geometries which may include two linked chambers. This geometrical simplification has been shown to have minimal effect on the resonance frequency of the bubbles. For extreme distortions in shape, increasing the aspect ratio up to 20, the monopole resonance frequency of a bubble of equal volume increases by less than a factor of 1.5 [19, 20], however the quality factor, $Q$, is reduced to aprroximately 30% of the value for an undistorted bubble [20]. Since for airbladder studies additional damping components are typically added, it is un-

6

clear how much additional damping is due to the fish body and how much is due to complex bubble geometry.

The following discussion on the background and development of fisheries acoustics is broken into three sub-sections, Fish school models, Experimental investigations, and Fish behavior. These sub-sections provide the basis on which we can compare the present approach and measurements. The field of fisheries acoustics has been active since the 1970s and for the most part has developed in isolation from the more general field of bubble acoustics. While the development of the field of bubble acoustics has a significant amount of crossover, it will be discussed in detail in Chapter 3. Beyond the difficulty of validating fish school scattering models due to the inability to directly record the size, species, and locations of schools *in situ*, it should also be noted that there is extreme variability in experimental estimation of fish populations due to [21]:

Fish schools avoiding the survey vessel

Acoustic shadowing as a result of non-linearity in back scattered echo energy

Daily horizontal migration

The strong directivity of scattering from fish and their movements relative to the vessel

The blind areas when fish are located close to the surface or the bottom

It is also interesting to note that even up to the 1950s there was confusion as to what caused the layer of scattering that is known as the deep scattering layer

(DSL). Many had hypothesized that the DSL was due to bubbles, but there was a strong belief that fish in the ocean lacked sufficient size swim-bladders and were dismissed as a cause of the DSL. Marshall cleared up this confusion in his 1951 review article on the subject [1].

### 1.2.2 Fish School Models

In an early formulation [22] of his fish school scattering model, Love was able to predict measured scattering strengths in several frequency bands within a few dB. He refined this model and published a thorough derivation of it three year later which is commonly known as Love's 1978 model, or simply Love's model [5].

Devin's [23] equation of motion for the monopole resonance of spherical bubbles was modified to account for the behavioral differences between pure bubbles and swim bladders, then a the scattering from an assumed fish school grid was calculated. The positions of the fish in the grid were varied with a normal offset distribution from the grid and ensemble averaged. The model has been shown to agree well with experimental measurements obtained from collections of model swim bladders [24].

Very similar expressions for the scattering from fish schools were proposed in 1964 by Andreeva [6] and in 1967 by Weston [7], the differences of which deal with the significance of the elasticity of the fish flesh on determining the resonance frequency. Both treat fish as a lumped-element system consisting of inertial and elastic components. Despite noting that the swim-bladder is similar to a prolate spheroid both dismiss the effect this has on the resonance frequency and use the Minneart frequency to determine the resonance of the swim bladder (with the exception of

Andreeva adding a term for the elasticity of the fish flesh). Neither note the effect that a change in bubble shape has on damping, though both note that additional damping is present that is not accounted for by the models.

In 1981 Love [8] proposed a model for estimating the target strength of distribution of fish schools. This model claims to take into account both multiple scattering and attenuation through the school. This model, however, is for estimating the target strength of a fish school for a known distribution of fish given the size, shape, and density of the school along with the scattering properties of an individual fish species.

While many models involve an assumption of a spherical swim-bladder, there have been several attempts to account for the non-spherical geometry. Clay [9] proposed models for straight and bent cylinders surrounded by a liquid that had an increased sound speed and density relative to water which represented the swim bladder and fish body respectively. The model also incorporated empirical viscous losses. These models were compared to experimental measurements by Love [25] and by Holiday [2] and showed good agreement. Clay concluded that a spherical bubble was a poor approximation for some fish swim-bladders.

Clay and Heist [10] proposed a two-parameter model for the scattering from individual fish. The model comprises an array of concentrated scatterers to represent the swimbladder and a distributed array of scatterers to represent other components such as the fish flesh and the skeletal structure. The total backscattering strength, $\sigma_{\text{bs}}$ is the sum of these two arrays and the ratio of the concentrated to distributed scatterer strength is defined as $\gamma$. The two parameters, $\sigma_{\text{bs}}$ and $\gamma$, are determined

by fitting the echo PDF to the Rician PDF given as:

$$w_{\mathrm{R}}(e) = \frac{2e(1+\gamma)}{\sigma_{\mathrm{bs}}} \exp\left(-\frac{(1+\gamma)e^2 + \gamma\sigma_{\mathrm{bs}}}{\sigma_{\mathrm{bs}}}\right) I_0(x) x \equiv \frac{2e[\gamma(1+\gamma)]^{(1/2)}}{\sigma_{\mathrm{bs}}^{(1/2)}}, \qquad (1.6)$$

where $I_0$ is the modified Bessel function. When $\gamma$ is zero, Equation (1.6) reduces to a Rayleigh PDF. This situation implies that the concentrated component (the swim bladder) is insignificant. The other extreme, when $\gamma \gg 1$, implies that the concentrated component dominates, and the PDF simplifies to a normal distribution. In the same paper, Clay and Heist also provide the results of experimental scattering measurements made of caged fish. They determined that both the backscattering cross section and the fluctuation parameter, $\gamma$, depend on the length of the fish relative a wavelength $L/\lambda$, the anatomy of the fish, and the fish behavior. They make a point that fish schools are not static, that any model should be able to simulate the "aliveness" of free swimming animals, and that this dynamic property of a fish school is captured in the probability density function of the backscatter.

A numerical model was proposed by Clay and Horne in 1994 [11] which broke fish down into cylinder-like sections based on x-rays of fish. The results were compared to experimental measurements, but not to prior fish scattering models. The discussion of the comparison is limited to high frequencies where the fish length is larger than the wavelength of ensonification.

In 1996 Feuillade, Nero, and Love [12] proposed a low-frequency scattering model that included all orders of multiple scattering. This model involved coupling

10

the scattering equations for each fish in a school with $N$ fish and coupling the equations in an $N \times N$ matrix with accounted for the scattered field from every fish affecting the field of every other fish. By assuming that the fish distribution followed an approximately body-centered cubic configuration and averaging the result over many ensembles were the fish were randomly moved around their cubic positions, the target strength as a function of frequency was determined. This resulted in an expected lowering of the resonance frequency and a peak level close to or lower than that produced by the assumption of incoherent scattering.

Another issue relevant to accurately measuring fish school densities is an effect called shadowing. Shadowing occurs when volume scattering measurements are made (as is the case with fish schools). Since energy is reflected or absorbed by the initial layers of fish, in dense schools the remaining fish do not receive the same incident energy as the initially ensonified fish. This reduces the amount of scattered energy that is detected since the fish further within the school are in the acoustic shadow of other fish. As a consequence any estimate of the number of fish is going to be low. Foote [13] proposed a method that involved assuming a horizontally stratified water column to correct single-ping vertical-distribution measurements. Recently, work has been done to estimate the effect of the shadowing effect on reflections from dense fish schools in a more general manner. Zhao and Ona [14] propose a linear model for the estimation of the ratio of the extinction cross section to the acoustic cross-section.

In 2013 Baik [15] reported an error in the original Love paper regarding the scattering cross section at resonance, though this correction is small for many physical

11

applications, when the ratio of the outer diameter to the inner diameter of the fish body is small and the swim bladder is small. While this correction is small for large fish in the ocean, it can be significant for small fish and other marine creatures such as gas-bearing zooplankton.

### 1.2.3 Experimental Investigations

*In situ* ocean studies are subject to many additional experimental variables such as ocean ambient noise, the presence of a thermocline, and uncertainty in fish spacing and fish school composition. In 1972, Holliday [2] conducted surveys of the scattering from schools of commercially important marine fish using explosive acoustic sources. After a school was found and the acoustic signature measured, a sample of the targets were captured in order to determine the species and size distributions. Results were reported in terms of the signal transfer function and then compared to model equations by Adreeva [6] and Weston [7]. Also in 1972 Scrimger, Turner, and Heyd [26] collected scattering measurements from a fish school while collecting background reference volume scattering data for the Saanich Inlet in British Columbia. They noted that the closely packed fish school (less then a fish length spacing) had a relatively flat response between 1 and 9 kHz and had a backscattering strength of approximately −47±3 dB.

In 1979 Blaxter, Denton, and Gray [3] studied how swim bladders in herring deform as pressure increases and discovered that the ends of the swim bladder generally remain fixed while the cross-section changes. In the same year Løvik and Hovem experimentally studied the resonance frequency of swim-bladders [4] of various fish

12

as a function of depth and fish length. They found that while the resonance frequency generally increases with depth, there is also a strong dependence on the fish adjusting to the depth, which can take between 12 to 24 hours. Adaptation to deeper water requires the production of gas and takes significantly longer than adaptation to shallower water, which requires the expulsion of gas. The same trend is noticed for the quality factor of the resonance, $Q$, and bladders smaller than required for equilibrium tend to have a higher $Q$ and those with larger bladders had a lower $Q$. They also discovered a strong trend that the fish swim-bladder resonance exhibited an inverse relationship with fish length according to:

$$f_0 = \frac{120}{L}, \tag{1.7}$$

where $f_0$ is the swimbladder resonance frequency in Hertz and $L$ is the fish length in meters. Also in 1979, Deuser et al. [27] at the University of Texas provided results that indicated that using an adaptive classification technique could significantly improve the ability to discriminate echos from fish and competing objects or distinguish general fish shoal densities.

Foote [16] experimentally verified that the swimbladder was in fact the primary scattering mechanism by comparing scattering from fish with and without swimbladders which were otherwise similar. The study shows that swimbladders account for approximately 90% to 95% of the scattered signal.

In 1983 Foote [28] conducted a series of experiments which supported the idea that fish school response was linear with respect to individual fish and that the echo-integration energy approach was sound for populations up to 40 fish, though

seven years later he published [13] that acoustic shadowing can be problematic.

Another issue with the concept of echo-integration is that the fish school response is convolved with the transducer response. In 1983 Clay [29] devised a method for deconvolving the fish scattering PDF from the ocho PDF for a single transducer sonar. While reasonable results are shown with respect to experiments, the method is susceptible to noise and can result in negative PDF values.

In 1984 Blaxter and Batty conducted a comprehensive study on the inflation and deflation of the physotome species of herring. They found that herring only replenish their swim bladder through the gulping of air at the surface, and found relationships between swim bladder volume and fish length and fish mass for fish ranging from 3 to 33 cm in length. They also noted that while oxygen appears to be absorbed into the blood stream over time, nitrogen takes 80 times longer to absorb into the blood.

In 1985 Foote [30] reported on a joint experimental/numerical study, where the were acoustically measured for back-scatter, flash frozen, and then sliced so that the swimbladder morphometry could be recorded. The back-scatter was then modeled for individual fish by representing them entirely by the swimbladder, which was equated to an ideal pressure release surface. His model was unique in that it used a very detailed representation of the swim bladder organ rather than approximating it with a simple shape. The agreement between experimental and numerical results showed that within a certain frequency limit a swimbladdered fish is little more than an ideal pressure-release surface and that high frequency scattering can be determined solely by the swimbladder morphometry.

In 1992 Furusawa, Ishii, and Miyanohana [31] conducted measurements of the extinction cross section of several species of fish. They concluded that the extinction cross section varies as 2/3 of the fish weight, and that there is a slight tend toward increasing extinction cross section as a function of frequency.

Love's 1993 paper on volume scattering [32] shows that while the general interest is to use acoustic data to extract fishery information, the converse case is also of interest. Using experimental volume reverberation data and fisery data from the same time period the study sought to determine if volume reverberation in an area can be predicted from fishery data. After making educated adjustments to the fishery data a good agreement was found between the acoustic theory for fishes and the measured volume reverberation levels.

Several studies found good agreement between, low frequency sound scattering in deep water at depth[33] and near the surface [34] and trawl data of Pacific hake [35] and Love's 1978 model [5].

In 1999 Orest Diachok [36] reported on experimental measurements of schools of sardines. The study noted that detected resonance frequencies of the fish school were in good agreement with theoretical computations. More notably that the collective resonance frequencies associated with sardines in schools were approximately 60% of the resonance frequency of dispersed shoals, and that the observation is consistent with a theoretical equation for the resonance frequency of the fundamental mode of a cloud of bubbles.

A 2003 paper by Love, Thompson, and Nero [37] showed that volume rever-

beration changed over time and in different ways for deep, slope, and shelf waters, depending upon the type of fish present.

In 2004, Nero, Thompson, and Jech [38] performed *in situ* acoustic estimates of the swim bladder volume using the response of a 1.5-5 kHz broadband sonar system and Love's original 1978 model [5] in conjunction with a correction factor for the resonance frequency by Weston [7]. Using this information they determined that Atlantic herring at a depth between 160 and 190 meters had swim bladder volumes estimated to be between 1.3 and 1.6 ml, which using Boyle's Law:

$$P_0 V_0 = P_z V_z, \tag{1.8}$$

would relate to uncompressed swim-bladder volumes $V_0$ between $22 - 32$ ml at the sea surface, and estimated that a neutrally buoyant herring would have a swim bladder volume of approximately 5 ml.

Since numerous uncertainties arise when comparing measurements and models of scattering from real fish schools *in situ*, Nero et al. measured the scattering from arrays of artificial fish swimbladders [24]. Measurements at sea were conducted on an array of plastic bubbles with a known number, size, and spacing, then explosive sources were used to obtain broadband target strength measurements. Due to variability in the size, position, and shape of the bubbles iterative simulations needed in order to get the model to approximately match the data.

In 2010 Gong et al. [39] reported on an extensive acoustic measurements of shoaling Atlantic herring conducted in 2006. Based on simultaneous length data

16

captured during the survey and by calculating a best fit for the swimbladder dimensions, good agreement was achieved with Love's model. Acoustic population estimates agree with simultaneous fish finder and trawl surveys.

You give motivation for the need for this work in terms of better fish population estimates, and reduced false alarms in sonar, etc.

### 1.2.4 Fish Behavior

An important aspect of fish behavior that plays into fishery acoustics is how the fish's swimbladder changes as a function of depth and what it's role is as an organ. The very interested reader is referred to Jones Marshall's [40] 60+ page review paper on the subject. The swimbladder is known to serve a hydrostatic function, contributing to the buoyancy of the fish in order to lessen the energy it takes to swim at a given depth. It also serves in some fish as a respitory organ, since oxygen the the swimbladder is readily absorbed into the blood stream. There has even been recent evidence [37] that some fish use oxygen stored in their swim bladder to survive in anoxic waters. Finally it can function as both a sound producer and a sound receiver as some fish have bones connecting the swim bladder to the inner ear, and it is believed that fish can detect high frequencies through the nonlinear radiation force on the swimbladder. According to Nero et al [38], herring may inflate their swimbladder with approximately 30% excess buoyancy at the surface in order to achieve the volume at observed depth, since herring can not inflate their swimbladder from their blood stream.

Next is the behavior known as schooling and shoaling. To avoid confusion

17

the definitions from Pitcher's *Behavious of Teleost Fishes* [41] are employed. A shoal is defined as a group of fish that remain together for social reasons. Shoaling fish are considered a social grouping and this term does not imply either structure or function. Groups of fish with synchronized movement and polarized swimming are termed schools. Schooling fish are a subset of shoals that exhibit a structure and synchronization in how they swim. Fish are believed to live in shoals for two reasons; predators and food [41] and that while we may talk about a shoal as a uniform entity, there are often subgroups with different configurations on smaller scales than the entire shoal [34]. It also merits noting that the unit of the school, which is primarily for defense against predators, makes fish much easier to detect and catch in large amounts by humans.

Another aspect of fish behavior is diurnal variability [21, 42]. It is well known that most pelagic fish migrate to further depths around dawn and travel in dense schools, whereas at dusk they rise to shallower depths and disperse. Fish gain advantages against predators by tightly schooling during the day and descending to depths, whereas at dusk fish tend to rise and spread into loose shoals for feeding [41]. At any time that the shoal feels threatened it can quickly reorganize into a tight school.

An interesting side discussion that usually appears when discussing fishery acoustics, is whether the fish can hear the active signals that are used for detection. If so, then it is possible that fish could change their behavior due to the signal of the test being performed. In a 1997 article in Nature, Mann, Lu, and Popper [43] dispute the traditional view that telost fishes cannot detect sounds higher than 2 or

18

3 kHz. More recent research indicates that swim-bladdered fish generally have two regions of hearing sensitivity. In the case of American shad these appeared to be 0.2-0.8 kHz and 25-130 kHz.

### 1.2.5 Acoustic Waveguides and Effective Medium Properties

The resonator technique used in this study grew out of research related to water-filled impedance tubes [44] which was used to conduct measurements of the phase speed and attenuation in bubbly liquids [45]. While the impedance tube technique achieved better agreement with models that previous measurements of phase speed and attenuation [45, 46], the present technique is better at extracting effective medium properties due to the build up of a resonant field within the effective medium. The resonator technique has been employed to measure the sound speed in fluid-like kaolinite sediment [47], liquids with freely rising bubbles [48], methane hydrate seeps [49], several varieties of seagrass [50, 51, 52], and encapsulated bubbles [53, 54].

## 1.3 Justification for Using Live Animals

The fish used in this study were zebrafish (*Danio rerio*). Goldfish (*Carassius auratus*) were originally supposed to be tested as well, however they were not used for considerations mentioned below. While these are not the fish that are of common interest in the ocean, they represent a major class of fish which have been studied in depth, namely swim bladdered fish. The two types of swim bladders previously discussed distinguish fish as either physostomes or physoclists. Both goldfish and ze-

brafish are physostomes. The physiology and acoustics of these fish are representative of many fish studied in the ocean and of general interest.

Swimbladders in zebrafish have been studied in detail and help the fish maintain both balance and neutral buoyancy at desired depths. An image of a zebrafish swimbladder is shown in Figure 1.1. The anterior chamber is believed to be used for audition and is connected to the inner ear through the Weberian ossicles. The posterior chamber is connected to the anterior chamber via the ductus communicans and to the esophagus via a pneumatic duct. The swimbladder was calculated to occupy $5.1 \pm 1.4\%$ of the whole-body volume and to have a gauge pressure of 7–8 mmHg [55]. The center of mass and buoyancy were observed to be approximately at the joining point of the two chambers.

Goldfish have a similar biology, except it has been noted that the anterior chamber has a firmer lining and as such changes minimally in volume [56]. The posterior chamber is more compliant and has the ability to collapse. Goldfish are also different because they have lipids in the posterior chamber that allow for gas exchange between the blood and the swimbladder, allowing them to change the swimbladder volume at depth. This also means that goldfish can change the mass of the air in the swimbladder during testing, which is why they have not been used. A schematic of a goldfish swimbladder is shown in Figure 1.2

Although balloons are freely rising bubbles can be used as models for fish, the effect of the fish flesh and the motion of the fish can not be satisfactorily represented by these physical substitutes. In order to advance the measurements of sound speed in fish schools live fish are necessary.

20
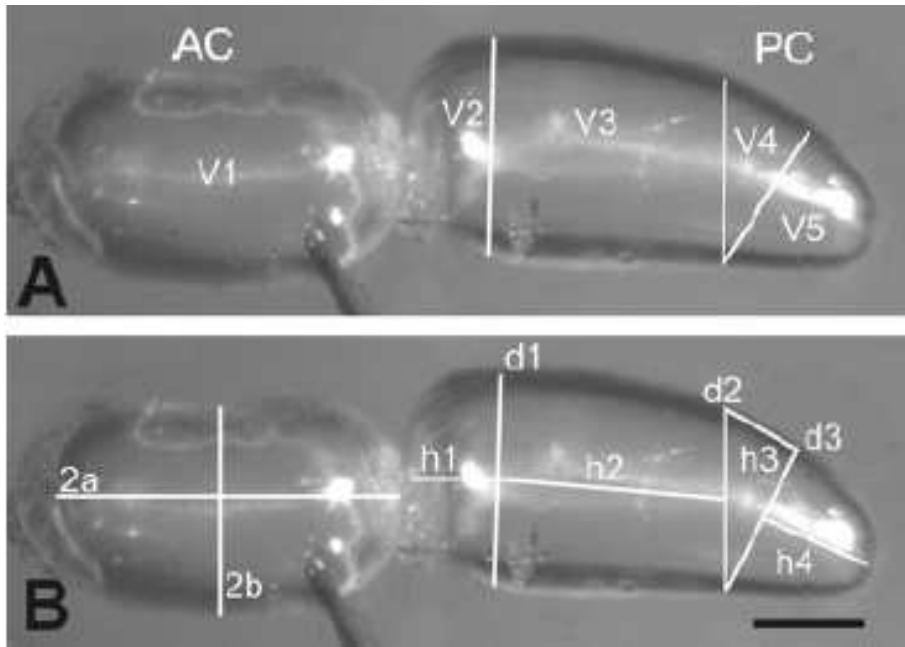
Figure 1.1: Photographs of a zebrafish swimbladder by Robertson et al [55]. Anterior chamber (AC) and posterior chamber (PC) along with volumes and linear dimensions used to approximate the total volume. The scale bar represents 1 mm. Figure adapted from Robertson et al [55].
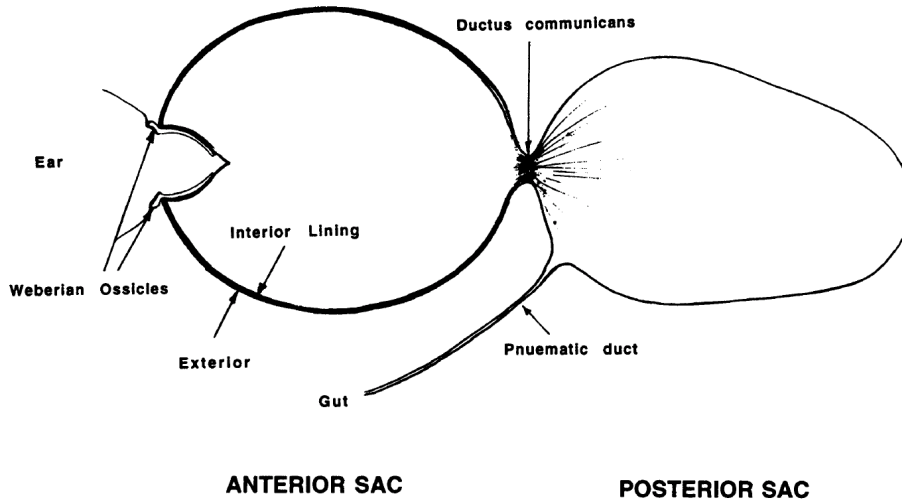
Figure 1.2: Schematic diagram of a goldfish swim bladder [56]. Figure adapted from Ref. [56]

There is still significant room for reducing the uncertainties in fishery surveys and sonar threat detection despite the extensive research conducted with respect to fish school acoustics. The present study works toward reducing these uncertainties through well-controlled laboratory measurements of sound propagation in model and real fish populations. The new method validated here can be extended to verify acoustic parameters for a wide variety of fish and provide data that will allow for comparisons with *in situ* measurements that were not possible before.

## 1.4 Dissertation Overview

This work is to extends the resonator technique to be able to be applied to live fish. This is in order to provide laboratory scale measurements of the effective acoustical properties of fish schools. The end product is a verified method for

measuring effective medium properties of schooling fish in the laboratory that can inform future fish school models. Measurements of phase speed for varying school densities of *Danio rerio* is presented. In addition tests were performed to validate the attenuation caused by the presence of fish.

The following chapters have been arranged in order to provide the background for understanding and interpreting the measurements made and analytical comparisons used. This begins with an introduction to the resonator technique in chapter 2. Starting with the basic definition of resonance, the method for extracting phase speed is discussed, along with considerations relating to deviations in the end conditions and the elastic waveguide effect. Then the theory is tied together with example dispersive sound speed profiles to show how phase speed is extracted.

Chapter 3 includes an overview of the many effective medium models available. They are introduced by starting with effective medium theory at the low-frequency quasi-static limit. Then the classic dispersion relation and the associated resonance and damping terms are discussed. Once the basic theory is discussed, several proposed multiple scattering corrections are presented and compared. Finally the chapter ends with a discussion of elasticity and shelled bubble effective medium theory.

Two series of experimental evaluations of sound propagation through shelled bubbles are presented in Chapter 4. The first set of tests correspond to resonator measurements of encapsulated balloons. The shell thickness and balloon volume were measured independently and the Church and Church-Kargl models were used to back out the shear modulus of the elastic shell.

23

Chapter 5 brings the study of effective medium theory full circle by exploring the scattered field from an effective medium. This starts with a look at the scattering coefficient of a single bubble, then scattering from a fluid sphere and a fluid sphere with effective medium properties. The results comparing an effective medium sphere to a full scattering model of discrete bubble position are presented with both the forward-scattering, back scattering, and directivity of scattering at various frequencies.

The experimental measurements of sound speed through populations of *Danio rerio* is presented in Chapter 6. Here the relevant parameters for fish acoustics are discussed. In addition the data obtained through micro-computed x-ray tomography imaging scans (CT scans) of fish is presented. The modifications to the standard resonator apparatus required for live fish testing are described, and the phase speed results are presented.

Finally, Chapter 7 provides a summary of the results. The results for each section of the study are looked at as a collection and concluding remarks are made of the study. Lastly, potential future work and applications are suggested for the research.

# Chapter 2

# The Resonator Method and Validation

## 2.1   Introduction

This study employs a resonator technique in order to determine the sound speed and attenuation through various effective media of encapsulated bubbles. The current technique has been used successfully to determine the effective acoustic properties of freely rising bubbles [48], methane hydrates [57, 49], seagrass [50], fluid-like gas-bearing sediments [47], and encapsulated bubbles [53]. This method relies on the fact that the effective acoustic properties of a material are directly related to the resonances of a tube filled with the material.

The classical modes in open-open pipes with rigid walls are well known. The method for determining sound speed in this study is based upon these resonances. The phase speed, $c_{\mathrm{phase}}$, of the medium in the resonator tube (see Figure 2.9) is determined by utilizing:

$$c_{\mathrm{phase}} = \lambda f, \tag{2.1}$$

where the wavelength, $\lambda$ is:

$$\lambda = 2L/m, \tag{2.2}$$

$f$ is the resonance frequency, the resonance mode is $m$, and the length of the resonator is $L$.

Ideally the end conditions would be pressure release and the side walls would be rigid, which would lead to the relationship $\lambda = 2L/m$. Unfortunately neither of these conditions are valid in the present experimental apparatus. With respect to the upper condition of the tube (an air-water interface) the pressure release assumption is reasonable; however, an unbaffled piston radiation impedance is used to account for energy radiating from the system. Generally closed-cell foam is used at the lower boundary to provide an approximately pressure release condition when performing tests with water alone as the fill material, however when encapsulated bubbles are added the specific acoustic impedance of the material in the resonator is much closer to that of closed-cell foam and the lower boundary condition deviates significantly from the expected pressure-release condition. However, this boundary can effectively be treated as a three-medium problem and accurately modeled as is done here, described below.

In order to compensate for the finite impedance of the lower boundary, a corrected wavelength is determined by adjusting the mode number. This is done by determining the non-dimensional location of the last node, $\bar{x} = x/L$, in the tube and finding the adjusted mode number $m_{\text{adj}}$:

$$m_{\text{adj}} = \frac{m}{\bar{x}}. \tag{2.3}$$

Then an appropriate phase speed can be determined by using the wavelength

indicated by the adjusted mode:

$$c_{\text{phase}} = \lambda f = 2L/m_{\text{adj}}. \tag{2.4}$$

Another departure from ideal conditions comes from the finite impedance of the tube walls. Since the acoustic impedance of the walls is often of the same order as the media contained in the resonator there is a large amount of coupling between the two. Several analytical models exist to determine how these fields couple, however for this work we used the model of Del Grosso [58] as implemented by Lafleur & Shields [59]. This provides an estimate of how the phase speeds in the elastic waveguide relate to those in free space. Through measuring the frequency at which each mode or resonance occurs, and then compensating for the elastic waveguide effect in order get the equivent free field values, we can accurately determine the frequency dependent sound speed of the contents of the resonator. The elastic wave guide correction procedure is described in Section 2.4.

## 2.2 Standard Definitions of Resonance Frequency and Modes

At this point it becomes very important to clarify what is meant by resonance and modes. Typically resonance is related to the frequency $f$, angular frequency $\omega = 2\pi f$, the sound speed in the medium $c$, the wavenumber of the system $k = \omega/c$, the wavelength $\lambda = c/f$, the mode number $n \in \mathbb{N}$, and either a critical dimension of the system or in this case the length of the tube $L$. Below are some definitions of resonance and normal modes. It is apparent from these definitions that a resonant

system often needs an application-tailored definition in order to avoid ambiguity. After introducing the basic system being studied we will present our particularized definitions of resonance and normal modes.

**Kinsler, Frey, Coppens, & Sanders** [60]: "The resonance frequencies of any mechanical system are defined in general as those frequencies for which the input mechanical reactance goes to zero." p. 48

**Pierce** [61]: "Resonance arises when the successive echoes reinforce the pressure on a piston face." p. 116

**Blackstock** [62]: "Resonance here means that the pressure amplitude becomes unbounded. If small losses are present, the amplitude at resonance is very high but bounded." p.136

**Temkin** [63]: "The energy becomes infinitely large for those values of $k$ that satisfy the condition $kL = n\pi$. That is resonance, for then the frequency of the piston $\omega = kc$ is equal to one of the characteristic frequencies for longitudinal waves in the tube." p. 134

Here are some definitions of normal modes:

**Kinsler, Frey, Coppens, & Sanders** [60]: "Application of the boundary conditions has limited the viable solutions of the wave equation to a series of discrete functions. These functions are called eigenfunctions or normal modes." p.53

**Pierce** [61]: "Such natural constant-frequency disturbances are referred to as modes and only occur for certain discrete frequencies termed natural frequencies." p.119

**Beranek**[64]: "The condition where the frequency equals $nc/2L$ so that a very large sound pressure builds up in the tube is called a resonance condition or a normal mode of vibration of the air space in the tube." p.286

**Temkin** [63]: "The frequencies of oscillation of the $n^{\text{th}}$ mode being, in this case, $\omega_n = n\pi c/L$. These modes and frequencies of oscillation are characteristic of the system. They are therefore called the characteristic modes (or eigenmodes) and the characteristic frequencies (or eigenfrequencies) of the system." p.99

## 2.3   Resonance Tubes

### 2.3.1   The Ideal Resonance Tube

The discussion of this method begins with an ideal tube resonator with rigid walls and pressure release end conditions that is filled with a non-dispersive fluid. Figure 2.1 shows the ideal mode shapes that are present in such a resonator. According to Temkin [63], at resonance:

$$k_n L = n\pi. \tag{2.5}$$

(a) Mode 1: $\lambda = 2L$      (b) Mode 2: $\lambda = L$      (c) Mode 3: $\lambda = \frac{2}{3}L$
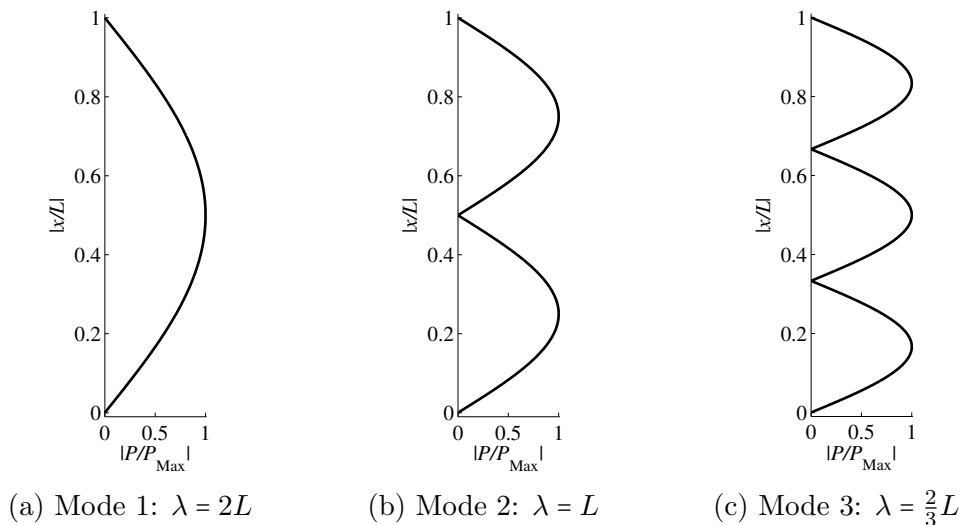
Figure 2.1: First three modes of an ideal open-open tube

Or alternitively,

$$\tag{2.6}$$

$$\lambda_n = \frac{2L}{n}, \tag{2.7}$$

$$f_n = \frac{nc}{2L}, \tag{2.8}$$

$$c = \frac{2Lf_n}{n}. \tag{2.9}$$

For the purpose of this study, we define resonance as occurring when equation (2.10) is satisfied,

$$c_{\text{phase}} = \frac{2Lf}{n}. \tag{2.10}$$

Hence, when the phase speed of the system at a given frequency is equivalent $2L/n$ times that frequency, the $n^{\text{th}}$ mode of resonance occurs. A graphical illustration of

30

(a) Phase speeds on a linear plot      (b) Phase speeds on a log-log plot
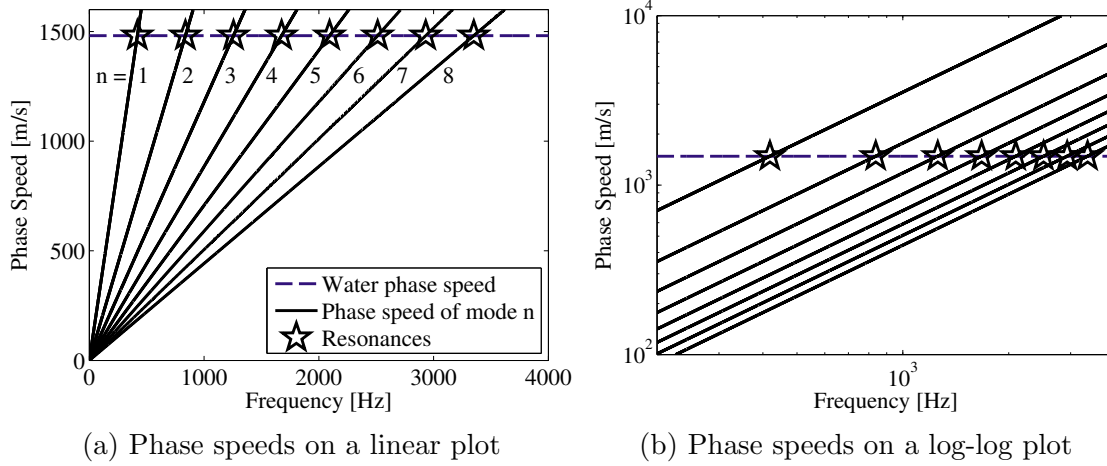
Figure 2.2: Location of resonances in an ideal system

Equation (2.10) is shown in Fig. 2.2 with both linear and logarithmic axes. Similarly, we associate the normal modes of the system with the spatial standing wave pattern in the tube each time the $n^{\text{th}}$ resonance occurs. For a system with a constant sound speed, this occurs once for each mode. As is shown in Section 2.6, when the fluid inside the waveguide has sufficient dispersion, the $n^{\text{th}}$ mode can occur at more than one frequency.

## 2.4   Elastic Waveguides

Up to this point we have considered a waveguide with rigid walls. In reality the walls have an acoustic impedance that is of the same order as medium being studied. As a result the walls do not act as if they are rigid; instead they couple with the acoustic field in the water. The response of the coupled system can be computed by relating the boundary conditions between the solid and fluid media. Multiple

31

forward models exist and in this study we are using an expression derived by Del Grosso [58]. This expression gives the phase speed in the coupled system as a function of the sound speed in the absence of the waveguide $c_0$, the density of the liquid $\rho_l$, frequency $f$, the inner and outer radius of the tube $b$ and $d$, the compressional and transverse sound speeds in the tube $c_c$ and $c_s$, and the density of the tube wall material $\rho_w$. The equations for the model can be found in Appendix B. The first four symmetric modes of a water-filled aluminum pipe with material properties listed in Table 2.1 were calculated by finding the solutions to Equation (B.7) and are shown in Figure 2.3a. Unlike a rigid waveguide, two modes can exist down to zero frequency; however for this study resonances are only present due to the (0,0) mode because the primary energy of the (0,1) mode is in the wall, and the $kb$ range study is below the cut-off for higher modes.

While the relationship can not be easily inverted, it is possible to solve the forward problem for all possible values of input free medium sound speed and then (since at a given frequency the free medium sound speed and the waveguide sound speed have an injective relationship) create an interpolation matrix that allows the desired sound speed (in the waveguide or in free space) to be determined. The mapping between free medium sound speeds and waveguide sound speeds is shown in Fig.2.3(b) where the color represents the free medium sound speed and the ordinate represents the corresponding waveguide sound speed. The primary limitations of this model is the fact that it is lossless and as such does not account for how attenuation is affected by the presence of the waveguide. The model also predicts that there is a maximum phase speed for the system and any phase speeds in the medium are

32
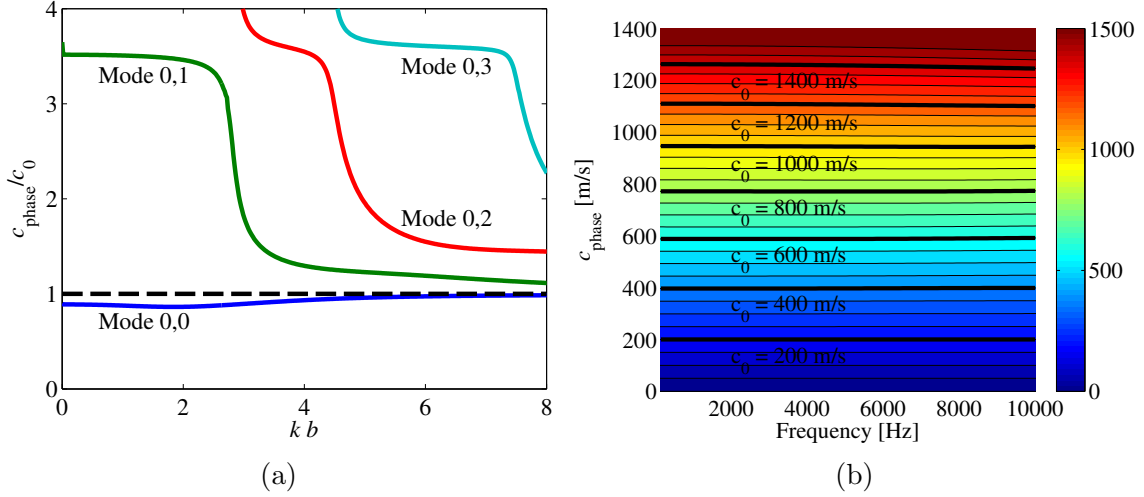
Figure 2.3: Dispersion relation for symmetric longitudinal modes calculated using expressions in Ref. [59] and included here in Appendix B. (a) Symmetric modes in an elastic waveguide. (b) Mapping between free medium and the (0,0) mode of the waveguide. The amplitude [m/s] represents the sound speed in a free field while the y-axis represents the sound speed in the waveguide.

reduced to this maximum value.

The correction is implemented here by computing a numerical correction function to predict the waveguide sound speed, $c_{\mathrm{wg}}$:

$$c_{\mathrm{wg}} = F_{\mathrm{free2wg}}(c_{\mathrm{free}}, f), \qquad (2.11)$$

for a given the free medium sound speed $c_{\mathrm{free}}$, and the frequency $f$. The function to compute the free medium sound speed from the waveguide sound speed was also determined:

$$c_{\mathrm{free}} = F_{\mathrm{wg2free}}(c_{\mathrm{wg}}, f). \qquad (2.12)$$

Both these relations were computed by solving Equation ([B.7](#)) over the range of expected free medium sound speeds and frequencies in order to create a reference data-set specific to the physical parameters for the apparatus used here. The functions then use a three point triangular interpolation scheme on that data set in order to determine the waveguide sound speed for a given free medium sound speed and frequency. Since the relationship between $c_{\text{free}}$ and $c_{\text{wg}}$ is injective at any given frequency, the same data set can be used for the inverse operation.

It is important to note that in an elastic waveguide the energy is not necessarily evenly distributed between the wall and the liquid, and that the waves are no longer purely planar. Lafleur & Shields [59] provide plots of the shape, amplitude, and phase of both the longitudinal and transverse motion in an aluminum waveguide for both the (0,0) and (0,1) modes. In their example the longitudinal motion of the (0,0) mode is within 1.5% of having uniform motion. Although there is a small radial component, the lowest mode is sufficiently plane to allow application of the equations of plane wave acoustics and the resonance frequency are associated with the phase speed in the usual manner. It is also noted that a significant fraction of the wave power is in the wall for the (0,1) mode. This is one of the reasons that the (0,1) mode is not expected in the measurements.

## 2.5    A Simple Analytical Model for the System

For the forward model of the system, it is assumed that propagation can be treated as consisting of only plane waves with a given phase speed and attenuation that only vary along the length of the resonator. The experimental system is excited
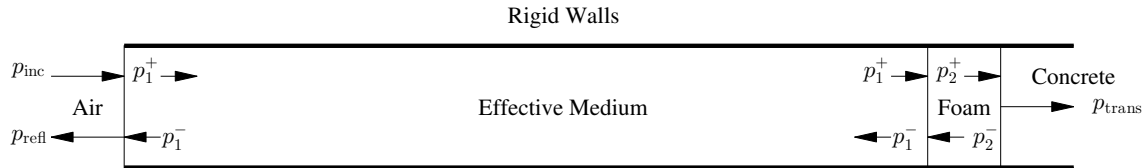
Figure 2.4: Resonator geometry

with a piston in the waveguide. The simplest analytical model has excitation coming from a plane wave parallel to one end of the resonator $p_{\text{inc}}$. The system is then treated like plane wave propagation through several layers, with a reflected wave $p_{\text{relf}}$ at one end of the resonator, left $p_m^-$ and right $p_m^+$ traveling waves in each layer $m$, and ultimately a transmitted wave $p_{\text{trans}}$ at the other end of the system. For the aluminum resonator, it was determined that the field in the resonator was coupled to the concrete floor despite a closed cell foam layer at the bottom, so both a layer of closed cell foam and radiation into the concrete floor are included. The model is shown in Figure 2.4.

For a water-filled resonator, the sound speed of water in the elastic waveguide is calculated as described in Section 2.4. Aside from radiation from the ends, other possible loss mechanisms are viscous-thermal wall damping and and viscous propagation losses. The attenuation coefficient for viscous-thermal damping in a tube is [62, 63]:

$$\alpha_{\text{w}} = \frac{1}{ac_0}\sqrt{\frac{\omega\mu}{2\rho}}\left(1 + \frac{\gamma - 1}{\sqrt{\text{Pr}}}\right), \tag{2.13}$$

35

where $c_0$, $\rho$, $\mu$, Pr, and $\gamma$ are the sound speed, density, viscosity, Prandtl number, and ratio of specific heats of water, respectively, and $a$ is the radius of the tube. The attenuation due to viscous propagation is [62, 63]:

$$\alpha_{\mathrm{v}} = \frac{\tilde{V}\mu\omega^2}{2\rho c_0^3},\tag{2.14}$$

where $\tilde{V}$ is the viscosity number and is approximately 4.42 for fresh water at room temperature. These attenuation for the narrowest resonator used in this study are shown in Figure 2.6 are secondary compared to the radiation loss from the ends of the tube, are less than 0.03 dB/m for the parameters in this study, and have been neglected in the models. An example of the pressure distribution in the tube calculated by the model is shown in Figure 2.5 and the derivation of the model is presented in Appendix C. Note the half-wavelength resonance in the foam at approximately 2500 Hz and that the nodes start from the origin (top) of the resonator.

## 2.6   The Inclusion of Highly Dispersive Effective Media and the Presence of Multiple Eigenfrequencies Per Mode

When acoustic waves propagate along a waveguide, the phase speed can vary as a function of frequency. The effect of waves of different frequencies traveling at different phase speeds is know as dispersion [60]. In distinction from the dispersion caused by the presence of a waveguide, acoustic waves in free space can also experience dispersion due to intrinsic properties of the medium. For the purpose of this study, the latter dispersion is defined as intrinsic dispersion, which is now added as the next level of complexity. In order to prevent confusion with the elastic waveg-

36
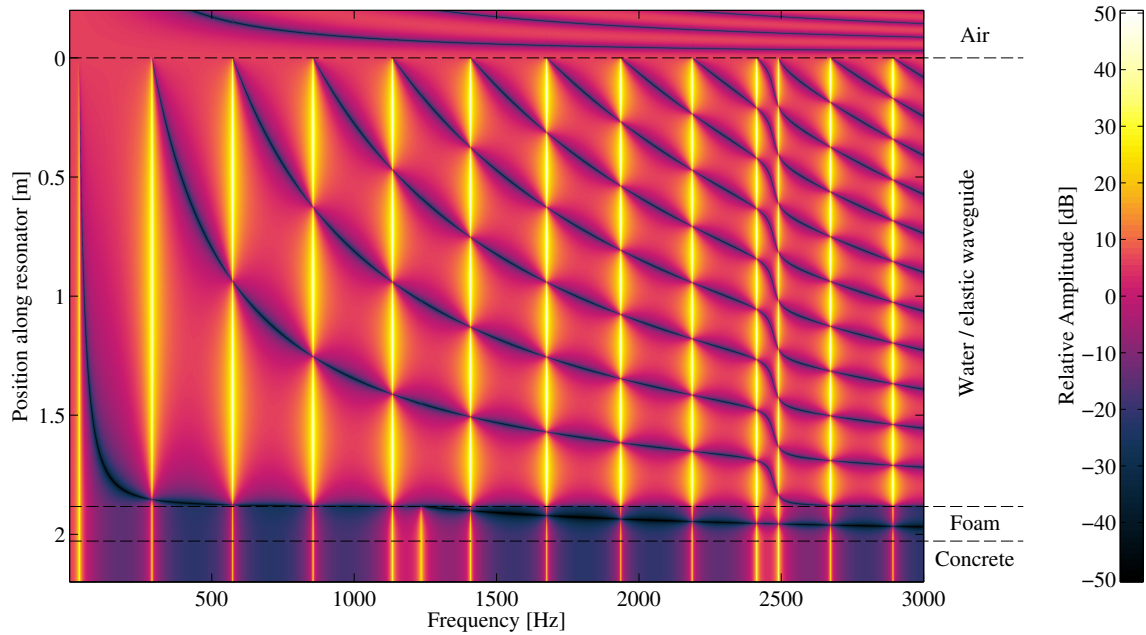
Figure 2.5: Analytical model of the spectra inside a water-filled aluminum waveguide.

uide effect and the non-ideal boundary conditions the walls are still considered to be infinitely rigid and both ends of the resonator terminate into half spaces of air.

Although effective medium models are discussed in Chapter 3, in this section we will be using the model by Commander & Prosperetti [46] for bubbly liquids in order to simulate a medium of increasingly large dispersion. The model is discussed in detail in Section 3.3.3. Figure 2.7 shows how the increasing VF affects the sound speed profile and the spectrum within a 1-D resonator. Air bubbles of a constant radius (2 cm) are gradually added to a water-filled resonator, which results in an increase in the volume fraction of air (VF). At this point the bubble size is chosen so that the bubble resonance is below the first natural resonance of the system. This is accomplished in the resonator model by inputting the complex sound speed

37
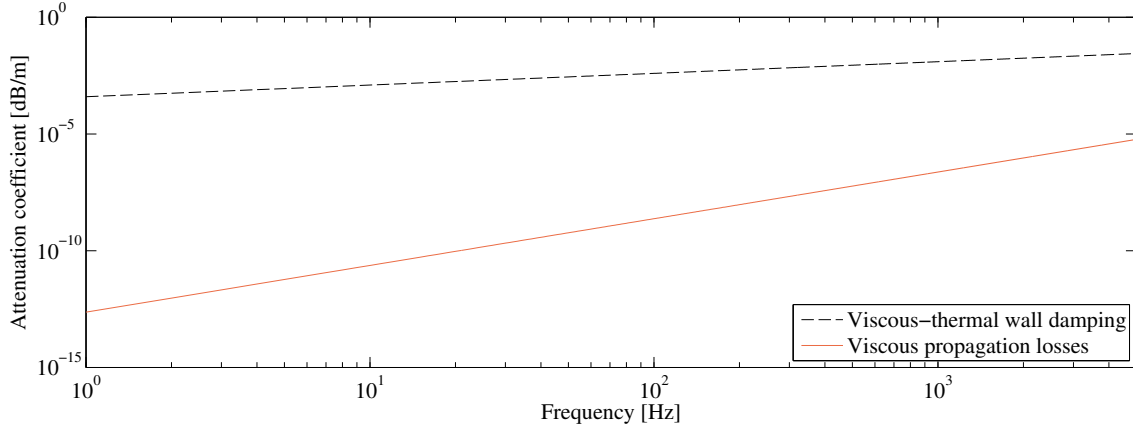
Figure 2.6: Attenuation due to motion at the wall of a tube and viscous propagation for the narrowest resonator.

calculated from the model presented by Commander and Prosperetti [46] into the resonator model which is discussed in Section 3.3.3 and in Appendix C. As was indicated in Section 2.1, the phase speed at resonance is described by Equation (2.1), and therefore this equation being satisfied (this happens at the intersection of the lines marked by stars in Figure 2.7) resonance occurs. At very low VFs the phase speed curve develops a bump. As this bump grows it eventually intersects the phase speed lines for the first resonance at an additional point, in this case when VF = $1.1 \times 10^{-5}$. Above this VF each resonance begins to occur at three distinct frequencies, the middle of which sees such excessive damping that it is not visible in the spectrum.

The appearance of individual modes occuring at multiple requencies was initially very surprising, however experimental scans of the hydrophone along the length of the resonator show that above the bubble resonance the fundamental modes do appear again. These measurements can be found in Section 2.8.
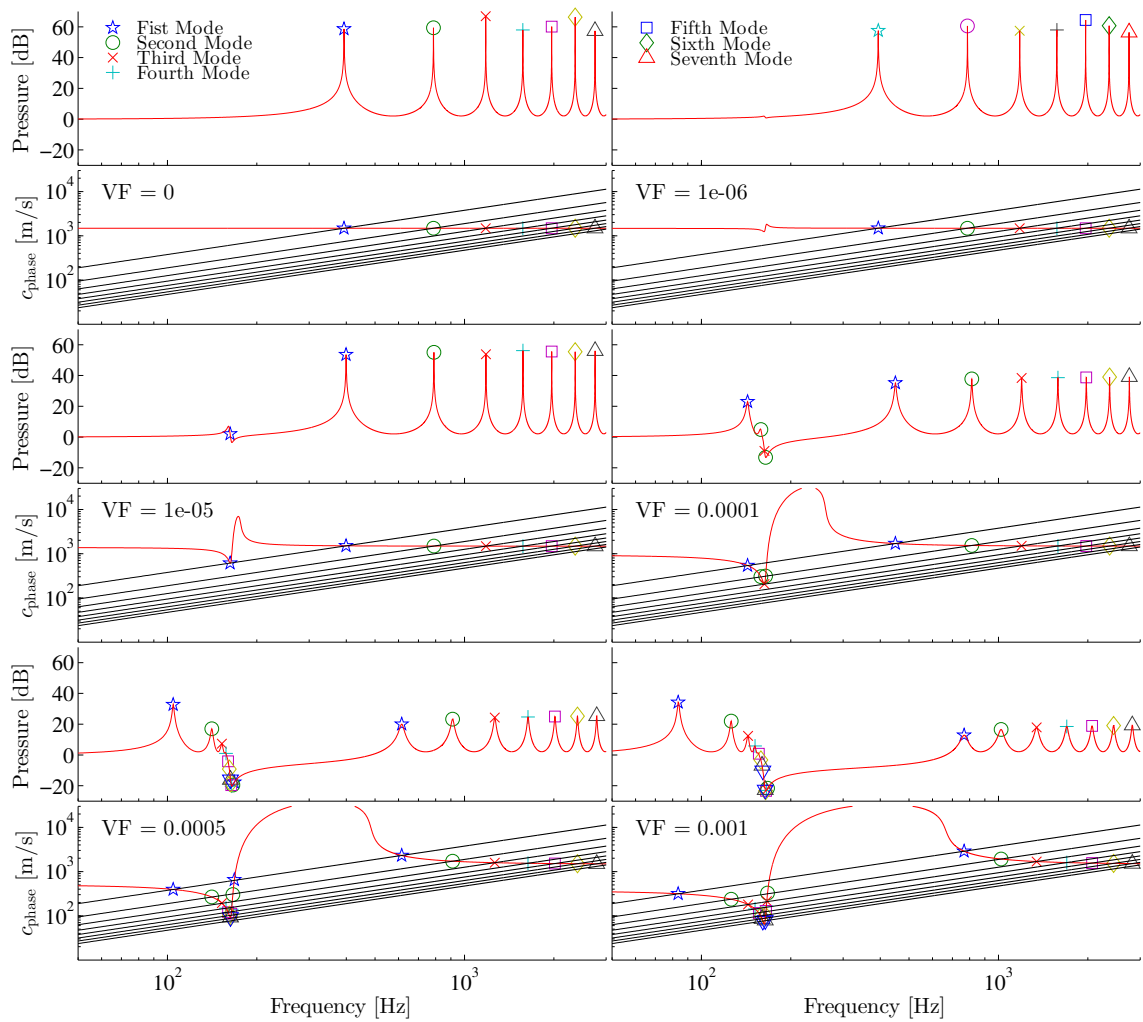
Figure 2.7: Plots showing how each resonance is related to the phase speed (top) and spectrum (bottom) for six volume fractions of air. The diagonal lines represent the condition required for each mode to appear. Each time the phase speed crosses a diagonal line, that resonance occurs ans is marked by a plot symbol that is unique for that mode or resonance. The associated resonance peaks are shown with the same plot symbol.

39

## 2.7    The Full Forward Model

Finally we can calculate a full forward prediction of the pressure field inside a resonator tube with the elastic waveguide effect and the dispersion due to the presence of bubbles. The first step is determining the effective medium properties from a model to get sound speed $c_{\text{eff,free}}$, and attenuation $\alpha_{\text{eff,free}}$. Then the sound speed is compensated for by using the correction function $F_{\text{free2wg}}(c_{\text{eff,free}}, f)$. From this we can calculate a complex wavenumber in the waveguide:

$$\tilde{k}_{\text{eff,wg}} = \frac{\omega}{F_{\text{free2wg}}(c_{\text{eff,free}}, f)} - i\alpha_{\text{eff,free}}, \tag{2.15}$$

and a complex sound speed:

$$\tilde{c}_{\text{eff,wg}} = \frac{\omega}{\tilde{k}_{\text{eff,wg}}}, \tag{2.16}$$

which is then used as the effective medium sound speed in the resonator model.

## 2.8    Validation of Resonator Method Theory

### 2.8.1    Multiple Eigenfrequencies for Individual Eigenmodes

Many acoustic systems exhibit dispersion and some can possess order-of-magnitude sound speed changes or more. The present research came about through investigating the acoustics of fish schools. Fish are often modeled as bubbles with viscoelastic shells. We use the acoustic resonator technique to determine the speed of sound through effective media. During this process the modes of the resonator need to be identified in order to relate the modal frequency to the phase speed. Figure 2.8

40

shows an experimental spectrum from a water-filled resonator with elastic-shelled air bubbles. Typically we had regarded the first few modes to be the fundamental lowest-order modes of the system (1, 2, 3, ...), followed by a region of high attenuation where no resonances are present. Above the high attenuation region there are higher-order modes, which require more information to properly identify. It is also useful to classify modes as either below or above the bubble resonance frequency, which occurs in the high attenuation region. In this paper mode shapes that posses multiple eigenfrequencies, found by scanning a hydrophone along the length of the resonator, are discussed.

### 2.8.2  Experimental Apparatus and Test Conditions

A picture of the experimental apparatus along with a schematic diagram are shown in Fig. 2.9. An aluminum pipe with the properties in Table 2.1 was filled with degassed water. The compressional $c_c$, and shear $c_s$, sound speeds of the wall material were determined by taking precise measurements of the dimensions, temperature, and sound speed in the water-filled resonator, then the values were optimized in order to obtain the best match with the elastic waveguide model (see Appendix B). These values are in agreement with tabulated values for aluminum, as expected. A Labworks shaker was used to drive a 3.81-cm-radius piston positioned 3 cm below the air-water interface, which excited the acoustic field inside the resonator with a linear chirp produced by an NI PCI 4461 card with two outputs and two inputs and amplified by a Crown power amplifier. For all measurements in this study except the lake tests the response was measured by scanning a Reson model TC4013 hydrophone

41

| | |
|---|---|
| $L$ | 1.985 m |
| $c_\mathrm{c}$ | 6420 m/s |
| $c_\mathrm{s}$ | 3205 m/s |
| $\rho$ | 2700 kg/m$^3$ |
| $b$ | 0.1015 m |
| $d$ | 0.1085 m |

Table 2.1: Material properties of the aluminum resonator.

along the length of the tube. A Brüel and Kjær Nexus was used for pre-amplification and signal conditioning after which the signal was recorded by the NI PCI 4461. The source signal was determined to have a flat frequency response. A baseline measurement was taken and then six evenly spaced latex balloons were inserted, each with a radius of 1.26 cm, yielding a volume fraction of air $8.2476 \times 10^{-4}$. At each position the response was averaged 8 times and then the power spectral density was calculated in order to create a map of energy as a function of frequency and space.

### 2.8.3  Comparison of Measurements and Model

Figure 2.10 shows a comparison between the experimental measurements and the results from the resonator model using fluid sound speeds calculated from the effective medium theory discussed in Section 3.3.3, and compensating for elastic waveguide effects. Only the upper three-quarters of the resonator tube could be scanned. The dashed line in the upper plot of Fig. 2.10 indicates the extent of the measurements. It is clear that there is a discrepancy between the amount of attenuation in the bubble resonance region between model and experiment. The dark blue region near 600 Hz is larger in the model (upper) plot than in the measured (lower) plot. This can be attributed to the fact that the compensation for waveguide

effects only takes into account how the sound speed is affected and not how the attenuation is affected. Despite the differences in attenuation the location and mode shapes outside the high attenuation area match well.

Now the phase speed is extracted from the spectrum using Equation (2.4). Using the standing wave pattern provided from scanning the hydrophone it is easy to identify the mode associated with each resonance frequency. Figure 2.11 displays mode determinations for the experimental spectrum first shown in Fig.2.8. There is one extra resonance present labeled "S", which was identified as the resonance of the piston structure by changing the length of the rod connecting the piston to the shaker, and noticing that only this resonance changed frequency.

The phase speeds that result from this mapping are shown in Fig. 2.12 along with effective medium theory (C&P see Section 3.3.3) which has been adjusted to reflect the presence of the waveguide. Figure 2.13 shows the same plot when the data are corrected to represent free field propagation. The elastic wave guide parameters from Table 2.1 were used along with 8 bubbles with a radius of 0.0076 m. The air-water interface was 0.213 m below the top of the tube, yielding a VF of air $2.55 \times 10^{-4}$. The air was taken to have a sound speed of 343 m/s and a density of 1.21 kg/m$^3$. The water was taken to have a sound speed of 1487.9 m/s and a density of 998 kg/m$^3$.

### 2.8.4 Resonances and Wall Motion

The elastic waveguide modeling presented so far is for axisymmetric modes. Additional modes of the flexural and torsional type can also exist and could potentially interfere with the sound speed inference algorithm previously described. To

43

explore this possibility laser doppler vibrometer (LDV) measurements were obtained from the wall of an water-filled 18-inch-long glass resonator while simultaneous acoustic measurements were made in the water. Twenty-three positions along the length of the tube were recorded with the LVD and for each longitudinal position five rotational positions were measured for a total of 115 measurements. A ensemble average of 16 sweeps from a single position in the water column, and of the wall motion at all the measurement positions are shown in Figure 2.14. Stars represent the dominant plane wave acoustic modes, whereas the square boxes represent other modes that appear in both the the water and the wall motion. The mode shapes of the acoustic plane wave modes labeled A are shown in Figure 2.15 and other modes labeled O are then shown in Figure 2.16.

The acoustic modes appear very clearly in the wall motion, quantitatively verifying part of the elastic waveguide model. The very first acoustic mode (Mode 1, Fig. 2.15) appears to be coupled to a bending mode in the wall, though this does not appear to have any impact of the sound speed of that mode.
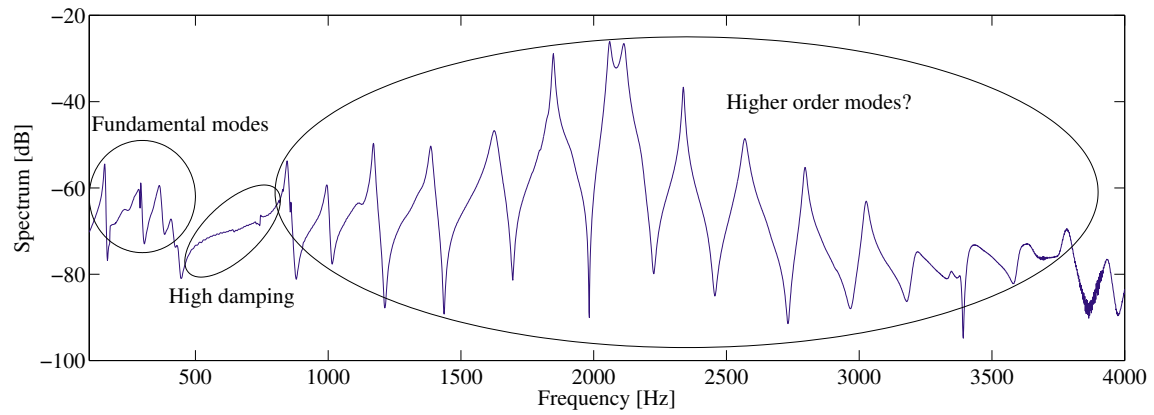
Figure 2.8: Spectrum with resonance peaks
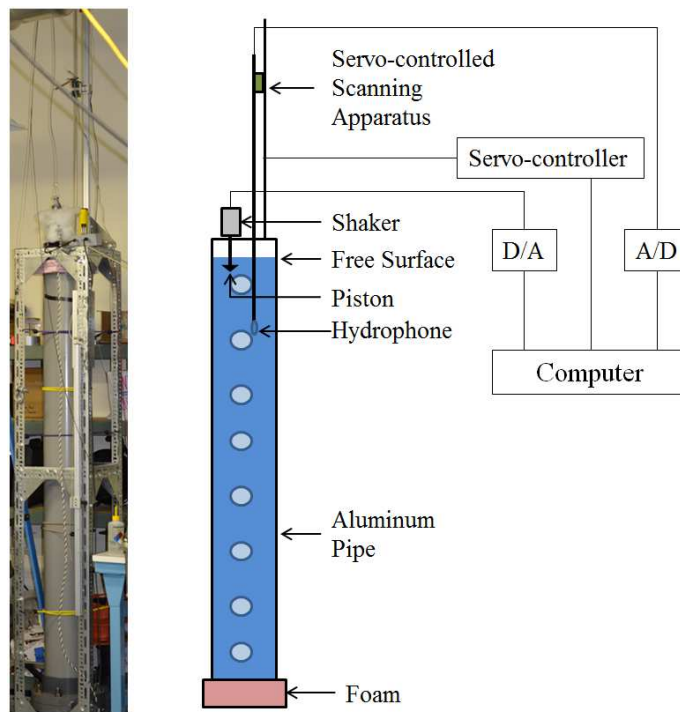


Figure 2.9: Photo (left) and schematic diagram (right) of the experimental apparatus
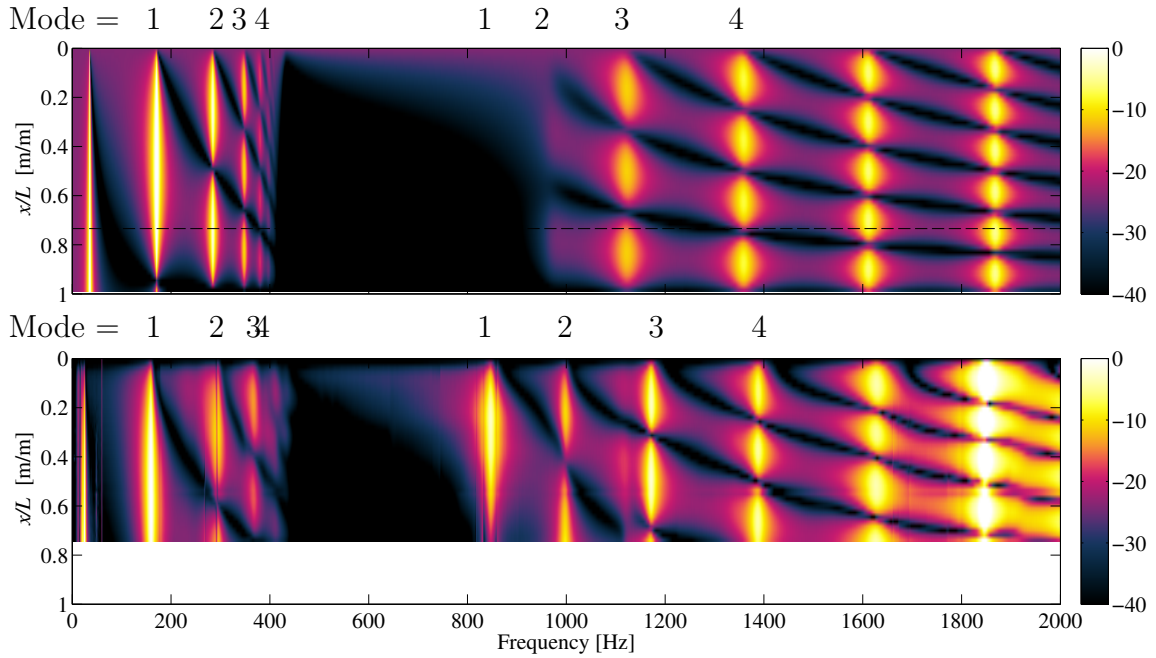
Figure 2.10: Comparison between a resonator model (top) with the fluid properties determined by Equations (3.33) and (3.34) and an experiment of the acoustic field in a resonator (bottom).
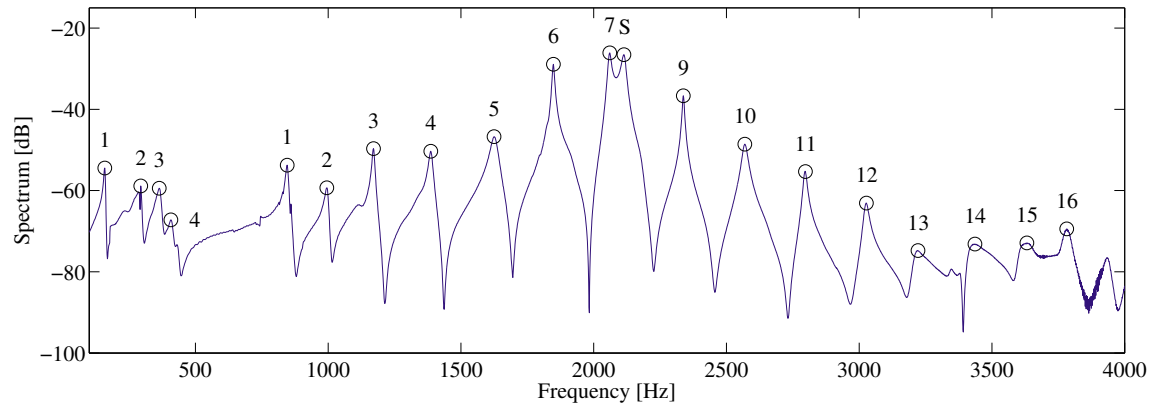


Figure 2.11: The resonance peaks are circled and the numbers correspond to the mode number. Hence peaks with the same number share an eigenmode shape, yet have distinct eigenfrequencies.
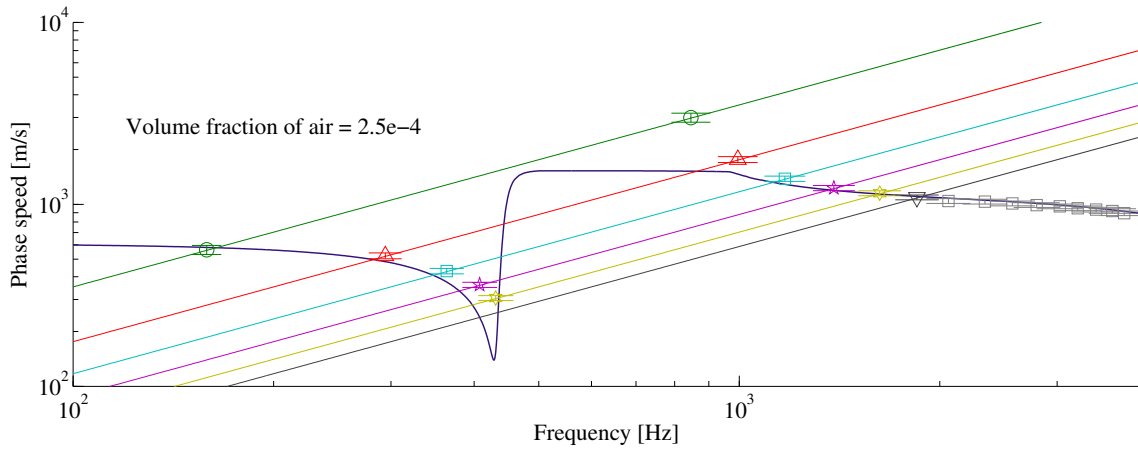
Figure 2.12: Experimental data with C&P model (adjusted to include waveguide effect).
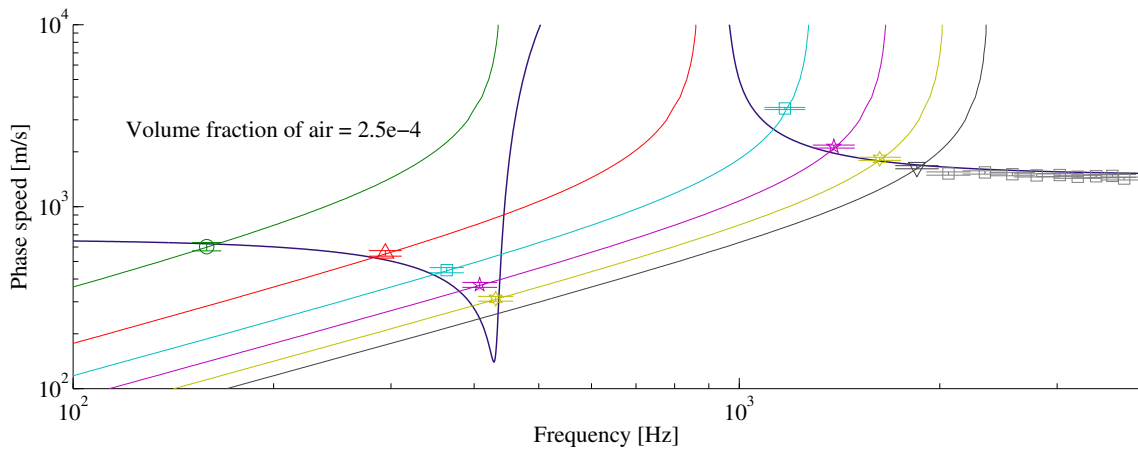


Figure 2.13: Experimental data (adjusted to remove the waveguide effect) with model.

47
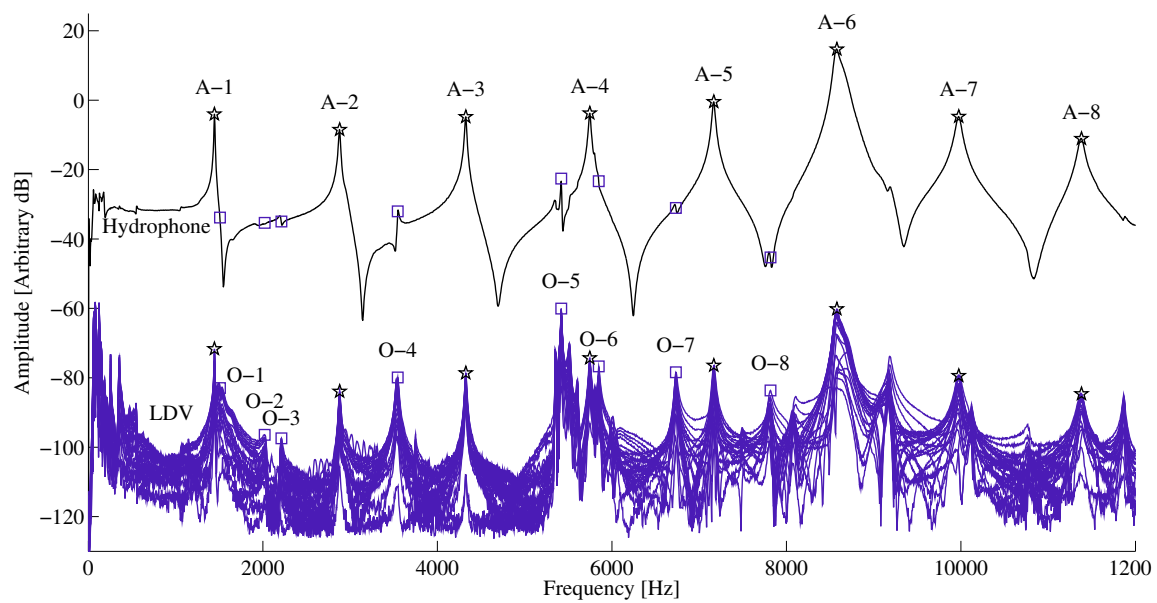
Figure 2.14: Resonant modes of a water-filled glass tube as measured by a hydrophone and an LDV. The notation A-$n$ indicates $(0,0,n)$ acoustic waveguide modes, the notation O-$n$ indicates other modes.

Mode 1      Mode 2      Mode 3      Mode 4

Mode 5      Mode 6      Mode 7      Mode 8
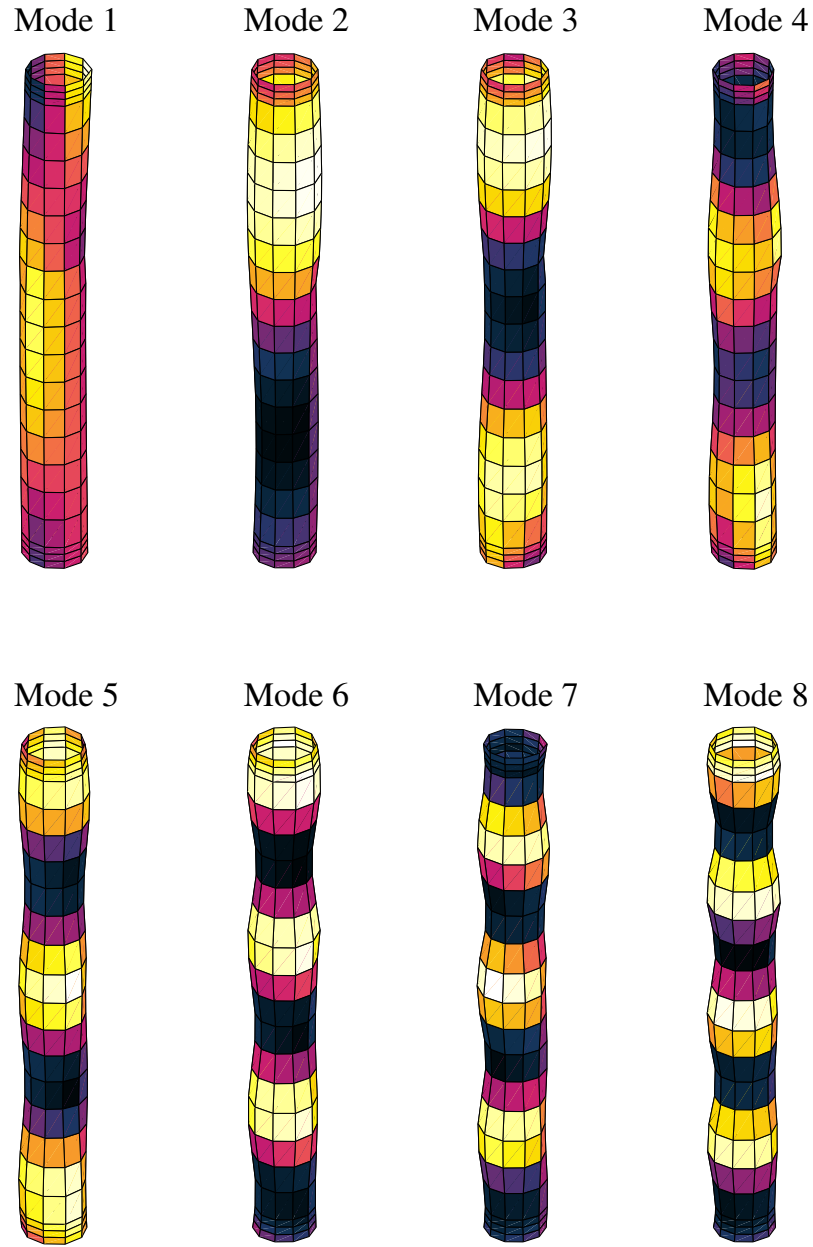
Figure 2.15: Wall displacement of first 8 plane wave acoustic (A) modes.

Mode 1      Mode 2      Mode 3      Mode 4

Mode 5      Mode 6      Mode 7      Mode 8
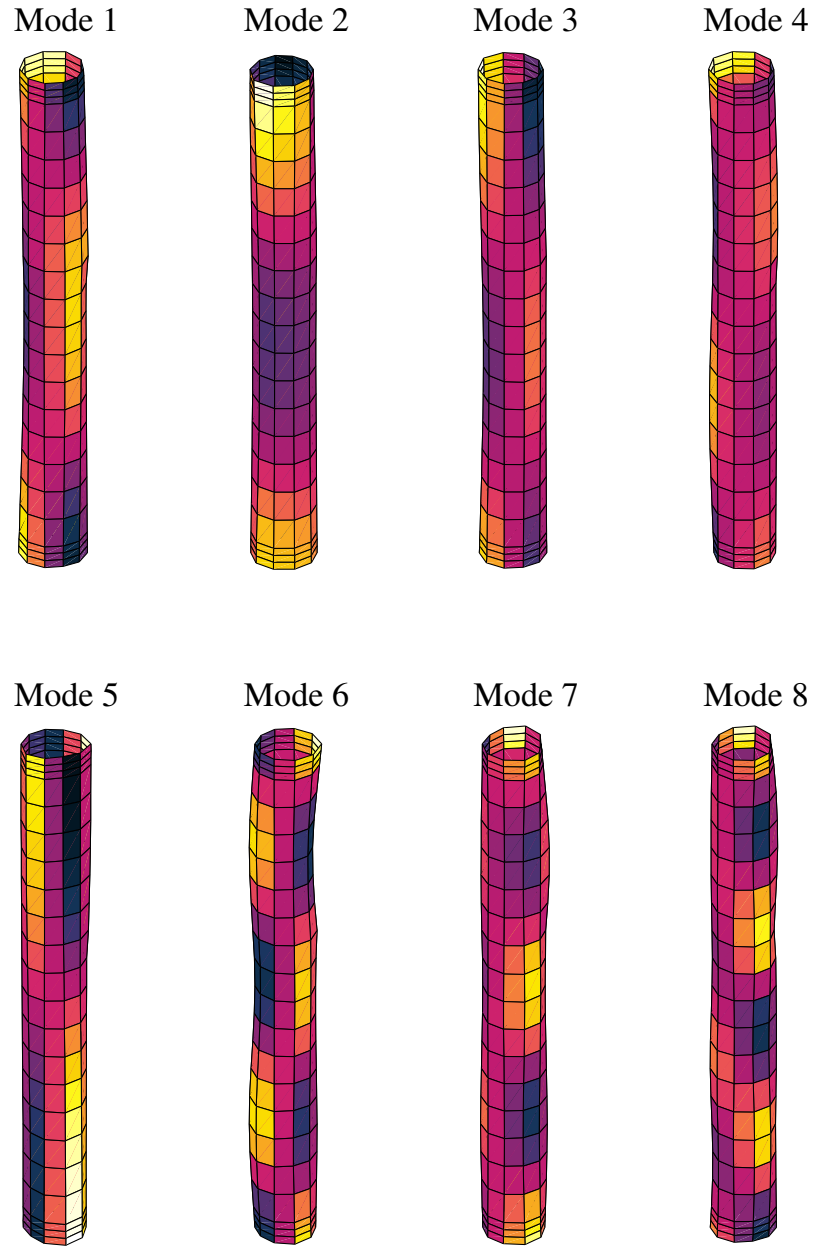
Figure 2.16: Relative wall displacement of first 8 other (O) modes

# Chapter 3

# Effective Medium Theory for Bubbly Liquids

## 3.1 Historical Overview

Up to this point effective medium theory has been mentioned quite a bit, but not formally defined. In the sense of this dissertation, effective medium theory is the representation of a complex heterogeneous system as a single homogeneous acoustic medium with an effective frequency dependent sound speed and a single frequency dependent attenuation. In the remainder of this chapter, effective medium models will be discussed ranging from quasi-static models which do not have any frequency dependence, to a variety of dynamic models which address multiple scattering effects. The study of effective media is often a branch of acoustics where exotic physcial properties such negative stiffnesses or mass are cited. The application to bubbly liquids is on the less exotic side. There is little consensus within the field as to which corrections for multiple scattering are appropriate due to the absence of measurements with sufficient accuracy and uncertainty to validate models. Some of the models discussed are for general mixtures and suspensions (Mallock-Wood and Temkin), however the majority are specifically for the case of gas bubbles in a homogeneous liquid.

The oldest paper concerning the propagation of sound through bubbly liquids

is Mallock's paper "The Damping by Frothy Liquids" published in 1910[65]. The paper begins with the problem statement "The fact that a tumbler containing a frothy liquid gives a dull sound when struck is familiar to every one, but I cannot find that any explanation of the rapid damping of the vibrations, which is indicated by the character of the sound, has been published." He goes on to propose that in bubbly liquids, the variations in pressure act entirely on the bubbles and that "the velocity of transmission of a wave in mixed fluid, such as a liquid containing bubbles, is the same as it would be in a homogeneous fluid of the same density and mean elasticity." The equations that result from this assumption are stated later on in section 3.2. He then goes on to calculate the work done due to viscous motion of the water caused by the vibrating bubble wall.

Mallock's work was reviewed and expanded upon in Wood's *A Textbook of Sound* [66] 20 years later. While the first edition of the textbook cited Mallock's work, subsequent (and more widely available) editions dropped the reference, causing many to falsely attribute the original derivation to Wood. Neither Mallock or Wood appear to define what elasticity should be used, though many have assumed that the isentropic elasticity, defined by $E = \rho c^2$, was intended. Although Mallock's argument of mean elasticity and density was made a priori, in 1933 Herzfeld [67] published a derivation of the sound speed in a suspension of small particles based on first principles and proved the concept of using mean elasticity and density for small spherical suspension of solids or fluids at quasi-static frequencies.

While the quasi-static nature of sound was being discussed, others were trying to solve the mystery of how bubbles resonated. In his 1919 lecture series "The World

of Sound" Sir William Henry Bragg [68] mentions an experiment by Sir Richard Paget where pieces of shot were dropped into still water. As with water drops an air cavity formed behind the shot. Sir Paget claimed to make measurements of these cavities and determined that upon making models of the cavities in plasticine the note produced by blowing across the top of the cavity was practically the same tone is produced as that of the bubble. Sir William Henry Bragg later noted in a personal correspondence to Minnaert [69] that Sir Paget's work was never published elsewhere. If anything is to be taken from this, it is that there was definitely awareness of bubbles having pitch and attempts to determine them prior to 1919.

The dynamics of a single bubble and its resonance frequency were revealed in 1933 by Minnaert [69] in his seminal paper *On Musical Air-Bubbles and the Sounds of Running Water*. Minnaert compares the potential energy in the bubble and the kinetic energy in the fluid, in essence reducing the system to a simple mass-spring analogy. He begins by noting that "by letting air escape in bubbles from the orifice of a tube immersed in water; each bubble gives a sound of very definite pitch." His paper includes experimental evidence that proves the relationship between bubble volume and pitch, the influence of the density of the liquid, and even makes a qualitative note that the bubble pitch reduces near the surface due to a lessening of the mass loading of the bubble. This expression for the resonance frequency of bubbles due to small acoustic perturbations holds to this day for sufficiently large bubbles, in which surface tension can be neglected, and aside from a small correction to account for themal effects added to the model in the 1980s, is accurate to within a few percent. Minneart's equation for the resonance frequency, $f_0$, of a single bubble is:

$$f_0 = \frac{1}{2\pi a}\sqrt{\frac{3\eta p_0}{\rho}}, \tag{3.1}$$

where $a$ is the radius of the bubble, $\eta$ is the polytropic index of the gas in the bubble, $p_0$ is the static pressure at the bubble, and $\rho$ is the density of the liquid.

The next advance in the determination of the sound speed in suspensions came in 1943, when Kennard [70] and Spitzer [71] appear to have independently published dispersion relations for the sound speed in bubbly liquids while working on WWII-related research. Both derivations arrive that what is now known as the classic dispersion relation for bubbly liquids:

$$\frac{1}{c^2} = \frac{1}{c_0^2} + \frac{4\pi}{\omega^2}\int \frac{n(r)r\mathrm{d}r}{\left(\frac{\omega_0^2}{\omega^2} - 1\right) + i\delta}, \tag{3.2}$$

where $c_0$ is the sound speed of the host liquid, $\omega$ is the angular frequency, $\omega_0 = 2\pi f_0$, $n$ is the number density of bubbles, and $\delta$ is the damping coefficient that was first mentioned in Section 1.2.

Kennard phrases the problem differently than Spitzer and instead of arriving at the form in equation 3.2, he arrives at a coupled set of equations which are similar to those later derived by Temkin [72, 73] and do not account for a polydisperse arrangement of bubbles. Kennard's equations do, however, simplify to the classic dispersion relation. The only attenuation Kennard includes in his derivation is due to acoustic re-radiation. Spitzer, on the other hand, mentions damping due to re-radiation, viscosity, and thermal effects. An expression for re-radiation damping is included, however he states that viscous damping can be ignored for bubbles greater

54

than $3 \times 10^{-6}$ m in radius and presents a theoretical determination of the damping costant, $\delta$. While Spitzer's derivation includes theoretical expressions for all three forms of damping he states that theoretical determination of $\delta$ is not to be trusted as it did not agree with the available experimental evidence.

A more general theory of the scattering of waves from a generic scatterer was published in 1945 by Foldy [74]. The seminal part of the paper deals with approaching multiple scattering from a wave propagation approach as opposed to the geometric optics limit. This is used to calculate the conditional averages of the the wave function, the average value of the square of its absolute value, and the average flux carried by the wave; however, it is often cited because the relation for an effective-medium wavenumber, which results as a consequence of the derivation. This relationship is:

$$k^2(\vec{r}) = k_0^2 + 2\pi g(\vec{r}), \tag{3.3}$$

where $\vec{r}$ is a position vector, $k(\vec{r})$ is the effective medium wavenumber, $k_0$ is the wavenumber in the host medium, and $g(\vec{r})$ is the scattering coefficient of scatterers integrated over their probability distribution. It is shown later that this is equivalent to (3.2).

Two additional technical reports based on WWII research from 1944 exist, are authored by Foldy, and specifically refer to the propagation of sound through bubbles, which extended Spitzer's work. It included distributions of bubbles and applied distributional averages to the bubbles in a bubble clouds. Both Foldy's

and Spitzer's work were summarized in Wildt's chapter on the "Acoustic theory of bubbles" in the book Physics of Sound in the Sea [75], where the classic dispersion relation was presented, but no description of the damping term included.

Between 1947 and 1957 the classical relation remained unchanged, and many authors proposed different damping terms [76, 77, 78, 79, 80, 81], apparently without knowledge of the earlier work mentioned above. Several experiments were conducted that provided a basis for comparison of the models [82, 83, 84]. The first comprehensive review of the bubbly liquid propagation theory came in 1959 with Devin's review [23].

Development of bubbly liquid theory was slower in the 60s than the 50s. Hsieh and Plesset [85, 86] published a paper on sound propagation in bubbly liquids, focusing particularly on heat conduction, and determined that attenuation due to heat conduction is very small. Crespo [87] worked on a synthesis of bubbly liquid theory and shock theory, showing that significant errors occur if the relative motion of gas bubbles was not included. Zabolotskaya and Soluyan [88] made a significant advancement in the non-linear theory of bubbly liquids by presenting a coupled expression for sound speed and the non-linear equations of motion for bubbles, allowing them to calculate the amplification of non-linear harmonics due to sound propagation through bubbly liquids. Near the end of the 1960s interest picked up again, with publications by Wijngaarden [89], Batchelor [90], and McWilliam and Duggins [91], all of whom failed to discover or cite the more complete work of Devin [23], and failed to cite the fundamental work of Spitzer [71], Kennard [70], and Foldy [74].

The beginning of the 1970s saw a large advancement in Devin's theory though

a letter to the editor of JASA by Anthony Eller [92], who extended Devin's theory of damping at resonance to all frequencies. This extension was clarified by Fairbank [93], in regards to the various definitions of the damping constants. Wijngaarden's 1972 review paper [94] did a better job at referencing the older literature, including citations of Foldy [74], Spitzer [71], and even Mallock's 1910 paper [65], though Mallock's mixture law was attributed to Wood's textbook [66]. Chapman and Plesset [95] and Prosperetti [96, 97] advanced the theory of a radius and frequency dependent polytropic index. Keiffer [98] focused on the low-frequency sound speed in mixtures of water and steam, Drumheller and Bedford [99, 100] worked on extending effective medium theory to general immiscible fluid mixtures, and Hsieh [101] and Marston [102] published a papers discussing possible second resonance frequencies for vapor bubbles.

The 1980s saw continued interest in tracking down the proper damping mechanisms and their associated amplitudes [103, 104, 105, 106, 107, 108, 109], nonlinearity [110, 111, 112], and multiple scattering [113, 114]. Commander and Prosperetti [46] published a complete set of equations for the sound speed and attenuation through bubbly liquids, and Temkin [115] published a review of the bubbly liquid research up to 1989.

From the 1990s on the critical question has been, how to correct for multiple scattering. From this debate has come a large amount of theoretical [116, 117, 12, 118, 119, 120, 121] and experimental [122, 123, 124, 47] literature. Some of the most commonly cited corrections for multiple scattering are described in Section 3.4. In addition Temkin [125, 72, 126, 73] published a unified theory for suspension

acoustics which applies to bubbly liquids and is unique from the classic bubbly liquid dispersion relation. Another important note is that up until 2003 there had been a dearth of experimental measurements of sound speed or attenuation at bubble resonance because of the excessive attenuation. In 2003 measurements were made in a liquid filled resonator [44] that indicated that multiple scattering corrections were not necessary, even up to volume fractions of air as high as $10^{-3}$. Studies involving higher void fractions at bubble resonance have not been published and the bubble concentration at which multiple scattering is important is not well known.

## 3.2 Acoustics at the Quasi-Static Limit

The discussion of effective media starts at the low-frequency or quasi-static limit. The important assumption here is that the system always stays in equilibrium. Two models are presented that account for plane wave propagation through an infinite medium with a given volume fraction (VF) of air $\chi$:

$$\chi_{\text{part}} = \frac{V_{\text{part}}}{V_{\text{whole}}}, \tag{3.4}$$

where $V_{\text{part}}$ is the volume of the component under consideration and $V_{\text{whole}}$ is the entire volume. If the subscript is omitted then the part under consideration is assumed to be the gas in the bubble.

Each model involves sound propagation in a bubbly liquid. Sound propagation is considered to be plane and wavelengths of the propagating sound $\lambda$, are larger than the bubble radius $a$.

### 3.2.1 Mallock-Wood Law for Sound Speed

Mallock's 1910 expression for sound speed in a heterogeneous mixture [65] was popularized in Wood's 1930 textbook of sound [66], is often attributed to Wood [127, 72] and is often cited as Wood's law; however, in deference to the earlier publication we refer to this derivation as the Mallock-Wood law. Mallock observes "It may be remarked that the velocity of transmission of a wave in mixed fluid, such as a liquid containing bubbles, is the same as it would be in a homogeneous fluid of the same density and mean elasticity." While the validity the *a priori* assumption that elasticities can be assumed to average has been challenged [72], more fundamental derivations [127, 67] have proven the point. If we consider the elasticity $E_m$, and the density $\rho_m$ ($m = 1$ or air, $m = 2$ for water), where the total volume fraction (volume of part / total volume) of air is known, we can arrive at the effective values through Equations (3.5a) and (3.5b). Then the elasticity, density, and sound speed are:

$$\rho_{\text{eff}} = \rho_1 \chi + (1 - \chi)\rho_2, \tag{3.5a}$$

$$\frac{1}{E_{\text{eff}}} = \frac{\chi}{E_1} + \frac{(1 - \chi)}{E_2}, \tag{3.5b}$$

$$c_{\text{eff}} = \sqrt{\frac{E_{\text{eff}}}{\rho_{\text{eff}}}}. \tag{3.5c}$$

Figure 3.1 show's a recreation of the sound speed plot from Mallock's 1910 paper, which has three different linear sections of its abscissa. In comparison, the second plot has a linear abscissa of $\chi$ and is in mks units. The Mallock-Wood law has seen success in various experiments [77, 78, 128]. One criticism of Mallock's
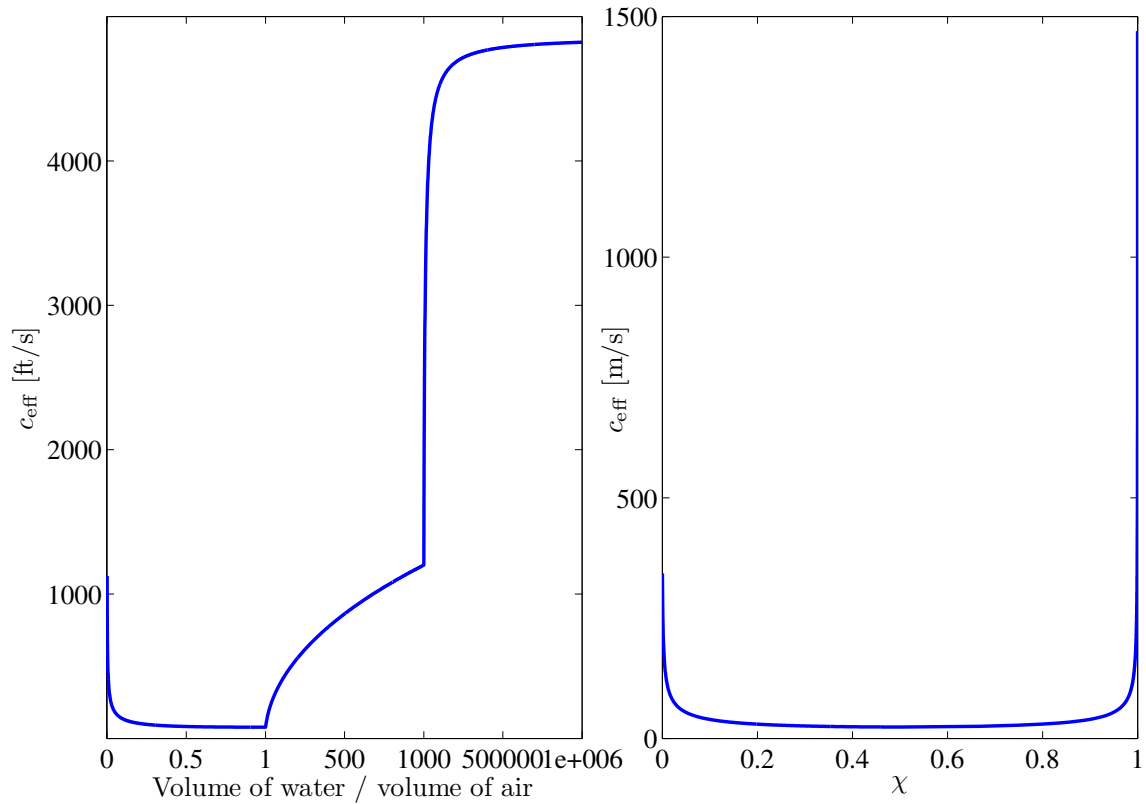
Figure 3.1: Recreation of Mallock's plot for the sound speed in a bubbly liquid for a given ratio of water to air with three different linear scales in the abscissa (left) and the modern convention of plotting the relation with the volume fraction of air $\chi$ (right).

low-frequency expression is that it only applies to isothermal conditions [72]. This has been countered by the argument [45] Wood [66] published a value of elasticity neither adiabatic nor isothermal, but somewhere in between, likely obtained by inference from measurements, and hence quite similar to what modern theory predicts for about millimeter-sized bubbles. This could be viewed as a mean low-frequency elasticity that is between the adiabatic and isothermal range.

**Temkin's Low and High Frequency Models for Suspension Acoustics**

Temkin [72, 129] derived an expression for near-zero and finite frequency sound propagation in suspensions using a first principles approach. The method starts with the definition of a homogeneous medium's adiabatic compressibility, $K_s$:

$$K_{\mathrm{s}} = -\frac{1}{\delta\tau}\frac{\mathrm{d}(\delta\tau)}{\mathrm{d}p}, \tag{3.6}$$

where $\delta\tau$ is a volume element and $\mathrm{d}p$ is the external pressure that deformes the element. The subscript s indicates an isentropic process. Once $K_{\mathrm{s}}$ is known, the isentropic sound speed can be determined:

$$c_{\mathrm{s}}^2 = \frac{1}{\rho_0 K_{\mathrm{s}}}, \tag{3.7}$$

where $\rho_0$ is the density of the medium.

While the homogenous definition can not generally be applied to suspensions, in can be applied at the low frequency limit where equilibrium exists within the medium. The zero-frequency-limit expression for sound speed, $c_s(0)$, in aerosols, bubbly liquids, emulsions, and hydrosols is:

$$\frac{c_{\mathrm{sf}}^2}{c_{\mathrm{s}}^2(0)} = \frac{1-\phi_{\mathrm{v}}}{1-\phi_{\mathrm{m}}}\left[\gamma_{\mathrm{f}}(1-\phi_{\mathrm{v}}) + \gamma_{\mathrm{p}}\phi_{\mathrm{v}}N_{\mathrm{s}}\right] - (\gamma_{\mathrm{f}}-1)\frac{(1-\phi_{\mathrm{v}}+\phi_{\mathrm{v}}\beta_{\mathrm{p}}/\beta_{\mathrm{f}})^2}{1+\phi_{\mathrm{m}}(c_{\mathrm{pp}}/c_{\mathrm{pf}}-1)}. \tag{3.8}$$

where $\phi_{\mathrm{v}}$ is the particle volume concentration, $\phi_m = (\rho_{\mathrm{p}}/\rho_{\mathrm{f}})\phi_{\mathrm{v}}/(1-\phi_{\mathrm{v}})$ is the mass concentration of the particulate, $N_s = (\rho_f c_{\mathrm{sf}}^2)/(\rho_{\mathrm{p}} c_{\mathrm{sp}}^2)$ is the ratio of particle to fluid

isentropic compressibilities, $c_s$ the isentropic sound speeds, $\gamma$ the specific heats ratio, $\beta$ the coefficient of thermal expansion, and $c_p$ the specific heat at constant pressure for the fluid (additional subscript f) and the particles (p). Temkin also presents a high-frequency limit known as the frozen-equilibrium speed ($c_s(\infty)$):

$$\frac{c_{sf}^2}{c_s^2(\infty)} = \frac{(1 - \phi_v)^2}{1 - \phi_m}. \tag{3.9}$$

This indicates a high-frequency limit where the particles are at rest. Note for very small volume fractions of air in water this is very close to the sound speed in water.

### 3.2.2 Quasi-Static Limit Summary

Using the models in this section we have our two frequency limits defined. The low frequency limit is valid below the resonance frequency and the high frequency limit is approached from some frequency above the resonance frequency. These models are shown in Figure 3.2. A region of high dispersion is necessary to connect the two limits.

## 3.3 Sound Propagation in Bubbly Liquids: Literature Highlights

### 3.3.1 Foldy's Multiple Scattering of Waves

Leslie L. Foldy took the problem of a medium filled with a random distribution of scatterers and evaluated it using statistical methods [74]. The solutions from this seminal paper are repeated here for clarity. The probability distribution that a

62
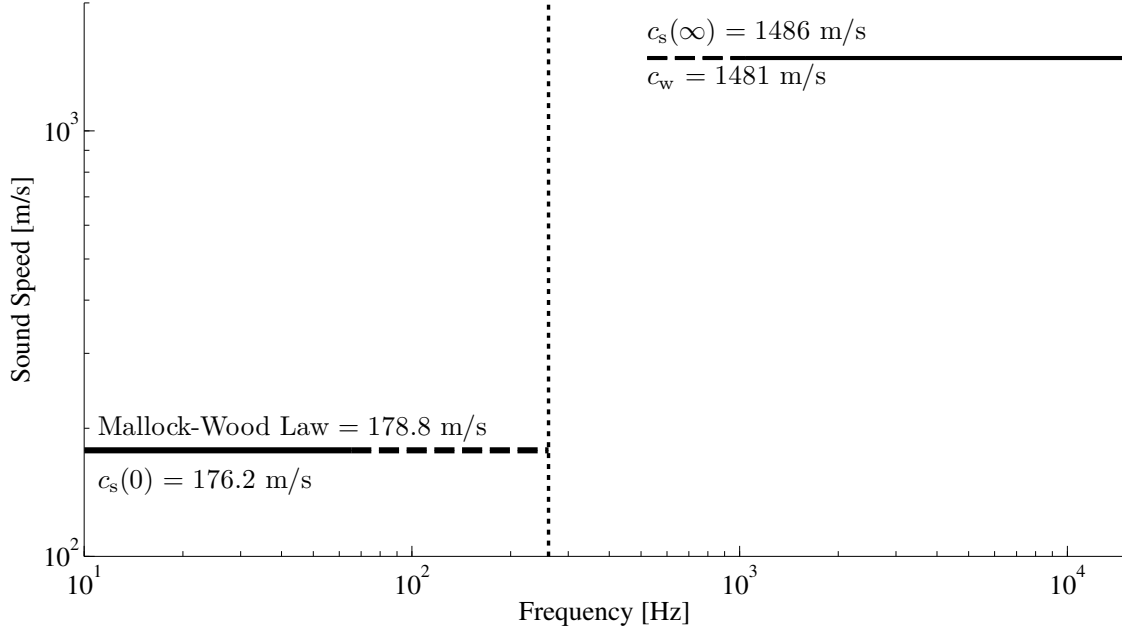
Figure 3.2: Quasi-static sound speeds limits for $\chi = 0.033$ and $a = 1.26$ cm.

scatterer is located in a volume element and has a scattering strength, $s$, is

$$P = (1/N)^N n(\mathbf{r}_1, s_1) n(\mathbf{r}_2, s_2) \cdots n(\mathbf{r}_N, s_N), \qquad (3.10)$$

where $N$ is the number of scatterers, $n(\mathbf{r}, s) \mathrm{d}s$ is the average number of scatterers per unit volume with strength between $s$ and $s + \mathrm{d}s$, and for the entire volume, $V$,

$$\iint_V n(\mathbf{r}, s) \, \mathrm{d}s \, \mathrm{d}r = N. \qquad (3.11)$$

The scalar wave function, $\psi(\mathbf{r})$, can be represented as the sum of the incident wave function, $\psi_0(\mathbf{r})$, and the sum of the field from all of the scatterers

63

$$\psi(\mathbf{r}) = \psi_0(\mathbf{r}) + \sum_j g_j \psi^j(\mathbf{r_j}) E(\mathbf{r}, \mathbf{r}_j), \qquad (3.12)$$

where $g_j$ is the scattering coefficient for the $j$th scatterer, $E(\mathbf{r}, \mathbf{r}') = \exp(-ik_0|\mathbf{r} - \mathbf{r}'|)/|\mathbf{r} - \mathbf{r}'|$, and the scattered field from the $j$th scatterer is defined implicetly as

$$\psi^j(\mathbf{r}_j) = \psi_0(\mathbf{r}_j) + \sum_{j'(\neq j)} g_j' \psi^{j'}(\mathbf{r}_j') E(\mathbf{r}, \mathbf{r}_j'). \qquad (3.13)$$

Equations (3.12) and (3.13) can be solved as a set of linear algebraic equations, however this becomes infeasible for a very large value of $N$ and it requires complete knowledge of the position and strength of every scatterer. In order to make the solution more useful for a statistical distribution of scatterers, Foldy set out to solve wave equations in order to determine the values of $\langle |\psi(\mathbf{r})| \rangle$ and $\langle |\psi(\mathbf{r})|^2 \rangle$, where the angular brackets signify an average.

After making the assumption that the summation of all but the current scatterer on the right hand of Equation (3.13) can be replaced with a summation over all of the scatterers without significant error if $N$ is large, and applying the physical operator $(\nabla^2 + k_0^2)$ to the average of Equation (3.13), applying the Liouville-Nuemann method of successive substitutions, and defining $G(\mathbf{r}) = \int g(s, \omega) n(\mathbf{r}, s) \mathrm{d}s$, the following iterative solution is found

$$\langle \psi(\mathbf{r}) \rangle = \sum_{m=0}^{\infty} \psi_m(\mathbf{r}), \qquad (3.14)$$

where

$$\psi_m(\mathbf{r}) = \int_V G(\mathbf{r}')\psi_{m-1}(\mathbf{r}')E(\mathbf{r},\mathbf{r}')\mathrm{d}\mathbf{r}' \quad (m \neq 0). \tag{3.15}$$

Through similar arguments the mean square value can be found to be

$$\langle|\psi(\mathbf{r})|^2\rangle = |\langle\psi(\mathbf{r})\rangle|^2 + \int_V H(\mathbf{r}')\langle|\psi(\mathbf{r}')|^2\rangle L(\mathbf{r},\mathbf{r};\mathbf{r}')\mathrm{f}\mathbf{r}', \tag{3.16}$$

$$L(\mathbf{r},\mathbf{r}_0;\mathbf{r}') = \sum_{p=0}^{\infty} L_p(\mathbf{r},\mathbf{r}_0;\mathbf{r}'), \tag{3.17}$$

$$L_p(\mathbf{r},\mathbf{r}_0;\mathbf{r}') = \frac{1}{4\pi}\iint_V [\{G(\mathbf{r}'')[\nabla'''^2 + k^{*2}(\mathbf{r}''')] + G^*(\mathbf{r}''')[\nabla''^2 + k^2(\mathbf{r}'')]\}$$
$$\times L_{p-1}(\mathbf{r}'',\mathbf{r}''';\mathbf{r}')]K(\mathbf{r},\mathbf{r}'') \times K^*(\mathbf{r}_0,\mathbf{r}''')\mathrm{d}\mathbf{r}''\mathrm{d}\mathbf{r}''', \tag{3.18}$$

$$L_0(\mathbf{r},\mathbf{r}_0;\mathbf{r}') = K(\mathbf{r},\mathbf{r}')K^*(\mathbf{r}_0,\mathbf{r}'), \tag{3.19}$$

and $K(\mathbf{r},\mathbf{r}')$ is a Green's function.

Most importantly Foldy derived a phase speed for waves traveling though the ensemble of scatteres, Equation (3.20), as a function of the scatter-free sound speed $c_0$, the angular frequency $\omega$, and the integral over the scattering strength and size probability density of the scatterers, Equation (3.3). By dividing by frequency we get an expression for the complex sound speed of the medium $\tilde{c_{\mathrm{eff}}}$:

$$\frac{1}{\tilde{c_{\mathrm{eff}}}^2} = \frac{1}{c_0^2} + \frac{4\pi G}{\omega^2}, \tag{3.20}$$

65

$$G(\mathbf{r}) = \int g(s,\omega)n(\mathbf{r},s)\mathrm{d}s. \tag{3.21}$$

For a mono-disperse size distribution of scatterers with a number density of $n$, these simplify to:

$$\frac{1}{\tilde{c_{\text{eff}}}^2} = \frac{1}{c_0^2} + \frac{4\pi ng}{\omega^2}. \tag{3.22}$$

The scattering coefficient, $g$, can be found in both the 1946 Navy volume Physics of Sound in the Sea [75] and in Clay and Medwin's book Acoustical Oceanography [130] to be:

$$g = \frac{a}{\left(\frac{\omega_0^2}{\omega^2} - 1\right) + i\delta}. \tag{3.23}$$

Substituting this into the original integral of Equation (3.21) and then into Equation (3.20) yeilds a phase speed entirely in terms of the bubble radius, resonance frequency, and damping:

$$\frac{1}{\tilde{c_{\text{eff}}}^2} = \frac{1}{c_0^2} + \frac{4\pi}{\omega^2} \int \frac{n(r)r\mathrm{d}r}{\left(\frac{\omega_0^2}{\omega^2} - 1\right) + i\delta}. \tag{3.24}$$

### 3.3.2 The Classic Dispersion Relation for Bubbly Liquids Without Damping

A useful exercise is to first look at the sound speed and attenuation predicted if the damping term is neglected, $\delta = 0$, which leaves us with:

$$\frac{1}{\tilde{c_\text{eff}}^2} = \frac{1}{c_0^2} + \frac{4\pi}{\omega^2} \int \frac{n(r)r\mathrm{d}r}{\left(\frac{\omega_0^2}{\omega^2} - 1\right)}, \qquad (3.25)$$

which can also be found in Zabolotskaya's 1967 paper [88]. Without damping, the sound speed becomes entirely imaginary, and the limits of this region can be found to be $[\omega_0, \omega_0\sqrt{(1 + \frac{4\pi c_0^2 na}{\omega_0^2})}]$ by setting $c = 0$. This indicates a stop band where no propagation is possible. The phase speed and attenuation plots for this model can be seen in Figure 3.3. The frequency-wavenumber plots are shown in Figure 3.4 are useful because the slope of the line at any point gives the group velocity and the slope between any point and the origin gives the phase velocity. At the beginning of the stop band the phase and group velocity trend to zero, while at the end of the stop band the group velocity is zero and the phase velocity is infinite. No real material is lossless, so this behavior is a mathematical abstraction and does not occur in nature.

### 3.3.3   Complete Model for Bubbles Without a Shell

The model used in this study for bubbles without a shell is by Kerry Commander and Andrea Prosperetti [46] and provides the phase speed and attenuation through a bubbly liquid in terms of the bubble number density $n$, bubble size $a$, and material properties of the gas and fluid.

The model introduced by Commander and Prosperetti [46], hereafter refered to as the C&P model, is a synthesis of all the prior work mentioned in Section 3.1 and predicts the net phase speed and absorption from bubbly media. This is accomplished through linearization of bubble equations of motion. The final expression for the complex sound speed through the bubbly-liquid is equivalent to the classic dispersion
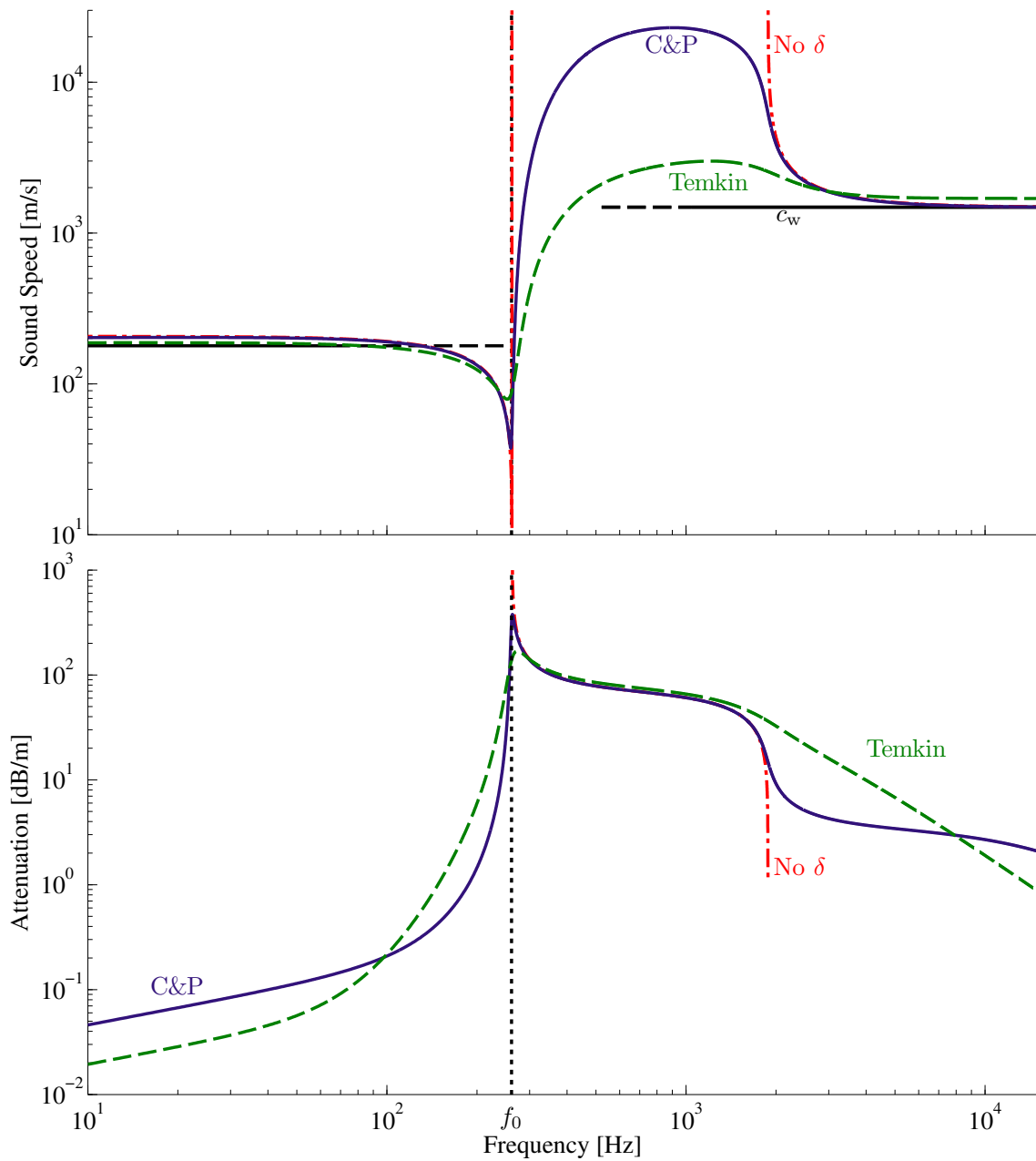
Figure 3.3: Sound speeds and attenuations for $\chi = 0.033$ and $a = 1.26$ cm for dynamic models C&P, C&P without damping (No $\delta$), and Temkin.
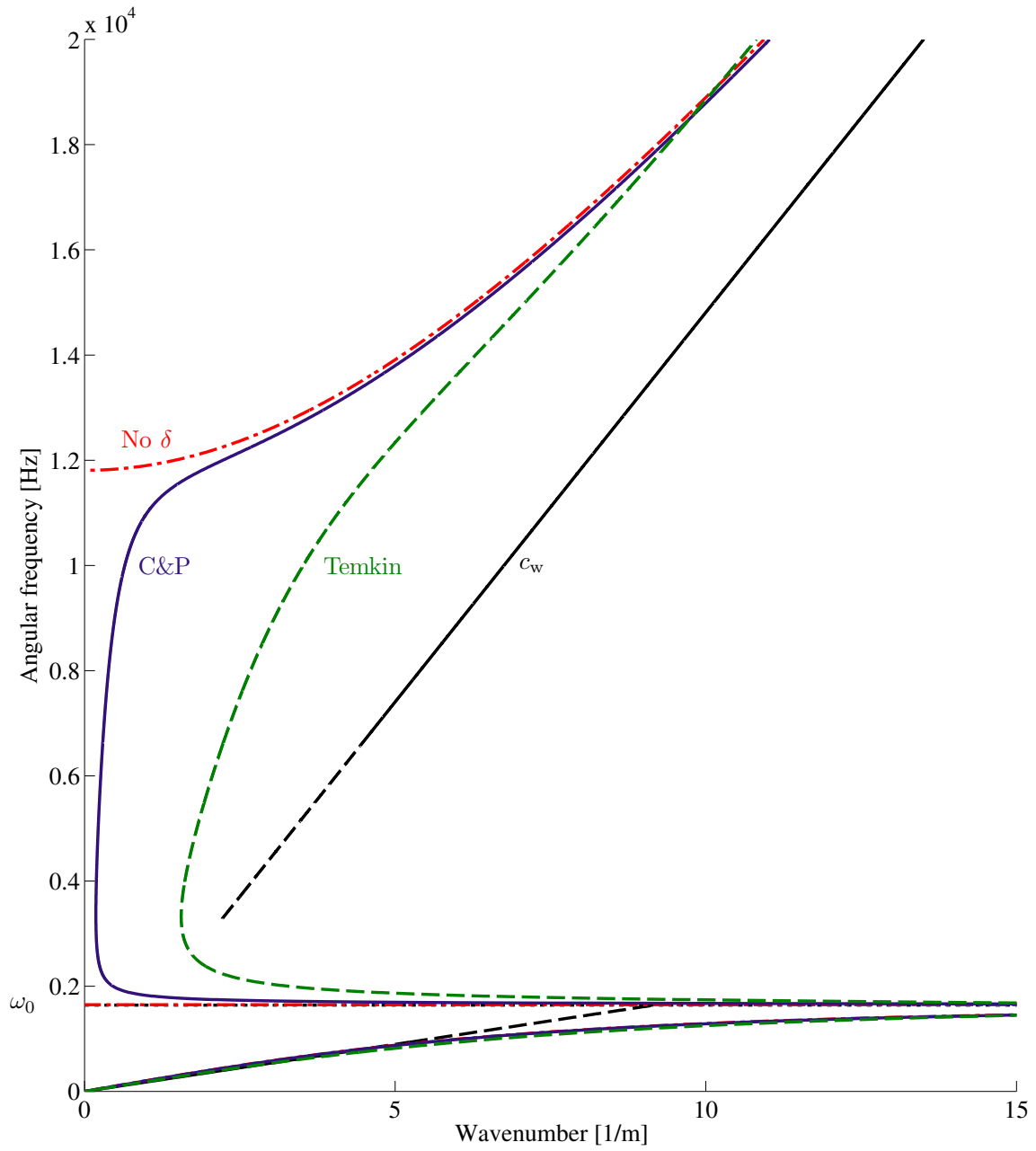
Figure 3.4: Frequency-wavenumber plots for $\chi = 0.033$ and $a = 1.26$ cm for dynamic models C&P, C&P without damping (No $\delta$), and Temkin.

relation, Equation 3.2, however uses a different definition for damping coefficient than that defined in Equation 1.5. Because of this difference in definition the complete set of equations are reproduced here using the previously specified definition for damping coefficient. Verification of some effective medium models are included in Appendix F.

The important definitions for the C&P model are for the damping coefficient $\delta$, and the resonance frequency $\omega_0$. The damping coefficient contains terms for three damping mechanisms, viscous damping, thermal damping, and acoustic re-radiation damping:

$$\delta = \underbrace{\frac{\mu_\mathrm{l}}{\rho a^2 \omega}}_{\text{viscous}} + \underbrace{\frac{4\mu_\mathrm{th}}{\rho a^2 \omega}}_{\text{thermal}} + \underbrace{\frac{a\omega}{c_0}}_{\text{acoustic}} , \tag{3.26}$$

where $c_0$ is the bubble free liquid sound speed, $\mu_\mathrm{l}$ is the viscosity of the liquid, $\rho$ is the density of the liquid, $\mu_\mathrm{th}$ is the thermal viscosity defined below. The thermal viscosity [108] $\mu_\mathrm{th}$, effective polytropic index $\gamma_\mathrm{eff}$, are both defined in terms of $\Phi$:

$$\mu_\mathrm{th} = \frac{p_\mathrm{stat}\mathfrak{I}\{\Phi\}}{4\omega}, \tag{3.27}$$

$$\gamma_\mathrm{eff} = \frac{\mathfrak{R}\{\Phi\}}{3}, \tag{3.28}$$

$$\Phi = \frac{3\gamma}{1 - 3(\gamma-1)iX[(i/X)^{1/2}\coth(i/X)^{1/2} - 1]}, \tag{3.29}$$

where $\mathfrak{I}\{\Phi\}$ and $\mathfrak{R}\{\Phi\}$ signify the imaginary and real parts of $\Phi$ respectively, and the following definitions for $X$, and the static pressure inside the bubble $p_\text{stat}$ have been used.

$$X = \frac{D}{\omega a^2}, \tag{3.30}$$

$$p_\text{stat} = p_\infty + \frac{2\sigma_\text{st}}{a}, \tag{3.31}$$

where $D$ is the thermal diffusivity of the gas inside the bubble, $P_\infty$ is what the pressure outside the bubble would be if there were no acoustic excitations, and $\sigma_\text{st}$ is the surface tension of the gas-water interface. We have now defined enough terms in order to produce an expression for the resonance frequency of the bubble $\omega_0 = 2\pi f_0$, which the reader should note is very similar to the Minneart frequency, Equation (3.1), except for the use of an effective polytropic index and compensation for the increased pressure due to surface tension at the gas-water interface:

$$\omega_0^2 = \frac{1}{a}\sqrt{\frac{3\gamma_\text{eff}p_\text{stat} - 2\sigma_\text{st}/a}{\rho}}. \tag{3.32}$$

Finally the the real phase velocity in the bubbly liquid $c_\text{ph}$ and the attenuation coefficient $\alpha$ can be calculated from the complex sound speed $\tilde{c}$ through:

$$c_\text{ph} = \left(\mathfrak{R}\left\{\frac{1}{\tilde{c}}\right\}\right)^{-1}, \tag{3.33}$$

$$\alpha = 20 \log_{10}(e)\omega \left( \Im \left\{ \frac{1}{\tilde{c}} \right\} \right)^{-1}, \qquad (3.34)$$

where $\alpha$ is in units of dB per meter.

One of the potential limitations of the C&P model is that it only includes multiple scattering within the field to first order. When scatterers are close to each other the multiple-scattering process causes a shift in the resonance frequency and the damping of the system. The field can no longer accurately be treated as an effective medium of non-interacting bubbles, but must be treated as a collective of mutually interacting scatterers[116]. The phase speed, attenuation and frequency-wavenumber plot for this model can be seen in Figure 3.3. It is worth noting that the attenuation for a broad range of frequencies above the bubble resonance frequency is almost equivalent to that provided by the no damping case. The frequency-wavenumber plot reveals a region of negative group velocity in the stop band predicted by the model without damping.

### 3.3.4 Temkin's Suspension Acoustics Model

Temkin's suspension acoustics model is a general formulation that applies for any dilute suspension of constant-mass particles that translate or pulsate in the presence of an external pressure field. It takes the quasi-static model for the compressibility of suspensions that was already discussed in Section 3.2 and adds dynamic compressibility terms for the particles' translational velocity, temperature, and pressure. It assumes that each mechanism that affects the dynamic compressibility acts independently:

$$\frac{K_s(\omega)}{K_s(0)} - 1 = \left[\frac{K_s(\omega)}{K_s(0)} - 1\right]_1 + \left[\frac{K_s(\omega)}{K_s(0)}\right]_2 + \dots \tag{3.35}$$

Upon specializing the equation (3.35) for monocromatic waves, the compressibilities are noted as being complex, $K_s(\omega) \to \tilde{K}_s(\omega)$, where the tilde is representative of a complex value. The complex compressibility can then be defined as $\tilde{K}_s(\omega) = [\rho_0 \tilde{c}_s{}^2(\omega)]^{-1}$, where $\tilde{c}_s(\omega)$ is a complex sound speed. The imaginary component of the complex sound speed is either due to attenuation or a reactive motion of the medium. This complex sound speed is better interpreted in terms of a complex wavenumber, which has the relationship:

$$\tilde{k} = \frac{\omega}{\tilde{c}_s(\omega)} = \frac{\omega}{c_s(\omega)} + i\alpha, \tag{3.36}$$

where $\alpha(\omega)$ is the amplitude-attenuation coefficient, and $c_s(\omega)$ is real and represents the phase velocity. After incorporating the complex wavenumber into the expression for complex compressibility, we arrive at equations (3.37) and (3.38).

$$\frac{c_s^2(0)}{c_s^2(\omega)} - \bar{\alpha}^2 = 1 + \mathfrak{R}\left[\frac{K_s(\omega)}{K_s(0)} - 1\right]_1 + \mathfrak{R}\left[\frac{K_s(\omega)}{K_s(0)} - 1\right]_2 + \dots \tag{3.37}$$

$$2\bar{\alpha}\frac{c_s(0)}{c_s(\omega)} = \left|\frac{\mathfrak{I}\{K_s(\omega)\}}{K_s(0)}\right|_1 + \left|\frac{\mathfrak{I}\{K_s(\omega)\}}{K_s(0)}\right|_2 + \dots \tag{3.38}$$

Temkin then focuses on two mechanisms that modify the dynamic compressibility, the translation and pulsation of the particles. These in turn can be solved for in terms of three complex and frequency dependent terms, $V$, for the ratio of the

73

particle velocity to the fluid velocity, $T$, for the ratio of the averages of temperature fluctuations in the particle to the fluid, and $\Pi$, for the ratio of the average pressure fluctuation in the particle to the fluid. Solving Equations (3.37) and (3.38) in terms of these complex ratios yeilds:

$$
\begin{aligned}
\frac{c_{sf}^2(0)}{c_s^2(\omega)} - \hat{\alpha}^2 = \frac{c_{sf}^2}{c_s^2(0)} = & \phi_v \left(1 + \frac{\phi_v}{\delta}\right) \left\{ \frac{1}{\delta}[\Re\{V\} - 1] \right. \\
& + (\gamma_f - 1) \left(\frac{\rho_{p0} c_{pp}}{\rho_{f0} c_{pf}} - \frac{\beta_p}{\beta_f}\right) [\Re\{T\} - 1] \right\} \\
& + \phi_v \left(1 + \frac{\phi_v}{\delta}\right) \left(\gamma_p N_s - (\gamma_f - 1)\frac{\beta_p}{\beta_f}\right) \\
& \times [\Re\{\Pi\} - 1],
\end{aligned} \tag{3.39}
$$

and

$$
\begin{aligned}
2\hat{a}\frac{c_{sf}^2(0)}{c_s^2(\omega)} = & \phi_v \left(1 + \frac{\phi_v}{\delta}\right) \\
& \times \left\{ \frac{1}{\delta}|\Im\{V\} - 1| \left| (\gamma_f - 1) \left(\frac{\rho_{p0} c_{pp}}{\rho_{f0} c_{pf}} - \frac{\beta_p}{\beta_f}\right) \Im\{T\} \right. \right. \\
& + \left. \left. \left(\gamma_p N_s - (\gamma_f - 1)\frac{\beta_p}{beta_f}\right) \Im\{\Pi\} \right| \right\},
\end{aligned} \tag{3.40}
$$

where $V$, $T$, and $\Pi$, are expressed in terms of constituent properties and frequency in Temkin's manuscripts[72, 73].

74

## 3.4 Multiple Scattering

There have been many proposals for corrections to the classic dispersion relation for bubbly liquids in order to account for higher-order interactions between the bubbles, also known as multiple scattering. All of corrections discussed in this section except for Kargl [119] focus on higher-order corrections to the Foldy effective medium wavenumber Equation (3.3), through a modification of the scattering coefficient for the bubble $g$, Equation (3.23).

### 3.4.1 Shielding in Bubble Clouds

Feuillade [12] re-derived the expression for the effective medium sound speed through bubbly liquids and found an additional field attenuation (or "sheilding") term that resulted in the scattering coefficient:

$$g_{(\text{Feuillade})} = \frac{a}{\left(\frac{\omega_0^2}{\omega^2} - 1\right) + i\delta - 4\pi n \int_0^\infty r e^{-i\tilde{k}_{\text{eff}}r} \mathrm{d}r}, \tag{3.41}$$

which is now dependent on the number density of bubbles $n$, and the complex effective medium wavenumber $\tilde{k}_{\text{eff}}$. The classic sound speed equation becomes implicit and needs to be solved iteratively.

### 3.4.2 Implicit Expansion of Scattering Coefficient

Henyey [118] focused on an expansion of the scattering coefficient and determined that when the next higher-order term is included, the result is:

$$g_{\text{(Henyey)}} = g + \frac{4\pi i n g \big(g_{\text{(Henyey)}}\big)^2}{\tilde{k}_{\text{eff}} + k_0},$$ (3.42)

which can be simplified to,

$$\frac{1}{g_{\text{(Henyey)}}} = \frac{1}{g} - i\big(\tilde{k}_{\text{eff}} - k_0\big),$$ (3.43)

which can then be substituted into Foldy's effective sound speed relation, Equation (3.20), to arrive at a cubic expression for the complex effective medium wave number or sound speed. Only one root of this equation will produce a valid wavenumber that possesses a positive real and complex component.

### 3.4.3 Explicit Expansion of Scattering Coefficient

Ye & Ding [117] also focused on expansions of the scattering function and arrived at a scattering function:

$$g_{\text{(Ye \& Ding)}} = g\left(1 + \frac{2\pi g^2}{k_0}\right).$$ (3.44)

This is the only formulation that results in an explicit equation for the scattering coefficient, though at high bubble concentrations this expression results in a negative phase velocity and a dip in attenuation not seen in any other model, or experiment.

### 3.4.4 Effective Medium Radiation

Kargl's [119] multiple scattering correction is based on the *a priori* assumption that since sound is radiating into the effective medium, the acoustic re-radiation damping should use the effective medium wavenumber. The adjusted damping coefficient is:

$$\delta_{(\text{Kargl})} = \underbrace{\frac{\mu_{\text{l}}}{\rho a^2 \omega}}_{\text{viscous}} + \underbrace{\frac{4\mu_{\text{th}}}{\rho a^2 \omega}}_{\text{thermal}} + \underbrace{\tilde{k}_{\text{eff}} a}_{\text{acoustic}} . \tag{3.45}$$

As with many of the other multiple scattering corrections the expression for sound speed and attenuation is not explicit and must be solved iteratively.

### 3.4.5 Comparison

The phase speeds and attenuations predicted by the various multiple scattering models are shown in Figure 3.5. The spread in values is quite wide even for a value of $\chi$ that has experimentally been shown to have minimal multiple scattering effects [44]. The frequency-wavenumber plot reveals that the EM radiation correction is very close to the phase speed without damping shown in Figure 3.3. The wide spread of the values attests to the fact that there is little consensus as to what role multiple scattering plays and when it is of consequence. The frequency-wavenumber plot of the multiple scattering models is shown in Figure 3.6. The large negative region of group velocity is visible along with the fact that the EM radiation correction displays a near infinite group velocity for a wide range of frequencies.

77
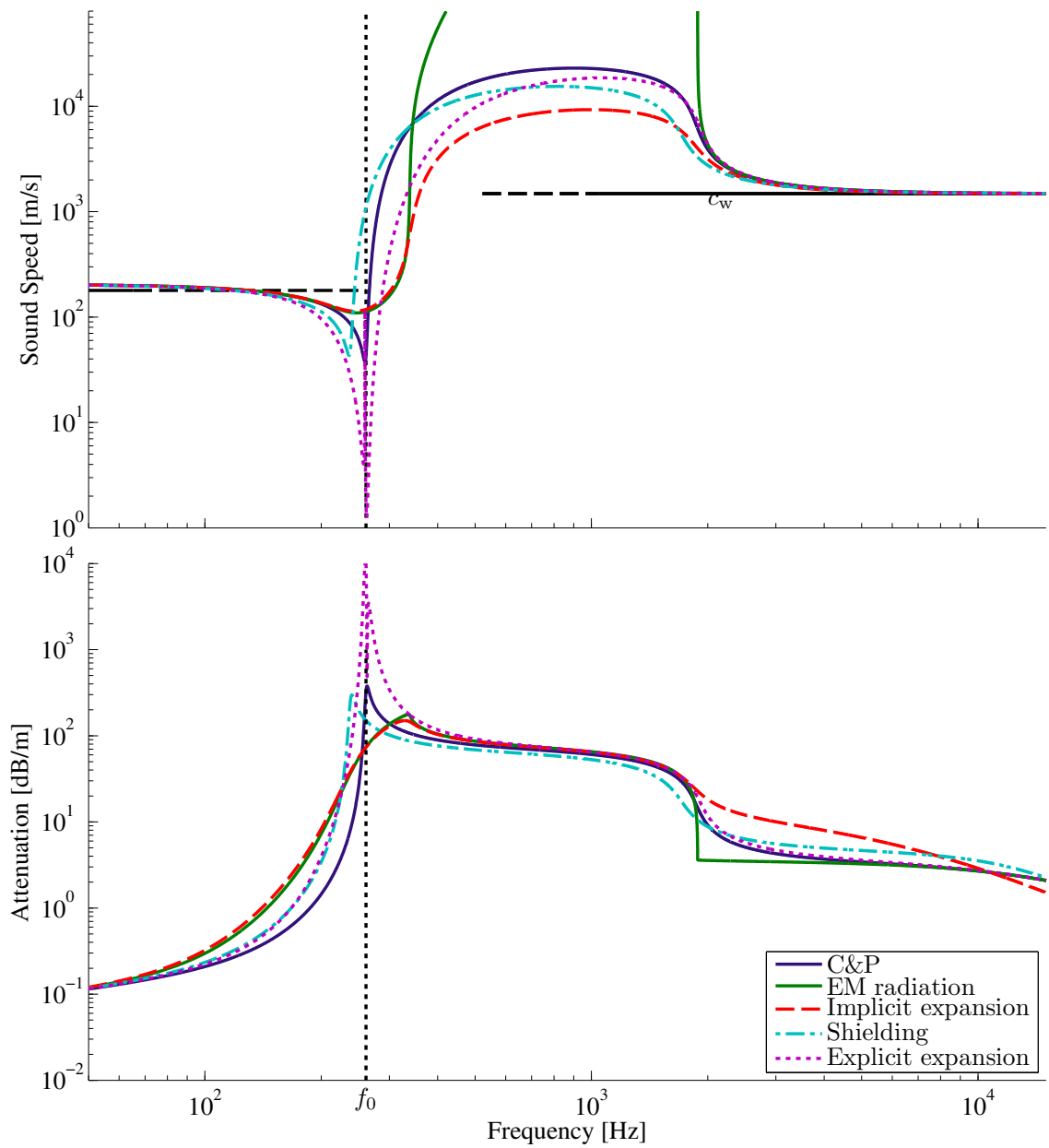
Figure 3.5: Sound speeds and attenuations for $\chi = 0.033$ and $a = 1.26$ cm for multiple scattering models.
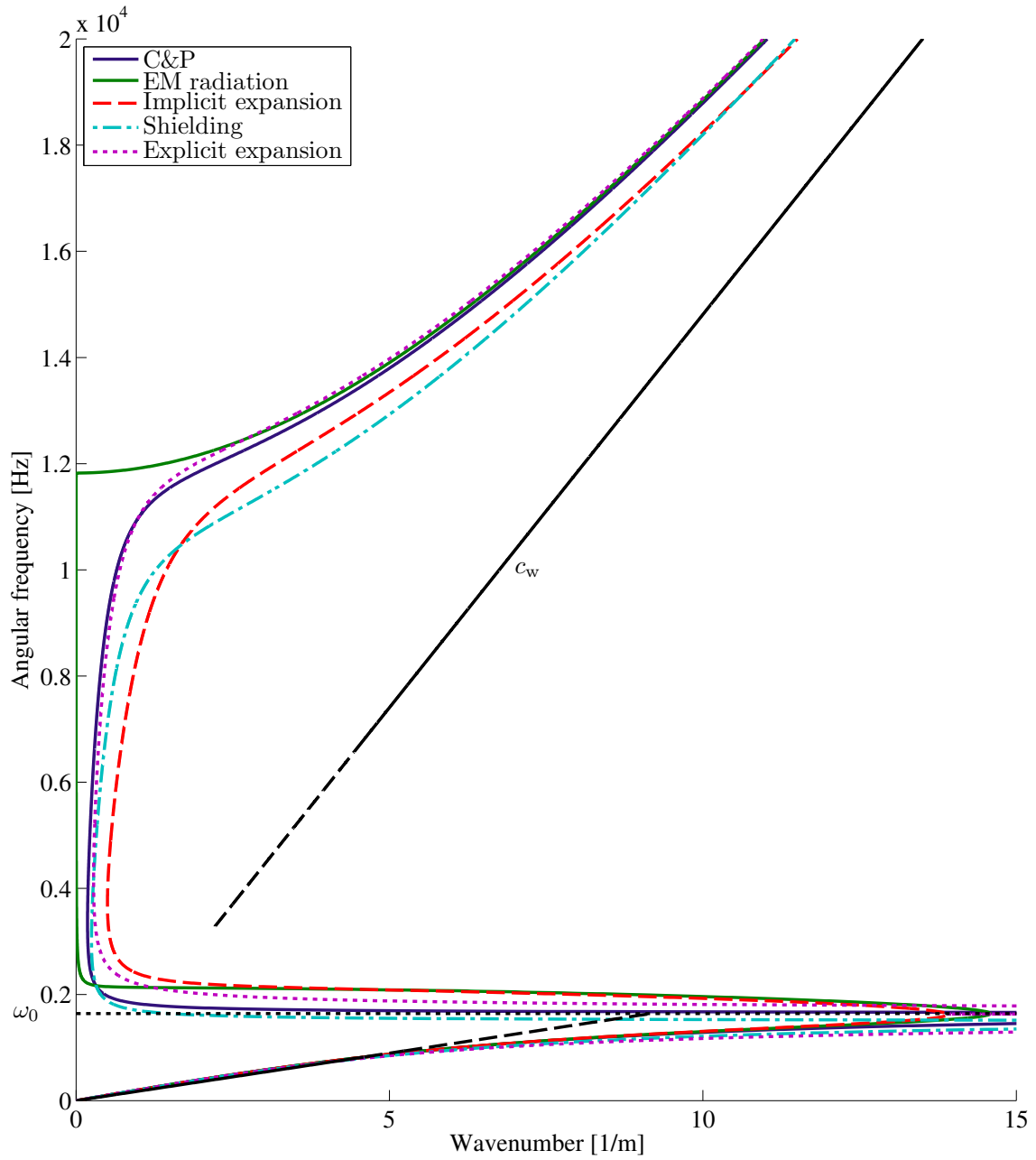
Figure 3.6: Frequency-wavenumber plots for $\chi = 0.033$ and $a = 1.26$ cm for multiple scattering models.

## 3.5  Elastic Shells

While stationary free bubbles would be an mathematically convenient model for fish, bubbles will rise due to buoyancy and larger bubbles are not stable, but will break into smaller bubbles. Since measurements with knowledge of precise bubble size and position are useful, often encapsulated bubbles are used. Unfortunately this adds an additional level of complexity to the system. This section describes the modeling that accounts for the addition of an elastic shell.

### 3.5.1  General Elasticity Relations

It can be difficult to find published values for the shear modulus $(G)$ and shear viscosity of even commonly-available shell material. The Young's modulus is defined as:

$$E = \frac{\sigma}{\epsilon},\tag{3.46}$$

where $\sigma$ is a longitudinal stress and $\epsilon$ is a longitudinal strain, and is more readily available. The Young's modulus is related to the shear modulus and Poisson's ratio $\nu$ through:

$$G = \frac{E}{2(1+\nu)} \approx \frac{E}{3}.\tag{3.47}$$

which can be simplified by assuming the shell material is incompressible $(\nu = 0.5)$.

Existing dynamic measurements for the longitudinal storage and loss modulus (effectively a dynamic and complex Young's Modulus) are expressed in the form:

$$E = E' + iE'', \tag{3.48}$$

where the real part $(E')$ is the dynamic Young's modulus and the imaginary part $(E'')$ is called the loss modulus.

If equation (3.48) is compared to the lumped element expression for the stress due to a viscosity $(\mu)$, and spherical loading is assumed, it can be seen that the stress and effective viscosity are:

$$\sigma = \mu \frac{\mathrm{d}\epsilon}{\mathrm{d}t}, \tag{3.49}$$

$$\mu = \frac{E''}{\omega}. \tag{3.50}$$

Therefore the shear modulus and shear viscosity are defined in terms of the longitudinal storage and loss modulus as shown:

$$G = \frac{E'}{3} \quad \& \quad \mu = \frac{E''}{3\omega}. \tag{3.51}$$

### 3.5.2 Church

Church [131] derived a model for the effective medium properties of a collection of encapsulated bubbles in a fluid. For the Church model, the radius of the bubble $a$ and surface tension $\sigma_{\text{st}}$, becomes the radius and surface tension of the gas-shell interface $(a_1, \sigma_{\text{st1}})$, and the shell-liquid interface $(a_2, \sigma_{\text{st2}})$ and contains three

additional parameters compared to the C&P model, the shear modulus $G_s$, viscosity $\mu_s$, and density $\rho_s$, of the shell material. The new damping coefficient has an additional term for the viscous damping due to the shell material, and the terms for the viscous damping in the liquid, the thermal damping, and acoustic re-radiation damping all contain modifications due to the presence of the shell:

$$\delta = \underbrace{\frac{4a_1\mu_l}{a_2^3\rho_s\aleph\omega}}_{\text{viscous liquid}} + \underbrace{\frac{4V_s\mu_s}{a_2^3a_1^2\rho_s\aleph\omega}}_{\text{viscous shell}} + \underbrace{\frac{4\mu_{\text{th}}}{a_1^2\aleph\omega}}_{\text{thermal}} + \underbrace{\frac{\omega a_2}{c_0(1+\omega a_2/c_0)^2}}_{\text{acoustic}}, \tag{3.52}$$

where the term $V_s$, and $\aleph$ are defined by:

$$V_s = a_2^3 - a_1^3, \tag{3.53}$$

$$\aleph = 1 + \frac{\rho - \rho_s}{\rho_s}\frac{a_1}{a_2}. \tag{3.54}$$

The resonance frequency as predicted by the Church model is:

$$\omega_0 = \frac{1}{a_1}\sqrt{\frac{3\gamma_{\text{eff}}p_{\text{stat}} - \frac{2\sigma_1}{a_1} - \frac{2\sigma_2 a_1^3}{a_2^4} + \frac{4V_sG_s}{a_2^3}\left(1 + Z\left(1 + \frac{3a_1^3}{a_2^3}\right)\right)}{\rho\aleph}}, \tag{3.55}$$

where

$$Z = \frac{a_2^3}{4V_sG_s}\left(\frac{2\sigma_1}{a_1} + \frac{2\sigma_2}{a_2}\right). \tag{3.56}$$

82

### 3.5.3 Church-Kargl

The Church-Kargl model simply applies the assumption that the effective medium wavenumber should be used for the acoustic re-radiation damping to the Church model, resulting in a damping coefficient of:

$$\delta = \underbrace{\frac{4a_1\mu_l}{a_2^3\rho_s\aleph\omega}}_{\text{viscous liquid}} + \underbrace{\frac{4V_s\mu_s}{a_2^3a_1^2\rho_s\aleph\omega}}_{\text{viscous shell}} + \underbrace{\frac{4\mu_{\text{th}}}{a_1^2\aleph\omega}}_{\text{thermal}} + \underbrace{\frac{\tilde{k}_{\text{eff}}a_2}{(1+\tilde{k}_{\text{eff}}a_2)^2}}_{\text{acoustic}}. \tag{3.57}$$

## 3.6 How Many Scatterers are Necessary in Order to Have an Effective Medium?

Relatively little has been published on exactly how many scatterers are required for effective medium theory (EMT) to be valid. In order to have a quantitative metric we will define the mean free paths per wavelength as:

$$\Upsilon = \lambda n^{1/3}, \tag{3.58}$$

where $\lambda$ is the wavelength, and $n$ is the number density of scatterers. The assumptions of EMT are very similar to continuum mechanics, where it is generally assumed that distances are large compared with the distance between molecules. The EMT analogy would be that wavelengths are large compared to the distance between scatterers. The experimental evidence presented later in this document, however seems to indicate that materials can act as effective media at wavelengths that are as small as twice the distance between scatterers. One reason for this could be that sound

speeds are generally reduced in bubbly liquids, and while the physical wavelength measured may be small compared to a wavelength, the wavelengths of the scatterer-free liquid would be much larger.

# Chapter 4

# Balloons and the Effect of Elastic Shells on Bubbles

## 4.1 Motivation

This chapter is dedicated to determining whether effective medium theory can be applied to clouds of elastic shelled bubbles. While typically fish are viewed as bubbles with a viscous shell and the elasticity of the fish flesh is generally considered negligible, balloons serve as a very stable proxy for fish. Balloons provide stable bubbles of almost any size and configuration, which allows much more latitude for experimental study than using live fish or bubbles without a shell. The last chapter ended with reviews of the Church [131] and Church-Kargl [119, 54] models, which will be utilized in this chapter.

The first experimental study in this chapter involved resonator measurements with precise knowledge of balloon shell thickness and volume. The pressure field in the resonator in the presence of the balloons was recorded and the resonances were used to extract phase speeds as described in Section 2.3. The system was then modeled using effective medium theory, and compared to the experimental results. After determining the wall thickness of the inflated balloon the only remaining sensitive parameter was the shear modulus, $G_s$ of the balloon rubber. The shear modulus was

used as a fitting parameter to determine consistence between the models, and which model can fit the data best.

The second experimental study was aimed at determining the validity of using effective medium theory to predict attenuation through bubble clouds. Arrays of balloons were lowered into at ARL's Lake Travis Test Facility (LTTS), a source was placed in the middle of the cloud, and the acoustic transfer function was recorded at several locations away from the balloon array. Comparing the pressure power spectra with and without the balloon array present allowed the computation of insertion loss, IL, which was compared to the predictions of several analytical models, including effective medium theory.

## 4.2 One-Dimensional Waveguide Resonator Measurements of Balloons

### 4.2.1 Experimental Apparatus

A 1.98-m-long aluminum pipe was oriented vertically to create the 1-D resonator. The bottom of the tube was capped with a latex membrane and a block of closed-cell foam was used to approximate a pressure release condition and support the pipe. The inner radius was 0.1015 m and the outer radius was 0.1085 m. A Labworks ET-216HF shaker attached to a 3.81-cm-diameter piston was used to excite the tube. The shaker rested on a layer of closed-cell foam which in turn rested on the top rim of the aluminum pipe. A Reson TC4013 hydrophone was held in place by a water-filled stainless steel sheath connected to a scanning apparatus. This scanning apparatus allowed the hydrophone to be scanned along the length of the tube in

86

order to map the modes. A schematic of the apparatus is presented in Figure 2.9 and a table of the material properties of the waveguide used in the analysis are in Table 2.1 and Appendix G.

### 4.2.2  Additional Experimental Details

Balloons of various radii $a$, and wall thicknesses $t$, were tested. Table 4.1 lists the different cases. For each day of measurement the temperature $T$ was recorded for the resonator and the water sound speed was calculated using the standard formulation by Chen and Miller [132] which is also shown Table 4.1. The thicknesses of the balloon walls were determined by two methods. The first method involved using a specific gravity flask to determine both the volume and the density of the shell material, which was then assumed to be uniformly distributed around a sphere. The second method involved drawing a circle on the inflated balloons, measuring the diameter, then measuring the area of the circle and thickness of the material when the balloon was deflated. The area of the circle when the balloon was inflated, $A_\mathrm{r}$, can be found using Equation (4.1) whereas the area of the circle when the balloon was deflated, $A_0$, was determined by flattening the circle and measuring the diameter.

$$A_\mathrm{r} = 2\pi r\big(r - \sqrt{r^2 - a_\mathrm{c}^2}\,\big), \tag{4.1}$$

where $r$ is the radius of the balloon, $a_\mathrm{c}$ is the radius of the circle on the balloon's surface. The reference thickness for the inflated balloon, $t_\mathrm{r}$, can be determined from these measurements using [133]:

Table 4.1: Experimental conditions

| test case | $a$ [cm] | $t$ [cm] | $N$ | $T$ [°C] | $c_0$ [m/s] |
|:---:|:---:|:---:|:---:|:---:|:---:|
| 0 | - | - | 0 | 27.2 | 1502.6 |
| 1 | 1.26 | 0.018 | 6 | 27.2 | 1502.6 |
| 2 | 1.26 | 0.018 | 24 | 27.2 | 1502.6 |
| 3 | 2.0 | 0.016 | 6 | 30.4 | 1510.2 |
| 4 | 2.0 | 0.008 | 6 | 30.4 | 1510.2 |
| 5 | 3.0 | 0.0036 | 6 | 21.9 | 1488.2 |
| 6 | 3.0 | 0.0018 | 6 | 21.9 | 1488.2 |

$$t_{\mathrm{r}} = t_0 \frac{A_0}{A_{\mathrm{r}}}. \tag{4.2}$$

The water in the tube was degassed before taking measurements, either through applying a vacuum to the resonator, or heating and then cooling the apparatus. Then balloons were tethered with a monofilament line, evenly spaced, anchored to the bottom of the tube with a pulley mechanism, and allowed to sit in the degassed water until the acoustic measurements appeared to be clear of the influence of tiny bubbles. A periodic chirp signal from 1 to 2000 Hz was sent to the shaker device eight times for each position and the response was recorded by the hydrophone. The hydrophone was scanned from above the free surface at the top of the tube to the bottom of the tube using a stepper motor with 102 measurements evenly spaced 1.91 cm apart. After the data was acquired, the ensemble average of the power spectral density was calculated from seven chirps at each location. The data acquisition used here is the same as described in Section 2.8.2.

### 4.2.3 Results

Both of the propagation models shown here require three additional parameters compared to models for a shell-less bubbly liquid; these are the thickness, $t$, the shear viscosity of the shell, $\mu_\mathrm{s}$, and the shear modulus of the shell $G_\mathrm{s}$. The thickness was determined using the area ratio method above. The shear viscosity has little effect on the results in the range of interest and was assumed to be 5 Pa·s and the rubber density was measured by means of a specific gravity flask to be 930 kg/m³. The shear modulus for natural latex rubber can range anywhere from 1.5 to 4.8 MPa in the frequency range studied [134], and likely varies much more than that. The shear modulus is also nonlinearly dependent on static tension, so the modulus changes as the balloon is inflated. The effect that this uncertainty (1.5 to 4.8 MPa) can have on the predictions of the Church and the Church-Kargl models is shown in Figure 4.1. The prediction of the Commander & Prosperetti model [46] for shell-free bubbles is included to illustrate the effect of the shell.

Figure 4.2 shows the depth-averaged spectra, the resulting measured phase speed, and the predictions of three models for sound propagation through bubbly liquids. For the the two elastic shell models, $G_\mathrm{s}$ was determined by a least-mean-square fit between all the phase speed measurements below the bubble resonance and the model predictions. The least mean square error, $\langle R^2 \rangle$, is indicated in each figure along with the shear modulus, $G_\mathrm{s}$. For the phase speeds below and near the bubble resonance the mean square error indicated that use of the Church-Kargl model leads to a better fit for 5 of the 6 experimental cases. These measurements were conducted in the Aluminum resonator and all of the physical properties utilized
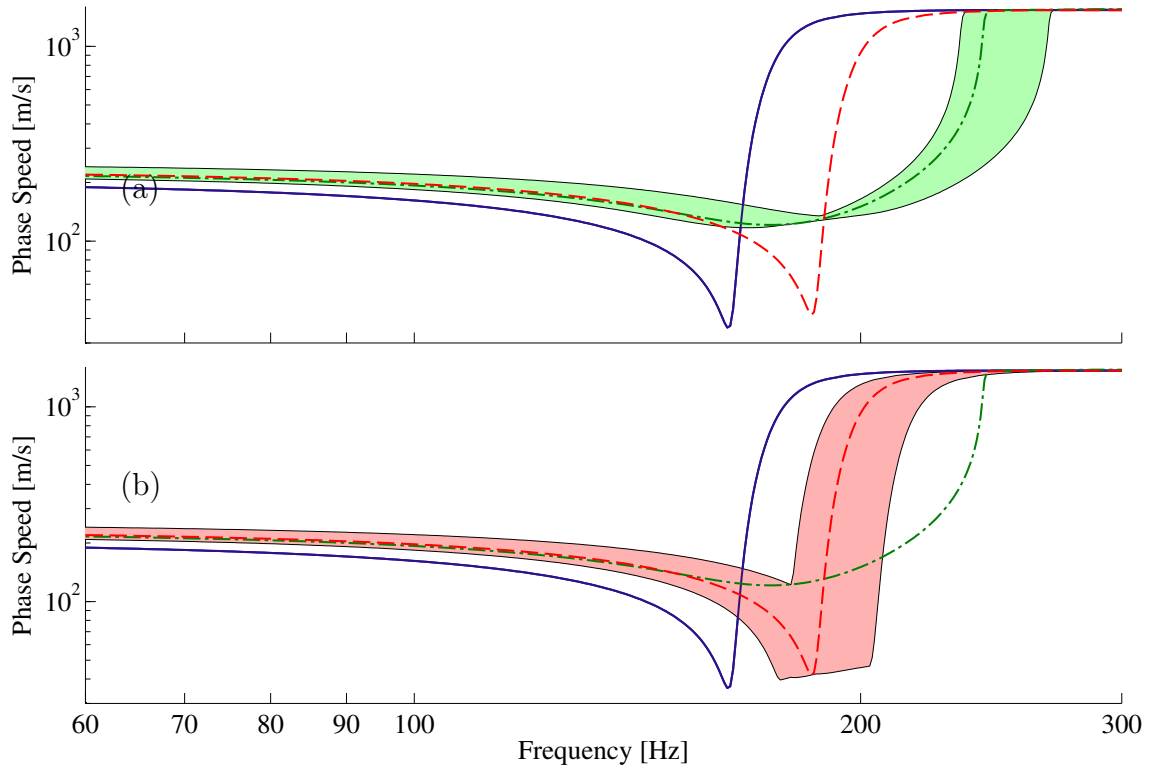
Figure 4.1: Uncertainty due to imprecise knowledge of the shear modulus shown using case 4. The range of values for phase speed produced by the Church-Kargl model (a), and by the Church model (b). Models of Commander & Prosperetti (——), Church (– – –), and Church-Kargl (– · –), in all cases modified to include the elastic waveguide effect.

in this experiment (unless otherwise noted) are listed in Appendix G.

The effect of the non-ideal bottom boundary condition is visible in Figure 4.4. For both Figure 4.3 and 4.4 an additional mode is present which appears to be approximately a quarter wavelength. This mode can not be used to determine a phase speed however, since there is no zero available to correct the mode number.
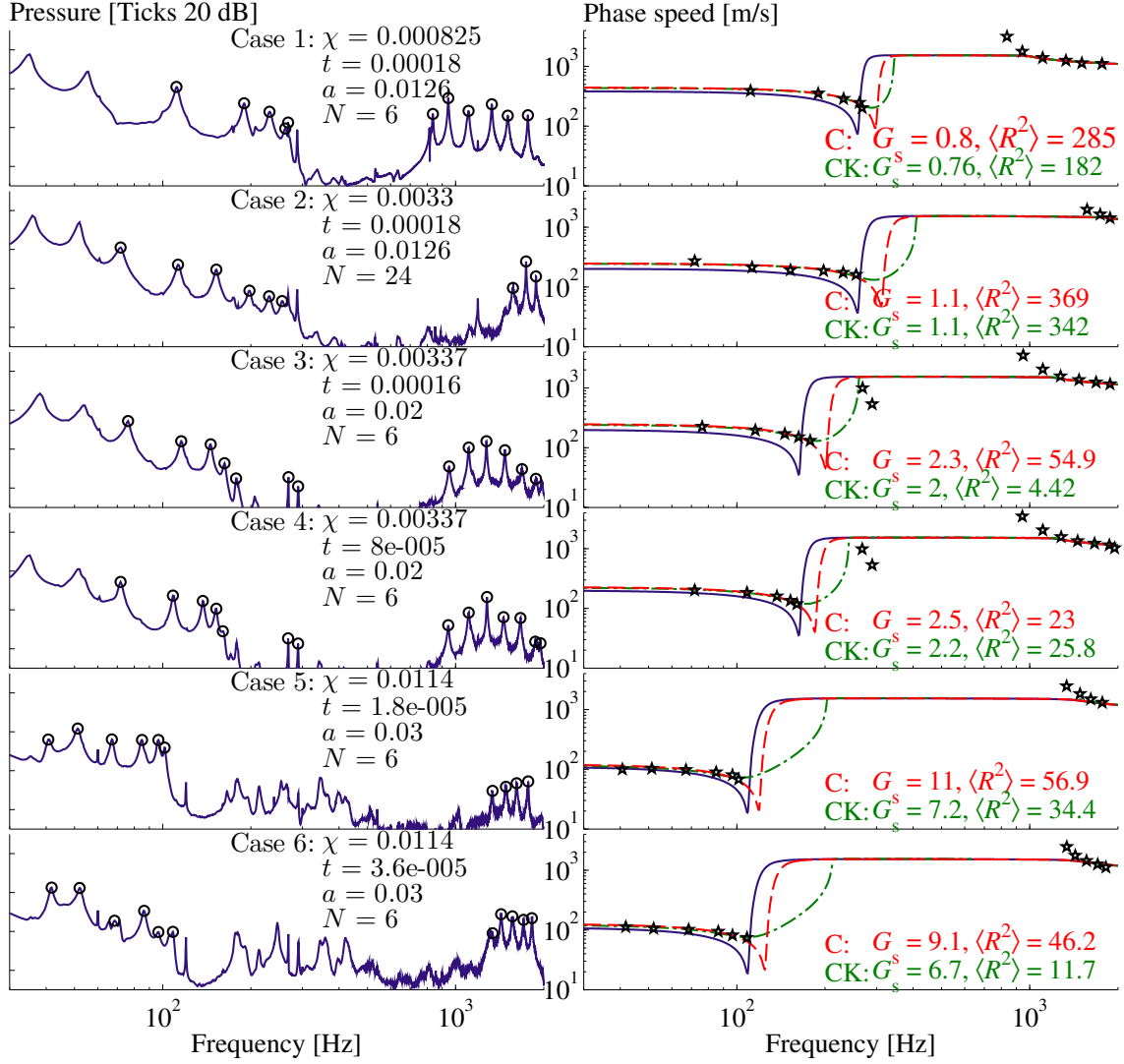
Figure 4.2: Spectra (left column) and resulting measured phase speeds (right column). The circles on the spectra indicate the peaks used to calculate phase speeds, which are shown with the symbol ☆. Models Shown are Commander & Prosperetti (——), Church (---), and Church-Kargl (-·-). Also included are the shear modulus $G_s$, and mean square error $\langle R^2 \rangle$, for the Church, C, and Church-Kargl, CK, models.
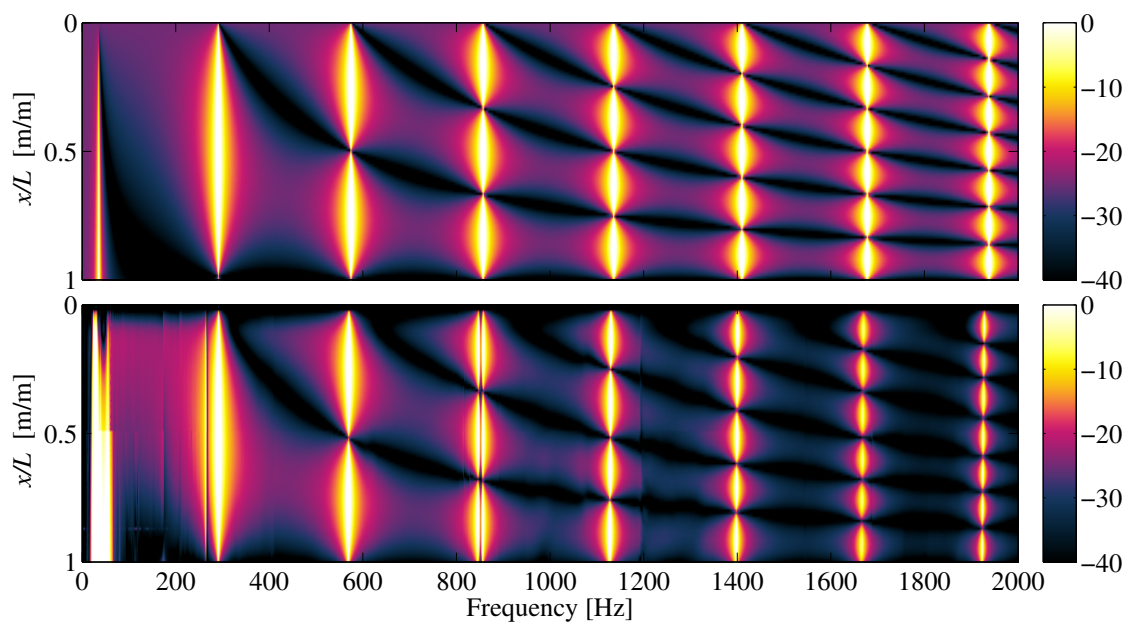
Figure 4.3: Analytical model (top) and experimental data (bottom) of case 0 using the C&P model. Amplitude colorbars are on a dB scale.
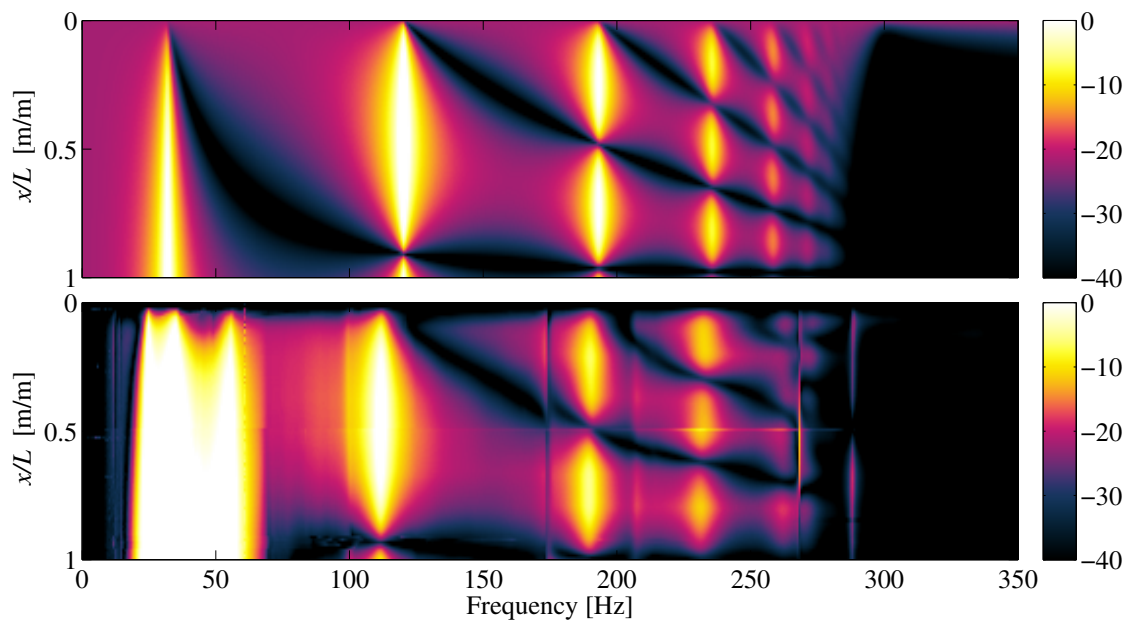
Figure 4.4: Analytical model (top) and experimental data (bottom) of case 1 using the Church model and the optimal fit wall shear elasticity. Amplitude colorbars are on a dB scale.

## 4.3   Lake Tests of Attenuation Through Bubble Clouds

### 4.3.1   Experimental Apparatus

A series of experiments were conducted at Lake Travis to measure the attenuation of sound through a cloud of balloons, to determine the amount of insertion loss due to placing the bubble cloud around a source, and provide base measurements to compare with effective medium theory. A steel unistrut cage 1.22 meters wide, and 1.30 meters long and deep was fitted with a nylon netting grid to allow balloons to be attached and is shown in Figure 4.5. The source was a Navy J-13, which is a moving coil loudspeaker designed to operate between 30 and 3000 Hz at depths up to 20 meters. During all tests the source was located at a depth of 1.11 m from the surface, which was also coincident with the center of the cage that held the bubble cloud. The directivity of the J-13 is approximately omnidirectional, within 5 dB up to 2500 Hz. Measurements of the acoustic pressure in the water column were recorded at 2 meter intervals of depth from 2 meters to 18 meters, at a horizontal distance of 11.7 meters from the center of the bubble cloud. Linear chirps from 30 Hz to 2 kHz produced by the J-13 were recorded by HTI-90-U hydrophones. The source signal output and data capture were performed by a DT9837B Data Translation [135] unit. The water depth at the source position was 19.6 m and the depth at the receiver position was 19.1 m. For the lake test all signal generation and data acquisition was performed by a DT9837B data translation transfer function unit. Each bubble cloud consisted of 14 Qualatex [136] balloons inflated to a radius of 4.68 cm at the surface. Three balloon configurations were used and the locations of the balloons were recorded, the arrangements of which are shown in Figure 4.6 and the exact balloon positions

95

Figure 4.5: Photo of unistrut cage and nylon netting used to attach balloons.

are noted in Appendix G. Using the dimensions of the cage as the total volume, the volume fraction of air at the depth of 1.11 meters was 0.26%.

The three configurations shown in Figure 4.6 will be referenced as Random, Quasi-Face Centered Cubic (Quasi-FCC), and Dense. This is because the Random configuration is the most evenly spread out configuration, Quasi-FCC is very close to being Face Centered Cubic, and the dense configuration is biased toward having more balloons toward the center.

The magnitude of the depth averaged frequency response function (FRF) is shown in Figure 4.7 along with the FRF for each configuration, the reference level,
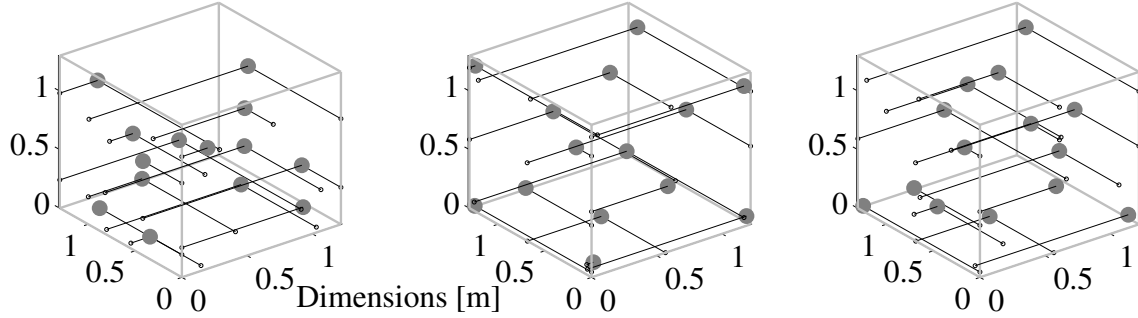
Figure 4.6: Positions of balloons for the three configurations discussed. The names of the configurations as referenced in the text are, Random, Quasi-FCC, and Dense, from left to right respectively.

and the background noise at each receiver position. The calculations for the FRF as the cross-spectral density of the hydrophone and source divided by the power spectral density of the source is discussed in Appendix A. One interesting observation is that the deeper receiver positions for cases with balloons present show higher amplitudes than the receiver positions near the surface around 60 Hz.

### 4.3.2 Analysis

At each depth, the insertion loss, IL, was calculated by computing the ratio of the FRFs before and after the balloons were put in place, and then the result was depth averaged and converted to dB. This calculation is shown in equation:

$$\text{IL} = 10 \log_{10} \frac{1}{9} \sum_{m=1}^{9} \frac{H_{\text{ref}}(f)}{H_{\text{bubs, m}}(f)}, \tag{4.3}$$

where $H_{\text{ref}}(f)$ is the FRF without balloons in the water and $H_{\text{bubs, m}}(f)$ is FRF at

97
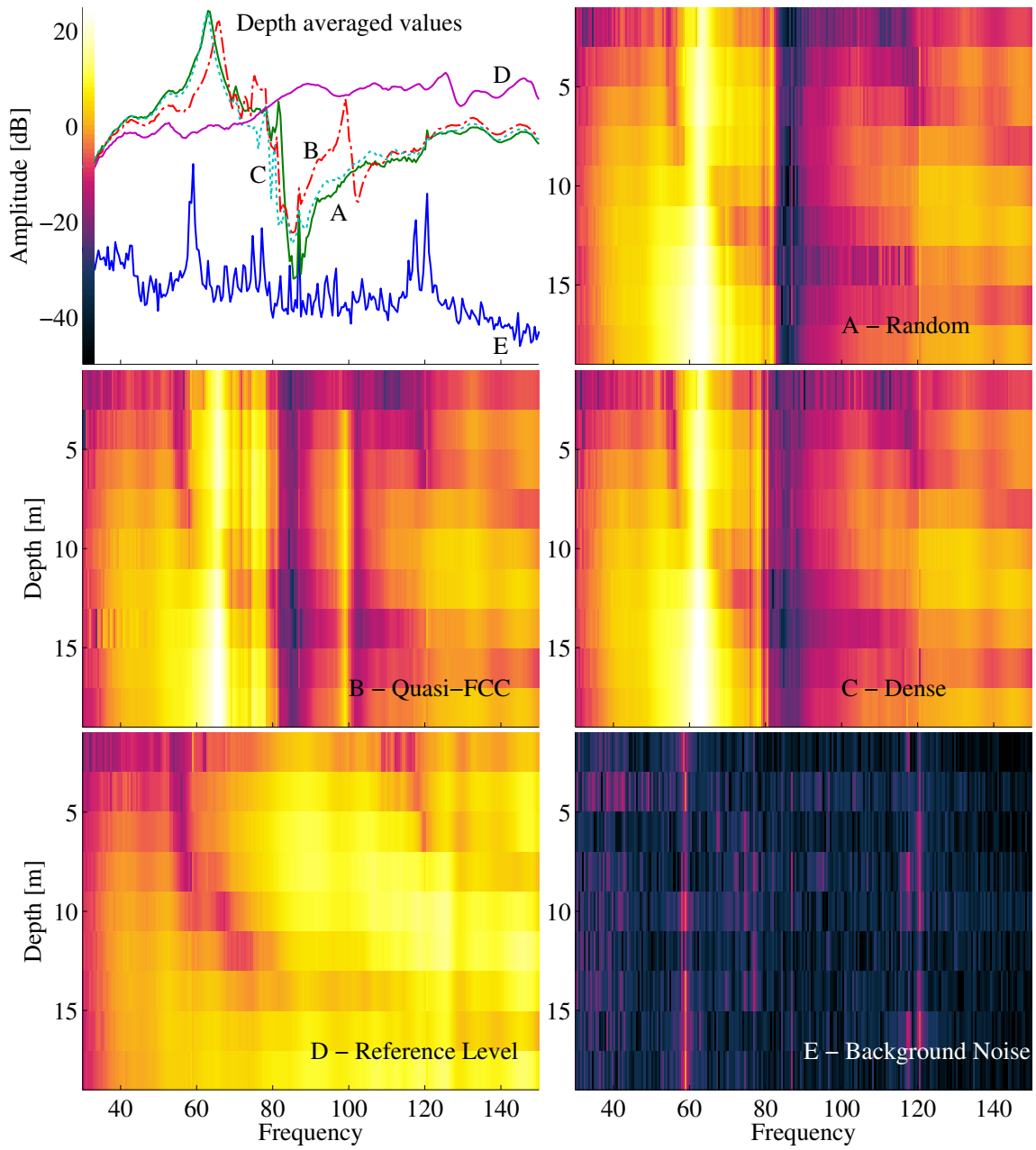
Figure 4.7: Depth averaged FRFs and the FRF at each array element (color maps A, B, C, D) and background noise E.

the $m^{\text{th}}$ depth at a total of nine depths. Using the known balloon radius at the surface, the hydrostatic pressure on the balloons and the depth adjusted radius were calculated for the mean depth of the bubble cloud, Eq. (1.8). Using these parameters three analytical tools were used to generate predictions of the depth-averaged IL, for comparison with the measurements. The first and more computationally intensive tool involved solving the coupled system of differential equations for the scattered field of the bubbles. This solution will be referred to as the full-scattering solution (FS) and is discussed in Appendix D. The second tool involves utilizing the attenuation per meter predicted by the Church model and multiplying it by the distance the acoustic wave travels through the bubble cloud from the source to the receiver, and is referred to as effective-medium theory (EMT). The EMT relations for free bubbles and bubbles with shells are described in detail in Sections 3.3.3 and 3.5.2 respectively. The third tool is to couple EMT with an analytical model for the acoustic reflections within the bubble cloud and is referred to as reflection EMT or REMT.

In order to derive the REMT solution, the bubble cloud was assumed to be represented by a sphere of the same volume, volume fraction of air, and mean bubble radius as the experimental configurations, with radius $r_{\text{cloud}}$. At the center of the effective medium sphere is another small sphere which will be defined to have a velocity source condition, namely the radial component of velocity at the source radius $r_{\text{source}}$ will be $u^{(r)}(t; r_{\text{source}}) = u_0 e^{j(\omega t)}$. All propagation is assumed to be spherical, inward and outward traveling waves are assumed in the interior of the sphere, and a transmitted outgoing traveling wave is present outside the bubble cloud with the properties of clear water. This system of equations is then solved for the

99

amplitude of the transmitted wave as a function of frequency. IL was then calculated in the same manner as it was for the experimental data. The derivation of this model is discussed in Appendix E.

### 4.3.3 Results

The measured IL can be seen in Figure 4.8. There are several noteworthy features of the data set. First, it is important to note that although the maximum measured IL was about 30 dB, in reality, the transmitted signal was lost in the noise floor, this means that the maximum IL might actually be higher. In other words, the maximum attenuation achieved by the bubble cloud may have reduced the transmit signal to a level below the noise floor, hence obscuring the maximum amount of insertion loss. The resonance frequency of the balloons tested should be around 76 Hz, according to a prediction based on the shell free bubble of equivalent volume. Below this frequency there is a significant negative peak, or amplification, in the IL. This amplification is believed to be due to acoustic reflections within the bubble cloud.

The model predictions can be seen in Figure 4.9. The sub-resonant amplification is predicted by the full-scattering model, however the amplitude is lower than in the experimental results. The maximum level of IL is within 1 dB for the Random case, however in the other two cases the IL is approximately 13 dB greater in the full-scattering model. This difference could be due to the noise floor issue previously discussed, but is significantly less than the difference between the experimental measurements and the Church model, which over predicts the measurements by as much

100
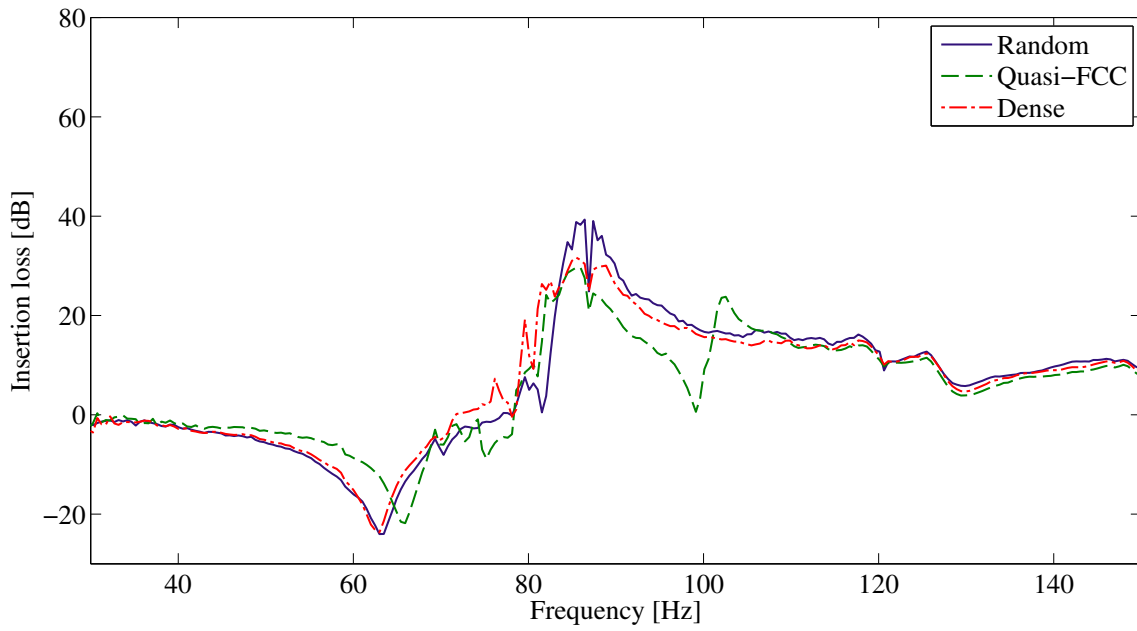
Figure 4.8: Experimental insertion loss for the three balloon configurations.
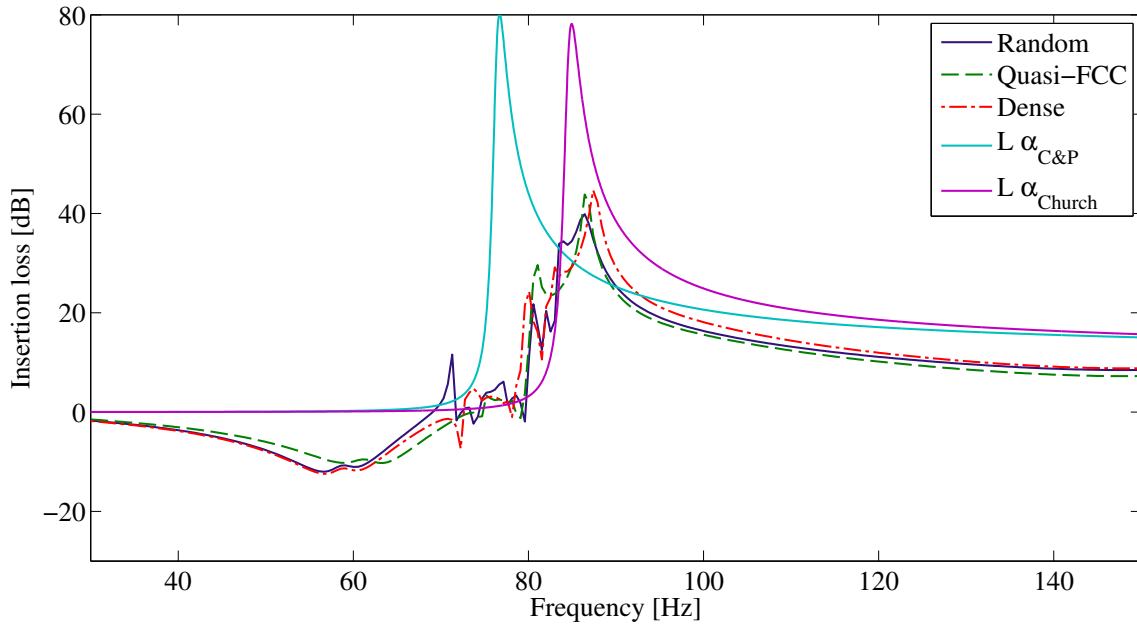


Figure 4.9: Analytical insertion loss for the three balloon configurations.

101

as 48 dB.

Figure 4.10 compares each experimental configuration with each analytical tool. FS stands for the full scattering model, which is the most computationally intensive and requires knowledge of the bubble geometry, but best captures the IL profile. EMT is the loss predicted by effective medium theory over the effective radius of the bubble cloud, this method captures the location of the IL peak, but does not predict and sub-resonant amplification. REMT accounts for reverberation within the bubble cloud and actually comes closer to predicting the amplification peak than the full scattering theory, however difference from the full-scattering theory prediction is partly due to the fact that both EMT and REMT assume a spherical bubble cloud.

## 4.4  Summary and Conclusions

This chapter involved the comparison of experiments involving sound propagation though balloons with effective medium theory. Church and Church-Kargl were compared measured pressure power spectra in a 1D aluminum resonator. The shear modulus was used as a fitting parameter for both models. The Church-Kargl generally provided a better fit and achieved an optimal fit an lower values of shear modulus.

Measurements of sound propagation through balloons was conducted at Lake Travis. Full-scattering modeling matched the experimental insertion loss extremely well, however using an effective medium model which took into account the acoustic reflections within the bubble cloud also provided reasonable agreement and predicted the amplification region observed at frequencies lower than the individual balloon

102
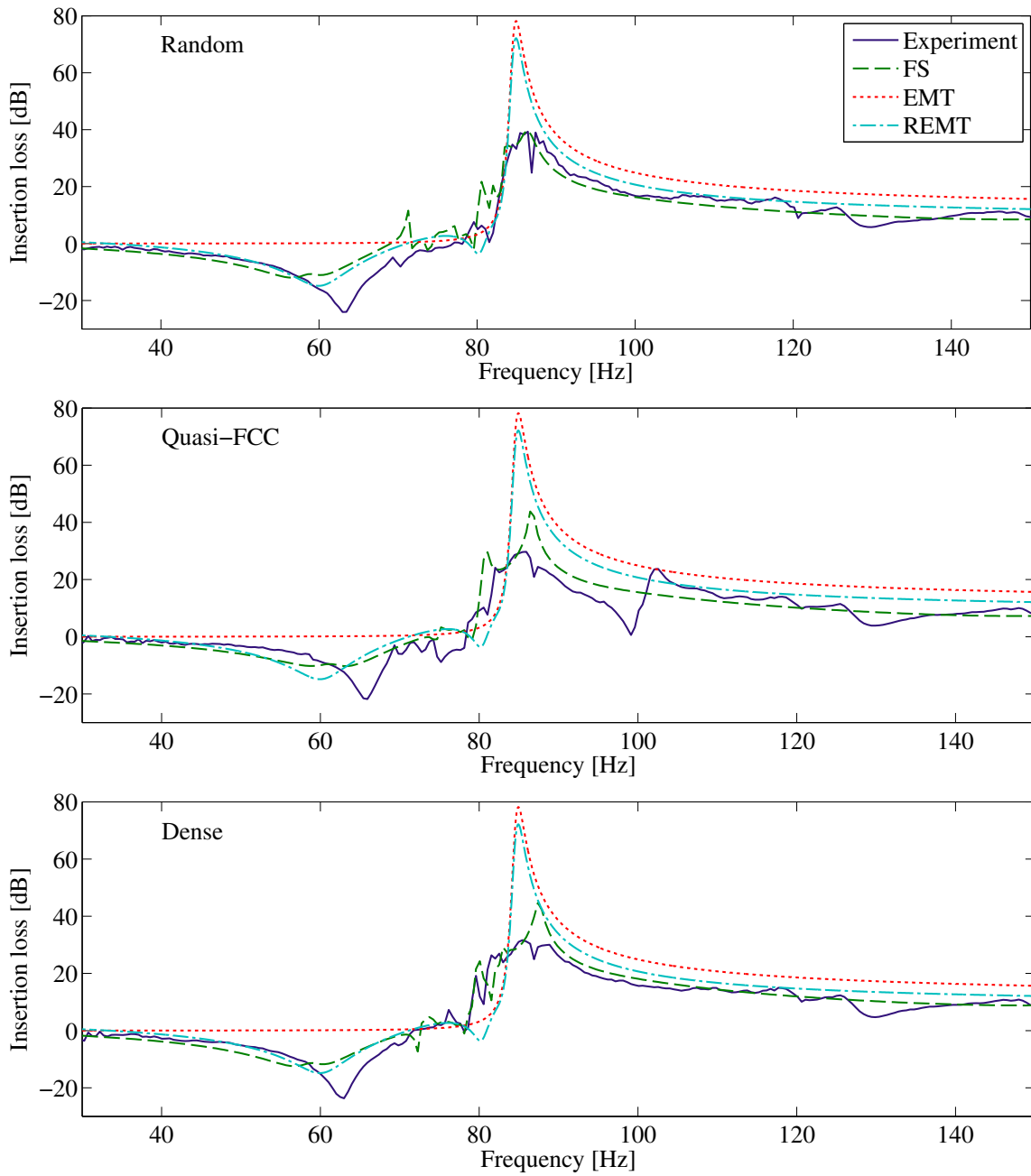
Figure 4.10: Comparison of the model predictions to the experimental measurements for all three balloon configurations.

resonance.

An important observation from both experiments is that the effective medium theories universally over-predict the attenuation above the individual bubble resonance frequency with respect to the experimental measurements.

# Chapter 5

# Scattering from an Effective Medium

## 5.1 Introduction

As useful as effective medium theories are to transform a system with many degrees of freedom into one with far fewer parameters, another leap needs to be made in order to make this information useful. In the ocean it is rare to directly observe phase speed and attenuation tests though an object. It is far more common to observe the scattering from an object. Thus in order to be ultimately useful, effective medium theory has to be applied in such a way to produce a useful prediction of the characteristic scattering from a target. In this chapter we will take the typical approach from underwater acoustics of indicating the scattering amplitude, SA, from an object in terms of its angle-dependent differential scattering cross-section, $\sigma(\theta, \phi)$ defined by:

$$\text{SA}(\theta, \phi) = 10 \log_{10} \left[\sigma(\theta, \phi)\right], \tag{5.1}$$

$$\sigma = \frac{r^2 I_{\text{scat}}(r, \theta, \phi) 10^{\alpha r/10}}{I_{\text{inc}}}, \tag{5.2}$$

where $r$ is the distance from the scatterer to the receiver, $I_{\text{scat}}(r, \theta, \phi)$ is the intensity of the scattered signal at the receiver, the term $10^{\alpha r/10}$ accounts for attenuation

between the scatterer and receiver, and $I_{\text{inc}}$ is the intensity incident on the scatterer. $\sigma(\theta, \phi)$ has units of m² and is equivalent to the backscattering cross-section when $\theta$ and $\phi$ are $\pi$ and 0, respectively [17], at that $\theta = \pi$ SA is equivalent to the target strength, TS.

## 5.2 Scattering from a Single Bubble

The differential scattering cross-section for an air bubble is:

$$\sigma = |g|^2 = \left| \frac{a}{\left(\frac{\omega_0^2}{\omega^2} - 1\right) + i\delta} \right|^2 , \tag{5.3}$$

where the scattering coefficient for an air bubble given by Eq. (3.23) is used.

For free bubbles the expressions for resonance frequency, $\omega_0$, and damping, $\delta$, are taken from Commander and Prosperetti [46], and for encapsulated bubbles the scattering coefficient and associated terms from the Church model [131] are used, see Section 3.5.2.

## 5.3 Scattering from a Fluid Sphere

The functional model for scattering from a fluid sphere is derived in Anderson's classic 1950 paper on the subject [137]. The boundary conditions on the sphere's surface are matched to a plane wave incident field in terms of spherical harmonics. The solution in terms of a complex, angle dependent, scattering coefficient after applying a large $kr$ approximation for the Hankel function (In order to eliminate distance dependence) is:

$$g_{\text{anderson}}(\theta) = \frac{p_{\text{scat}}(r,\theta)re^{-i(\omega t - kr)}}{p_{\text{incident}}} = \frac{i}{k}\sum_{m=0}^{\infty} P_m(\cos(\theta))(2m+1)D_m, \qquad (5.4)$$

where $P_m(\cos(\theta))$ are the Legendre polynomials and $D_m$ contains spherical Bessel functions $j_m$, spherical Hankel functions $h_m$, and their derivatives $j'_m$, $h'_m$, and is:

$$D_m = \frac{j'_m(k_1 a)j_m(ka) - ghj_m(k_1 a)j'_m(ka)}{j'_m(k_1 a)h_m(ka) - hgj_m(k_1 a)h'_m(k1)}, \qquad (5.5)$$

where $g = \rho_1/\rho$, $h = c_1/c$, $k_1 = k/h$, the subscript 1 indicates properties of the sphere and absence of subscript refers to properties of the fluid surrounding the sphere.

## 5.4 Comparison of Scattering from an Effective Medium and Bubble Cloud

In this section two of the analysis techniques previously discussed in Section 4.3.2 will be employed for various bubble distributions. The first will be the FS model (discussed in Appendix D) for free bubbles and the second will be a combination of the C&P effective medium model and Anderson's scattering model, and will be referred to as FS and A-EM respectively. Figure 5.1 compares the geometry of these two models. In the FS model a random distribution of bubbles with a given bubble size distribution and volume fraction of air is chosen. That same bubble size distribution and volume fraction is used to calculate the effective medium sound speed from the Commander and Prosperetti model [46], which is then used as the fluid sphere's properties in Anderson's model.

(a) Sphere of randomly located scatterers          (b) Sphere of effective medium
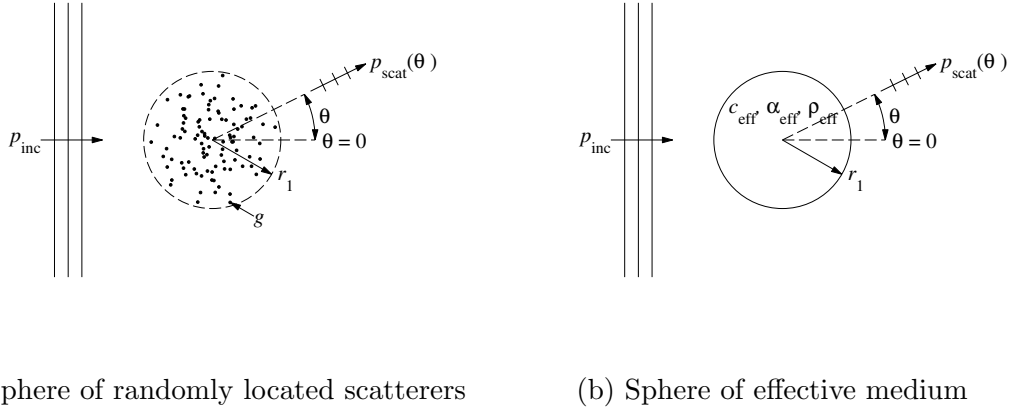
Figure 5.1: Geometries for scattering from (a) a sphere of randomly placed scatterers and for (b) a sphere of effective medium.

Recently Raveau and Feuillade compared these two approaches and made two assertions [138]. The first is that generally these approaches show good agreement in the forward scattering direction, but not in the back scattering direction. The second was that the models agree at low frequencies, but diverge when the wavelength $\lambda$ is smaller than four times the average spacing $s$ between scatterers. The reason that forward-scattering agrees better than back-scattering stems from the phase dependence of reflection, which is shown diagrammatically in Figure 5.2.

Figure 5.3 and 5.4 show the comparison of these models in a mono-disperse spherical cloud of radius 1 m with 100 bubbles while varying the bubble radius. The randomization was accomplished by generating a random radius and angles in spherical coordinates so that there is in equal likelihood that the bubble will be contained at any element of volume. Then the bubble position was checked to ensure none of them are within 3 radii of another bubble. Bubble locations not meeting

this criteria are removed and new locations are generated. This continues until a complete set of 100 randomized bubble locations is achieved. The Matlab code to used for the random distribution is in Section A.3.

Each plot is an is marked with a vertical dashed line at the frequency where the wavelength is equal to 4 mean free paths ($\Upsilon = \lambda/s = 4$). Both forward-scattering and back-scattering for the FS and A-EM models agree well below $\Upsilon = 4$, usually within a dB below the individual bubble resonance frequency $f_0$ and within 5 dB near $f_0$. Above the $\Upsilon = 4$ criteria the back-scattering of A-EM diverges quickly from the FS solution and us under-predicted by more than 20 dB. The forward-scattering on the other hand is generally in agreement between the models to the high frequency limit and only differs significantly around $f_0$. As the size of the bubble radius $a$ decreases $f_0$ increases and consequently the mean free paths at resonance $\Upsilon_0$ decreases. As $\Upsilon_0$ decreases the polar pattern for the FS solution becomes less symmetric, whereas the A-EM is based on an assumption of symmetry.

In order to get an idea of how much variation occurs due to fish movement, Figure 5.5 displays the result of 100 independent realizations of 100 random bubble positions and the mean value. An actual school the fish generally maintain a regular spacing and are not distributed in a purely random fashion, however this provides the range of variation. It is clear that the distribution is different for FS and BS. Figure 5.6 shows the FS and BS histogram probability density functions (PDFs) at four frequencies, each with 20 bins divided across the result range. It is clear from the PDFs that there is much less variability in the forward scattering, and that the distribution of the back-scattering SA is not normal for frequencies higher than

109

(a) Back-scattering  (b) Forward-scattering
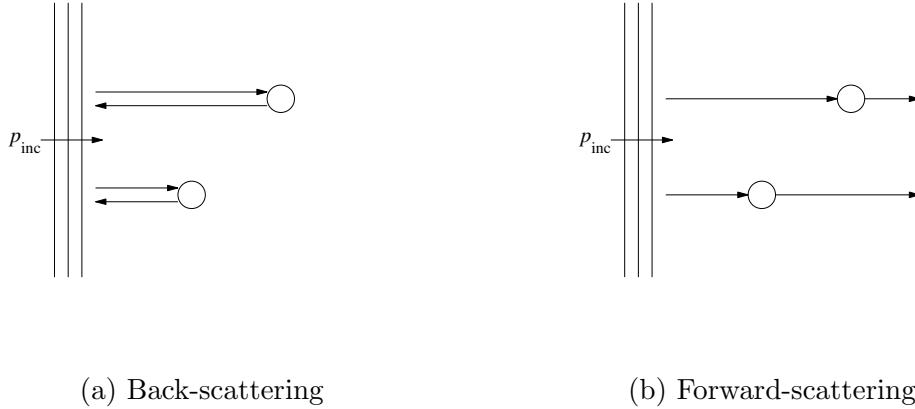
Figure 5.2: This simple ray diagram illustrates why back-scattering is much more sensitive to the positioning of the individual scatters, since the phase of each scatterer plays a larger role. This figure is adapted from Feuillade and Raveau [139].

the individual bubble resonance. This appears to be because the nulls can change significantly, leading to a large likelihood the SA will be near the mean, but a definite chance that the value could be 60 dB lower.

The directivity of one case at several frequencies is shown in Figure 5.7. Here the ensemble average of the SA is taken from the 100 realizations shown in Figures 5.5 and 5.6. In these plots, the trend that the two methods agree below the individual bubble resonance frequency and toward forward scattering are apparent. While Figures 5.3 and 5.4 show that the scattering from one realization of the FS model is not symmetric, Figure 5.7 shows that the average value of many realizations is symmetric.

This can be repeated for the balloon configurations studied in Section 4.3. The results for each bubble configuration is shown in Figure 5.8. The FS model shows
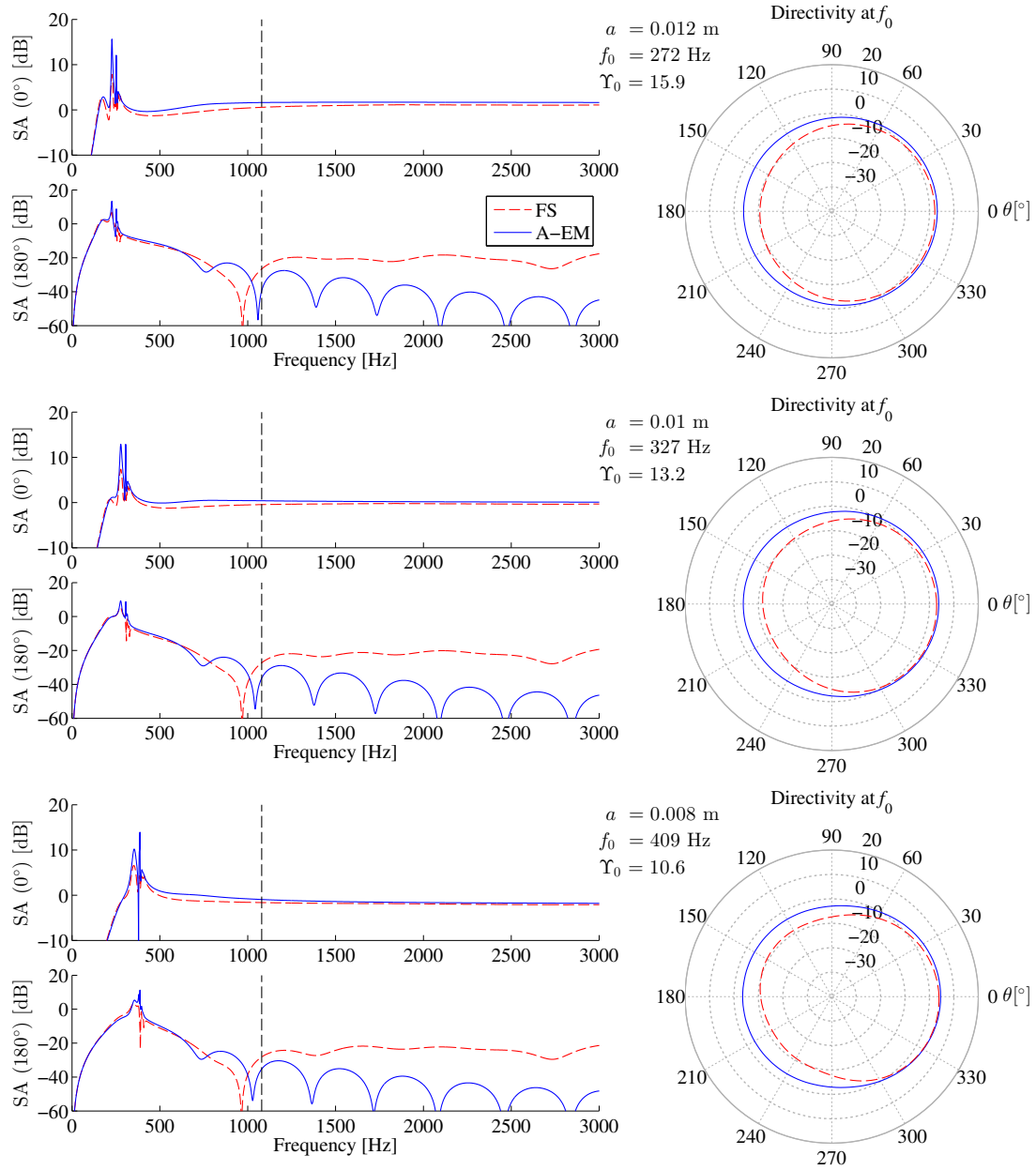
Figure 5.3: The FS scattering amplitude (0°) and BS scattering amplitude (180°) for various values of $10.6 < \Upsilon_0 < 15.9$ and the directivity of the SA at the individual bubble resonance frequency, where $a$ is the radius of the mono-disperse bubbles. The vertical dashed line represents a value of $\lambda/s = 4$.

111
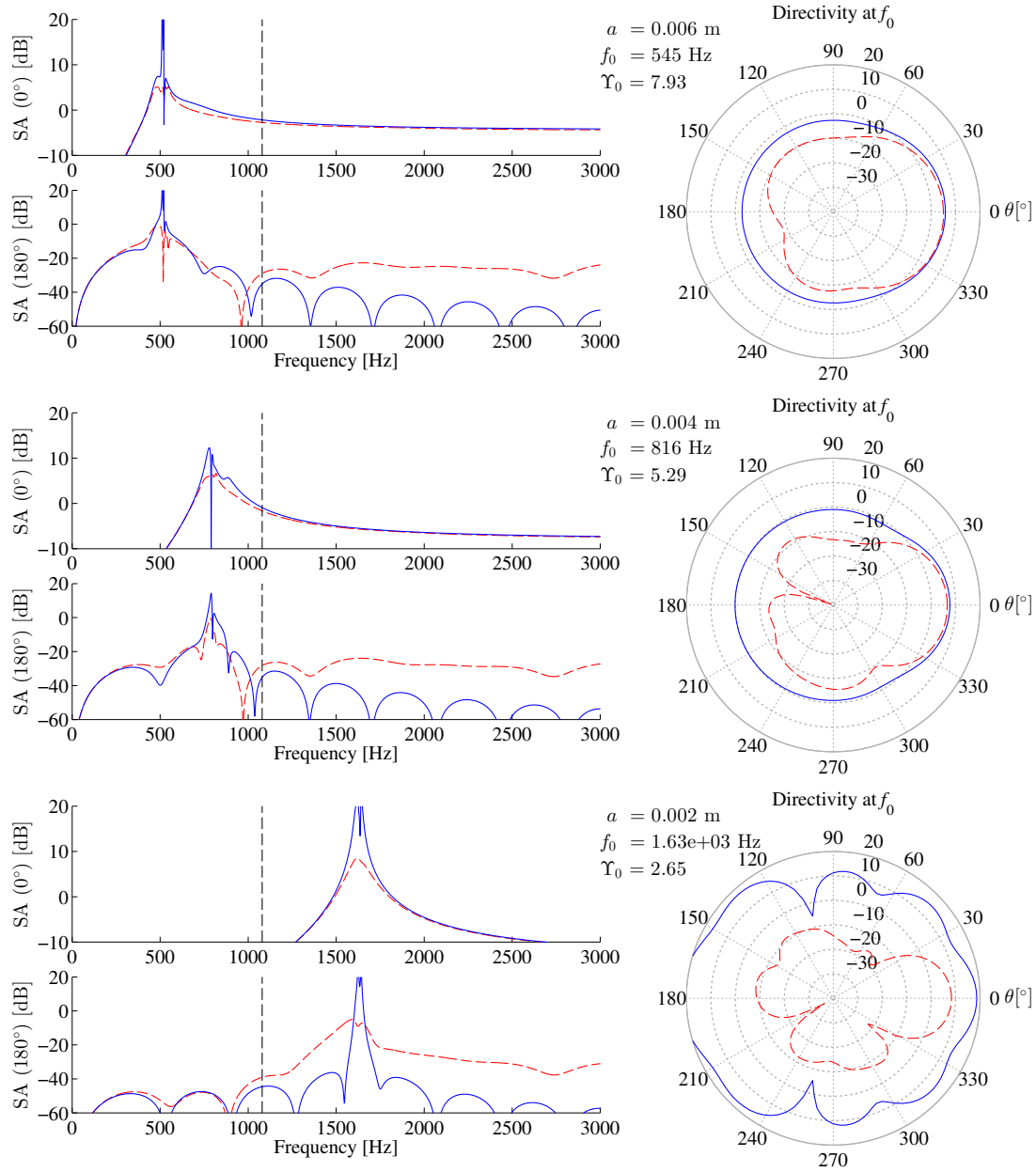
Figure 5.4: The FS scattering amplitude (0°) and BS scattering amplitude (180°) for various values of $2.65 < \Upsilon_0 < 7.3$ and the directivity of the SA at the individual bubble resonance frequency, where $a$ is the radius of the mono-disperse bubbles. The vertical dashed line represents a value of $\lambda/s = 4$.

112
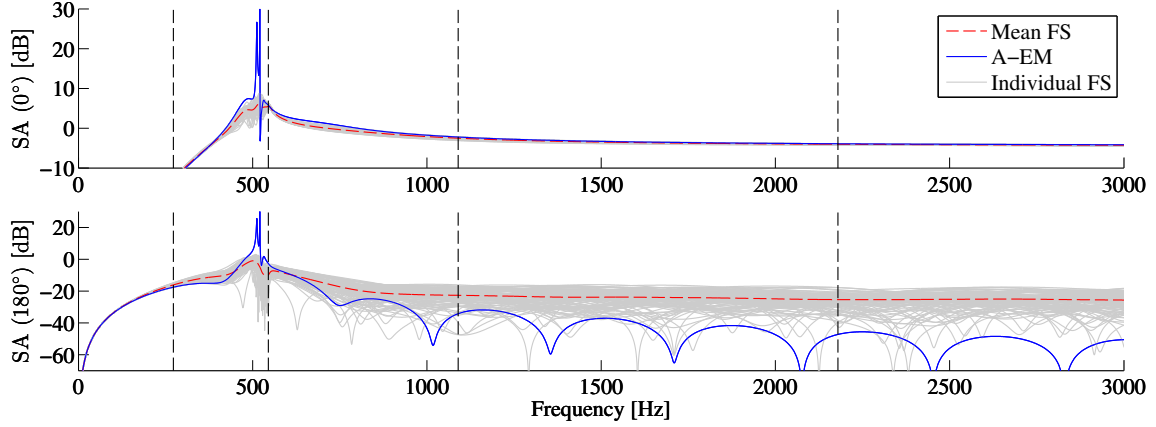
Figure 5.5: The FS scattering amplitude (0°) and BS scattering amplitude (180°) with 100 randomized arrangements of 100 mono-disperse bubbles with a radii $a = 0.006$ m and $\Upsilon_0 = 7.93$ within a sphere of radius 1 m at atmospheric pressure. The four verticle lines indicated the frequencies at which the PDFs are shown in Figure 5.6, and are $1/2f_0$, $f_0$, $2f_0$, and $4f_0$.
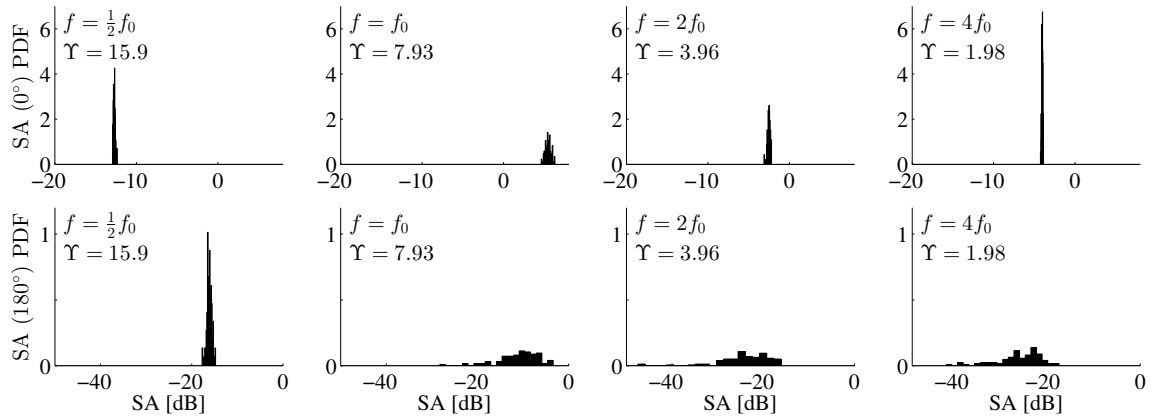


Figure 5.6: PDFs of the SA from Figure 5.5.

113
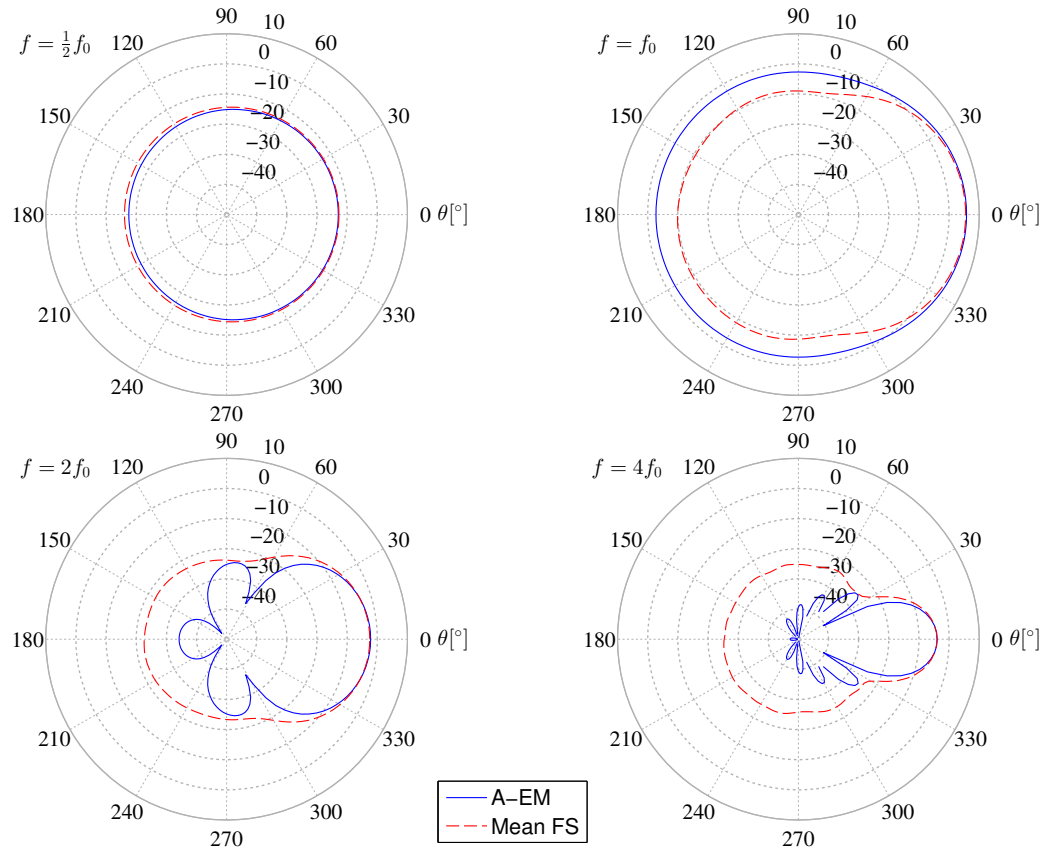
Figure 5.7: The angle dependent SA at four frequencies for the average of 100 randomized arrangements of 100 mono-disperse bubbles with a radii $a = 0.006$ m and $\Upsilon_0 = 7.93$ within a sphere of radius 1 m at atmospheric pressure

that the collective mode resonates at a higher frequency than A-EM predicts. This is to be expected since the geometry of cage was a cube, while A-EM as implemented here assumes a sphere. The Random case and the Dense case mach most closely with A-EM. Since the number of bubbles and bubble sizes are the same for each configuration the A-EM plots are identical. The dip in the back scattering above the individual bubble resonance frequency is predicted by both the FS and A-EM Models.

For the test conditions presented in Chapter 6, the ratio $\Upsilon_0 = \lambda_0/s$ ranges from 6.0 to 8.5, which implies according to Raveau and Feuillade's hypothesis, effective medium scattering should be valid for these densities.
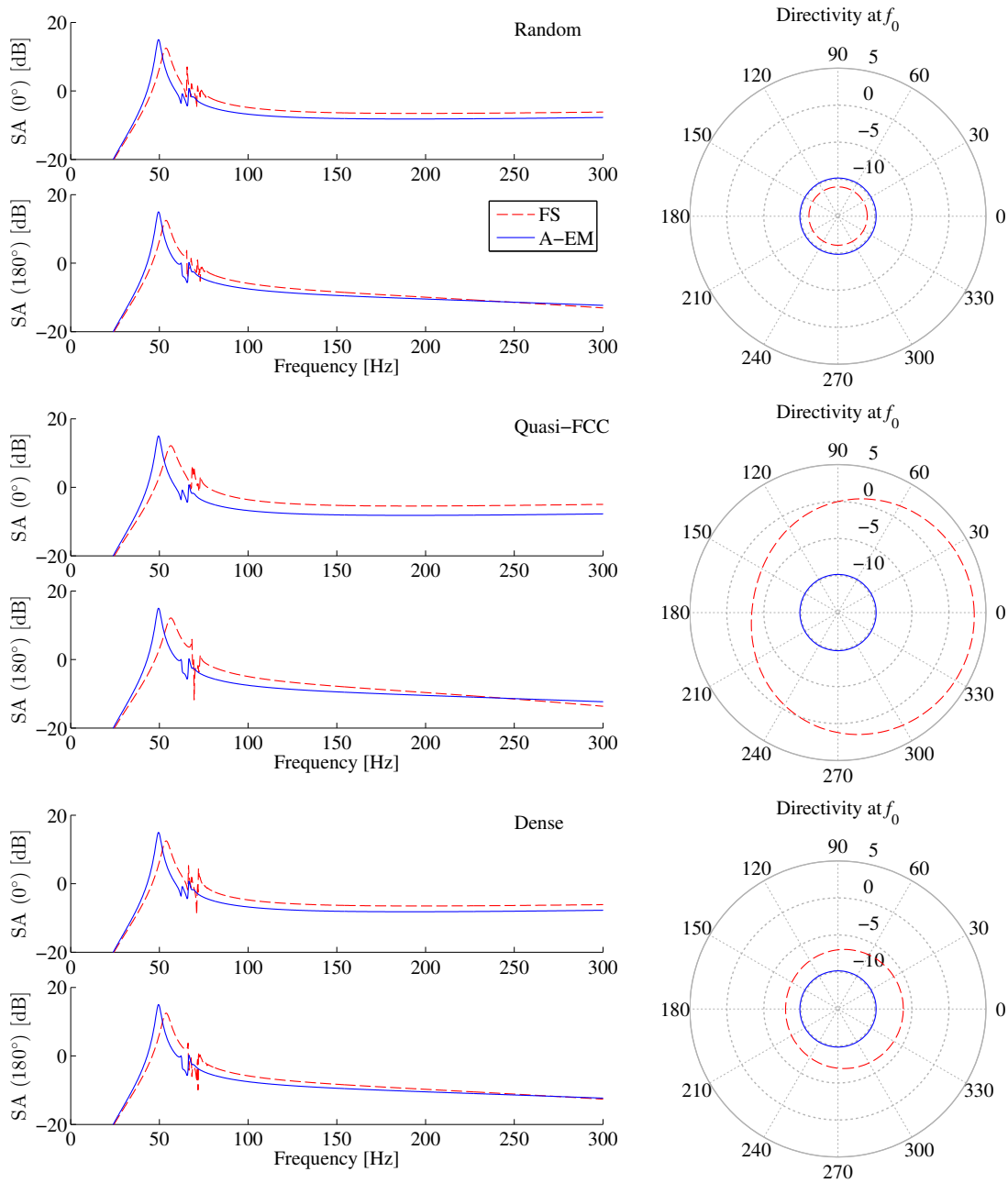
Figure 5.8: The FS scattering amplitude (0°) and BS scattering amplitude (180°) for bubble configurations from Section 4.3.

# Chapter 6

# Speed of Sound within Model Schools of *Danio Rerios*

This chapter presents measurements of the sound speed through schools of fish using the resonator method. The method of analysis is the same as for the balloons discussed in Section 4.2. While insight into effective medium theory is possible by using balloons and freely rising bubbles, the ultimate interest is in determining the bio-acoustic relevant factors for fish schools. While information regarding the scattering of fish schools can be made at sea, the interest here is the application and development of a laboratory measurement of the acoustic properties of fish. Laboratory measurements allow for increased knowledge of important parameters such as fish species, size, orientation, and biology, that aren't accessible in the field.

## 6.1 Determination of Bio-Acoustic Parameters

In order to extract important biological data, micro-computed x-ray tomography imaging scans (CT scans) were performed on multiple batches of *Danio rerio* after testing. The intention was to determine the volume of the swim bladder and fish flesh. Although not utilized in this study, the skeletal structure was also resolved. A small subset (12 of 48) of the fish in the acoustic study were scanned, and for each

117

| Swim bladder volume [m$^3$] | Fish body volume [m$^3$] | Length [m] |
|---|---|---|
| $1.27031 \times 10^{-8}$ | $2.30939 \times 10^{-7}$ | - |
| $1.32834 \times 10^{-8}$ | $2.16233 \times 10^{-7}$ | - |
| $1.41937 \times 10^{-8}$ | $3.0026 \times 10^{-7}$ | 0.0305 |
| $1.19829 \times 10^{-8}$ | $2.21701 \times 10^{-7}$ | 0.0325 |
| $1.9803 \times 10^{-8}$ | $3.50581 \times 10^{-7}$ | 0.0338 |
| $1.5259 \times 10^{-8}$ | $3.58723 \times 10^{-7}$ | 0.0321 |
| $1.88127 \times 10^{-8}$ | $4.31611 \times 10^{-7}$ | 0.0371 |
| $1.05275 \times 10^{-8}$ | $1.95627 \times 10^{-7}$ | 0.0298 |
| $2.47594 \times 10^{-8}$ | $4.14205 \times 10^{-7}$ | 0.0322 |
| $4.32598 \times 10^{-9}$ | $2.26313 \times 10^{-7}$ | 0.0361 |
| $1.62929 \times 10^{-8}$ | $3.06988 \times 10^{-7}$ | 0.0295 |
| $9.50288 \times 10^{-8}$ | $2.66979 \times 10^{-7}$ | 0.0333 |

Table 6.1: Swim bladder and fish volume (determined from CT scan imagery) and measured length for a subset of the fish used in acoustic tests.

fish the length, volume of swim bladder, and total body volume were cataloged. The CT scan was performed at low energy (60kV) and the reconstructed images had a voxel size of 31 micrometers. The swim bladder feature was extracted by thresholding the image to provide a clear distinction between the fish flesh and the air filled swim bladder. Example slices from the results of a CT scan are shown in Figure 6.1. The average swim bladder volume was $1.429 \times 10^{-8}$ m$^3$ and the standard deviation was $5.09 \times 10^{-9}$ m$^3$ (35.6%). The individual results are presented in Table 6.1.

## 6.2   Experimental Method

The experimental apparatus for use with live fish was significantly more complex than for the balloon measurements and followed the approved IACUC protocol AUP-2010-00176 (shown in Appendix I). The first complicating factor was to pro-
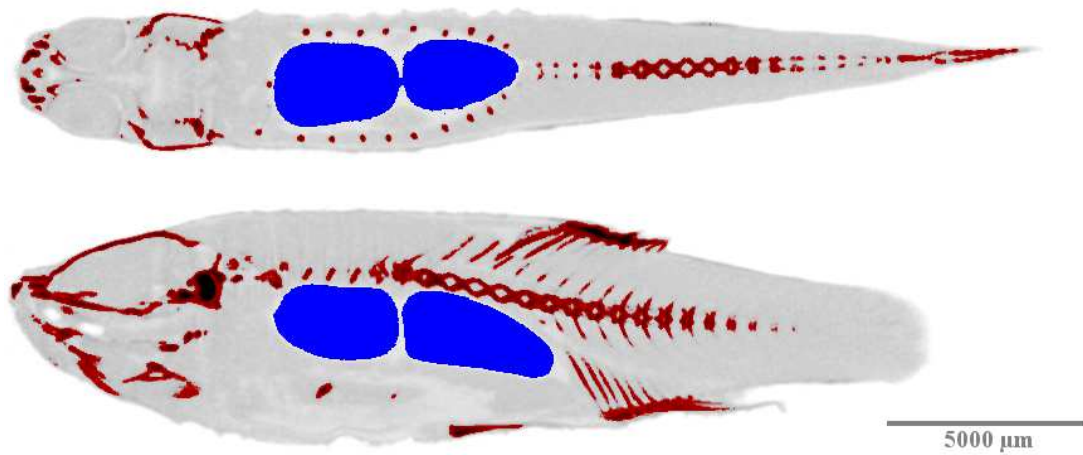
Figure 6.1: Slices taken from a CT scan of one of the fist tested. Blue is the swim bladder, red is the skeletal structure, and light gray is the fish flesh.

vide oxygenated water to the fish during testing. This is significantly different from the protocol for testing inanimate objects, which calls for the use of degassed water in order to remove any tiny bubbles that might affect the test results. In order to provide a continuous flow of oxygenated water a small tube was inserted through the foam layer at the bottom of the tube, and an overflow catchment was added to the top of the tube. The tube was filled with degassed water prior to testing and then oxygenated water was pumped into the bottom of the tube. The water flowed over the rim at the top of the tube into the catchment, where it entered a tube that returned it to the reservoir. The reservoir was a conventional fish tank with an aerating filter. A schematic of this process is represented in Figure 6.2 and a photo of the resonator and reservoir is shown in Figure 6.3.

The second complication comes from the fact that *Danio rerios* are a schooling species of fish. When their tendency for schooling is combined with the unfamiliar
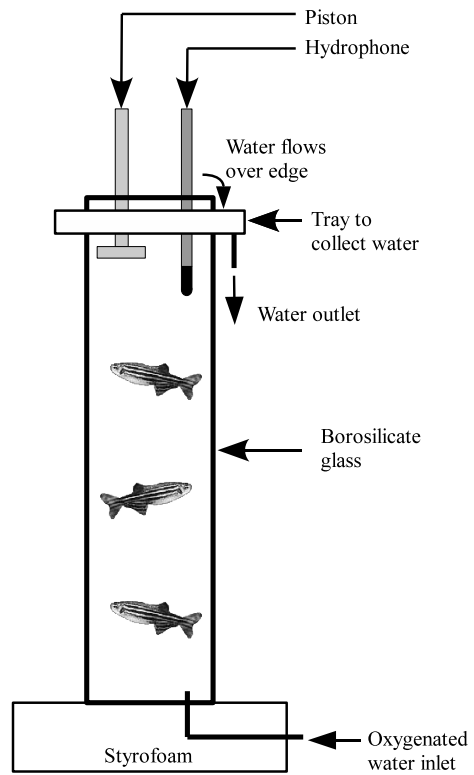
Figure 6.2: Schematic of resonator oxygenation. The reservoir in the text is not shown.
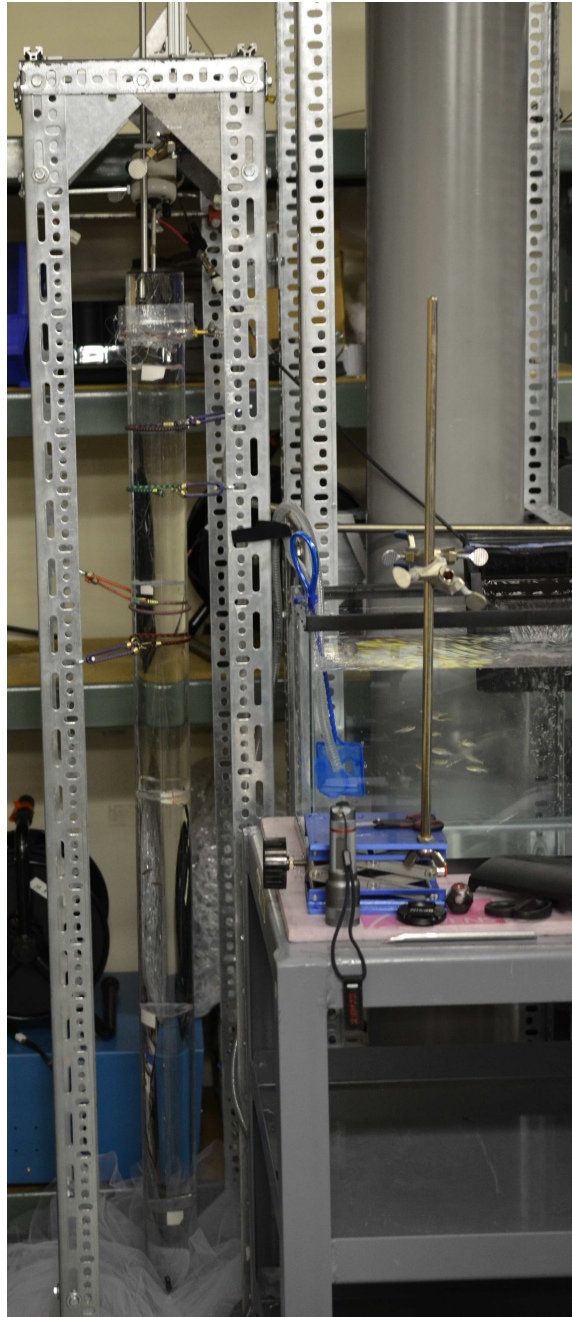
Figure 6.3: Photo of resonator apparatus with catchment and fish reservoir.

environment of a vertical tube the fish quickly form a tight school at the very bottom of the tube, which results in an inhomogeneous sound speed within the tube, and causes failure of the resonator method. A means to separate and evenly distribute the fish had to be devised. The dividers used to do this presented the additional risks of modifying the acoustic field, and providing extra surfaces on which small bubbles could be trapped or could form. The goal of the design was to minimize these complications. The final design involved creating cylinders out of thin plastic sheets and affixing them with either epoxy or electrical tape so that their outer radius was just smaller than the inner radius of the glass tube. A fine mesh was then attached to the top of the cylinder with hot glue and two monofilament lines were attached to the sides in order to suspend the dividers in the tube. The bottom divider was attached to a lead weight. One of these dividers in place within a resonator with a fish is shown in Figure 6.4. Spectra were taken for the water-filled tube with and without the resonator dividers and are shown in Figure 6.5. The presence of the cages damped the resonances slightly and reduced the resonance frequency of some peaks a minor amount; however, no significant difference was noted. The average relative error between sound speeds measured with and without dividers is 1.3%. The estimated sound speed error $\epsilon_c$ due to uncertainty in the water column length $\epsilon_L$ and the finite frequency resolution $\epsilon_f$ was estimated with the expression:

$$\pm \epsilon_c = \pm 2 \left( L\epsilon_f + f\epsilon_L + \epsilon_f \epsilon_L \right) / m_{\text{eff}}, \tag{6.1}$$

where $m_{\text{eff}}$ is the effective mode number. Equation (6.1) is not plotted because it is below 1% for all cases.

122
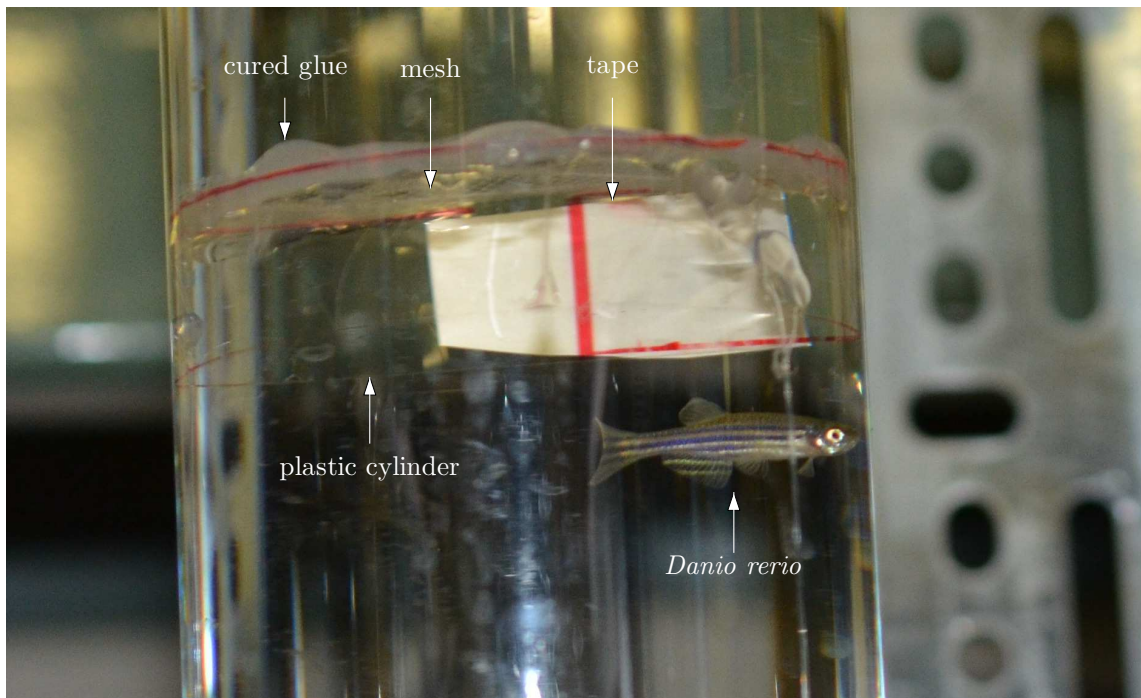
Figure 6.4: Picture of resonator divider. The cured glue and the remains of dried water drops may look like bubbles in this photograph, but the degassed water initially used inside the tube effectively removed any unwanted air bubbles from the system.
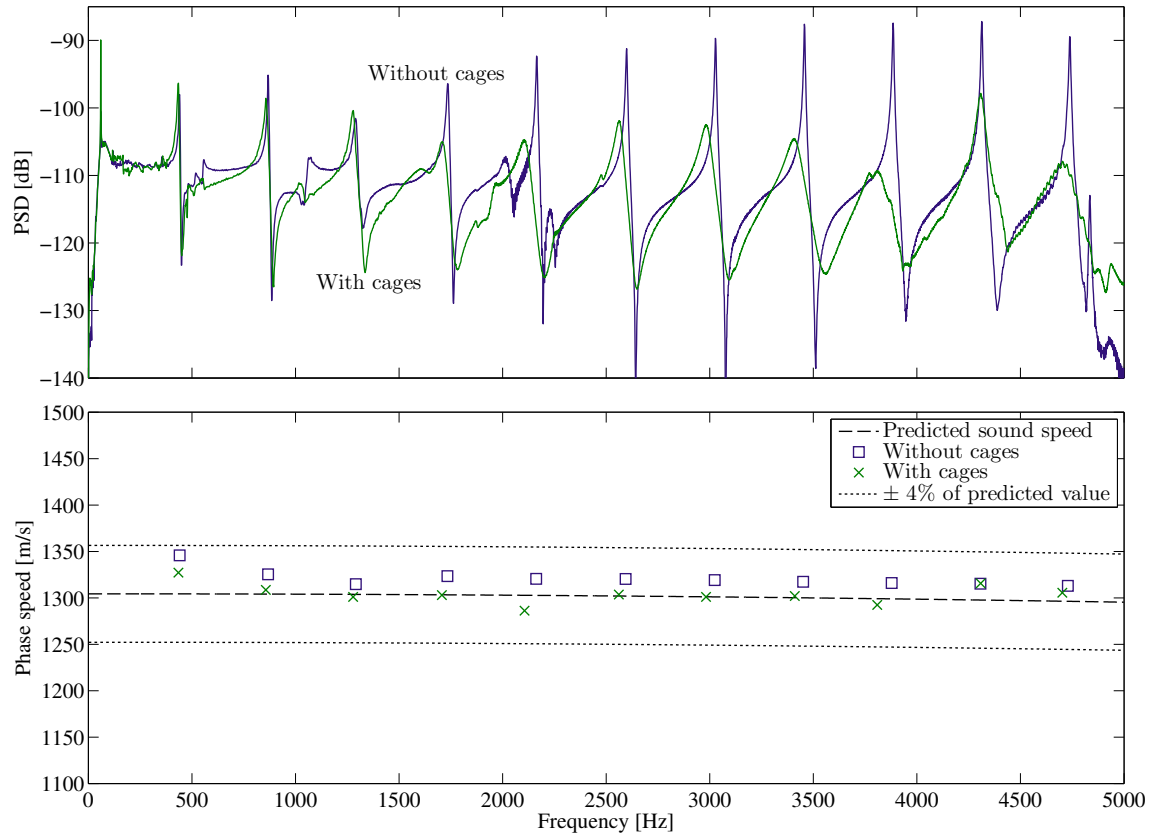
Figure 6.5: The effect of the fish divider/cages on the acoustic spectrum is shown (top). The phase speed calculated from the resonances compared to the value predicted by the forward model.

| Glass properties | Short resonator | Long resonator |
|---|---|---|
| $c_c = 5584.4$ m/s | $L$ = 0.6121 m | $L = 1.5270$ m |
| $c_s = 3376.1$ m/s | $b = 0.0265$ m | $b = 0.0309$ m |
| $\rho = 2199.4$ kg/m$^3$ | $d = 0.0347$ m | $d = 0.0400$ m |

Table 6.2: Material properties of the borosilicate glass resonators

Four rounds of fish testing were conducted. The first three rounds used a resonator with the properties of the short resonator shown in Table 6.2, while the last round of testing used a larger resonator with the same glass properties and the dimensions stated in Table 6.2. The shear and compressional sound speed used for the glass tube wall material were determined by calibration using experimental measurements of a water-filled glass resonator. The sound speeds were adjusted until a best fit from the L&S disperion relation was found. The inner $b$ and outer $d$ radii were calculated from multiple measurements of the inner and outer diameters.

## 6.3 Determination of Fish Equivalent Bubble Volume

While it is possible that the resonance frequency of an individual fish is higher due to the fish flesh or tension in the muscles surrounding the swim bladder, in this study this simplification is made that the resonance frequency of a fish is that of a spherical bubble with the equivalent volume as the swim bladder. In the bubble size range studied, Minnaert's resonance frequency [69] is a reasonable approximation.

Because there are no known studies of the functional relationship between the length of a *Danio rerio* and the volume of the swimbladder, it is assumed that the linear dimensions of an adult swimbladder are proportional to the length of the fish.

Based on this assumption and the volumes and lengths measured of the set of fish that were CT scanned, the empirical relationship of Equation (6.2) is used based on a least mean-square errors fit.

$$V = (7.2722 \times 10^{-5}L)^3. \tag{6.2}$$

The mono-disperse bubble size used in the model for Figure 6.9 was determined by applying Equation (6.2) to the average of the lengths presented in Table 6.3. Figure 6.6 shows that this functional relationship has a weak correlation. There are a myriad of reasons that there is little evidence of a functional relationship between swim bladder volume and fish length. Firstly it was not possible to conduct the CT scans immediately after testing had occurred. In all cases after euthanization the fish were refrigerated and delivered to the CT facility the next morning. This is due to the limited time windows for testing and the fact that the CT scan facility was geographically separate from the site where the resonator tests were conducted. Even if direct transportation had been used the CT scan facility would have closed for the evening. Another reason for the lack of correlation is due to the fact that fish can voluntarily inflate and deflate their swim bladder. There was not time to let the fish sit for a long time and re-equilibriate between testing and euthanasia. Despite this weak fit this relationship is still used because it was not possible to get swim-bladder volume measurements for all of the fish, while it was possible to measure their length. Gong *et al.* [39] analyzed weight and length of Atlantic herring and found a that the weight of herring varies as the length to the power of 3.35. There was also considerable scatter in their data, which is included here as Figure 6.7.
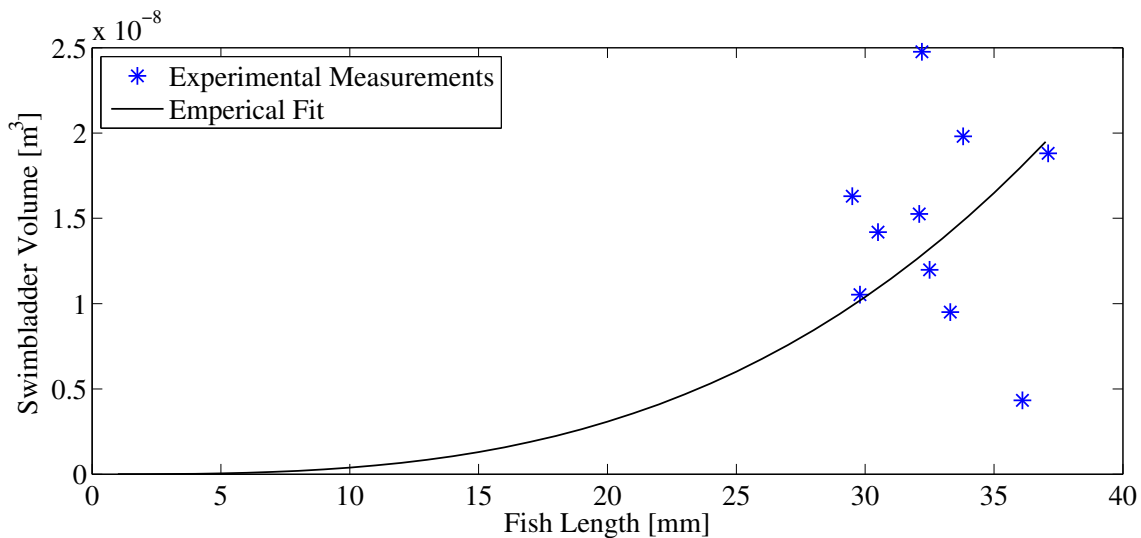
Figure 6.6: Fish length and swim bladder volume.

Gong *et al.* [39] also mention that the swim bladder volume is typically proportional to weight in order for fish to maintain neutral buoyancy. How constant of proportion varies with different collections of fish. The mass of the fish were not measured in this study.

## 6.4 Sound Speed as a Function of School Density

The four rounds of fish testing took place on the 14th of December, 2011, the 19th of December, 2012, the 8th of August, 2013, and the 17th of December, 2013. The first round of testing occurred without dividers and consequently the majority of the fish resided at the bottom of the tube with a few fish occasionally swimming toward top of the resonator for short periods of time. The second round of testing involved testing two types of dividers. Both types of dividers turned out
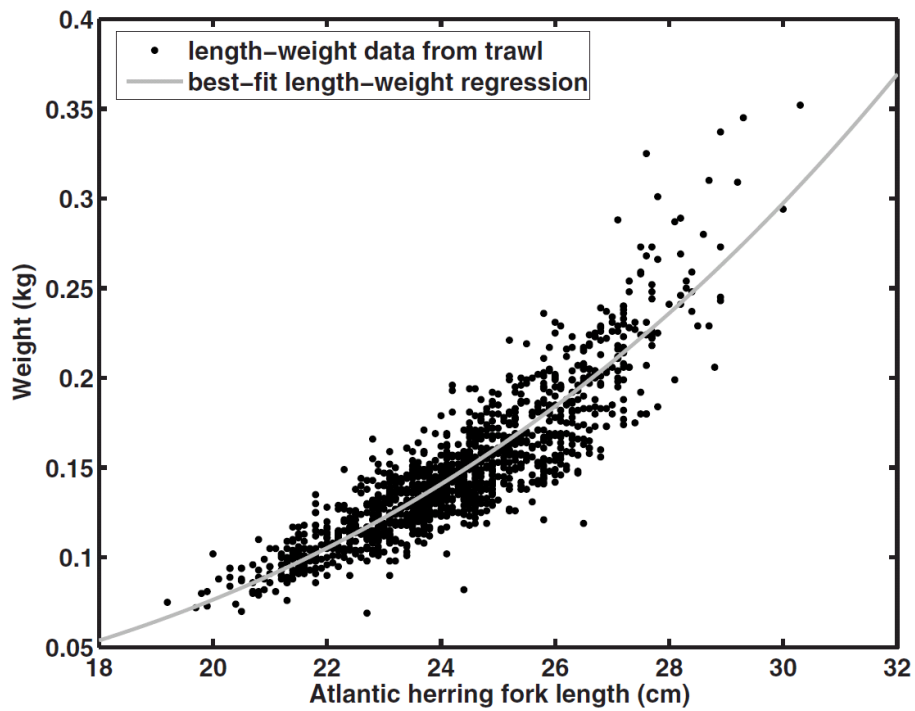
Figure 6.7: Figure from Gong *et al.* [39] showing the experimentally determined Atlantic herring length-weight relationship.

to capture stray bubbles extremely easily and the extra damping for excess bubbles masked the measurements. From these trials, several lessons were learned about the divider design which were incorporated into the third round of testing. The third round was successful, aside from the fact that only one resonator mode was present below the individual fish resonance frequency. This motivated the move to a much larger tube for the last round of testing. Even with the dividers, getting an even distribution of fish in the resonator proved difficult. *Danio rerios* are very active and do not appreciate being in an enclosed space. As such the fish constantly try to swim around the edge of the dividers and sometimes they succeeded. The fish also wiggle as much as possible when being deployed into or recovered from the apparatus, which prompted the use of netting all around the resonator for the inevitable cases where a fish launched itself out of the resonator or to the ground when being handled.

The results of the third round of testing are shown in Figure 6.8. The number of clear resonance modes visible below the individual fish resonance frequency ranges between 1 and 3 and the number of fish lengths per mean free path ranged from 3.3 to 1.7. For some reason the fish were very calm during this test and the approximate fish positions throughout each test are included as a subset schematic in each graph. The bubble size subsequently used to model this case was based on the equivalent spherical radius of the average swim bladder volume as determined by CT scans of the fish. Three of the CT scans showed a vertical division within both chambers of the swim bladder. If this occurred the total swim bladder volume was used. The bubble size distribution for Figure 6.8 is considered mono-disperse with an equivalent spherical volume to the average swim bladder volume from the CT scans. The

129

| 0.0128 | 0.0132 | 0.0113 | 0.0111 | 0.0100 |
|--------|--------|--------|--------|--------|
| 0.0105 | 0.0109 | 0.0119 | 0.0122 | 0.0118 |
| 0.0108 | 0.0104 | 0.0098 | | |

Table 6.3: Lengths of the fish in the fourth round of testing in meters.

effective medium model for free bubbles (see Equations (3.33) and (3.34)) was used for comparison with model parameters states in Appendix G.

The sound speed dispersion plot for the fourth round of fish test is shown in Figure 6.9. The fish in these tests were much more active and consequently were at different positions throughout the test. The fish densities for these cases ranged from 8.6 to 6.1 fish lengths per mean free path. Since there were no CT scans for this experiment and the fish size was significantly smaller than the prior test, the swim bladder size and effective radius was extrapolated as discussed in Section 6.3. The lengths of the fish used in the fourth round of fish testing are presented in Table 6.3. The average length was used to determine the swim bladder volume.

The movement of individual fish can affect the effective sound speed inside the tube. Each case was sampled for a number of 1 second time segments. The number of time segments for each case are [33, 33, 38, 232, 51, 104], respectively for [0, 0, 5, 8, 11, 14] fish in the tube, respectively. The eight fish case was let run for more than twice the length of any other case and shows much greater variation. This suggests that future tests require a much larger measurement period. Figures 6.10 and 6.11 show the resonator measurements for each case as function of time. Each dot in the figure represents the peak of a resonance in that time segment as it is being tracked across time. The motion of the fish changes the effective medium properties, which

130
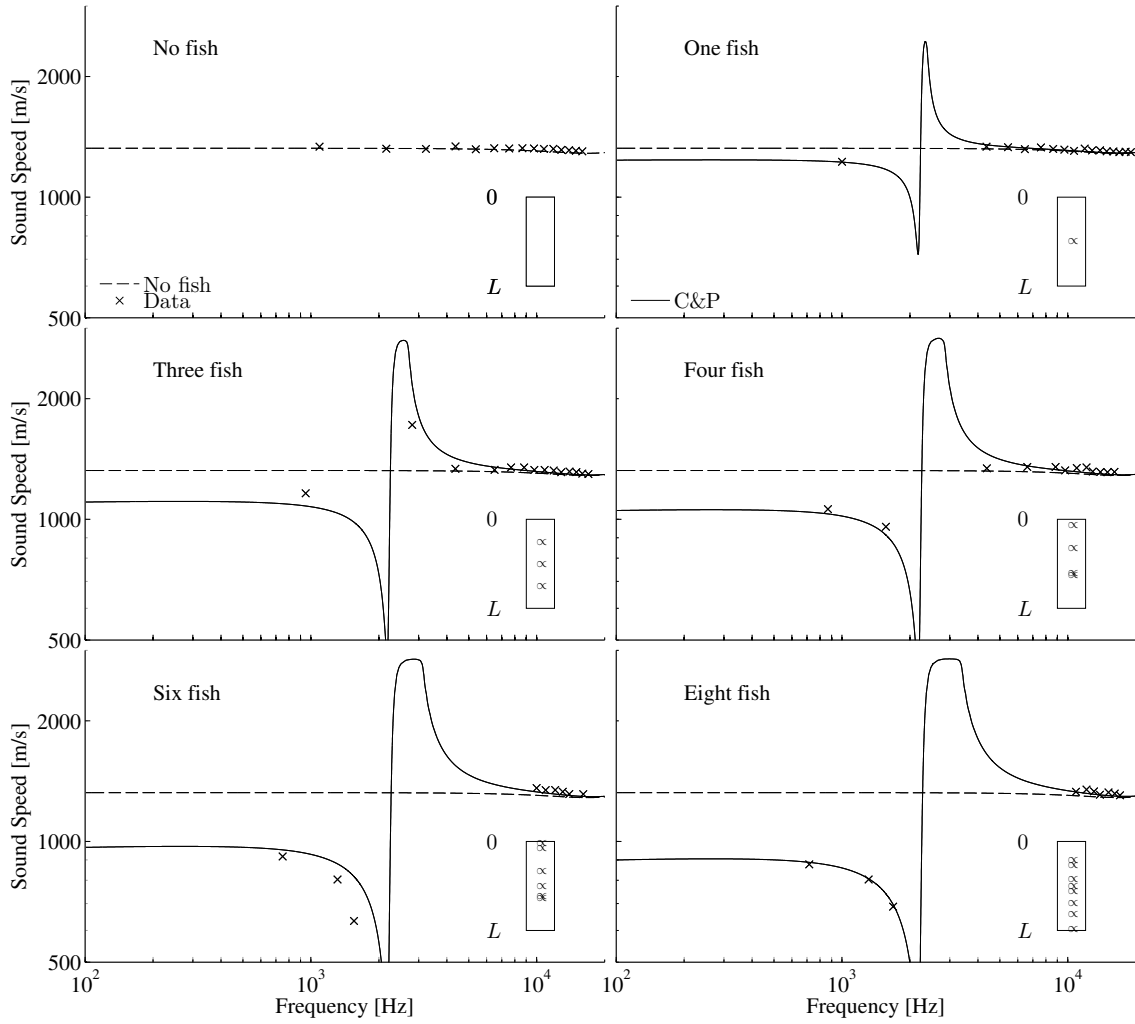
Figure 6.8: Fish school sound speed measurement in 0.6121 m resonator. The figure at the lower right of each graph indicates the approximate position of the fish when the measurement was taken. The free bubble effective medium model (C&P) was used and is plotted for comparison.

131
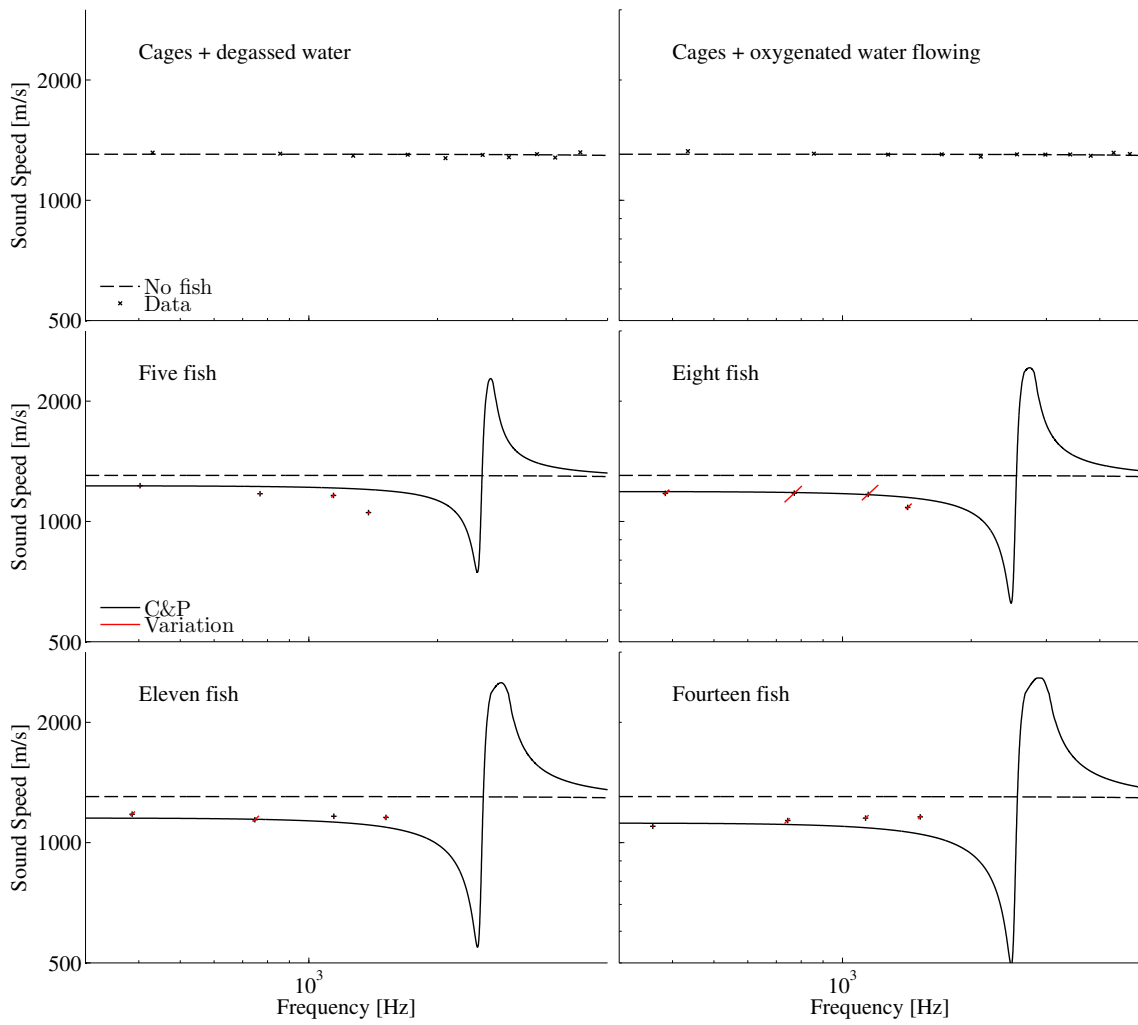
Figure 6.9: Fish school sound speed calculation in 1.5270 m resonator.

causes variation in the resonance frequencies. The shift in the resonance frequencies was used to estimate the variation in sound speed due to the fish. This variation is shown in Figure 6.12 for the eight fish case. This case was chosen because it was the only experiment of sufficient length to capture large variations. The measured phase speed has been normalized by the mean value. The first mode has the least variation, which is expected since any fish movement would be smaller relative to a wavelength. The largest difference was ±5.6% variation from the mean value.
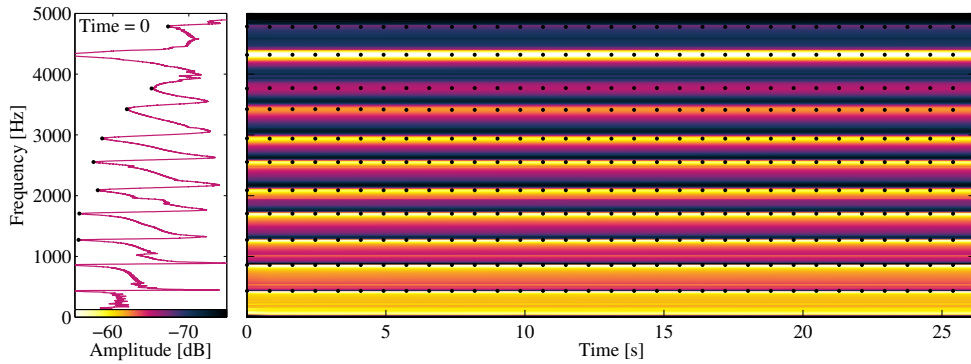
(a) Water filled tube with cages and degassed water.
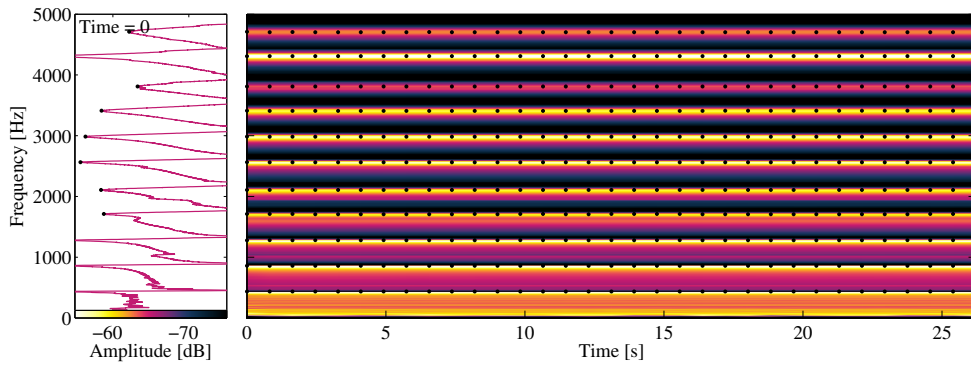


(b) Water filled tube with cages and oxygenated water flowing, but no fish.
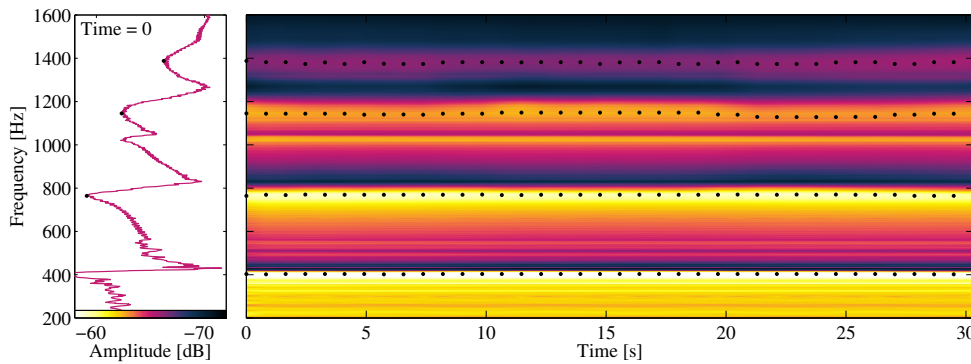


(c) Same as (b) but with five fish.

Figure 6.10: Variation in resonances due to fish movement during the test. The spectrum for the first time segment indicates the peaks that are tracked and the color scale (left), The spectrum as a function of time shows how the tracked peaks change (right).
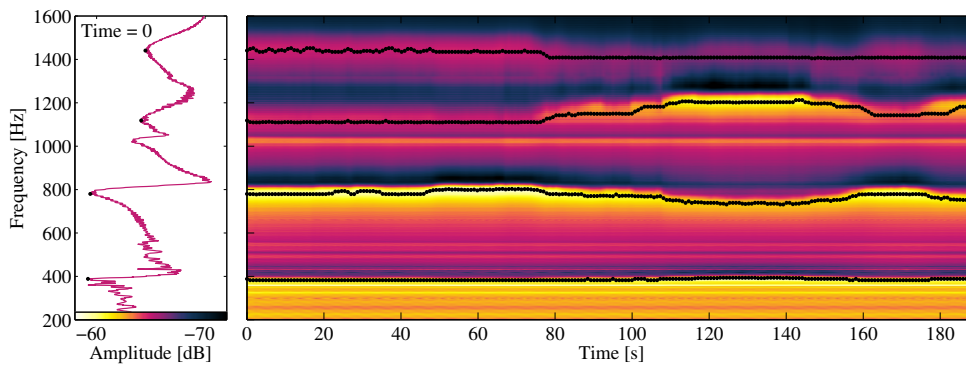
(a) Water filled tube with eight fish.
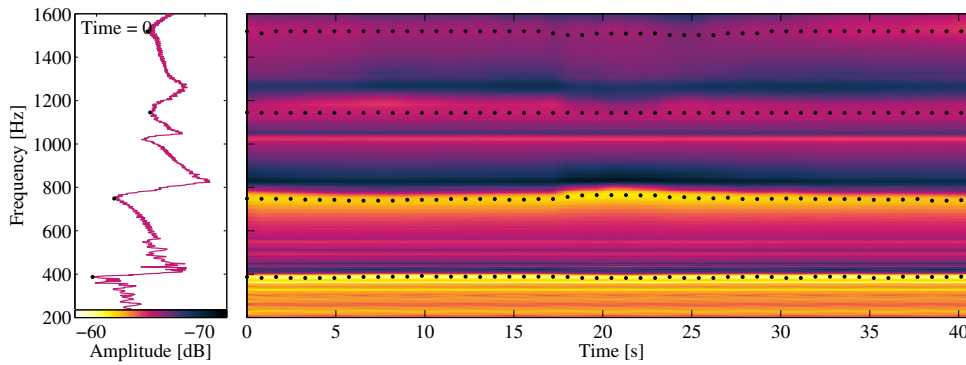


(b) Water filled tube with eleven fish.
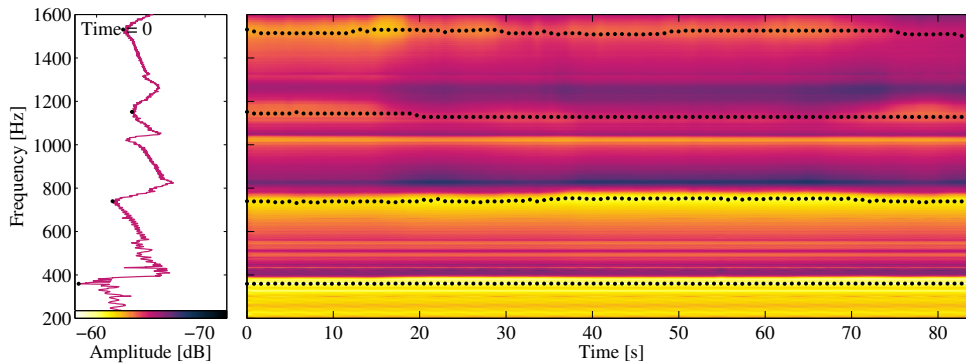


(c) Water filled tube with fourteen fish.

Figure 6.11: Variation in resonances due to fish movement during the test. The spectrum for the first time segment indicates the peaks that are tracked and the color scale (left), The spectrum as a function of time shows how the tracked peaks change (right).

135
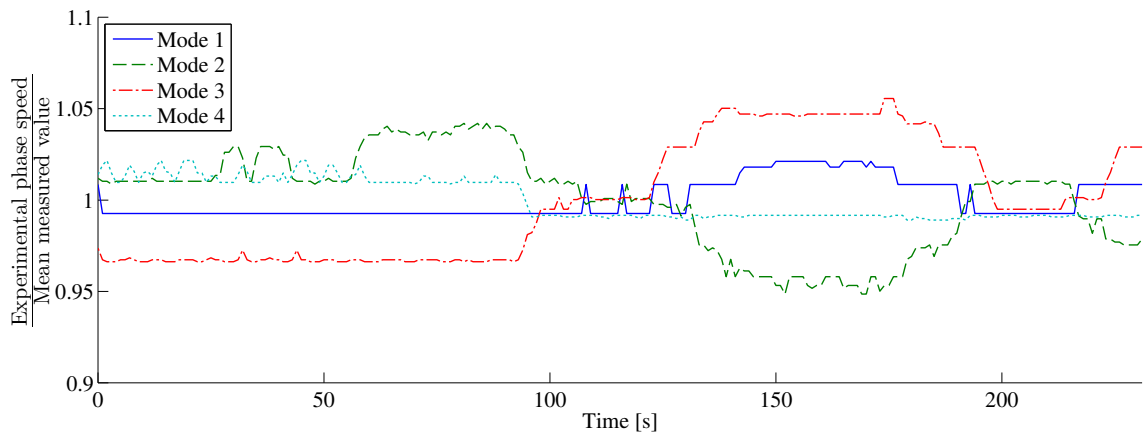
Figure 6.12: The changes in phase speed as a function of time for the eight fish case.

# Chapter 7

# Summary and Future Work

The purpose of this work was to increase the understanding of the acoustic response of fish. Fish are an important biological scatterer and the primary contributor to the deep scattering layer. Improved knowledge of the acoustic response of fish will allow more accurate classification of the abundance, type, and size of fish when performing acoustic surveys, which would be an invaluable advance for the field of fishery acoustics. These advances would also aid in the classification of potential threats for defense applications and specifically the reduction in false threat detection due to the presence of fish for active sonar applications.

Despite years of study there is still an inherent uncertainty in available measurement datasets that is hard to quantify and these measurements have been unable to validate existing competing predictive models. In order to begin to address this deficiency, laboratory measurements of sound speed and attenuation have been conducted. The advantage of laboratory measurements lies in the ability to have precise control of the parameters, such as bubble size, bubble position, and number of bubbles. Laboratory measurements also allow better estimates of the uncertainties present.

Sound speed measurements of elastic-shelled bubbles and model fish schools

composed of real but artificially contained fish were conducted using a resonator technique. Testing of elastic-shelled balloons allowed investigation of the mode shapes present in the resonator and validation of the technique. Corrections were needed to account for the elastic waveguide effect of the resonator, which allowed sound speeds for free space to be calculated from the measured phase speed. The elastic waveguide corrections also allowed for waveguide sound speeds to be calculated from free field models in order to predict the acoustic field in the resonator. Spatial scans allowed characterization of the modal shapes at each resonance.

Two unanticipated phenomena were observed. When the sound speed through encapsulated bubbles that exhibited strong positive and negative dispersion was being measured, particular standing wave patterns were found both above and below the individual bubble resonance frequency, indicating that the first few acoustic modes (half-wavelength, two half-wavelengths, three half-wavelengths) occurred twice at different frequencies simultaneously. Secondly, at low frequencies the foam layer that had previously provided a reasonable approximation of a pressure release boundary was coupling to the system, causing the nodes to shift away from the boundary resulting in an over-estimation of the phase speed. The cause for the coupling was the reduced acoustic impedance of the bubbly liquid. Compensation for this was achieved by noting the location of the last node of each mode and adjusting the phase speed calculation accordingly. The measurements of elastic-shelled bubbles also revealed that the rubber shell material stiffened as the inflation was increased, a result that while anticipated does not have an accurate predictive model.

Acoustic resonator sound speed measurements of fish were conducted and

agreed unexpectedly well with the effective medium model for air-bubbles with no shell, which indicted that the fish flesh and swimbladder morphology for the species tested (*Danio rerio*) had little effect on the sound speed. The size of the bubbles for the model was determined through analysis of micro-computed x-ray tomography imaging scans (CT scans) of the fish used in the acoustic tests. Fish motion during the tests had a significant impact on the sound speed measurements, causing variations up to ±5.6% in one case. One can imagine both beneficial and detrimental effects of this acoustic variation. If the level of variation correlates with species, this effect could be exploited for classification purposes. Alternatively, variation could potentially confound abundance estimates. More work is required to fully understand the impact of the observed sound speed variation.

Insertion loss measurements of a model school composed of elastic-shelled bubbles was performed at UT Austin's Lake Travis Testing Station. This allowed precise knowledge of the bubble locations relative to the source and receiver. The measurements were compared to a full scattering model, which took into account the positions of each bubble and considered all orders of scattering between the bubbles, and an effective medium model that treated the bubble cloud as a uniform sphere with effective medium properties. Both models predicted the observed amplification effect below the individual bubble resonance frequency and the high insertion loss observed above that frequency, however effective medium theory over predicted the insertion loss by up to 45 dB whereas the full scattering model was within a few dB for one bubble position arrangement and 15 dB for the other two. Both models under-predicted the amount of amplification observed.

The work is brought full circle by investigating the predicted scattering from an effective medium. Here effective medium theory was compared to the full scattering solution. The results indicated that the effective medium theory only provides accurate back-scattering estimates if the wavelength of ensonification is greater than four times the mean spacing between fish, which verifies the findings of Raveau and Feuillade [138]. Forward-scattering measurements on the other hand provide accurate predictions for all frequencies except for those immediately around the individual fish resonance frequency or a collective resonance of the fish school.

The techniques reported here were successful in achieving the primary goal by providing experimental measurements with sufficient knowledge of the measurement uncertainty to quantify the amount of variation in sound speed and provide validation and comparison of predictive models. Repeating these measurements for various species of interest and expansion to include multiple scattering measurements of model fish schools composed of both real and artificially contained fish can be performed to provide even further insight into the acoustic response of fish. Other beneficial extensions of this work involve measuring the sound speed of model schools over longer time periods in order to determine if there is a quantifiable effect from the fish acclimating to the apparatus.

# Appendices

# Appendix A

# Statistical and Spectral Methods and Matlab Code

This appendix is provided in order to establish the statistical and spectral conventions used in this study. It will refer to the analysis of two time series of data with an input output relationship, $x(t)$ and $y(t)$, respectively. This section also contains content that is designed as a primer in the application of spectral analysis for the Austin Acoustical Society of America student chapter.

## A.1 Statistics

There are a few fundamental statistical definitions that need to be presented before discussing spectral methods.

### Mean

The definition of the arithmetic mean $\bar{x}$ for a signal of duration $T$ is:

$$\bar{x} = \frac{1}{T} \int_0^T x(t)\,\mathrm{d}t. \tag{A.1}$$

When cast in terms of a discrete series of $N$ values $x_n$, it becomes:

$$\bar{x} = \frac{1}{N} \sum_{n=1}^{N} (x_n). \tag{A.2}$$

**Variance**

The variance of a signal is the average of the squared difference between the instantaneous amplitude and the mean amplitude. For physical systems is often related to the signal power. For a continuous signal of duration $T$ it is defined as:

$$\text{Var}(x) = \frac{1}{T} \int_0^T [x(t) - \bar{x}]^2 \, \text{d}t. \tag{A.3}$$

When cast in terms of a discrete series of $N$ values $x_n$, it becomes:

$$\text{Var}(x) = \frac{1}{N} \sum_{n=1}^{N} \left[ (x_n - \bar{x})^2 \right]. \tag{A.4}$$

## A.2 Spectral Methods

**Fast Fourier Transform (FFT)**

The Fourier transform is an analytical tool that transforms time domain signals into the frequency domain, and is defined as:

$$X(\omega) = \int_{-\infty}^{\infty} x(t) e^{-j\omega t} \, \text{d}t, \tag{A.5}$$

where $\omega = 2\pi f$ is angular frequency. It is impossible to capture a signal for all time, so for discrete signal of finite time the discrete Fourier transform is used:

$$X_k = \sum_{n=1}^{N} \left( x_n e^{-j2\pi k(n-1)/N} \right), \tag{A.6}$$

where in this equation $k$ is an element of the integer set, and due to the periodicity of the discrete Fourier transform is generally evaluated on the range $[-N/2, N/2-1]$ if $N$ is even and $[-(N-1)/2, (N-1)/2]$ of $N$ is odd.

The FFT is an efficient numerical implementation of the discrete Fourier transform and its inverse and is most efficient when $N = 2^{\mathbb{N}}$, where $\mathbb{N}$ is a natural number. The FFT is properly implemented in Matlab by multiplying the function fft by the sampling interval d$t$:

```
N = 8;                  % Number of samples [#]
dt = 0.1;               % Sampling interval [s]
T = dt*N;               % Total sampling time [s]
df = 1/(dt*N);          % Frequency interval [Hz]
x = randn(N,1);         % Random values
X = fft(x)*dt;          % FFT of random values.
```

**Power Spectral Density (PSD)**

The PSD is used to describe the distribution of a time signal's variance over the frequency domain and is sometimes also called the autospectra or autospectral density function. It should not be confused with the energy spectral density which has an amplitude that will increase with measurement duration. The PSD is also usually described in terms of an ensemble average. Assume that the total measurement of $x(t)$ with a duration $T_r$ is stationary (A function whose joint probability distribution does not vary with time. This is a requirement for using the the Fourier Transform)

144

and has a zero mean ($\bar{x} = 0$). This record is divided into $n_d$ contiguous segments which each have a duration $T$. The two-sided PSD is defined as:

$$S_{xx}(f) = \frac{1}{n_d T} \sum_{n=1}^{n_d} [X_n^*(f) X_n(f)], \qquad (A.7)$$

where $X_n(f)$ is the FFT of the segment $x_n(t)$ and $^*$ indicates a complex conjugate. One of the convenient features of the properly scaled PSD is that its integral is equal to the variance of the original signal due to Parseval's theorem. The PSD can be calculated in Matlab and Parseval's theorem verified as:

```
N = 8;              % Number of samples [#]
dt = 0.1;           % Sampling interval [s]
T = dt*N;           % Total sampling time [s]
df = 1/(dt*N);      % Frequency interval [Hz]
x = randn(N,1);     % Random values
X = fft(x)*dt;      % FFT of random values.

Sxx = conj(X).*X/T; % PSD

Var = sum(conj(x).*(x))/N;  % Variance calculated from the time signal

VarPSD = sum(Sxx*df);       % Variance calculated from the PSD

RatioCheck = VarPSD/Var;    % This value should always be 1
```

**Cross-Spectral Density (CSD)**

The CSD is very similar to the PSD but deals with the relationship of the power between both signal $x(t)$ and signal $y(t)$. It is implemented in this study using:

145

$$S_{xy}(f) = \frac{1}{n_d T} \sum_{n=1}^{n_d} [X_n^*(f) Y_n(f)]. \tag{A.8}$$

**Frequency Response Function (FRF)**

The FRF is also some times referred to as a transfer function, though the FRF specifically refers to the ratio of a CSD to a PSD, whereas the transfer function is often simply the ratio of the Fourier transforms of two signals. The FRF is:

$$H(f) = \frac{S_{xy}(f)}{S_{xx}(f)}. \tag{A.9}$$

**Coherence**

The coherence is a good metric for whether the energy in an output signal is linearly related to the input signal. It is defined as:

$$\gamma_c^2 = \frac{S_{xy}^* S_{xy}}{S_{xx} S_{yy}}, \tag{A.10}$$

where $S_{yy}$ is the PSD for signal $y(x)$.

## A.3 Random Distribution Matlab Code

```matlab
a_bub = 0.006;   % radius of bubbles [m]
r1 = 1;          % radius of bubble cloud [m]
NumBub = 100;

x_bub = zeros(NumBub,3);
for ii = 1:NumBub
    k = 0;
    while k == 0;
        count = 0;
        % random point in spherical coordinates
        r = (rand)^(1/2)*r1;
        theta_pop = rand*2*pi;
        phi = acos(2*rand-1);

        % convert to cartesian coordinates
        x_bub(ii,1) = r*cos(theta_pop)*sin(phi);
        x_bub(ii,2) = r*sin(theta_pop)*sin(phi);
        x_bub(ii,3) = r*cos(phi);

        % check if new bubble is within 3 radii of other bubbles
        d = sqrt((x_bub(1:(ii-1),1)-x_bub(ii,1)).^2 + ...
            (x_bub(1:(ii-1),2)-x_bub(ii,2)).^2 + ...
            (x_bub(1:(ii-1),3)-x_bub(ii,3)).^2);
        if any(d<3*a_bub)
            count = count + 1;
            if count == 1000
                error('unable to find random position after 1000 ...
                    attempts')
            end
        else
            k = 1;
        end
    end
end
```

# Appendix B

# Elastic Waveguide Correction

The model used to describe sound propagation in a cylindrical elastic waveguide was originally derived by Del Grosso [58] and later put into a more intuitive form by Lafleur & Sheilds [59]. This model applies to an elastic cylinder of inner radius $b$ and outer radius $d$ made of a material with a compressional sound speed of $c_c$, a shear sound speed of $c_s$, and density $\rho_w$. The liquid that fills the resonator is assumed to have a sound speed $c_0$, and density $\rho_l$. The phase speed for the $m^{th}$ axisymmetric mode of the entire waveguide system is defined as $c_{0m}$. The geometry of the system is shown in Figure B.1.

Del Grosso assumed a coupled system with axisymmetric waves in both the elastic shell and the liquid. The axial $S_z^L(r, z; t)$ and radial $S_r^L(r, z; t)$ components of
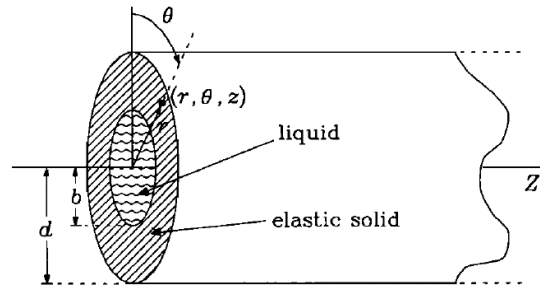


Figure B.1: Adapted from Lafleur & Sheilds [59]. Coordinate system used to define propagation in a liquid filled elastic tube.

particle displacement in the liquid are defined as:

$$S_z^{\mathrm{L}}(r,z;t) = i\phi_0 q_{0m} J_0(rX_{0m}/b)e^{i(q_{0m}z-\omega t)}, \tag{B.1a}$$

$$S_r^{\mathrm{L}}(r,z;t) = -(\phi_0 X_{0m}/b)J_1(rX_{0m}/b)e^{i(q_{0m}z-\omega t)}, \tag{B.1b}$$

and the axial $S_z^{\mathrm{W}}(r,z;t)$ and radial $S_r^{\mathrm{W}}(r,z;t)$ components of particle displacement in the wall are defined as:

$$\begin{aligned} S_z^{\mathrm{W}}(r,z;t) = \{&iq_{0m}[AJ_0(rP_m) + BY_0(rP_m)] \\ &+ T_m[CJ_0(rT_m) + DY_0(rT_m)]\}e^{i(q_{0m}z-\omega t)}, \end{aligned} \tag{B.2a}$$

$$\begin{aligned} S_r^{\mathrm{W}}(r,z;t) = \{&-P_m[AJ_1(rP_m) + BY_1(rP_m)] \\ &+ -iq_{0m}[CJ_1(rT_m) + DY_1(rT_m)]\}e^{i(q_{0m}z-\omega t)}, \end{aligned} \tag{B.2b}$$

where various wavenumbers in the system are defined as:

$$X_{0m} = b\sqrt{k_1^2 - q_{0m}^2}, \quad P_m = \sqrt{k_l^2 - q_{0m}^2}, \quad T_m = \sqrt{k_t^2 - q_{0m}^2},$$

$$q_{0m} = \omega/c_{0m}, \quad k_c = \omega/c_{\mathrm{c}}, \quad k_s = \omega/c_{\mathrm{s}}, \quad k_1 = \omega/c_0.$$

and $J_n$ and $Y_n$ are the $n^{\mathrm{th}}$ order Bessel functions of the first and second kind respectively.

The constants $\phi_0$, $A$, $B$, $C$, and $D$ are obtained from the boundary conditions. Del Grosso [58] shows that the latter four satisfy the following equations:

$$A\left(E_m J_0(dP_m) + \frac{P_m}{d}J_1(dP_m)\right) + B\left(E_m Y_0(dP_m) + \frac{P_m}{d}Y_1(dP_m)\right)$$

$$+ C \left( -i q_{0m} T_m J_0(dT_m) + i \frac{q_{0m}}{d} J_1(dT_m) \right)$$

$$+ D \left( -i q_{0m} T_m Y_0(dT_m) + i \frac{q_{0m}}{d} Y_1(dT_m) \right) = 0, \tag{B.3}$$

and

$$A \left[ i q_{0m} P_m J_1(dP_m) \right] + B \left[ i q_{0m} P_m Y_1(dP_m) \right]$$

$$+ C \left[ -E_m J_1(dT_m) \right] + D \left[ -E_m Y_1(dT_m) \right] = 0, \tag{B.4}$$

and

$$A \left[ i q_{0m} P_m J_1(bP_m) \right] + B \left[ i q_{0m} P_m Y_1(bP_m) \right]$$

$$+ C \left[ -E_m J_1(bT_m) \right] + D \left[ -E_m Y_1(bT_m) \right] = 0, \tag{B.5}$$

and

$$A \left( E_m J_0(bP_m) + \frac{1 + Q_m b}{b} P_m J_1(bP_m) \right)$$

$$+ B \left( E_m Y_0(bP_m) + \frac{1 + Q_m b}{b} Y_1(bP_m) \right)$$

$$+ C \left( -i q_{0m} T_m J_0(bT_m) + i \frac{q_{0m}}{d}(1 + Q_m b) J_1(bT_m) \right)$$

$$+ D \left( -i q_{0m} T_m Y_0(bT_m) + i \frac{q_{0m}}{d}(1 + Q_m b) Y_1(bT_m) \right) = 0, \tag{B.6}$$

where the following definitions have been used,

$$E_m = q_{0m}^2 - k_s^2/2, \qquad Q_m = \frac{\rho_l \omega^2 b J_0(X_{0m})}{2 \rho_w c_s^2 X_{0m} J_1(X_{0m})},$$

and where $\rho_w$ and $\rho_l$ are the densities of the tube wall and the liquid, respectively.

Nonzero values for the four constants, $A$, $B$, $C$, and $D$ are found by requiring the determinant of their coefficients to vanish, which results in a characteristic equation relating $q_{0m}$ to $\omega$,

$$1 + \left[ L_{11}(P_m) L_{00}(T_m) \right] \left( \frac{\pi^2 q_{0m}^2 bd P_m^2 T_m^2}{8 E_m^2} \right) + \left[ L_{11}(T_m) L_{00}(P_m) \right] \left( \frac{\pi^2 bd E_m^2}{8 q_{0m}^2} \right)$$

$$+\left[L_{10}(P_m)L_{01}(T_m) + L_{01}(P_m)L_{10}(T_m)\right]\left(\frac{\pi^2 bd P_m T_m}{8}\right)$$

$$+\left[bL_{11}(P_m)L_{10}(T_m) + d(1+Q_m b)L_{11}(P_m)L_{01}(T_m)\right]\left(\frac{\pi^2 P_m^2 T_m}{8E_m} - \frac{\pi^2 P_m^2 q_{0m}^2 T_m}{8E_m^2}\right)$$

$$+\left[bL_{11}(T_m)L_{10}(P_m) + d(1+Q_m b)L_{11}(T_m)L_{01}(P_m)\right]\left(\frac{\pi^2 P_m E_m}{8q_{0m}^2} - \frac{\pi^2 P_m}{8}\right)$$

$$+\left[(1+Q_m b)L_{11}(T_m)L_{11}(P_m)\right]\left(\frac{\pi^2 P_m^2}{8q_{0m}^2} + \frac{\pi^2 P_m^2 q_{0m}^2}{8E_m^2} - \frac{\pi^2 P_m^2}{4E_m}\right) = 0, \qquad \text{(B.7)}$$

where $L_{mn}(\xi) = J_m(d\xi)Y_n(b\xi) - J_n(b\xi)Y_m(d\xi)$.

Values of $c_{0m}$ that satisfy Equation (B.7) result in propagating modes. In practice $c_{0m}$ is varied until Equation (B.7) is satisfied in order to determine the phase speed in the system.

# Appendix C

# Resonator Model Derivation

This is an appendix detailing the derivation of the analytical resonator model used in this study. This model predicts the acoustic field in of an N-layers fluid medium excited by a plane acoustic wave normal to the layers. A diagram of the model theory is presented in Figure C.1. There is a reflected wave from the incident wave hitting the first layer, a forward and backward traveling wave in each intermediate layer, and the last layer is assumed to be an acoustic half-space. The originating half space has a sound speed $c_0$ and density $\rho_0$ and each subsequent layer has a sound speed $c_n$ and density $\rho_n$ for the remaining $N$ layers. Each layer also has an associated wavenumber $k_n = \omega/c_n$. The waves in the first half space and last half space are taken to be:
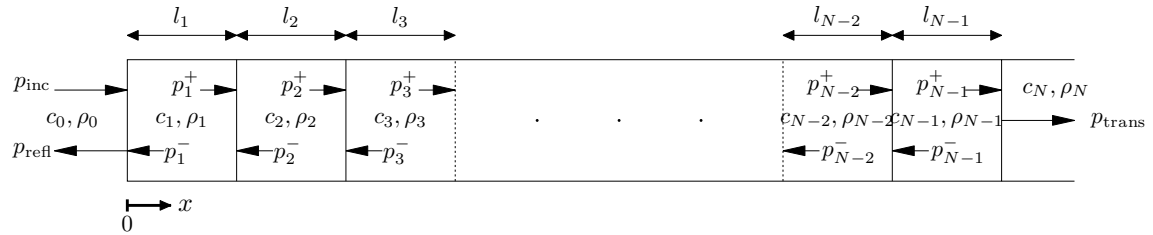


Figure C.1: Naming convention for $N$-layered resonator model

$$p_{\text{inc}} = e^{j(\omega t - k_0 x)}, \tag{C.1}$$

and

$$p_{\text{refl}} = R e^{j(\omega t + k_0 x)}. \tag{C.2}$$

The remaining expressions for layers 1 through $N-1$ are:

$$p_n^+ = A_n^+ e^{j(\omega t - k_n x)}, \tag{C.3}$$

$$p_n^- = A_n^- e^{j(\omega t + k_n x)}, \tag{C.4}$$

and for layer $N$,

$$p_{\text{trans}} = T e^{j(\omega t - k_n x)}. \tag{C.5}$$

At the first boundary, continuity of pressure and particle velocity yield:

$$1 + R = A_1^+ + A_1^-, \tag{C.6a}$$

$$\frac{1}{Z_0} - \frac{R}{Z_0} = \frac{A_1^+}{Z_1} - \frac{A_1^-}{Z_1}, \tag{C.6b}$$

where $Z_n = c_n \rho_n$ is the acoustic impedance of each layer. The boundary conditions for the interfaces between layer 1 through $N-1$ result in:

$$A_n^+ e^{-jk_n l_n} + A_n^- e^{jk_n l_n} = A_{n+1}^+ + A_{n+1}^-, \tag{C.7a}$$

$$\frac{A_n^+ e^{-jk_n l_n}}{Z_n} - \frac{A_n^- e^{jk_n l_n}}{Z_n} = \frac{A_{n+1}^+}{Z_{n+1}} - \frac{A_{n+1}^-}{Z_{n+1}}, \tag{C.7b}$$

and the relations for the final boundary are:

$$A_{N-1}^+ e^{-jk_{N-1} l_{N-1}} + A_{N-1}^- e^{jk_{N-1} l_{N-1}} = T, \tag{C.8a}$$

$$\frac{A_{N-1}^+ e^{-jk_{N-1} l_{N-1}}}{Z_{N-1}} - \frac{A_{N-1}^- e^{jk_{N-1} l_{N-1}}}{Z_{N-1}} = \frac{T}{Z_N}. \tag{C.8b}$$

Equations C.6, C.7, and C.8 can be arranged into matrix equations:

$$\begin{bmatrix} 1 & 1 \\ \frac{1}{Z_0} & -\frac{1}{Z_0} \end{bmatrix} \begin{bmatrix} 1 \\ R \end{bmatrix} = \begin{bmatrix} 1 & 1 \\ \frac{1}{Z_1} & -\frac{1}{Z_1} \end{bmatrix} \begin{bmatrix} A_1^+ \\ A_1^- \end{bmatrix}, \tag{C.9a}$$

$$\begin{bmatrix} e^{-jk_n l_n} & e^{jk_n l_n} \\ \frac{e^{-jk_n l_n}}{Z_n} & -\frac{e^{jk_n l_n}}{Z_n} \end{bmatrix} \begin{bmatrix} A_n^+ \\ A_n^- \end{bmatrix} = \begin{bmatrix} 1 & 1 \\ \frac{1}{Z_{n+1}} & -\frac{1}{Z_{n+1}} \end{bmatrix} \begin{bmatrix} A_{n+1}^+ \\ A_{n+1}^- \end{bmatrix}, \tag{C.9b}$$

$$\begin{bmatrix} e^{-jk_{N-1} l_{N-1}} & e^{jk_{N-1} l_{N-1}} \\ \frac{e^{-jk_{N-1} l_{N-1}}}{Z_{N-1}} & -\frac{e^{jk_{N-1} l_{N-1}}}{Z_{N-1}} \end{bmatrix} \begin{bmatrix} A_{N-1}^+ \\ A_{N-1}^- \end{bmatrix} = \begin{bmatrix} 1 \\ \frac{1}{Z_N} \end{bmatrix} T. \tag{C.9c}$$

The system can then be reduced to:

$$\begin{bmatrix} 1 \\ R \end{bmatrix} = I \left( \prod_{n=1}^{N-1} M_n \right) FT, \tag{C.10}$$

where,

154

$$I = \begin{bmatrix} 1 & 1 \\ \frac{1}{Z_0} & -\frac{1}{Z_0} \end{bmatrix}^{-1} \begin{bmatrix} 1 & 1 \\ \frac{1}{Z_1} & -\frac{1}{Z_1} \end{bmatrix} \tag{C.11a}$$

$$M_n = \begin{bmatrix} e^{-jk_n l_n} & e^{jk_n l_n} \\ \frac{e^{-jk_n l_n}}{Z_n} & -\frac{e^{jk_n l_n}}{Z_n} \end{bmatrix}^{-1} \begin{bmatrix} 1 & 1 \\ \frac{1}{Z_{n+1}} & -\frac{1}{Z_{n+1}} \end{bmatrix} \tag{C.11b}$$

$$F = \begin{bmatrix} e^{-jk_{N-1} l_{N-1}} & e^{jk_{N-1} l_{N-1}} \\ \frac{e^{-jk_{N-1} l_{N-1}}}{Z_{N-1}} & -\frac{e^{jk_{N-1} l_{N-1}}}{Z_{N-1}} \end{bmatrix}^{-1} \begin{bmatrix} 1 \\ \frac{1}{Z_N} \end{bmatrix}. \tag{C.11c}$$

Equation C.10 can be solved for $T$ and $R$, then Equations C.9c and C.9b can be used to find each $A_n^+$ and $A_n^-$.

# Appendix D

# Full Scattering Model

This appendix details the solution of the full scattering problem as described at the beginning of Foldy's 1945 paper [74]. This model assumes that each scatterer is affected by the incident field and the scattered field from every other scatterer. Each scatterer experiences a velocity potential $\psi_i$ consisting of the incident field and the radiated field from every other scatterer, where $i$ represents the $i^{\text{th}}$ scatterer. The velocity potential that drives each scatterer can then be represented as:

$$\psi_i = \psi_0(\vec{r}_i) + \sum_{h \neq i} g_h \psi_h \frac{\exp(-jk_0|\vec{r}_i - \vec{r}_h|)}{|\vec{r}_i - \vec{r}_h|}, \tag{D.1}$$

where $\psi_0(\vec{r})$ is the incident field at the position in space $\vec{r}$, $\vec{r}_i$ is the location of the $i^{\text{th}}$ scatterer, $k_0$ is the wavenumber in the host medium, and $g_i$ is the scattering coefficient for the $i^{\text{th}}$ scatterer as presented in Equation 3.23. For $N$ scatterers with equivalent scattering coefficients $g$, this can be represented in matrix form as:

$$\begin{bmatrix} \psi_1 \\ \psi_2 \\ \vdots \\ \psi_N \end{bmatrix} = \begin{bmatrix} \psi_0(\vec{r}_1) \\ \psi_0(\vec{r}_2) \\ \vdots \\ \psi_0(\vec{r}_N) \end{bmatrix} + g \begin{bmatrix} 0 & E(\vec{r}_1, \vec{r}_2) & \cdots & E(\vec{r}_1, \vec{r}_N) \\ E(\vec{r}_2, \vec{r}_1) & 0 & \cdots & E(\vec{r}_2, \vec{r}_N) \\ \vdots & & \ddots & \vdots \\ E(\vec{r}_N, \vec{r}_1) & \cdots & E(\vec{r}_N, \vec{r}_{N-1}) & 0 \end{bmatrix} \begin{bmatrix} \psi_1 \\ \psi_2 \\ \vdots \\ \psi_N \end{bmatrix}, \tag{D.2}$$

where $E(\vec{r}_1, \vec{r}_2)$ accounts for the finite phase and amplitude difference from the acoustic wave traveling between the $i^{\text{th}}$ and $h^{\text{th}}$ scatterer, and is defined as:

$$E(\vec{r}_i, \vec{r}_h) = \frac{\exp(-jk_0|\vec{r}_i - \vec{r}_h|)}{|\vec{r}_i - \vec{r}_h|}. \tag{D.3}$$

This system of equations can be rearranged in order to solve explicit for $\psi_i$:

$$\begin{bmatrix} \psi_0(\vec{r}_1) \\ \psi_0(\vec{r}_2) \\ \vdots \\ \psi_0(\vec{r}_N) \end{bmatrix} = \begin{bmatrix} 1 & -E(\vec{r}_1, \vec{r}_2) & \cdots & -E(\vec{r}_1, \vec{r}_N) \\ -E(\vec{r}_2, \vec{r}_1) & 1 & \cdots & -E(\vec{r}_2, \vec{r}_N) \\ \vdots & & \ddots & \vdots \\ -E(\vec{r}_N, \vec{r}_1) & \cdots & -E(\vec{r}_N, r_{N-1}) & 1 \end{bmatrix} \begin{bmatrix} \psi_1 \\ \psi_2 \\ \vdots \\ \psi_N \end{bmatrix}. \tag{D.4}$$

Once $\psi_i$ is known, the total field $\psi_{\text{total}}(\vec{r})$ at the location $\vec{r}$ can be determined by the sum of the incident field and the scattered field:

$$\psi_{\text{total}} = \psi_0(\vec{r}) + g \begin{bmatrix} E(\vec{r}_1, \vec{r}) & E(\vec{r}_2, \vec{r}) & \cdots & E(\vec{r}_N, \vec{r}) \end{bmatrix} \begin{bmatrix} \psi_1 \\ \psi_2 \\ \vdots \\ \psi_N \end{bmatrix}. \tag{D.5}$$

Here is the code used to implement this model:

```
function [p_tot, p_0] = FSBubble(fVec,c,rho,sigma,a_bub,p_bub,x_bub,...
    x_rec,varargin)

% This code solves the full-scattering problem for an known ...
    configuration
% of bubbles by jointly solving for the interacting scattered ...
    fields of
% each bubble. By default the source is spherical and at the origin.
%
% [p_tot, p_0] = ...
    FSBubble(c,fVec,rho,sigma,x_bub,a_bub,x_rec,p_bub,options)
```

```
%
% Outputs:
% p_tot       - The resultant pressure field froms source and ...
%    scatterers [Pa]
% p_0         - The source pressure signal [Pa]
%
% Inputs:
% fVec        - Frequency vector [Hz]
% c           - Speed of sound in liquid absent of scatterers [m/s]
% rho         - Density of liquid absent of scatterers [kg/m^3]
% sigma       - Bubble surface tension [N/m]
% a_bub       - Radius of bubbles (mono-disperse population) [m]
% p_bub       - Static pressure at bubbles [Pa]
% x_bub       - Locations of bubbles in cartesian coordinates,
%                   eg. [x(:,1); x(:,2); x(:,3)] = [x; y; z] [m; m;m]
% x_rec       - Locations of receivers in cartesian coordinates [m; ...
%    m; m]
%
% Options:
%
% 'Church'
% Utilizes the scattering coefficient for a bubble with an elastic ...
%    shell
% from Church's 1995 effective medium model.
% FSBubble(c,fVec,rho,sigma,x_bub,a_bub,x_rec,p_bub,...
%       'Church',t,Gs,mus,rhos,sigma2))
%
% Additional Inputs:
% t           - Shell thickness [m]
% Gs          - Shear modulus of the shell [Pa]
% mus         - Shell viscosity [N s/m^2]
% rhos        - Density of shell [kg/m^3]
% simga2      - Suface tension between shell and liquid [N/m]
%
% 'PlaneWave'
% Uses a plane wave as a source as opposed to a spherical source at the
% origin.
% FSBubble(c,fVec,rho,sigma,x_bub,a_bub,x_rec,p_bub,...
%       'PlaneWave',sVec))
%
% Additional Inputs:
% sVec        - Cartesian vector determining the direction of the source.
%                   eg. vector normal to planes of constant phase [m]
%
% Record of revisions:
```

158

```matlab
%       Date         Programmer           Description of change
%       ====         ==========           =====================
%    13-Mar-2014   Craig N. Dolder      Initial programming
%
% Features to add:
% Polydisperse bubble parameters.
% Images from ideal reflection (surface)
%
% Citations:
%
% L. L. Foldy, Physical Rev., 67 (3), 107-119 (1945)
% A. Prosperetti, J. Acoust. Soc. Am. 61, 17-27 (1977)
% K. Commander, A. Prosperetti, J. Acoust. Soc. Am. 85, 732-746 (1989)
% C. Church, J. Acoust. Soc. Am. 97, 1510-1521 (1995)

arg = 9;
while arg ≤ nargin
    if strcmp(varargin{arg-8},'Church')
        t = varargin{arg+1-8};
        Gs = varargin{arg+2-8};
        mus = varargin{arg+3-8};
        rhos =  varargin{arg+4-8};
        sigma2 = varargin{arg+5-8};
        arg = arg+6;
    elseif strcmp(varargin{arg-8},'PlaneWave')
        sVec = varargin{arg+1-8};
        arg = arg+2;
    else
        error('Unknown input')
    end
end

gamma = 1.4; % Ratio of specific heat in air
mul = 0.001; % Liquid visocity in Pa s
D=2e-5; % Thermal diffusivity of air in m^2/s
omega = 2*pi*fVec;
k = omega./c;

% Number of bubbles
[N, ¬] = size(x_bub);

% Number of receivers
[M, ¬] = size(x_rec);

% Initialize variables
```

```matlab
p_0 = zeros(M,length(fVec),1);
p_tot = zeros(M,length(fVec),1);
%% Solve problem for each frequency
for ii = 1:length(fVec)
    % Damping of a bubble at frequency ii
        chi = D./(omega(ii).*a_bub.^2);      % Variable in phi
        phi = (3.*gamma)./(1-3.*(gamma-1).*1i.*chi.*...
            ((1i./chi).^0.5 .* coth((1i./chi).^0.5) - 1));
        p_stat = p_bub + 2*sigma./a_bub;
        kappa = real(phi)/3; %effective polytropic index
        muth = 0.25.*p_stat.*imag(phi)./omega(ii);

    % If there is no shell use parameters from C&P
    if exist('t','var') == 0
        % Thermal viscosity from  Propseretti, Crum, Commannder ...
            JASA(1989)

        omega_0 = ((1./(rho*a_bub.^2)).*...
            (3*kappa.*p_stat-2*sigma./a_bub)).^(1/2);

        b_vis = 4*mul./(rho*a_bub.^2.*omega(ii));
        b_th = 4*muth./(rho*a_bub.^2.*omega(ii));
        b_rad = a_bub.*omega(ii)./c;
        b = b_vis + b_th + b_rad;

        % Scattering coefficient of individual bubbles
        g = a_bub./(((omega_0./omega(ii)).^2 - 1) - 1i*b);
    else % If there is a sheel use parameters for Church
        aleph = 1 + ((rho-rhos)./rhos).*a_bub./(a_bub+t); % Church ...
            Eq. 18a
        Vs = (a_bub+t).^3 - a_bub.^3;          % Church after Eq. 12
        Z = (2.*sigma./a_bub+2.*sigma2./(a_bub+t)).*...
            ((a_bub+t).^3./Vs).*(4.*Gs).^(-1);

        omega_0 = (1./(rhos.*a_bub.^2.*aleph).*...
            (3*kappa.*p_stat-2*sigma./a_bub-...
            2*sigma2.*a_bub.^3./(a_bub+t).^4 + ...
            4.*Vs.*Gs./(a_bub+t).^3.*...
            (1+Z.*(1+3.*a_bub.^3./(a_bub+t).^3)))).^(1/2);

        b_visL = 4*a_bub.^3.*mul./(a_bub+t).^3.*...
            (rhos.*a_bub.^2.*aleph.*omega(ii)).^(-1);
        b_visS = 4*Vs.*mus./(a_bub+t).^3 .*...
            (rhos.*a_bub.^2.*aleph.*omega(ii)).^(-1);
        b_th = 4*(muth).*(rhos.*a_bub.^2.*aleph.*omega(ii)).^(-1);
```

160

```matlab
    b_rad = omega(ii).*(a_bub+t)./(c).*...
        (1+(omega(ii).*(a_bub+t)./c).^2).^(-1);

    b = b_visL + b_visS + b_th + b_rad;

    g = a_bub./(((omega_0./omega(ii)).^2 - 1) - 1i*b);
end

%% Phase Matrix
% Matrix of the distance from each bubble to every other bubble
dMat(:,:,1) = x_bub(:,1)*ones(1,N) - ones(N,1)*x_bub(:,1).';
dMat(:,:,2) = x_bub(:,2)*ones(1,N) - ones(N,1)*x_bub(:,2).';
dMat(:,:,3) = x_bub(:,3)*ones(1,N) - ones(N,1)*x_bub(:,3).';
rMat = sqrt(dMat(:,:,1).^2+dMat(:,:,2).^2+dMat(:,:,3).^2);

PhaseMat = exp(1i*k(ii)*rMat)./rMat;

% Ensure that the diagonal elements are zero
PhaseMat(PhaseMat==Inf) = 0;

% If point source, compute incomming field for every bubble ...
    position
if exist('sVec','var') == 0
    r_0 = sqrt(x_bub(:,1).^2+x_bub(:,2).^2+x_bub(:,3).^2);
    p_i = exp(1i*k(ii)*r_0)./r_0;
% If plane source, compute incomming field for every bubble ...
    position
else
    % Ensure source vector is a unit vector;
    sVec = sVec/sqrt(sVec(1).^2+sVec(2).^2+sVec(3).^2);
    % Compute distance from plane of constant phase at origin,
    % which is the dot product of the vectors.
    r_0 = x_bub(:,1)*sVec(1) + x_bub(:,2)*sVec(2) + ...
        x_bub(:,3)*sVec(3);
    % Then the source signal is simply the phase difference.
    p_i = exp(1i*k(ii)*r_0);
end

% Identity matrix minus the scattering coeffeicient, phase and
% amplitude difference
ScatMat = eye(N) - diag(g)*PhaseMat;

A = diag(g)*(ScatMat\p_i).';

% Compute the scattered field at the receiver position
```

```matlab
    d_rec(:,:,1) = x_bub(:,1)*ones(1,M)-ones(N,1)*x_rec(:,1).';
    d_rec(:,:,2) = x_bub(:,2)*ones(1,M)-ones(N,1)*x_rec(:,2).';
    d_rec(:,:,3) = x_bub(:,3)*ones(1,M)-ones(N,1)*x_rec(:,3).';
    r_rec = sqrt(d_rec(:,:,1).^2+d_rec(:,:,2).^2+d_rec(:,:,3).^2);
    Phase_rec = exp(1i*k(ii)*r_rec)./r_rec;

    % If point source, compute source field at each receiver
    if exist('sVec','var') == 0
        r_srec = sqrt(x_rec(:,1).^2+x_rec(:,2).^2+x_rec(:,3).^2);
        p_0(:,ii) = exp(1i*k(ii)*r_srec)./r_srec;
    % If plane source, compute source field at each receiver
    else
        % Compute distance from plane of constant phase at origin,
        % which is the dot product of the vectors.
        r_srec = ...
            x_rec(:,1)*sVec(1)+x_rec(:,2)*sVec(2)+x_rec(:,3)*sVec(3);
        % Then the source signal is simply the phase difference.
        p_0(:,ii) = exp(1i*k(ii)*r_srec);
    end

    % Scattered field from each of the bubbles at the receiver position
    p_rec = diag(A)*Phase_rec;
    % Total field is the sum of the source field and the scattered ...
        field
    p_tot(:,ii) = p_0(:,ii) + sum(p_rec).';

end
```

# Appendix E

# Reflection Effective Medium Theory Model

This model consists of a sphere of effective medium with sound speed $c_1$ and density $\rho_1$ with a small source at the center with a transmitted wave traveling away from the effective medium into a space with sound speed $c_2$ and density $\rho_2$, as shown in Figure E.1. The source is assumed to have a radius $a_s$ and the effective medium sphere a radius of $a_1$. All waves are assumed to be spherically symmetric. Three waves are considered, the outgoing $p_{\text{out}}$ and incoming $p_{\text{in}}$ waves between the source and the outer radius of the effective medium and a transmitted wave $p_{\text{tr}}$:

$$p_{\text{out}} = A\frac{a_1}{r}e^{j(\omega t - k_1(r-a_1))}, \tag{E.1a}$$

$$p_{\text{in}} = B\frac{a_1}{r}e^{j(\omega t + k_1(r-a_1))}, \tag{E.1b}$$

$$p_{\text{tr}} = C\frac{a_1}{r}e^{j(\omega t - k_2(r-a_1))}. \tag{E.1c}$$

where $k_1 = \omega/c_1$ and $k_2 = \omega/c_2$. The acoustical impedance seen by an outgoing spherical acoustic wave is:

$$Z_{\text{out}} = \rho_0 c_0 \frac{jkr}{1 + jkr}, \tag{E.2}$$

and for an incoming spherical waves is:
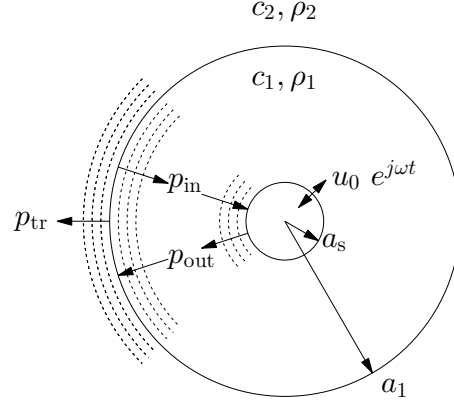
Figure E.1: Geometry for the reflection effective medium theory model

$$Z_{\text{in}} = \rho_0 c_0 \frac{jkr}{1 - jkr}. \tag{E.3}$$

There are three boundary conditions that have to be met.

1. Continuity of pressure at $r_1$: $p_{\text{out}} + p_{\text{in}} = p_{\text{tr}}|_{r=a_1}$

2. Continuity of particle velocity at $r_1$: $u_{\text{out}} + u_{\text{in}} = u_{\text{tr}}|_{r=a_1}$

3. Continuity of particle velocity at $a_{\text{s}}$: $u_{\text{out}} + u_{\text{in}} = u_0 e^{j\omega t}|_{r=a_1}$

After applying the impedance relations these the boundary conditions produce the relations:

$$A + B = C, \tag{E.4a}$$

$$A\left(\frac{1 + jk_1 a_1}{jk_1 a_1 \rho_1 c_1}\right) + B\left(\frac{1 - jk_1 a}{jk_1 a_1 \rho_1 c_1}\right) = C\left(\frac{1 + jk_2 a_1}{jk_2 a_1 \rho_2 c_2}\right), \tag{E.4b}$$

$$A\frac{1 + jk_1 a_{\text{s}}}{jk_1 a_{\text{s}} \rho_1 c_1}\frac{a_1}{a_{\text{s}}}e^{-jk_1(a_s - a_1)} + B\frac{1 - jk_1 a_{\text{s}}}{jk_1 a_{\text{s}} \rho_1 c_1}\frac{a_1}{a_{\text{s}}}e^{jk_1(a_s - a_1)} = u_0 \tag{E.4c}$$

164

After defining $B/A = R$ and $C/A = T$, Equations E.4a and E.4b can be solved to yeild:

$$R = \frac{(1 - Z_1/Z_2) - j\alpha_1(1 - \rho_1/\rho_2)}{(1 + Z_1/Z_2) + j\alpha_1(1 - \rho_1/\rho_2)}, \tag{E.5}$$

where $Z_1 = \rho_1 c_1$, $Z_2 = \rho_2 c_2$, and $\alpha_1 = 1/k_1 a_1$. $T$ is then:

$$T = 1 + \frac{(1 - Z_1/Z_2) - j\alpha_1(1 - \rho_1/rho_2)}{(1 + Z_1/Z_2) + j\alpha_1(1 - \rho_1/rho_2)}. \tag{E.6}$$

Now Equation E.4c can be used to solve for $A$, yielding:

$$A = \frac{jk_1 a_s^2 Z_1 u_0}{a_1}\left((1 + jk_1 a_s)e^{-jk_1(a_s - a_1)} + R(1 - jk_1 a_s)e^{jk_1(a_s - a_1)}\right)^{-1}. \tag{E.7}$$

The transmitted field can not be expressed as:

$$p_{\text{tr}} = AT\frac{a_1}{r}e^{j(\omega t - k_2(r - a_1))}, \tag{E.8}$$

and can be compared to what the field would be if no effective medium sphere were present:

$$p_{\text{No EM}} = u_0 Z_2 \frac{(jk_2 a_s^2)}{(a_1(1 + jk_2 a_s))}\frac{e^{(-jk_2(r - a_s))}}{r}. \tag{E.9}$$

# Appendix F

# Code Verifications

## F.1   Complete Model for Bubbles Without a Shell

This section compares curves generated with the code used in this work to Commander and Prosperetti's model for a bubble without a shell, Ref. [46]. Figures F.1 and F.2 are for a mono-disperse collection of air bubbles in water with a volume fraction of air $\chi = 0.000377$ and a radius of $a = 0.000994$ m.
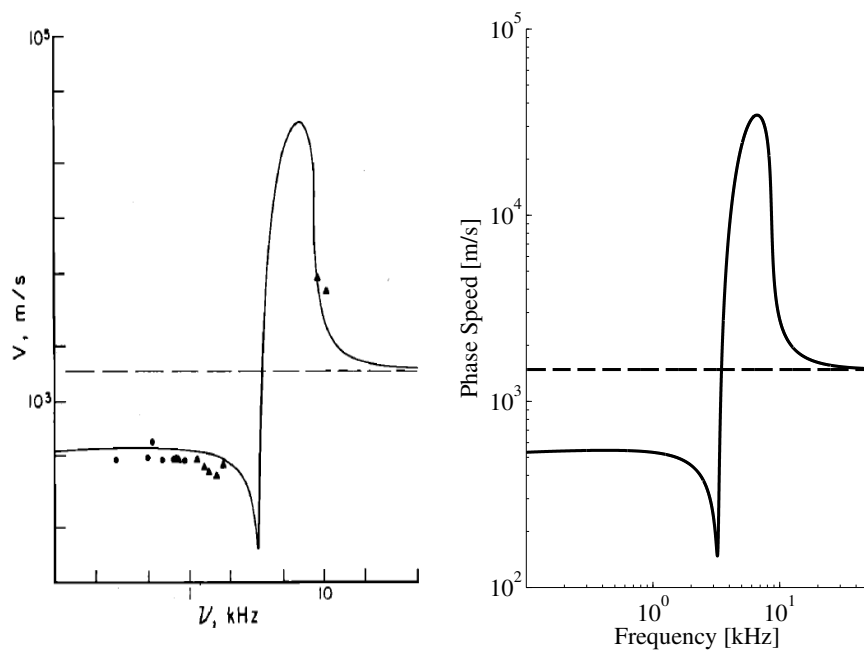
Figure F.1: Left: Adapted from Figure 8 of Commander and Prosperetti [46]. Right: Curves generated with same input parameters.
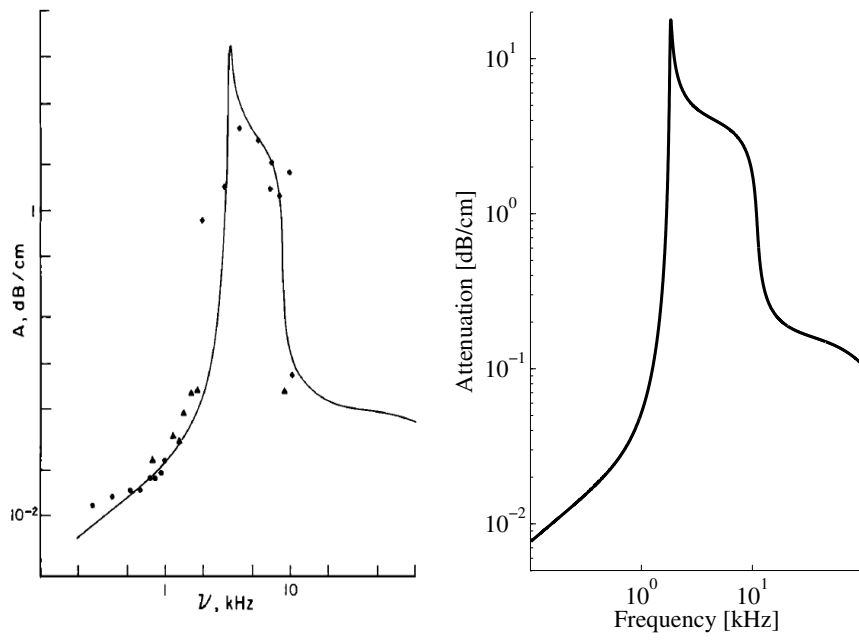
Figure F.2: Left: Adapted from Figure 1 of Commander and Prosperetti [46]. Right: Curves generated with same input parameters.

## F.2 Model for bubbles with an elastic shell

This section compares curves generated with the code used in this work to the shelled bubble model by Church [131]. Because Church's sound speed and attenuation curves are generated from an experimental bubble distribution, an attempt was made to duplicate these plots by pulling points from Figure 12 of Church [131]. The results shown in Figures F.4 and F.5.
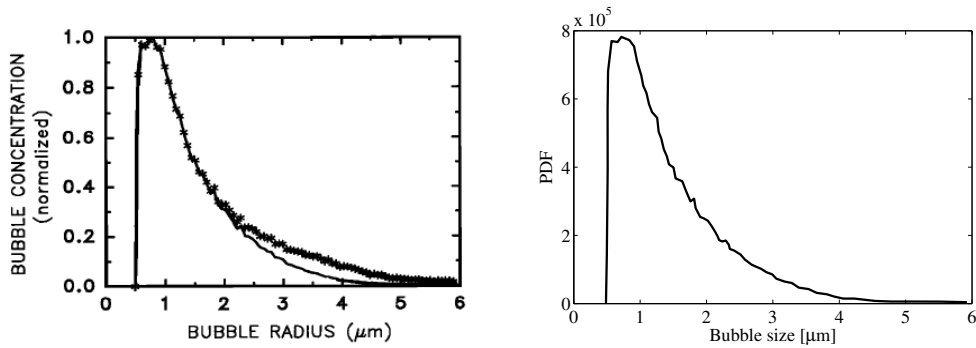


Figure F.3: Left: Adapted from Figure 12 of Church [131], distribution of bubble sizes. Right: PDF generated from plot on left.
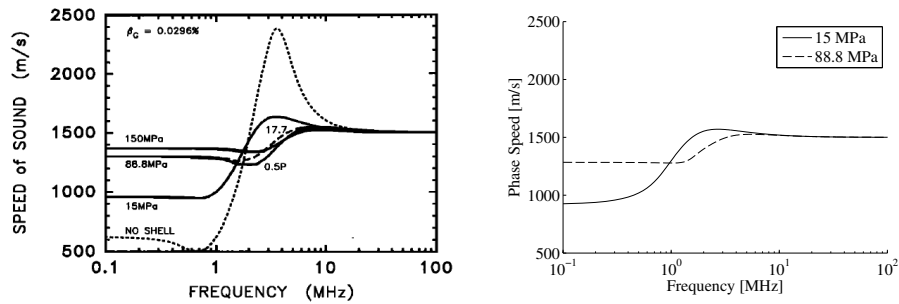


Figure F.4: Left: Adapted from Figure 13 of Church [131]. Right: Curves generated with same input parameters.

169
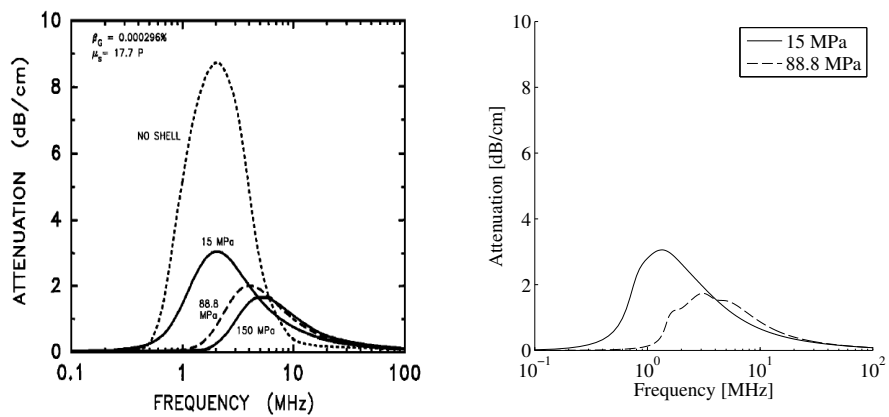
Figure F.5: Left: Adapted from Figure 19 of Church [131]. Right: Curves generated with same input parameters.

## F.3    Multiple Scattering with Bubble Shielding

This section compares curves generated with the code used in this work to Feuillade's paper on multiply interacting bubbles [12].
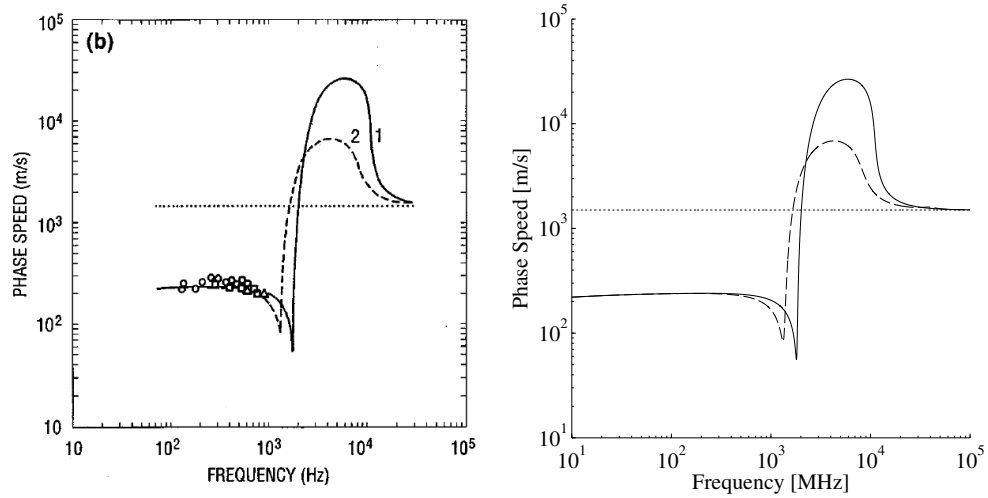


Figure F.6: Left: Adapted from Figure 6 of Feuillade [12]. Right: Curves generated with same input parameters.
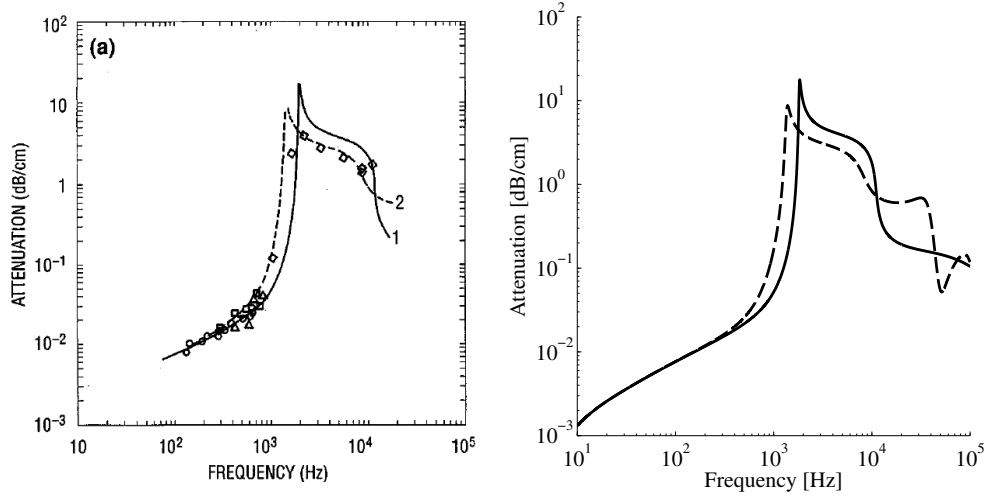
Figure F.7: Left: Adapted from Figure 6 of Feuillade [12]. Right: Curves generated with same input parameters.

# Appendix G

# Physical Constants and Balloon Positions

## G.1  Physical Constants

Physical constants needed in this dissertation are tabulated here.

| Length of resonator | $L$ | 1.985 m |
|---|---|---|
| Compressional sound speed in wall | $c_\mathrm{c}$ | 6420 m/s |
| Shear sound speed in wall | $c_\mathrm{s}$ | 3205 m/s |
| Density of wall | $\rho$ | 2700 kg/m$^3$ |
| Inner radius | $b$ | 0.1015 m |
| Outer radius | $d$ | 0.1085 m |
| Length of foam layer | $l$ | 0.145 m |

Table G.1: Material properties of the aluminum resonator.

| Sound speed in water | $c_1$ | 1481 m/s |
|---|---|---|
| Density of water | $\rho_w$ | 998.2 kg/m$^3$ |
| Sound speed in air | $c_a$ | 343 m/s |
| Density of air | $\rho_a$ | 1.210 kg/m$^3$ |
| Sound speed in foam | $c_f$ | 717 m/s |
| Density of foam | $\rho_f$ | 29 kg/m$^3$ |
| Sound speed in concrete | $c_c$ | 3100 m/s |
| Density of concrete | $\rho_c$ | 2600 kg/m$^3$ |
| Atmospheric pressure | $p_0$ | 101325 Pa |
| Dynamic viscosity of water | $\mu$ | $1.002 \times 10^{-3}$ Pa s |

Table G.2: Physical properties

| $x$ [m] | $y$ [m] | $z$ [m] |
| --- | --- | --- |
| 0.92964 | 0 | 0.254 |
| 0.19812 | 0 | 1.03124 |
| 0.70104 | 0.3048 | 1.04648 |
| 1.2192 | 0.41656 | 0.31496 |
| 1.0668 | 0.81788 | 0.35306 |
| 1.2192 | 0.9906 | 0.9017 |
| 0.41148 | 0.99695 | 0.23622 |
| 0.9144 | 1.30175 | 0.2413 |
| 0.28956 | 1.30175 | 0.98298 |
| 0 | 0.8763 | 0.19304 |
| 0.1778 | 0.76962 | 0.8128 |
| 0 | 0.41402 | 0.80518 |
| 1.03124 | 0.80264 | 0.04572 |
| 0.14732 | 0.54356 | 0.04572 |

Table G.3: Balloon positions for "Random" configuration.

## G.2   Balloon Positions

Balloon Positions for work presented in Chapter 4 are presented here.

| $x$ [m] | $y$ [m] | $z$ [m] |
|---------|---------|---------|
| 1.1684 | 0 | 1.19888 |
| 0.5842 | 0 | 0.56134 |
| 0.0508 | 0.0508 | 0.08636 |
| 1.2192 | 1.2065 | 1.13538 |
| 1.2192 | 0.6858 | 0.66802 |
| 1.2192 | 0.04318 | 0.0508 |
| 0.04572 | 1.30175 | 1.19888 |
| 0.64262 | 1.30175 | 0.58674 |
| 1.1684 | 1.24968 | 0.0762 |
| 0 | 0.16256 | 1.03632 |
| 0 | 0.70104 | 0.4445 |
| 0 | 1.2446 | 0.04572 |
| 0.56642 | 0.68326 | 0 |
| 0.6096 | 0.65024 | 1.22682 |

Table G.4: Balloon positions for "Quasi-FCC" configuration.

| $x$ [m] | $y$ [m] | $z$ [m] |
|---------|---------|---------|
| 0.6096 | 0.3048 | 0.94742 |
| 0.5842 | 0 | 0.56134 |
| 1.17348 | 0.0508 | 0.0762 |
| 1.2192 | 1.2065 | 1.13538 |
| 1.2192 | 0.6858 | 0.66802 |
| 1.0668 | 0.63754 | 0.3937 |
| 0.66294 | 1.30175 | 0.59436 |
| 0.6223 | 0.99695 | 0.9652 |
| 0 | 1.2446 | 0.04572 |
| 0 | 0.16256 | 1.03632 |
| 0 | 0.70104 | 0.4445 |
| 0.1778 | 0.70104 | 0.22098 |
| 0.56642 | 0.68326 | 0 |
| 0.6096 | 0.65024 | 1.22682 |

Table G.5: Balloon positions for "Dense" configuration.

# Appendix H

# Sound Propagation in Bubbly Liquids Publication Timeline

T - Theoretical Papers | E - Experimental Papers | R - Review Papers

1910, Dec - Mallock - The Damping by Frothy Liquids [65] (T)

1930, xxx - Wood - A Textbook of Sound [66] (T)

1930, May - Herzfeld - Propagation of Sound in Suspensions [67] (T)

1933, xxx - Minnaert - On Musical Air-Bubbles and the Sounds of Running Water [69] (E T)

1943, Sep - Kennard - Radial Motion of Water Surrounding a Sphere or Gas in Relation to Pressure Waves [70] (T)

1943, xxx - Spitzer - Acoustic Properties of Gas Bubbles in a Liquid [71] (T)

1945, Feb - Foldy - The Multiple Scattering of Waves [74] (T)

1946, xxx - Wildt Ed. - Acoustic Theory of Air Bubbles - Physics of Sound in the Sea [75] (T)

1947, May - Cartensen and Foldy - Propagation of Sound Through a Liquid Containing Bubbles [76] (E)

1947, Nov - Urick - A Sound Velocity Method for Determining the Compressibility of Finely Divided Substances [77] (E)

1949, Mar - Urick and Ament - The Propagation of Sound in Composite Media [78] (T)

1953, xxx - Meyer und Skudrzyk - Uber die akustishen eigensschaften von gasblasenschleiern in wasser [79] (T)

1953, xxx - Exner and Hampe - Experimental Determination of the Damping of Pulsating Air Bubbles in Water [80] (E)

1954, May - Chambré - Speed of a Plane Wave in a Gross Mixture [127] (T)

1954, xxx - Strasberg - Concerning the Article by M,L. Exner and W. Hampe [81] (T)

1955, May - Fox, Curley, and Larson - Phase Velocity and Absorption Measurements in Water Containing Air Bubbles [82] (E)

1957, Sep - Silberman - Sound Velocity and Attenuation in Bubbly Mixtures Measured in Standing Wave Tubes [83] (E)

1957, xxx - Macpherson - The Effect of Gas Bubbles on Sound Propagation in Water [84] (E)

1959, Dec - Devin Jr. - Survey of Thermal, Radiation, and Viscous Damping of Pulsating Air Bubbles in Water [23] (R)

1961, Aug - Hsieh and Plesset - On the Propagation of Sound in a Liquid Containing Gas Bubbles [85] (T)

1961, Nov - Hsieh and Plesset - Theory of the Acoustics Absorption by a Gas Bubble in a Liquid [86] (T)

1969, Nov - Crespo - Sound and Shock Waves in Liquids Containing Bubbles [87] (T)

1967, Dec - Zabolotskaya and Soluyan - A Possible Approach to the Amplification of Sound Waves [88] (T)

1968, xxx - Wijngaarden - On the equations of motion for mixtures of liquid and gas bubbles [89] (T)

1969, xxx - Batchelor - Compression Waves in a Suspension of Gas Bubbles in Liquid [90] (T)

1969, Sep - McWilliam and Duggins- Speed of sound in bubbly liquids [91] (T)

1970, Feb - Eller - Damping Constants of Pulsating Bubbles [92] (T)

1972, Sep - Chapman and Plesset - Thermal Effects in the Free Oscillations of Gas Bubbles [95] (T)

1972, xxx - Wijngaarden - One-dimensional flow of liquids conatining small gas bubbles [94] (R)

1973, Mar - Zabolotskaya and Soluyan - Emission of Harmonic and Combination-Frequency Waves by Air Bubbles [140] (T)

1975, Sep - Fairbank Jr. - Damping constants for nonresonant bubbles [93] (T)

1977, Jan - Properetti - Application of the subharmonic threshold to the measurement of the damping of oscillating gas bubbles [96] (T)

1977, Jan - Properetti - Thermal effects and damping mechanisms in the forces radial oscillations of gas bubbles in liquids [97] (T)

179

1977, Jul - Kieffer - Sound Speed in Liquid-Gas Mixtures: Water-Air and Water-Steam [98] (T)

1977, xxx - Clay and Medwin - Acoustical Oceanography [141] (R)

1978, Mar - SA. Bedford and D. S. Drumheller - A variational Theory of Immiscible Fluid Mixtures [99] (T)

1979, Jul - Drumheller and Bedford - A theory of bubbly liquids [100] (T)

1979, Nov - Hsieh - On Oscillation of Vapor Bubbles [101] (T)

1979, Nov - Marston - Evaporation-condensation resonance frequency of oscillating vapor bubbles [102] (T)

1980, Aug - Keller and Miksis - Bubble oscillations of large amplitude [110] (T)

1981, Feb - Gaunaurd and Überall - Resonance theory of bubbly liquids [103] (T)

1981, xxx - Fanelli, Prosperetti, and Reali - Radial Oscillations of Gas-Vapour Bubbles in Liquids. Part I: Mathematical Formulation [104] (T)

1981, xxx - Fanelli, Prosperetti, and Reali - Radial Oscillations of Gas-Vapour Bubbles in Liquids. Part II: Numerical Examples [105] (T)

1982, xxx - Drumheller, Kipp, and Bedford - Transient wave propagation in bubbly liquids [106] (T)

1982, Jun - Bruno and Novarini - Coherence and multiple scattering effects on acoustic backscattering from linear arrays of gas-filled bubbles [113] (T)

1983, Jan - Crum - The Polytropic Exponent of Gas Contained within Air Bubbles Pulsating in a Liquid [107] (E)

180

1984, Mar - Prosperetti - Bubble phenomena in sound fields: part one [108] (R)

1985, xxx - Caflisch, Miksis, Papanicolaou, and Ting - Effective equations for wave propagation in bubbly liquids[109] (T)

1987, Sep - Omta - Oscillations of a cloud of bubbles of small and not so small amplitude [114] (T)

1988, xxx - Nigmatulin, Khabeev, and Hai - Waves in liquids with vapour bubbles [111] (T)

1989, Feb - Commander and Prosperetti - Linear pressure waves in bubbly liquids: Comparison between theory and experiment[46] (R)

1989, Apr - Temkin - Sound Propagation in Bubbly Liquids. A Review [115] (R)

1989, Dec - Miksis and Ting - Effects of bubbly layers on wave propagations [112] (T)

1991, xxx - Sangani - A pairwise interaction theory for determining the linear acoustic properties of dilute bubbly liquids [142] (T)

1994, Jun - Nicholas, Roy, Crum, Oğuz, and Prosperetti - Sound emissions by a laboratory bubble cloud [122] (E)

1995, Aug - Feuillade - Scattering from collective modes of air bubbles in water and the physical mechanism of superresonances [116] (T)

1995, Sep - Ye and Ding - Acoustic dispersion and attenuation relations in bubbly mixture [117] (T)

1995, Mar - Cheyne, Stebbings, and Roy - Phase velocity measurements in bubbly liquids using a fiber optic laser interferometer [123] (E)

181

1996, Jun - Feuillade - The attenuation and dispersion of sound in water containing multiply interacting air bubbles [143] (T)

1999, Feb - Temkin - Radial pulsations of a fluid sphere in a sound wave [125] (T)

1999, Apr - Henyey - Corrections to Foldy's effective medium theory for propagation in bubble couds and other collections of very small scatterers [118] (T)

2000, Jul - Temkin - Attenuation and dispersion of sound in dilute suspensions of spherical particles [72] (T)

2001, Mar - Temkin - Corrigendum: Radial pulsations of a fluid sphere in a sound wave [126] (T)

2002, Jan - Kargl - Effective medium approach to linear acoustics in bubbly liquids [119] (T)

2002, Feb - Temkin - Erratum: Attenuation and dispersion of sound in dilute suspensions of spherical particles [73] (T)

2002, Apr - Feuillade - Comment on "'Corrections to Foldy's effective medium theory for propagation in bubble couds and other collections of very small scatterers"' [120] (T)

2002, Apr - Henyey - Reply to "Comment on 'Corrections to Foldy's effective medium theory for propagation in bubble clouds and other collections of very small scatterers' " [121] (T)

2002, Oct - Leighton et al - The effect of reverberation on the damping of bubbles [124] (T E)

2005, Jun - Wilson - Low-frequency dispersion in bubbly liquids [45] (T)

2008, Oct - Wilson and Roy - An audible demonstration of the speed of sound in bubbly liquids [47] (E)

2009, Nov - Ainslie and Leighton - Near resonant bubble acoustic cross-section corrections, including examples... [18] (R)

2011, Nov - Ainslie and Leighton - Review of scattering and extinction cross-sections, damping factors, and resonance frequencies of a spherical gas bubble [144] (R)

# Appendix I

# IACUC Protocol Animal Use Policy

**The University of Texas at Austin**
**INSTITUTIONAL ANIMAL CARE AND USE COMMITTEE (IACUC)**
**NIH ASSURANCE #A4107-01**
**Animal Utilization Proposal Form**

Protocol #
AUP-2010-00176

--------------------------------------------------------------------------

**Protocol Title:**    Laboratory Studies of the Acoustic Impact of Fish School Density and Individual Distribution
**Approval Period:**    11/26/2012 - 12/15/2013
**Important Notice:**    **This Print View may not reflect all comments and contingencies for approval. Please check the comments section of the online protocol.**

--------------------------------------------------------------------------

## * * * Renewal Form * * *

To renew this protocol, answer the following renewal questions. If you would like to make changes to the information in the protocol, add/remove/update personnel, add/modify a procedure, etc., click on the appropriate section on the left side menu.

1)    **How many animals (of each approved species) were used as part of this protocol during the previous project year?**

**Project Summary**

| Species | Number of Animals Used | | Reported Used | Total Approved | Remaining Approved | Additional Requested |
|---|---|---|---|---|---|---|
| | Year1 | Year2 | | | | |
| **Carassius auratus** | 0 | 0 | 0 | 120 | 120 | 0 |
| **Danio rerio** | 0 | 24 | 24 | 120 | 120 | 0 |

2)    **N**    **During the past year, were there any unexpected problems or complications? (If yes, explain)**

3)    **Do you wish to amend/change/modify any sections of the protocol?**

If you would like to make changes to the information in the protocol, add/remove/update personnel, add/modify a procedure, etc., click on the appropriate section on the left side menu.

Remember, ANY change in the care and use of animals involved in this protocol that would affect animal welfare must be promptly forwarded to the IACUC for review. Such changes must not be implemented until approval is obtained from the IACUC. Animals will not be transferred between investigators without prior approval.

## * * * Protocol Personnel * * *

**Principal Investigator**

| | | | |
|---|---|---|---|
| **Name:** | Preston Wilson | **Title:** | Associate Professor |
| **E-mail Address:** | pswilson@mail.utexas.edu | **UT EID:** | wilsonps |
| **Phone Number:** | +1 512 475 9093 | **Mail Code:** | C2200 |
| **Department:** | Mechanical Engineering | | |

| Training Details | | | |
|---|---|---|---|
| Course ID | Course | Completion Date | Expiration Date |
| RC0410 | Financial Conflict of Interest | 09/18/2012 | |
| 3219 | Working with Laboratory Zebrafish | 12/10/2010 | 12/09/2013 |
| 3198 | Orientation | 11/18/2010 | 11/17/2013 |
| 3199 | Care and Use of Laboratory Animals | 11/18/2010 | 11/17/2013 |
| AN0020 | HealthPoint OHP (Low Risk) | 11/01/2010 | 10/31/2013 |

Y    **Working with animal models?**

**Describe experience/training have had or will have with this/these specific animal model(s).**
 I have worked with catfish on similar studies, and kept fish as pets at home.

**Administrative Contact**

| | | | |
|---|---|---|---|
| **Name:** | Julia, Cindy Raman | **Title:** | Administrative Associate |

185

- - - - - - - - - - - - - - - - - - - - - - - - - - - - - - - - - - - - - - - - - - - - - - - -

| | |
|---|---|
| **Protocol Title:** | Laboratory Studies of the Acoustic Impact of Fish School Density and Individual Distribution |
| **Approval Period:** | 11/26/2012 - 12/15/2013 |
| **Important Notice:** | **This Print View may not reflect all comments and contingencies for approval. Please check the comments section of the online protocol.** |

- - - - - - - - - - - - - - - - - - - - - - - - - - - - - - - - - - - - - - - - - - - - - - - -

| | | | |
|---|---|---|---|
| **E-mail:** | cindy.raman@austin.utexas.edu | **UT EID:** | mgjcr |
| **Phone Number:** | +1 512 471 3087 | **Mail Code:** | C2200 |
| **Department:** | Department of Mechanical Engineering, Cockrell School of Engineering | | |

| Training Details | | | |
|---|---|---|---|
| **Course ID** | **Course** | **Completion Date** | **Expiration Date** |
| | | | |

N       **Working with animal models?**

**Describe experience/training have had or will have with this/these specific animal model(s).**

**Other Personnel**

| | | | |
|---|---|---|---|
| **Name:** | Michael Ryan | **Title:** | Professor |
| **E-mail:** | mryan@mail.utexas.edu | **UT EID:** | ryanmj |
| **Phone Number:** | +1 512 471 5078 | **Mail Code:** | C0930 |
| **Department:** | Section of Integrative Biology, College of Natural Sciences | | |

| Training Details | | | |
|---|---|---|---|
| **Course ID** | **Course** | **Completion Date** | **Expiration Date** |
| RC0410 | Financial Conflict of Interest | 08/26/2012 | |
| AN0023 | HealthPoint OHP (High Risk) | 05/01/2012 | 04/30/2013 |
| 260 | Introduction to Mice | 04/23/2012 | 04/22/2015 |
| 2601 | Introduction to Amphibians | 11/30/2011 | 11/29/2014 |
| AN0020 | HealthPoint OHP (Low Risk) | 09/01/2011 | 08/31/2014 |
| AN0023 | HealthPoint OHP (High Risk) | 09/01/2011 | 08/31/2012 |
| 3219 | Working with Laboratory Zebrafish | 12/15/2010 | 12/14/2013 |
| AN0020 | HealthPoint OHP (Low Risk) | 04/01/2010 | 03/31/2013 |
| AN0023 | HealthPoint OHP (High Risk) | 04/01/2010 | 03/31/2011 |
| AN0020 | HealthPoint OHP (Low Risk) | 03/01/2010 | 02/28/2013 |
| AN0023 | HealthPoint OHP (High Risk) | 03/01/2010 | 02/28/2011 |
| 3198 | Orientation | 01/07/2010 | 01/06/2013 |
| 3199 | Care and Use of Laboratory Animals | 01/07/2010 | 01/06/2013 |
| AN0020 | HealthPoint OHP (Low Risk) | 01/01/2010 | 12/31/2012 |
| AN0023 | HealthPoint OHP (High Risk) | 01/01/2010 | 12/31/2010 |

186

- - - - - - - - - - - - - - - - - - - - - - - - - - - - - - - - - - - - - - - - - - - - - - - - - - -

**Protocol Title:**        Laboratory Studies of the Acoustic Impact of Fish School Density and Individual Distribution

**Approval Period:**       11/26/2012 - 12/15/2013

**Important Notice:**      **This Print View may not reflect all comments and contingencies for approval. Please check the comments section of the online protocol.**

- - - - - - - - - - - - - - - - - - - - - - - - - - - - - - - - - - - - - - - - - - - - - - - - - - -

| Training Details | | | |
|---|---|---|---|
| **Course ID** | **Course** | **Completion Date** | **Expiration Date** |
| AN0001 | ARC Orientation Class | 02/13/2007 | 02/12/2010 |
| AN0003 | Humane Care and Use of Laboratory Animals | 12/30/2006 | 12/29/2009 |
| AN0014 | Humane Care and Use of Laboratory Fish | 11/30/2006 | 11/29/2009 |
| AN0020 | HealthPoint OHP (Low Risk) | 11/01/2006 | 10/31/2009 |

Y        **Working with animal models?**

**Describe experience/training have had or will have with this/these specific animal model(s).**

Mike Ryan has had 25 years experience working with small freshwater fish.

| | | | |
|---|---|---|---|
| **Name:** | Craig Dolder | **Title:** | Graduate Research Assistant |
| **E-mail:** | dolder@utexas.edu | **UT EID:** | cnd345 |
| **Phone Number:** | +1 512 835 3130 | **Mail Code:** | F0260 |
| **Department:** | Applied Research Laboratories | | |

| Training Details | | | |
|---|---|---|---|
| **Course ID** | **Course** | **Completion Date** | **Expiration Date** |
| 3198 | Orientation | 05/16/2011 | 05/15/2014 |
| 3199 | Care and Use of Laboratory Animals | 05/16/2011 | 05/15/2014 |
| 3219 | Working with Laboratory Zebrafish | 05/16/2011 | 05/15/2014 |
| AN0020 | HealthPoint OHP (Low Risk) | 05/01/2011 | 04/30/2014 |

Y        **Working with animal models?**

**Describe experience/training have had or will have with this/these specific animal model(s).**

Craig is a new graduate student working on this project. This will be his first laboratory experience with small freshwater fish, but has kept them as pets.

- - - - - - - - - - - - - - - - - - - - - - - - - - - - - - - - - - - - - - - - - - - - - - - - - - -

## * * * Species * * *

**Common Name:** Fish, Goldfish                    **Scientific Name:** Carassius auratus

**Strain/Breed:** Comet                            **Animal Sex:** Either

**Weight Range:** 0.000 - 4.500gm(s)               **Age Range:** 45 - 60Day(s)

**Housing Location:** PAT                          **Room Number:** 108

**Maximum number of animals for three year project period:**                    120

**Common Name:** Fish, Zebrafish                   **Scientific Name:** Danio rerio

187

- - - - - - - - - - - - - - - - - - - - - - - - - - - - - - - - - - - - - - - - - - - - - - - - - - - - - - - -

**Protocol Title:**        Laboratory Studies of the Acoustic Impact of Fish School Density and Individual Distribution

**Approval Period:**       11/26/2012 - 12/15/2013

**Important Notice:**      **This Print View may not reflect all comments and contingencies for approval. Please**
                           **check the comments section of the online protocol.**

- - - - - - - - - - - - - - - - - - - - - - - - - - - - - - - - - - - - - - - - - - - - - - - - - - - - - - - -

                 **Strain/Breed:** casper                          **Animal Sex:** Either

              **Weight Range:** 0.200 - 0.700gm(s)                 **Age Range:** 12 - 24Month(s)

                 **Housing Location:** PAT                          **Room Number:** 108

**Maximum number of animals for three year project period:**                      120

- - - - - - - - - - - - - - - - - - - - - - - - - - - - - - - - - - - - - - - - - - - - - - - - - - - - - - - -

## * * * Are You Using * * *

**Are you using?**

1.      N      **Live animals for teaching?**

               ARC contacted regarding procurement and disposal of animals?

        Source of the animals and disposal plan?

        Goals of the course and intended audience?

2.      N      **Dead animals for teaching purposes?**

               ARC contacted regarding procurement and disposal of animals?

        Source of the animals and disposal plan?

        Goals of the course and the intended audience?

3.      N      **Collaboration with another institution(s)**

4.      N      **Biological Material / Animal Product(s)**

5.             **Hazardous Agent(s)**

a)      N      Recombinant DNA (rDNA - including transgenic and knock-out animals)

b)      N      Infectious Agent(s)?

c)      N      Controlled Substance(s)?

d)      N      Toxic Agent(s) (Carcinogens, reproductive hazards, etc.)

6.      N      **Radiological Agent(s)**

7.      N      **Field Study or Wildlife Study**

        **Field Study or Wildlife Study**

188

December 20, 2012
Page 5 of 20

**The University of Texas at Austin**
**INSTITUTIONAL ANIMAL CARE AND USE COMMITTEE (IACUC)**
**NIH ASSURANCE #A4107-01**
**Animal Utilization Proposal Form**

Protocol #
AUP-2010-00176

- - - - - - - - - - - - - - - - - - - - - - - - - - - - - - - - - - - - - - - - - - - - - - - - - - - - - - - - - - -

**Protocol Title:**      Laboratory Studies of the Acoustic Impact of Fish School Density and Individual Distribution

**Approval Period:**      11/26/2012 - 12/15/2013

**Important Notice:**      **This Print View may not reflect all comments and contingencies for approval. Please check the comments section of the online protocol.**

- - - - - - - - - - - - - - - - - - - - - - - - - - - - - - - - - - - - - - - - - - - - - - - - - - - - - - - - - - -

- - - - - - - - - - - - - - - - - - - - - - - - - - - - - - - - - - - - - - - - - - - - - - - - - - - - - - - - - - -

## * * * Funding Sources * * *

**Funding - Sponsored Projects**

**PI / Fellow:**      Preston Wilson

**OSP #:**      201002116

**Source:**      DOD-NAVY

**Project #:**      10656458, P-3987

**Title:**      Laboratory Studies of the Impact of Fish School Density and Individual Distribution on Acoustic Propagation and Scattering

**Date Range:**      10/01/2010- 09/30/2014

- - - - - - - - - - - - - - - - - - - - - - - - - - - - - - - - - - - - - - - - - - - - - - - - - - - - - - - - - - -

## * * * Rationale * * *

**1. STUDY OBJECTIVES**

     a) **What is the overall aim and purpose of this research?**

     The long-term scientific objective of this project is to increase our understanding of acoustic propagation and scattering in the presence of schools of fish.

     b) **How will the information gained be important to human or animal health, the advancement of knowledge, or the good of society?**

     This research benefits sonar operation and acoustic communication in shallow water ocean environments, and will increase the accuracy of acoustically-based fisheries surveys.

**2. RATIONALE FOR USE OF ANIMALS**

     a) **Why must animals be used? Discuss why non-vertebrate alternatives such tissue culture, invertebrate animals, computer simulations, or human epidemiological studies can't provide the information to be gained.**

     Mathematical models and phantoms have been used to reach the current state-of-the-art. (Nero et al., 2007) The next step toward understanding the acoustic properties of fish in nature is to validate the aforementioned state-of-the-art with real fish in the laboratory.

     Reference:

     R.W. Nero, C. Feuillade, C.H. Thompson, and R.H. Love, "Near-resonance scattering from arrays of artificial fish swimbladders," J. Acoust. Soc. Am. 121, pp. 132-143 (2007).

     b) **Why are the species you have selected the most appropriate for these studies?**

     Goldfish are readily available, inexpensive, easy to keep and possess the most important anatomical features of the fish in nature that are of interest, namely any fish with a swim bladder. Further, the upper limit of acoustic exposure that causes no permanent hearing damage is known for goldfish, (Smith et al, 2004) but for few other small fresh water fish otherwise suitable for this study.

     Zebrafish are included because as they have a different type of swim bladder, namely one that is more like two swim bladders. They are also inexpensive and easy to keep and readily available. There is a strain that has transparent scales

189

**The University of Texas at Austin**
**INSTITUTIONAL ANIMAL CARE AND USE COMMITTEE (IACUC)**
**NIH ASSURANCE #A4107-01**
**Animal Utilization Proposal Form**

Protocol #
AUP-2010-00176

**Protocol Title:** Laboratory Studies of the Acoustic Impact of Fish School Density and Individual Distribution

**Approval Period:** 11/26/2012 - 12/15/2013

**Important Notice:** **This Print View may not reflect all comments and contingencies for approval. Please check the comments section of the online protocol.**

and skin, and hence one can see the swim bladder without any special procedures. Finally, many hearing characteristics of zebrafish are known, although it does not appear that the upper limit of acoustic exposure that causes no permanent hearing damage is known. It is believed that this exposure level is similar to that in goldfish, due to the similarity of other aspects of their hearing. (Higgs et al., 2002)

Both types of swim bladders are present in nature, hence we wish to study both types.

References:

D.M. Higgs, M.J. Souza, H.R. Wilkins, J.C. Presson, and A.N. Popper, "Age- and Size-Related Changes in the Inner Ear and Hearing Ability of the Adult Zebrafish (Danio rerio)," Journal of the Association for Research in Otolaryngology 3, pp. 174-184 (2002).

M.E. Smith, A.S. Kane, and A.N. Popper, "Noise-induced stress response and hearing loss in goldfish (Carassius auratus)," J Exp Biol 207, pp. 427-435 (2004).

**c) How have you determined that the numbers provided in the Species section of this protocol represent the smallest number of animals needed to fulfill the goals of the study over a three year period? Provide a detailed rationale that includes information on statistically-determined minimum group sizes, how animals will be allocated to different portions of the project, requirements for breeding, etc.**

We will be comparing measurements of the acoustic properties of these fish to deterministic, rather than statistical mathematical models. Namely, the acoustic response for any particular experiment will be compared to a model that takes into account the exact size and mass of each fish, rather than statistically-determined metrics. The number was selected to achieve a range of fish density (number per unit volume) similar to that of interest in the ocean, which is about 1 fish per body length cubed (Pitcher and Partridge, 1979) and also considering the physical volume of the experimental apparatus.

For the 1-D resonator, its physical volume is about 1000 ml, and the fish of both proposed species have body lengths of about 3 cm. Therefore to achieve school density in nature mentioned above, this requires about 20 fish. We will then use the same fish in the 3-D tank experiments.

Finally, the aforementioned acoustic measurements will be replicated 6 times each, to investigating a total of 120 fish for each species, as was done to achieve statistical significance in a recent study of zebrafish swim bladder morphology. (Robertson, et al., 2008)

We will work with one species at a time, and 20 individuals at a time, performing first the 1-D resonator measurements and the the 3-D tank measurements.

We will not be working with any type of breeding.

References:

T.J. Pitcher and B.L. Partridge, "Fish School Denisty and Volume," Marine Biology 54, pp. 383-394 (1979).

G.N. Robertson, B.W. Lindsey, T.C. Dumbarton, R.P. Croll, and F.M. Smith, "The contribution of the swimbladder to buoyancy in the adult zebrafish (Danio rerio): A morphometric analysis," Journal of Morphology 269, pp. 666-673 (2008).

* * * **Procedures** * * *

Note: Animal Welfare Act regulations require that you consult a veterinarian when designing or renewing applications which involve Category D or E studies. If you describe Category D or E studies below, please indicate the name of the veterinarian you consulted and the approximate number of animals undergoing the procedure

**Other**

190

- - - - - - - - - - - - - - - - - - - - - - - - - - - - - - - - - - - - - - - - - - - - - -

**Protocol Title:** Laboratory Studies of the Acoustic Impact of Fish School Density and Individual Distribution

**Approval Period:** 11/26/2012 - 12/15/2013

**Important Notice:** **This Print View may not reflect all comments and contingencies for approval. Please check the comments section of the online protocol.**

- - - - - - - - - - - - - - - - - - - - - - - - - - - - - - - - - - - - - - - - - - - - - -

| | | | |
|---|---|---|---|
| **Procedure Type:** | Other | **Procedure Title:** | 1-dimensional acoustic resonator (goldfish) |
| **Species:** | Carassius auratus (PAT) | **Pain/Distress Category:** | C |
| **Approximate number of animals to be used in this procedure:** | 120 | **Name of the veterinarian consulted (for D or E studies):** | |
| **Use Location:** | UT-Austin Main Campus | **Building Name:** | ARL |
| | | **Room Number:** | N632 |

* * * Procedure Description * * *

**Procedure Description**

For each of the six replicates of this procedure, 20 fish will be transferred from their housing facility tank in PAT 108 into a 20 gallon insulated cooler that was previously filled with fresh water treated with commercially-available aquarium tap water conditioner and allowed to equilibrate with the temperature in PAT 108 for three hours. Supplemental oxygen will be provided to the fish while in the cooler using a battery powered pump and an airstone. The fish-filled cooler will be transferred to ARL N632 in a university vehicle where it will be allowed to equilibrate with the local temperature for 1 hour.

Each fish will be transferred to another fish tank in the form of a 54 mm inner diameter pipe, 23 cm in height made of clear borosilicate glass. The tank water will be tap water at room temperature that has been treated with commercially-available aquarium tap water conditioner. This will form a one-dimensional acoustic resonator. A low amplitude acoustic field will be established inside the tank. The acoustic resonance frequencies of the resonator with fish inside will be measured with a underwater microphone and the acoustic sound speed and attenuation is inferred from these measurements. These acoustic properties will be determined for a range of fish number density inside the tank and for a range of fish distributions within the tank. The number of fish used for a given acoustic measurement, and hence the fish density will be varied from about 4 fish in the tank (16 fish/gal) to 20 (80 fish/gal), the latter being the high end of fish school density observed in nature for species of the size used here, about 3 cm in length. (Pitcher and Partridge, 1979) The fish distribution is observable from outside the tank, since it is made of clear glass. A video camera will be used to record the position of the fish during the acoustic measurements. Ensonification time is about 30 seconds per trial. We expect to perform about three hour's worth of trials per day. Supplemental oxygen will be provided to the fish while in the tank using a properly-sized aquarium aerator pump, which provides a flow of aerated but bubble-free water to the system and can be used continuously during the acoustics experiments.

Upon completion of the acoustic trials the fish will be placed back in the cooler and returned to PAT 108 and kept in a separate tank from the rest of the colony until the tomography procedure. The testing tank will be sanitized with commercially available aquarium cleaner.

**List any significant effects this procedure may have on the health or behavior of the animals. Describe both expected outcomes and potential complications.**

Fish are exposed to a wide variety of acoustic stimuli in nature. We are not interested in the effects of high amplitude sound, rather will only use low amplitude sound, similar to the sound levels found in nature. We do not expect any adverse effects on the fish. The maximum exposure levels that result in no permanent hearing damage are known for goldfish, (170 dB re 1 microPa, Smith et al., 2004) and believed to be similar for zebrafish, since other aspects of their hearing are similar to goldfish (Higgs et al., 2002).

References:

D.M. Higgs, M.J. Souza, H.R. Wilkins, J.C. Presson, and A.N. Popper, "Age- and Size-Related Changes in the Inner Ear and Hearing Ability of the Adult Zebrafish (Danio rerio)," Journal of the Association for Research in Otolaryngology 3, pp. 174-184 (2002).

M.E. Smith, A.S. Kane, and A.N. Popper, "Noise-induced stress response and hearing loss in goldfish (Carassius auratus)," J Exp Biol 207, pp. 427-435 (2004).

**What criteria will be used to determine if animals exhibiting clinical or behavioral changes should be euthanized?**

191

- - - - - - - - - - - - - - - - - - - - - - - - - - - - - - - - - - - - - - - - - - - - - - - - - - - - - - - -

**Protocol Title:**       Laboratory Studies of the Acoustic Impact of Fish School Density and Individual Distribution
**Approval Period:**      11/26/2012 - 12/15/2013
**Important Notice:**     **This Print View may not reflect all comments and contingencies for approval. Please
                          check the comments section of the online protocol.**

- - - - - - - - - - - - - - - - - - - - - - - - - - - - - - - - - - - - - - - - - - - - - - - - - - - - - - - -

After trials, fish will be returned to a husbandry tank and observed.  A control husbandry tank will also be kept.  The behavior of the fish that have underdone acoustic tests will be compared to the behavior of the fish in the control tank.  Significant changes might be erratic swimming patterns, inability to right themselves, or significantly reduced activity.  Individuals exhibiting significantly different behavior as compared to the control group will be euthanized.

- - - - - - - - - - - - - - - - - - - - - - - - - - - - - - - - - - - - - - - - - - - - - - - - - - - - - - - -

## Other

| | | | |
|---|---|---|---|
| **Procedure Type:** | Other | **Procedure Title:** | 3-D Tank Measurements (goldfish) |
| **Species:** | Carassius auratus (PAT) | **Pain/Distress Category:** | C |
| **Approximate number of animals to be used in this procedure:** | 120 | **Name of the veterinarian consulted (for D or E studies):** | |
| **Use Location:** | UT-Austin Main Campus | **Building Name:** | ARL |
| | | **Room Number:** | N632 |

* * * Procedure Description * * *

**Procedure Description**

For each of the six replicates of this procedure, 20 fish will be transferred from their housing facility tank in PAT 108 into a 20 gallon insulated cooler that was previously filled with fresh water treated with commercially-available aquarium tap water conditioner and allowed to equilibrate with the temperature in PAT 108 for three hours.  Supplemental oxygen will be provided to the fish while in the cooler using a battery powered pump and an airstone.  The fish-filled cooler will be transferred to ARL N632 in a university vehicle where it will be allowed to equilibriate with the local temperature for 1 hour.

While still within the cooler, the fish will be transferred into to a single 1000 ml plastic bag, of the type used to transport fish home from a pet store.  This fish-filled bag will then be transferred into a rectangular fish tank of dimensions 1.5 m x 0.9 m x 0.9 m with borosilicate glass walls.  The bag will be used to keep the fish at the desired density and localized near the center of this large tank.  The tank water will be tap water at room temperature that has been treated with commercially-available aquarium tap water conditioner.  This will form a 3-dimensional acoustic resonator.  A low amplitude acoustic field will be established inside the tank.  The acoustic resonance frequencies of the resonator with fish inside will be measured with a underwater microphone and the acoustic sound scattering properties will be inferred from these measurements.  These acoustic properties will be determined for a range of fish number density inside the bag and for a range of fish distributions within the bag.  The number of fish used for a given acoustic measurement, and hence the fish density will be varied from about 4 fish in the bag (16 fish/gal) to 20 (80 fish/gal), the latter being the high end of fish school density observed in nature for species of the size used here, about 3 cm in length. (Pitcher and Partridge, 1979) The fish distribution is observable from outside the tank and bag, since it is made of clear glass.  A video camera will be used to record the position of the fish during the acoustic measurements.  Ensonification time is about 30 seconds per trial.  We expect to perform about three hour's worth of trials per day.  No active aeration will occur inside the bag during an acoustic trial, but the water in the bag will be replaced after thirty minutes of trials with fully oxygenated water from the cooler.

Upon completion of the acoustic trials the fish will be placed back in the cooler and returned to PAT 108 and kept in a separate tank from the rest of the colony until the tomography procedure.

**List any significant effects this procedure may have on the health or behavior of the animals. Describe both expected outcomes and potential complications.**

Fish are exposed to a wide variety of acoustic stimuli in nature.  We are not interested in the effects of high amplitude sound, rather will only use low amplitude sound, similar to the sound levels found in nature.  We do not expect any adverse effects on the fish.  The maximum exposure levels that result in no permanent hearing damage are known for goldfish, (170 dB re 1 microPa, Smith et al., 2004) and believed to be similar for zebrafish, since other aspects of their hearing are similar to goldfish (Higgs et al., 2002).

192

- - - - - - - - - - - - - - - - - - - - - - - - - - - - - - - - - - - - - - - - - - - - - - - - - - - - - -

**Protocol Title:**          Laboratory Studies of the Acoustic Impact of Fish School Density and Individual Distribution

**Approval Period:**          11/26/2012 - 12/15/2013

**Important Notice:**          **This Print View may not reflect all comments and contingencies for approval. Please check the comments section of the online protocol.**

- - - - - - - - - - - - - - - - - - - - - - - - - - - - - - - - - - - - - - - - - - - - - - - - - - - - - -

References:

D.M. Higgs, M.J. Souza, H.R. Wilkins, J.C. Presson, and A.N. Popper, "Age- and Size-Related Changes in the Inner Ear and Hearing Ability of the Adult Zebrafish (Danio rerio)," Journal of the Association for Research in Otolaryngology 3, pp. 174-184 (2002).

M.E. Smith, A.S. Kane, and A.N. Popper, "Noise-induced stress response and hearing loss in goldfish (Carassius auratus)," J Exp Biol 207, pp. 427-435 (2004).

**What criteria will be used to determine if animals exhibiting clinical or behavioral changes should be euthanized?**

After trials, fish will be returned to a husbandry tank and observed. A control husbandry tank will also be kept. The behavior of the fish that have underdone acoustic tests will be compared to the behavior of the fish in the control tank. Significant changes might be erratic swimming patterns, inability to right themselves, or significantly reduced activity. Individuals exhibiting significantly different behavior as compared to the control group will be euthanized.

- - - - - - - - - - - - - - - - - - - - - - - - - - - - - - - - - - - - - - - - - - - - - - - - - - - - - -

## Other

| | | | |
|---|---|---|---|
| **Procedure Type:** | Other | **Procedure Title:** | micro X-ray computed tomography (goldfish) |
| **Species:** | Carassius auratus (PAT) | **Pain/Distress Category:** | C |
| **Approximate number of animals to be used in this procedure:** | 50 | **Name of the veterinarian consulted** (**for D or E studies**): | |
| **Use Location:** | UT-Austin Main Campus | **Building Name:** | JGB |
| | | **Room Number:** | 1.120 |

* * * Procedure Description * * *

**Procedure Description**

After both the 1-D resonator measurements and the 3-D tank measurements, the fish that were used in the acoustic measurements will be collected for micro-CT scans, which will provide high-resolution 3-D anatomical size, shape, and volume information. These individuals will be euthanized using immersion in an MS-222 solution, described elsewhere in this protocol. They will then be transported in this solution to the UT micro-CT facility in the Geology building on campus. The micro-CT scan will be performed, the fish weighed, and the carcass will be disposed of as described elsewhere in this protocol.

**List any significant effects this procedure may have on the health or behavior of the animals. Describe both expected outcomes and potential complications.**

This procedure will only be performed on euthanized animals.

**What criteria will be used to determine if animals exhibiting clinical or behavioral changes should be euthanized?**

n/a, see above

- - - - - - - - - - - - - - - - - - - - - - - - - - - - - - - - - - - - - - - - - - - - - - - - - - - - - -

## Other

193

December 20, 2012         **The University of Texas at Austin**        Protocol #
Page 10 of 20    **INSTITUTIONAL ANIMAL CARE AND USE COMMITTEE (IACUC)**    AUP-2010-00176
**NIH ASSURANCE #A4107-01**
**Animal Utilization Proposal Form**

- - - - - - - - - - - - - - - - - - - - - - - - - - - - - - - - - - - - - - - - - - - - - - - -

**Protocol Title:**      Laboratory Studies of the Acoustic Impact of Fish School Density and Individual Distribution

**Approval Period:**    11/26/2012 - 12/15/2013

**Important Notice:**    **This Print View may not reflect all comments and contingencies for approval. Please check the comments section of the online protocol.**

- - - - - - - - - - - - - - - - - - - - - - - - - - - - - - - - - - - - - - - - - - - - - - - -

| | | | |
|---|---|---|---|
| **Procedure Type:** | Other | **Procedure Title:** | 1-dimensional acoustic resonator (zebrafish) |
| **Species:** | Danio rerio (PAT) | **Pain/Distress Category:** | C |
| **Approximate number of animals to be used in this procedure:** | 120 | **Name of the veterinarian consulted (for D or E studies):** | |
| **Use Location:** | UT-Austin Main Campus | **Building Name:** | ARL |
| | | **Room Number:** | N632 |

* * * Procedure Description * * *

**Procedure Description**

This procedure is identical to the one of the same name described for goldfish.

For each of the six replicates of this procedure, 20 fish will be transferred from their housing facility tank in PAT 108 into a 20 gallon insulated cooler that was previously filled with fresh water treated with commercially-available aquarium tap water conditioner and allowed to equilibrate with the temperature in PAT 108 for three hours.  Supplemental oxygen will be provided to the fish while in the cooler using a battery powered pump and an airstone.  The fish-filled cooler will be transferred to ARL N632 in a university vehicle where it will be allowed to equilibriate with the local temperature for 1 hour.

Each fish will be transferred to another fish tank in the form of a 54 mm inner diameter pipe, 23 cm in height made of clear borosilicate glass.  The tank water will be tap water at room temperature that has been treated with commercially-available aquarium tap water conditioner.  This will form a one-dimensional acoustic resonator.  A low amplitude acoustic field will be established inside the tank.  The acoustic resonance frequencies of the resonator with fish inside will be measured with an underwater microphone and the acoustic sound speed and attenuation is inferred from these measurements.  These acoustic properties will be determined for a range of fish number density inside the tank and for a range of fish distributions within the tank.  The number of fish used for a given acoustic measurement, and hence the fish density will be varied from about 4 fish in the tank (16 fish/gal) to 20 (80 fish/gal), the latter being the high end of fish school density observed in nature for species of the size used here, about 3 cm in length. (Pitcher and Partridge, 1979) The fish distribution is observable from outside the tank, since it is made of clear glass.  A video camera will be used to record the position of the fish during the acoustic measurements.  Ensonification time is about 30 seconds per trial.  We expect to perform about  three hour's worth of trials per day.  Supplemental oxygen will be provided to the fish while in the tank using a properly-sized aquarium aerator pump, which provides a flow of aerated but bubble-free water to the system and can be used continuously during the acoustics experiments.

Upon completion of the acoustic trials the fish will be placed back in the cooler and returned to PAT 108 and kept in a separate tank from the rest of the colony until the tomography procedure.  The testing tank will be sanitized with commercially available aquarium cleaner.

**List any significant effects this procedure may have on the health or behavior of the animals. Describe both expected outcomes and potential complications.**

Fish are exposed to a wide variety of acoustic stimuli in nature.  We are not interested in the effects of high amplitude sound, rather will only use low amplitude sound, similar to the sound levels found in nature.  We do not expect any adverse effects on the fish.  The maximum exposure levels that result in no permanent hearing damage are known for goldfish, (170 dB re 1 microPa, Smith et al., 2004) and believed to be similar for zebrafish, since other aspects of their hearing are similar to goldfish (Higgs et al., 2002).

References:

D.M. Higgs, M.J. Souza, H.R. Wilkins, J.C. Presson, and A.N. Popper, "Age- and Size-Related Changes in the Inner Ear and Hearing Ability of the Adult Zebrafish (Danio rerio)," Journal of the Association for Research in Otolaryngology 3, pp. 174-184 (2002).

M.E. Smith, A.S. Kane, and A.N. Popper, "Noise-induced stress response and hearing loss in goldfish (Carassius auratus)," J Exp Biol 207, pp. 427-435 (2004).

194

- - - - - - - - - - - - - - - - - - - - - - - - - - - - - - - - - - - - - - - - - - - - - - - - - - -

**Protocol Title:**     Laboratory Studies of the Acoustic Impact of Fish School Density and Individual Distribution
**Approval Period:**    11/26/2012 - 12/15/2013
**Important Notice:**   **This Print View may not reflect all comments and contingencies for approval. Please check the comments section of the online protocol.**

- - - - - - - - - - - - - - - - - - - - - - - - - - - - - - - - - - - - - - - - - - - - - - - - - - -

**What criteria will be used to determine if animals exhibiting clinical or behavioral changes should be euthanized?**

After trials, fish will be returned to a husbandry tank and observed.  A control husbandry tank will also be kept.  The behavior of the fish that have underdone acoustic tests will be compared to the behavior of the fish in the control tank.  Significant changes might be erratic swimming patterns, inability to right themselves, or significantly reduced activity.  Individuals exhibiting significantly different behavior as compared to the control group will be euthanized.

- - - - - - - - - - - - - - - - - - - - - - - - - - - - - - - - - - - - - - - - - - - - - - - - - - -

## Other

| | | | |
|---|---|---|---|
| **Procedure Type:** | Other | **Procedure Title:** | 3-D Tank Measurements (zebrafish) |
| **Species:** | Danio rerio (PAT) | **Pain/Distress Category:** | C |
| **Approximate number of animals to be used in this procedure:** | 120 | **Name of the veterinarian consulted (for D or E studies):** | |
| **Use Location:** | UT-Austin Main Campus | **Building Name:** | ARL |
| | | **Room Number:** | N632 |

*** Procedure Description ***

**Procedure Description**

This is the same procedure as that with the same name described for goldfish.

For each of the six replicates of this procedure, 20 fish will be transferred from their housing facility tank in PAT 108 into a 20 gallon insulated cooler that was previously filled with fresh water treated with commercially-available aquarium tap water conditioner and allowed to equilibrate with the temperature in PAT 108 for three hours.  Supplemental oxygen will be provided to the fish while in the cooler using a battery powered pump and an airstone.  The fish-filled cooler will be transferred to ARL N632 in a university vehicle where it will be allowed to equilibriate with the local temperature for 1 hour.

While still within the cooler, the fish will be transferred into to a single 1000 ml plastic bag, of the type used to transport fish home from a pet store.  This fish-filled bag will then be transferred into a rectangular fish tank of dimensions 1.5 m x 0.9 m x 0.9 m with borosilicate glass walls.  The bag will be used to keep the fish at the desired density and localized near the center of this large tank.  The tank water will be tap water at room temperature that has been treated with commercially-available aquarium tap water conditioner.  This will form a 3-dimensional acoustic resonator.  A low amplitude acoustic field will be established inside the tank.  The acoustic resonance frequencies of the resonator with fish inside will be measured with a underwater microphone and the acoustic sound scattering properties will be inferred from these measurements.  These acoustic properties will be determined for a range of fish number density inside the bag and for a range of fish distributions within the bag.  The number of fish used for a given acoustic measurement, and hence the fish density will be varied from about 4 fish in the bag (16 fish/gal) to 20 (80 fish/gal), the latter being the high end of fish school density observed in nature for species of the size used here, about 3 cm in length. (Pitcher and Partridge, 1979) The fish distribution is observable from outside the tank and bag, since it is made of clear glass.  A video camera will be used to record the position of the fish during the acoustic measurements.  Ensonification time is about 30 seconds per trial.  We expect to perform about  three hour's worth of trials per day.  No active aeration will occur inside the bag during an acoustic trial, but the water in the bag will be replaced after thirty minutes of trials with fully oxygenated water from the cooler.

Upon completion of the acoustic trials the fish will be placed back in the cooler and returned to PAT 108 and kept in a separate tank from the rest of the colony until the tomography procedure.

**List any significant effects this procedure may have on the health or behavior of the animals. Describe both expected outcomes and potential complications.**

Fish are exposed to a wide variety of acoustic stimuli in nature.  We are not interested in the effects of high amplitude sound, rather will only use low amplitude sound, similar to the sound levels found in nature.  We do not expect any adverse effects on

195

December 20, 2012
Page 12 of 20

**The University of Texas at Austin**
**INSTITUTIONAL ANIMAL CARE AND USE COMMITTEE (IACUC)**
**NIH ASSURANCE #A4107-01**
**Animal Utilization Proposal Form**

Protocol #
AUP-2010-00176

- - - - - - - - - - - - - - - - - - - - - - - - - - - - - - - - - - - - - - - - - - - - - - - - - - - - - -

**Protocol Title:**     Laboratory Studies of the Acoustic Impact of Fish School Density and Individual Distribution

**Approval Period:**    11/26/2012 - 12/15/2013

**Important Notice:**   **This Print View may not reflect all comments and contingencies for approval. Please check the comments section of the online protocol.**

- - - - - - - - - - - - - - - - - - - - - - - - - - - - - - - - - - - - - - - - - - - - - - - - - - - - - -

the fish.  The maximum exposure levels that result in no permanent hearing damage are known for goldfish, (170 dB re 1 microPa, Smith et al., 2004) and believed to be similar for zebrafish, since other aspects of their hearing are similar to goldfish (Higgs et al., 2002).

References:

D.M. Higgs, M.J. Souza, H.R. Wilkins, J.C. Presson, and A.N. Popper, "Age- and Size-Related Changes in the Inner Ear and Hearing Ability of the Adult Zebrafish (Danio rerio)," Journal of the Association for Research in Otolaryngology 3, pp. 174-184 (2002).

M.E. Smith, A.S. Kane, and A.N. Popper, "Noise-induced stress response and hearing loss in goldfish (Carassius auratus)," J Exp Biol 207, pp. 427-435 (2004).

**What criteria will be used to determine if animals exhibiting clinical or behavioral changes should be euthanized?**

After trials, fish will be returned to a husbandry tank and observed.  A control husbandry tank will also be kept.  The behavior of the fish that have underdone acoustic tests will be compared to the behavior of the fish in the control tank.  Significant changes might be erratic swimming patterns, inability to right themselves, or significantly reduced activity.  Individuals exhibiting significantly different behavior as compared to the control group will be euthanized.

- - - - - - - - - - - - - - - - - - - - - - - - - - - - - - - - - - - - - - - - - - - - - - - - - - - - - -

## Other

| | | | |
|---|---|---|---|
| **Procedure Type:** | Other | **Procedure Title:** | micro X-ray computed tomography (zebrafish) |
| **Species:** | Danio rerio (PAT) | **Pain/Distress Category:** | C |
| **Approximate number of animals to be used in this procedure:** | 50 | **Name of the veterinarian consulted (for D or E studies):** | |
| **Use Location:** | UT-Austin Main Campus | **Building Name:** | JGB |
| | | **Room Number:** | 1.120 |

* * * Procedure Description * * *

**Procedure Description**

This is the same procedure as that with the same name described for goldfish.

After both the 1-D resonator measurements and the 3-D tank measurements, the fish that were used in the acoustic measurements will be collected for micro-CT scans, which will provide high-resolution 3-D anatomical size, shape, and volume information.  These individuals will be euthanized using immersion in an MS-222 solution, described elsewhere in this protocol.  They will then be transported in this solution to the UT micro-CT facility in the Geology building on campus.  The micro-CT scan will be performed, the fish weighed, and the carcass will be disposed of as described elsewhere in this protocol.

**List any significant effects this procedure may have on the health or behavior of the animals. Describe both expected outcomes and potential complications.**

This procedure will only be performed on euthanized animals.

**What criteria will be used to determine if animals exhibiting clinical or behavioral changes should be euthanized?**

n/a, see above

196

- - - - - - - - - - - - - - - - - - - - - - - - - - - - - - - - - - - - - - - - - - - - - - - - - - - - - - - - - -

**Protocol Title:**     Laboratory Studies of the Acoustic Impact of Fish School Density and Individual Distribution

**Approval Period:**     11/26/2012 - 12/15/2013

**Important Notice:**     **This Print View may not reflect all comments and contingencies for approval. Please check the comments section of the online protocol.**

- - - - - - - - - - - - - - - - - - - - - - - - - - - - - - - - - - - - - - - - - - - - - - - - - - - - - - - - - -

- - - - - - - - - - - - - - - - - - - - - - - - - - - - - - - - - - - - - - - - - - - - - - - - - - - - - - - - - -

## * * * Procedure Relationships * * *

**Please describe the sequence and timing of the manipulations:**

If more than one surgery or procedure will be performed on some or all animals used under this protocol, describe the sequence and timing of these manipulations. Use enough detail to allow reviewers to understand what each animal may undergo.

There will be no surgery procedures. Fish will be removed from the husbandry tank in PAT 108, transferred to ARL N632, and placed in the acoustic test tank, either the 1-D resonator or the 3-D tank. A single acoustic trial will last about 30 seconds many trials will be conducted over the course of a maximum of three hours. Fish will be transported back to campus after the acoustic trials.

If time permits on a given day, the the micro-CT imagery procedure will be conducted directly after the completion of the acoustic procedures. Hence the fish will be transported to the Geology building micro-CT imaging lab. This procedure requires euthanasia, hence after the procedure is completed, the carcasses will be transported back to PAT 108, where they will be double bagged, frozen, and picked up by Environmental Services.

Otherwise, the fish will be transported back to PAT 108 and placed in their husbandry tanks, after one hour acclimation for temperature. The next day, the fish will be euthanized and transported to the imaging lab in the Geology building for the micro-CT procedure. This procedure requires euthanasia, hence after the procedure is completed, the carcasses will be transported back to PAT 108, where they will be double bagged, frozen, and picked up by Environmental Services.

Fish will not remain away from their husbandry tanks for more than 12 hours at a time.

**Multiple Major Survival Surgery Description:**

Describe why it is necessary to perform multiple major surgical procedures on the same animal.

- - - - - - - - - - - - - - - - - - - - - - - - - - - - - - - - - - - - - - - - - - - - - - - - - - - - - - - - - -

## * * * Husbandry * * *

**Emergency Contact Information**

**List all individuals/phone numbers that are to be notified by veterinary staff or others in the event of an emergency. One or more of the provided telephone numbers must be a non-University line for off-hours contact** (**e.g. home, cell or pager**).

Preston S. Wilson, 512-963-4883
Michael J. Ryan, 512-471-5078
Glenn Otto, 512-471-2392

**Special Husbandry or Care**

**List any special housing, equipment, animal care** (**i.e., special caging, water, feed, or waste disposal, etc.**) **and animal identification methods** (**e.g., ear punches/notches, ear tags, tattoos, collars, cage cards, etc.**)

Comet goldfish (Carassius auratus) and zebrafish (Danio rerio) will be purchased from Carolina Biological Supply Company; PO Box 6010; Burlington, NC 27216-6010 [336-584-0381].

Fish will be housed in aquaria in Patterson Labs 108, which currently is approved as a satellite fish husbandry facility under the supervision of Prof. Michael Ryan. They will be housed in standard 20 gal fish aquaria (24x8x12 in) with recirculating filter systems. Fish density will be 10 fish per tank for goldfish and 20 fish per tank for zebrafish. Room and water temperature are maintained at 25 )C. Water will be tested daily and maintained with pH between 6 to 8, ammonia between 0 and 0.25 mg/L, nitrite between 0 and 0.5 mg/L and nitrate between 0 and 2 mg/L. Light is 12 hours on, 12 hours off full bandwidth fluorescent.

- - - - - - - - - - - - - - - - - - - - - - - - - - - - - - - - - - - - - - - - - - - - - - - -

**Protocol Title:**     Laboratory Studies of the Acoustic Impact of Fish School Density and Individual Distribution

**Approval Period:**    11/26/2012 - 12/15/2013

**Important Notice:**   **This Print View may not reflect all comments and contingencies for approval. Please check the comments section of the online protocol.**

- - - - - - - - - - - - - - - - - - - - - - - - - - - - - - - - - - - - - - - - - - - - - - - -

Aquarium water is changed every 10 days with treated tap water or when above water parameters are not met.  Fish are fed daily. Fish health will be visually assessed daily, 7 days a week, including weekends, holidays and shut downs by Mike Ryan or Preston Wilson. Fish health will be logged daily on a chart kept on the door of PAT 108 and initialed by the keepers.  Any unhealthy fish or emergency situations will be reported to Preston Wilson or Michael Ryan and the attending veterinarian, Dr. Glenn Otto.  Note that this protocol is for batch procedures, in which fish will only be present in the facility for a couple of days at a time.  There is no long-term colony in this protocol.  In addition to spontaneous disease conditions, monitoring and reporting will also include unanticipated consequences or adverse events associated with research use, including, but not limited to, handling, mechanical failures in environmental control systems, and transport or shipping (including animals that are injured or dead upon arrival).

Significant incidents involving unanticipated illness or death, as part of a research project, must be reported to the IACUC. The ARC will work with the research group to assure that the IACUC is informed about such complications as needed.

**If animals will be transported between facilities** (**e.g., hand carried, vehicular, etc.**) **describe the methods and containment measures to be utilized. Transportation of animals must conform to all Institutional guidelines/policies.**

Fish will be transported between the husbandry facility in PAT 108 to experimental facilities in ARL N632 and in the Geology building.  Fish will be transported either in the container they were purchased in, or within an insulated cooler filled with tap water that has been treated with aquarium tap water conditioner.  Supplemental oxygen will be provided to the fish while in the cooler using a battery powered pump and an airstone.  This will in turn be transported in a University vehicle, personal car or carried by hand.

The fish will be transported DIRECTLY from their holding room to the laboratory use location. We will insure that the top of the transport enclosure is closed and secure.

If a cart is used, we will minimize noise and vibration by using a cart with wheels in good repair. If more than two transportation enclosures are used, we will not stack them. They will be placed on second and/or lower tiers of cart, whenever possible, which leaves top shelf to support the weight of the drape or cover.

We will use opaque coolers to ensure that the fish are shielded from
public view.

Fish will not be left unattended during transport.

We will return the cooler and discarded carcasses to PAT 108 at the end of each experimental procedure.  Carcasses will be double bagged, frozen, and picked up by Environmental Services.

Transport vehicles and carts will be cleaned and sanitized between uses.

**Non-standard Experimental Requirements**

**Food or Fluid restriction**

| Species | Food Restriction | Length of Restriction | Fluid Restriction | Length of Restriction | Reason for Restriction |
|---|---|---|---|---|---|
| Carassius auratus (PAT) | | | | | |
| Danio rerio (PAT) | | | | | |

**Restraint of Conscious Animals**

| Species | Type restraint (manual, commercial, manual and commercial) | Please describe acclimation to restraint | Length of restraint |
|---|---|---|---|
| Carassius auratus (PAT) | | | |
| Danio rerio (PAT) | | | |

198

December 20, 2012        The University of Texas at Austin        Protocol #
Page 15 of 20      INSTITUTIONAL ANIMAL CARE AND USE COMMITTEE (IACUC)      AUP-2010-00176
NIH ASSURANCE #A4107-01
Animal Utilization Proposal Form

**Protocol Title:**    Laboratory Studies of the Acoustic Impact of Fish School Density and Individual Distribution

**Approval Period:**    11/26/2012 - 12/15/2013

**Important Notice:**    **This Print View may not reflect all comments and contingencies for approval. Please check the comments section of the online protocol.**

**Non-Standard Housing Requirements**

| Species | Cage/Pen size | Cage Sanitation Interval | Wire-bottom rodent cages or grids | Animals outside dedicated animal housing for greater than 12 hours | Exemption from exercise (dogs only) |
|---|---|---|---|---|---|
| Carassius auratus (PAT) | | | | | |
| Danio rerio (PAT) | | | | | |

## * * * Euthanasia * * *

**Euthanasia**

| Species | Primary euthanasia method | Route of Administration | Dosage mg/kg (if possible) | Secondary euthanasia method |
|---|---|---|---|---|
| Carassius auratus (PAT) | Tricane methanesulfonate | Immersion bath (IB) | 500 mg/liter | |
| Danio rerio (PAT) | Tricane methanesulfonate | Immersion bath (IB) | 500 mg/liter | |

**Provide specific details for carcass disposal.**

Carcasses will be double bagged in zip-lock bags and disposed of in the normal laboratory trash. This carcass disposal protocol was specified for this project by the Assistant Director of Biological and Lab Safety, Environmental Health and Safety Office. The pH of the MS-222 euthanizing solution will be tested and buffered to neutrality as needed with sodium bicarbonate.

## * * * Attachments * * *

**Attachment(s)**

| Attachment Name | Attached Date | Attached By | Submitted Date |
|---|---|---|---|
| sponsor review comments | 2/23/2011 | Preston Wilson | 03/01/2011 |
| summary of changes | 3/1/2011 | Preston Wilson | 03/01/2011 |

## * * * Guidelines * * *

**Mandatory Guidelines**

      Guidelines for Endpoint Monitoring and Humane Termination

**Non-Mandatory Guidelines**

199

**The University of Texas at Austin**
**INSTITUTIONAL ANIMAL CARE AND USE COMMITTEE (IACUC)**
**NIH ASSURANCE #A4107-01**
**Animal Utilization Proposal Form**

---

**Protocol Title:** Laboratory Studies of the Acoustic Impact of Fish School Density and Individual Distribution

**Approval Period:** 11/26/2012 - 12/15/2013

**Important Notice:** **This Print View may not reflect all comments and contingencies for approval. Please check the comments section of the online protocol.**

---

**None**

----------------------------------------------------------------

200

December 20, 2012
Page 17 of 20

**The University of Texas at Austin**
**INSTITUTIONAL ANIMAL CARE AND USE COMMITTEE (IACUC)**
**NIH ASSURANCE #A4107-01**
**Animal Utilization Proposal Form**

Protocol #
AUP-2010-00176

- - - - - - - - - - - - - - - - - - - - - - - - - - - - - - - - - - - - - - - - - - - - - - - - - - - - - -

**Protocol Title:**     Laboratory Studies of the Acoustic Impact of Fish School Density and Individual Distribution

**Approval Period:**     11/26/2012 - 12/15/2013

**Important Notice:**     **This Print View may not reflect all comments and contingencies for approval. Please check the comments section of the online protocol.**

- - - - - - - - - - - - - - - - - - - - - - - - - - - - - - - - - - - - - - - - - - - - - - - - - - - - - -

## * * * Certification * * *

By submitting this Animal Utilization Proposal to the Institutional Animal Care and Use Committee (IACUC) of The University of Texas at Austin, the Principal Investigator certifies the following:

1) I assure that all students, staff, and faculty on this project are familiar with the Animal Welfare Act (AWA) and the Public Health Service (PHS) Policy on Humane Care and Use of Laboratory Animals, the National Institute of Health (NIH) Guide for the Care and Use of Laboratory Animals, and recognize their responsibility in strictly adhering to approved protocols.

2) I assure that all individuals listed on this project are qualified or will be trained to conduct procedures involving animals under this proposal, and that they have attended an approved UT-Austin ARC Orientation Course and received training in the biology, handling, and care of this species; aseptic surgical methods and techniques (if necessary); the concept availability and use of research or testing methods that limit the use of animals or minimize distress; the proper use of anesthetics, analgesics, and tranquilizers (if necessary), and procedures for reporting animal welfare concerns.

3) I assure that all procedure will be conducted in accordance with The University of Texas at Austin safety procedures, including those pertaining to personal protective equipment.

4) I assure that all individuals working on this proposal are enrolled in the HealthPoint Occupational Health Program (OHP).

5) I assure that ANY change in the care and use of animals involved in this protocol that would affect their welfare will be promptly forwarded to the IACUC for review. Such changes will not be implemented until approval is obtained from the IACUC. Animals will not be transferred between investigators without prior approval.

6) I assure that I have reviewed the pertinent scientific literature and the sources and/or databases and have found no valid alternative to any procedures described herein which may cause more than momentary or slight pain, distress, or generalized discomfort to animals, whether it is relieved or not.

7) I assure that every effort has been made to minimize the number of animals used and reduce the amount of pain, distress, and/or discomfort these animals must experience.

8) I assure that the activities described with in this document submitted for IACUC review are consistent with those described in any related grant, contract, or subcontract.

9) I assure that the information contained in this application for animal use is accurate to the best of my knowledge.

10) I understand that this application and/or my animal use privileges may be revoked by the IACUC if I violate any of the aforementioned assurance statements.

☐     The Principal Investigator has read and agrees to abide by the above obligations.

- - - - - - - - - - - - - - - - - - - - - - - - - - - - - - - - - - - - - - - - - - - - - - - - - - - - - -

**Appendix A**

**Guidelines**

**The University of Texas at Austin**
**INSTITUTIONAL ANIMAL CARE AND USE COMMITTEE (IACUC)**
**NIH ASSURANCE #A4107-01**
**Animal Utilization Proposal Form**

- - - - - - - - - - - - - - - - - - - - - - - - - - - - - - - - - - - - - - - - - - - - - - - - - - -

**Protocol Title:** Laboratory Studies of the Acoustic Impact of Fish School Density and Individual Distribution

**Approval Period:** 11/26/2012 - 12/15/2013

**Important Notice:** **This Print View may not reflect all comments and contingencies for approval. Please check the comments section of the online protocol.**

- - - - - - - - - - - - - - - - - - - - - - - - - - - - - - - - - - - - - - - - - - - - - - - - - - -

       **Guidelines for Endpoint Monitoring and Humane Termination**

---

**Guidelines for Endpoint Monitoring and Humane Termination**

The University of Texas at Austin
Institutional Animal Care and Use Committee

*These guidelines have been written to assist faculty, staff, and students in performing vertebrate animal procedures in a humane manner and complying with pertinent regulatory requirements. Under some circumstances deviations from these procedures may be indicated but such variances must be approved in advance by the IACUC.*

---

**Guideline # 008**
**Approved: 07/14/2008**

This document provides information to be used when planning and performing procedures in vertebrate animals used for research, teaching, or other purposes at The University of Texas at Austin.  It is organized into three sections:


Section A - Definitions
Section B - Specific Considerations
Section C - Acknowledgements


**Section A - Definitions**


**Moribund** is defined as "in a dying state." Animals are considered to be clinically moribund if they manifest any of the following clinical signs:
- Inability to ambulate that prevents the animal's easy access to food and/or water
- Inability to maintain itself in an upright position.
- Prolonged (greater than 48 hours) in appetence and/or clinical dehydration.
- Agonal breathing and cyanosis.
- Chronic unrelieved diarrhea or constipation.
- Hematological or biochemical parameters that indicate organ failure incompatible with life.
- Unconsciousness with no response to external stimuli such as a toe-pinch withdrawal test.


**Section B - Specific Considerations**


1. Whenever possible, experiments should be designed and refined so that animals will never predictably be subjected to potentially life-threatening conditions.
2. In order to minimize animal pain or distress, and to comply with guidelines governing the use of animals in experimentation, animals that show evidence of pronounced, terminal debilitation should be humanely euthanized rather than being allowed to progress to death.
3. If experiments will result in predictable debilitation, the PI must describe the expected time frame for this to occur, and provide a plan in the approved protocol, which documents that:
   - The minimum number of animals necessary to achieve statistical significance will be used;
   - Animals reaching the terminal phase of the study will be monitored at least twice daily (in the early morning and late afternoon including weekends and holidays);
   - Any animals evidencing clinically abnormal behavior will be removed from group housing situations and housed individually with easy access to food and water; and
   - Written records of all monitoring sessions, indicating the time of the observations, the person observing the animals, and any observations such as the number of animals evidencing clinically abnormal behavior and the number of animals found dead, must be maintained and made available to the IACUC, the ARC staff, or outside regulatory personnel upon request.

4. Researchers must perform euthanasia on all moribund experimental animals unless there is an IACUC approved scientific

202

- - - - - - - - - - - - - - - - - - - - - - - - - - - - - - - - - - - - - - - - - - - - - - - - - - - - -

**Protocol Title:**      Laboratory Studies of the Acoustic Impact of Fish School Density and Individual Distribution

**Approval Period:**     11/26/2012 - 12/15/2013

**Important Notice:**    **This Print View may not reflect all comments and contingencies for approval. Please
                         check the comments section of the online protocol.**

- - - - - - - - - - - - - - - - - - - - - - - - - - - - - - - - - - - - - - - - - - - - - - - - - - - - -

     justification that euthanasia would invalidate experimental data collection.

5.   If euthanizing a moribund animal would invalidate the study, the scientific justification for using death as an endpoint must be provided in writing as part of the animal care protocol and must be approved by the IACUC prior to initiating this procedure. In addition to following the requirements listed in "3" above, the PI must assure that dead animals will be promptly collected and removed from the cage.

NOTE: ANY APPROVED USE OF DEATH AS AN EXPERIMENTAL ENDPOINT WILL BE NOTED ON ALL PROTOCOL FORMS AND REGULATORY DOCUMENTS AS BEING IN THE HIGHEST PAIN LEVEL CATEGORY, "E," UNLESS ANALGESICS OR ANESTHETICS ARE PROVIDED TO ALLEVIATE PAIN OR DISTRESS IN THE EXPERIMENTAL ANIMALS.

**Section C - Acknowledgements**

This document contains content that was adapted from materials obtained from Stanford University.

203

**The University of Texas at Austin**
**INSTITUTIONAL ANIMAL CARE AND USE COMMITTEE (IACUC)**
**NIH ASSURANCE #A4107-01**
**Animal Utilization Proposal Form**

------------------------------------------------------------------------------------------------

**Protocol Title:**      Laboratory Studies of the Acoustic Impact of Fish School Density and Individual Distribution

**Approval Period:**     11/26/2012 - 12/15/2013

**Important Notice:**    **This Print View may not reflect all comments and contingencies for approval. Please check the comments section of the online protocol.**

------------------------------------------------------------------------------------------------

**Guidelines for Veterinary Care, Health Checks, and Illness Reporting**

204

# Bibliography

[1] N. B. Marshall. Bathypelagic fishes as sound scatterers in the ocean. *J. Mar. Res.*, 10(1):1–17, 1951.

[2] D. V. Holliday. Resonance structure in echoes from schooled pelagic fish. *J. Acoust. Soc. Am.*, 51(4-2):1322–1332, 1972.

[3] J. H. S. Blaxter, E. J. Denton, and J. A. B. Gray. The herring swimbladder as a gas reservoir for the acoustico-lateralis system. *Journal of the Marine Biological Association of the United Kingdom*, 59(1):1–10, 1979.

[4] A. Løvik and J. M. Hovem. An experimental investigation of swimbladder resonance in fishes. *J. Acoust. Soc. Am.*, 66(3):850–854, 1979.

[5] R. H. Love. Resonant acoustic scattering by swimbladder-bearing fish. *J. Acoust. Soc. Am.*, 64(2):571–580, 1978.

[6] I. Andreeva. Scattering of sound by air bladders of fish in deep sound-scattering ocean layers. *Sov. Phys. Acoust*, 10(1):17–20, 1964.

[7] D. E. Weston. Sound propagation in the presence of bladder fish. In V. M. Albers, editor, *Underwater Acoustics*, pages 55–88. Plenum Press, 1967.

[8] R. H. Love. A model for estimating distributions of fish school target strengths. *Deep-Sea Res.*, 28(7):705–725, 1981.

[9] C. S. Clay. Low-resolution acoustic scattering models: fluid-filled cylinders and fish with swim bladders. *J. Acoust. Soc. Am.*, 89(5):2168–2179, 1991.

[10] C. S. Clay and B. G. Heist. Acoustic scattering by fish — acoustic models and a two-parameter fit. *J. Acoust. Soc. Am.*, 75(4):1077–1083, 1984.

[11] C. S. Clay and J. K. Horne. Acoustic models of fish: the Atlantic cod (*Gadus morhua*). *J. Acoust. Soc. Am.*, 96(3):1661–1668, 1994.

[12] C. Feuillade, R. W. Nero, and R. H. Love. A low-frequency acoustic scattering model for small schools of fish. *J. Acoust. Soc. Am.*, 99(1):196–208, 1996.

[13] K. G. Foote. Correcting acoustic measurements of scatterer density for extinction. *J. Acoust. Soc. Am.*, 88(3):1543–1546, 1990.

[14] X. Zhao and E. Ona. Estimation and compensation models for the shadowing effect in dense fish aggregations. *ICES J. Mar. Sci.*, 60(1):155–163, 2003.

[15] K. Baik. Comment on resonant acoustic scattering by swimbladder-bearing fish [J. Acoust. Soc. Am. 64, 571–580 (1978)](L). *J. Acoust. Soc. Am.*, 133(1):5–8, 2013.

[16] K. G. Foote. Importance of the swimbladder in acoustic scattering by fish: A comparison of gadoid and mackerel target strengths. *J. Acoust. Soc. Am.*, 67(6):2048–2089, 1980.

[17] D. N. Maclennan, P. G. Fernandes, and J. Dalen. A consistent approach to definitions and symbols in fisheries acoustics. *ICES J. Mar. Sci.*, 59(2):365–369, 2002.

[18] M. A. Ainslie and T. G. Leighton. Near resonant bubble acoustic cross-section corrections, including examples from oceanpgraphy, volcanology, and biomedical ultrasound. *J. Acoust. Soc. Am.*, 126(5):2163–2175, 2009.

[19] M. Strasberg. The pulsation frequency of nonspherical gas bubbles in liquids. *J. Acoust. Soc. Am.*, 25(3):536–537, 1953.

[20] C. Feuillade and M. F. Werby. Resonances of deformed gas bubbles in liquids. *J. Acoust. Soc. Am.*, 96(6):3684–3692, 1994.

[21] P. Fréon, M. Soria, C. Mullon, and F. Gerlotto. Diurnal variation in fish density estimate during acoustic surveys in relation to spatial distribution and avoidance reaction. *Aquat. Living Resour.*, 6(3):221–234, 1993.

[22] R. H. Love. Predictions of volume scattering strengths from biological trawl data. *J. Acoust. Soc. Am.*, 57(2):300–306, 1975.

[23] C. Devin. Survey of thermal, radiation, and viscous damping of pulsating air bubbles in water. *J. Acoust. Soc. Am.*, 31(12):1654–1667, 1959.

[24] R. W. Nero, C. Feuillade, C. H. Thompson, and R. H. Love. Near-resonance scattering from arrays of artificial fish swimbladders. *J. Acoust. Soc. Am.*, 121(1):132–143, 2007.

[25] R. H. Love. Dorsal-aspect target strength of an individual fish. *J. Acoust. Soc. Am.*, 49(3-2):816–823, 1971.

[26] J. Scrimger, R. Turner, and G. Heyd. Backscattering of underwater sound in saanich inlet, british columbia, including observations of scattering from a fish school. *J. Acoust. Soc. Am.*, 51(3-2):1098–1105, 1972.

[27] L. M. Deuser, D. Middleton, T. D. Plemons, and J. K. Vaughan. On the classification of underwater acoustic signals. ii. experimental applications involving fish. *J. Acoust. Soc. Am.*, 65(2):444–455, 1979.

[28] K. G. Foote. Linearity of fisheries acoustics, with addition theorems. *J. Acoust. Soc. Am.*, 73(6):1932–1940, 1983.

[29] C. S. Clay. Deconvolution of the fish scattering pdf from the echo pdf for a single transducer sonar. *J. Acoust. Soc. Am.*, 73(6):1989–1994, 1983.

[30] K. G. Foote. Rather-high-frequency sound scattering by swimbladdered fish. *J. Acoust. Soc. Am.*, 78(2):688–700, 1985.

[31] M. Furusawa, K. Ishii, and Y. Miyanohana. Attenuation of sound by schooling fish. *J. Acoust. Soc. Am.*, 92(2):987–994, 1992.

[32] R. H. Love. A comparison of volume scattering strength data with model calculations based on quasisynoptically collected fishery data. *J. Acoust. Soc. Am.*, 94(4):2255–2268, 1993.

[33] R. W. Nero, C. H. Thompson, and R. H. Love. Abyssopelagic grenadiers: the probable cause of low frequency sound scattering at great depths off the oregon and california coasts. *Deep-sea Res. Pt. I*, 44(4):627–645, 1997.

[34] R. W. Nero and M. E. Huster. Low frequency acoustic imaging of pacific salmon on the high seas. *Can. J. Fish Aquat. Sci.*, 53(11):2513–2523, 1996.

[35] R. W. Nero, C. H. Thompson, and R. H. Love. Low-frequency acoustic measurements of pacific hake, merluccius productus, off the west coast of the united states. *Fishery Bulletin*, 96(2):329–343, 1998.

[36] O. Diachok. Effects of absorptivity due to fish on transmission loss in shallow water. *J. Acoust. Soc. Am.*, 105(4):2107–2128, 1999.

[37] R. H. Love, C. H. Thompson, and R. W. Nero. Changes in volume reverberation from deep to shallow water in the eastern gulf of mexico. *J. Acoust. Soc. Am.*, 114(5):2698–2708, 2003.

[38] R. W. Nero, C. H. Thompson, and J. M. Jech. In situ acoustic estimates of the swimbladder volume of atlantic herring (clupea harengus). *ICES J. Mar. Sci.*, 61(3):323–337, 2004.

[39] Z. Gong, M. Andrews, S. Jagannathan, R. Patel, J. M. Jech, N. C. Makris, and P. Ratilal. Low-frequency target strength and abundance of shoaling atlantic herring (clupea harengus) in the gulf of maine during the ocean acoustic waveguide remote sensing 2006 experiment. *J. Acoust. Soc. Am.*, 127(1):104–123, 2010.

[40] F. H. Jones and N. Marshall. The structure and functions of the theleostean swembladder. *Biol. Rev.*, 28(1):16–82, 1953.

[41] T. J. Pitcher. *Behaviour of Teleost Fishes.* Number 7 in Fish and Fisheries. Springer, London, 2 edition, 1993.

[42] P. Fréon, F. Gerlotto, and M. Soria. Diel variability of school structure with special reference to transition periods. *ICES J. Mar. Sci.*, 53(2):459–464, 1996.

[43] D. A. Mann, Z. Lu, and A. N. Popper. A clupeid fish can detect ultrasound. *Nature*, 389:341, 1997.

[44] P. S. Wilson, R. A. Roy, and W. M. Carey. An improved water-filled impedance tube. *J. Acoust. Soc. Am.*, 113(6):3245–3252, 2003.

[45] P. S. Wilson. Low-frequency dispersion in bubbly liquids. *Acoust. Res. Let. Online*, 6(3):188–194, 2005.

[46] K. W. Commander and A. Prosperetti. Linear pressure waves in bubbly liquids: Comparison between theory and experiments. *J. Acoust. Soc. Am.*, 85(2):732–746, 1989.

[47] P. S. Wilson, A. H. Reed, W. T. Wood, and R. A. Roy. The low-frequency sound speed of fluid-like gas-bearing sediments. *J. Acoust. Soc. Am.*, 123(4):EL99–EL104, 2008.

[48] P. S. Wilson and R. A. Roy. An audible demonstration of the speed of sound in bubbly liquids. *Am. J. Phys.*, 76(10):975–981, 2008.

[49] C. A. Greene, P. S. Wilson, and R. B. Coffin. Acoustic determination of methane hydrate dissociation pressures. In *7th International Conference on Gas Hydrates (ICGH 2011)*, pages 1–11, 2011.

[50] P. S. Wilson and K. H. Dunton. Laboratory investigation of the acoustic response of seagrass tissue in the frequency band 0.5–2.5 kHz. *J. Acoust. Soc. Am.*, 125(4):1951–1959, 2009.

[51] C. J. Wilson, P. S. Wilson, and K. H. Dunton. Assessing the low frequency acoustic characteristics of *Macrocystis pyrifera*, *Egregia menziessi*, and *Laminaria solidungula*. *J. Acoust. Soc. Am.*, 133(6):3819–3826, 2013.

[52] G. Enenstein, C. Dolder, P. S. Wilson, and J.-P. Hermand. Investigation of low-frequency acoustic tissue properties of seagrass. In *Proc. Meetings Acoust.*, volume 19, page 005007. Acoustical Society of America, 2013.

[53] K. M. Lee, K. T. Hinojosa, M. S. Wochner, T. F. Argo, P. S. Wilson, and R. S. Mercier. Sound propagation in water containing large tethered spherical encapsulated gas bubbles with resonance frequencies in the 50 Hz to 100 Hz range. *J. Acoust. Soc. Am.*, 130(5):3325–3332, 2011.

[54] K. M. Lee. personal communication, 2012.

[55] G. N. Robertson, B. W. Lindsey, T. C. Dumbarton, R. P. Croll, and F. M. Smith. The contribustion of the swimbladder to buoyancy in the adult zebrafish (*Danio rerio*): A morphometric analysis. *J. Morph.*, 269(6):666–673, 2008.

[56] C. B. Daniels and C. H. Skinner. The composition and function of surface-active lipids in the goldfish swim bladder. *Physiol. Zool.*, 67(5):1230–1256, 1994.

[57] C. A. Greene. Low-frequency acoustic classication of methane hydrates. Master's thesis, The University of Texas at Austin, 2010. ETD-UT-2010-12-2632.

[58] V. A. Del Grosso. Analysis of multimode acoustic propagation in liquid cylinders with realistic boundary conditionsapplication to sound speed and absorption measurements. *Acta Acust. United Ac.*, 24(6):299–311, 1971.

[59] L. D. Lafleur and F. D. Shields. Low-frequency propagation modes in a liquid-filled elastic tube waveguide. *J. Acoust. Soc. Am.*, 97(3):1435–1445, 1995.

[60] L. E. Kinsler, A. R. Frey, A. B. Coppens, and J. V. Sanders. *Fundamentals of Acoustics.* John Wiley & Sons, Inc., Danvers, fourth edition edition, 1999.

[61] A. D. Pierce. *Acoustics.* the Acoustical Society of America, Melville, 1994 edition edition, 1994.

[62] D. T. Blackstock. *Fundamentals of Physical Acoustics.* John Wiley & Sons, Inc., New York, 2000.

[63] S. Temkin. *Elements of Acoustics.* John Wiley & Sons, Inc., New York, 1981.

[64] L. L. Beranek. *Acoustics.* The Acoustical Society of America, Woodbury, 1993 edition edition, 1996.

[65] A. H. R. Mallock. The damping of sound by frothy liquids. *P. Roy. Soc. Lond.*, 84(572):391–395, 1910.

[66] A. B. Wood. *A Textbook of Sound.* G. Bell and Sons LTD, New York, first edition edition, 1930.

[67] K. Herzfeld. Propagation of sound in suspensions. *Lond. Edinb. Dublin Philos. Mag.*, 9(59):752–768, 1930.

[68] S. W. H. Bragg. *The World of Sound: Six Lectures Delivered Before a Juvenile Auditory at the Royal Institution, Christmas, 1919.* G. Bell and Sons Ltd., London, 1920.

[69] M. Minnaert. On musical air-bubbles and the sounds of running water. *Lond. Edinb. Dublin Philos. Mag.*, 16(104):235–248, 1933.

[70] E. H. Kennard. Radial motion of water surrounding a sphere of gas in relation to pressure waves. In G. K. Hartmann and E. G. Hill, editors, *Underwater Explosion Research*, volume 2, chapter Theory of Pulsations, pages 183–226. Office of Naval Research, Department of the Navy, 1950.

[71] L. Spitzer Jr. Acoustic properties of gas bubbles in a liquid. Technical Report NRDC No. 6.1-sr20-918, Columbia University - Division of War Research, 1943.

[72] S. Temkin. Attenuation and dispersion of sound in dilute sespensions of spherical particles. *J. Acoust. Soc. Am.*, 108(1):126–146, 2000.

[73] S. Temkin. Erattum: "Attenuation and dispersion of sound in dilute suspensions of spherical particles" [J. Acoust. Soc. Am. 108, 126–146 (2000)]. *J. Acoust. Soc. Am.*, 111(2):1126–1128, 2002.

[74] L. L. Foldy. The multiple scattering of waves. *Physical Rev.*, 67(3–4):107–119, 1945.

[75] N. D. R. Committee. *Physics of Sound in the Sea.* Department of the Navy, Washington, D.C., 1946.

[76] E. L. Cartensen and L. L. Foldy. Propagation of sound through a liquid containing bubbles. *J. Acoust. Soc. Am.*, 19(3):481–501, 1947.

[77] R. J. Urick. A sound velocity method for determining the compressibility of finely divided substances. *J. Appl. Phys.*, 18(11):983–987, 1947.

[78] R. J. Urick and W. S. Ament. The propagation of sound in composite media. *J. Acoust. Soc. Am.*, 21(2):115–119, 1949.

[79] V. E. Meyer and E. Skudrzyk. Über die akustischen eigenshaften von gasblasenscheiern in wasser. *Acustica*, 3:434–440, 1953.

[80] M. L. Exner and W. Hampe. Experimental determination of the damping of pulsating air bubbles in water. *Acustica*, 3:67–71, 1953.

[81] M. Strasberg. Letter to the editor concerning the article by "M. L. Exner and W. Hampe, Experimental determination of the damping of pulsating air bubbles in water". *Acustica*, 4:450, 1954.

[82] F. E. Fox, S. R. Curley, and G. S. Larson. Phase velocity and absorption measurements in water containing air bubbles. *J. Acoust. Soc. Am.*, 27(3):534–539, 1955.

[83] E. Silberman. Sound velocity and attenuation in bubbly mixtures measured in standing wave tubes. *J. Acoust. Soc. Am.*, 29(8):925–933, 1957.

[84] J. D. Macpherson. The effect of gas bubbles on sound propagation in water. *Proc. Phys. Soc. London*, 70:85–92, 1957.

[85] D. Hsieh and M. S. Plesset. On the propagation of sound in a liquid containing gas bubbles. *Phys. Fluids*, 4(8):970–975, 1961.

[86] D. Hsieh and M. S. Plesset. Theory of the acoustic absorption by a gas bubble in a liquid. Technical Report 85-19, Engineering Division of California Institute of Technology, 1961.

[87] A. Crespo. Sound and shock waves in liquids containing bubbles. *Phys. Fluids*, 12(11):2274–2282, 1969.

[88] E. A. Zabolotskaya and S. I. Soluyan. A possible approach to the amplification of sound waves. *Sov. Phys. Acoust*, 13(2):254–256, 1967.

[89] L. V. Wijngaarden. On the equations of motion for mixtures of liquid and gas bubbles. *J. Fluid Mech.*, 33(3):465–474, 1968.

[90] G. K. Batchelor. Compression waves in a suspension of gas bubbles in liquid. *Fluid Dynam. Trans.*, 4:425–445, 1969.

[91] D. McWilliam and R. Duggins. Speed of sound in bubbly liquids. *Proc. Inst. Mech. Eng., Conference Proceedings*, 184(3):102–107, 1969.

[92] A. I. Eller. Damping constants of pulsating bubbles. *J. Acoust. Soc. Am.*, 47:1469–1470, 1970.

[93] W. M. F. Jr. Damping constants for nonresonant bubbles. *J. Acoust. Soc. Am.*, 58(3):746, 1975.

[94] L. V. Wijngaarden. One-dimensional flow of liquids containing small gas bubbles. *Annu. Rev. Fluid Mech.*, 4:369–396, 1972.

[95] R. B. Chapman and M. S. Plesset. Thermal effects in the free oscillations of gas bubbles. *J. Basic Eng.*, 94:373–276, 1971.

[96] A. Prosperetti. Application of the subharmonic threshold to the measurement of the damping of oscillating gas bubbles. *J. Acoust. Soc. Am.*, 61(1):11–16, 1977.

[97] A. Prosperetti. Thermal effects and damping mechanisms in the forced radial oscillations of gas bubbles in liquids. *J. Acoust. Soc. Am.*, 61(1):17–27, 1977.

[98] S. W. Kieffer. Sound speed in liquid-gas mixtures: Water-air and water-steam. *J. Geophys. Res.*, 2:2895–2904, 1977.

[99] S. A. Bedford and D. S. Drumheller. A variational theory of immiscible fluid mixtures. *Arch. Rational Mech. Anal.*, 68(1):37–51, 1978.

[100] D. S. Drumheller and A. Bedford. A theory of bubbly liquids. *J. Acoust. Soc. Am.*, 68(1):197–208, 1979.

[101] D. Y. Hsieh. On oscillation of vapor bubbles. *J. Acoust. Soc. Am*, 66(5):1514–1515, 1979.

[102] P. L. Marston. Evaporation-condensation resonance frequency of oscillating vapor bubbles. *J. Acoust. Soc. Am*, 66(5):1516–1521, 1979.

[103] G. C. Gaunaurd and H. Überall. Resonance theory of bubbly liquids. *J. Acoust. Soc. Am*, 69(2):362–370, 1981.

[104] M. Fanelli, A. Prosperetti, and M. Reali. Radial oscillations of gas-vapour bubbles in liquids. part I: Mathematical formulation. *Acustica*, 47:253–265, 1981.

[105] M. Fanelli, A. Prosperetti, and M. Reali. Radial oscillations of gas-vapour bubbles in liquids. part II: Numerical examples. *Acustica*, 49:98–109, 1981.

[106] D. S. Drumheller, M. E. Kipp, and A. Bedford. Transient wave propagation in bubbly liquids. *J. Fluid Mech.*, 119:347–365, 1982.

[107] L. A. Crum. The polytropic exponent of gas contained within air bubbles pulsating in a liquid. *J. Acoust. Soc. Am*, 73(1):116–120, 1983.

[108] A. Prosperetti. Bubble phenomena in sound fields: part one. *Ultrasonics*, 22(2):69–77, 1984.

[109] R. E. Caflisch, M. J. Miksis, G. C. Papanicolaou, and L. Ting. Effective equations for wave propagation in bubbly liquids. *J. Fluid Mech.*, 153:259–273, 1985.

[110] J. B. Keller and M. Miksis. Bubble oscillations of large ampliture. *J. Acoust. Soc. Am.*, 68(2):628–633, 1980.

[111] R. I. Nigmatulin, N. S. Khabeev, and Z. N. Hai. Waves in liquids with vapour bubbles. *J. Fluid Mech.*, 186:85–117, 1988.

[112] M. J. Miksis and L. Ting. Effects of bubbly layers on wave propagations. *J. Acoust. Soc. Am*, 86(6):2349–2358, 1989.

[113] D. R. Bruno and J. C. Novarini. Coherence and multiple scattering effects on acoustic backscattering from linear arrays of gas-filled bubbles. *J. Acoust. Soc. Am.*, 71(6):1359–1367, 1982.

[114] R. Omta. Oscillations of a cloud of bubbles of small and not so small amplitude. *J. Acoust. Soc. Am*, 82(3):1018–1033, 1987.

[115] S. Temkin. Sound propagation in bubbly liquids: A review. Technical Report NRL Memorandum Report 6403, Naval Research Laboratory, 1989.

[116] C. Feuillade. Scattering from collective modes of air bubbles in water and the physical mechanism of superresonances. *J. Acoust. Soc. Am.*, 98(2):1178–1190, 1995.

[117] Z. Ye and L. Ding. Acoustic dispersion and attenuation relations in bubbly mixture. *J. Acoust. Soc. Am.*, 98(3):1629–1636, 1995.

[118] F. S. Henyey. Corrections to foldys effective medium theory for propagation in bubble clouds and other collections of very small scatterers. *J. Acoust. Soc. Am.*, 105(4):2149–2154, 1999.

[119] S. G. Kargl. Effective medium approach to linear acoustics in bubbly liquids. *J. Acoust. Soc. Am.*, 111(1):168–173, 2002.

[120] C. Feuillade. Comment on "Corrections to foldys effective medium theory for propagation in bubble clouds and other collections of very small scatterers [J. Acoust. Soc. Am. 105, 2149–2154 (1999)]. *J. Acoust. Soc. Am.*, 111(4):1552–1555, 2002.

[121] F. S. Henyey. Reply to "Comment on 'Corrections to foldys effective medium theory for propagation in bubble clouds and other collections of very small scatterers' " [J. Acoust. Soc. Am. 111, 1552–1555 (2002)]. *J. Acoust. Soc. Am.*, 111(4):1556–1559, 2002.

[122] M. Nicholas, R. A. Roy, L. A. Crum, H. Og̃uz, and A. Prosperetti. Sound emissions by a laboratory bubble cloud. *J. Acoust. Soc. Am*, 95(6):3171–3182, 1994.

[123] S. A. Cheyne, C. T. Stebbings, and R. A. Roy. Phase velocity measurements in bubbly liquids using a fiber optic laser interferometer. *J. Acoust. Soc. Am*, 97(3):1621–1624, 1995.

[124] T. G. Leighton, P. R. While, C. L. Morfey, J. W. L. Clarke, G. J. Heald, H. A. Dumbrell, and K. R. Holland. The effect of reverberation on the damping of bubbles. *J. Acoust. Soc. Am.*, 112(4):1366–1376, 2002.

[125] S. Temkin. Radial pulsations of a fluid sphere in a sound wave. *J. Fluid Mech.*, 380:1–38, 1999.

[126] S. Temkin. Corrigendum: Radial pulsations of a fluid sphere in a sound wave. *J. Fluid Mech.*, 430:407–410, 2001.

[127] P. L. Chambr. Speed of a plane wave in a gross mixture. *J. Acoust. Soc. Am.*, 26(3):329–331, 1954.

[128] J. Pierre, R.-M. Guillermic, F. Elias, W. Drenckhan, and V. Leroy. Acoustic characterisation of liquid foams with an impedance tube. *Eur. Phys. J. E*, 36(10):1–10, 2013.

[129] S. Temkin. Sound speeds in suspensions in thermodynamic equilibrium. *Phys. Fluids A*, 4:2399, 1992.

[130] C. S. Clay and H. Medwin. *Acoustical Oceanography.* John Wiley & Sons, Inc., New York, 1977.

[131] C. C. Church. The effects of elastic solid surface layer on the radial pulsations of gas bubbles. *J. Acoust. Soc. Am.*, 97(3):1510–1521, 1995.

[132] C.-T. Chen and F. J. Millero. Speed of sound in seawater at high pressures. *J. Acoust. Soc. Am.*, 62(5):1129–1135, 1977.

[133] A. N. Gent. *Engineering with Rubber*, pages pp. 74–75. Hanser Verlag, Munich, 2nd edition, 2001.

[134] R. N. Capps. Elastomeric materials for acoustical applications. Technical Report AD-A216 872, Underwater Sound Ref. Detach. Naval Research laboratory, 1989.

[135] Data Translation, Inc. About data translation. http://www.datatranslation.com/, March 2014.

[136] Pioneer Balloon Company. Qualatex balloons. http://www.qualatex.com/pages/pioneer.php, March 2014.

[137] V. C. Anderson. Sound scattering from a fluid sphere. *J. Acoust. Soc. Am.*, 22(4):426–431, 1950.

[138] M. P. Raveau and C. Feuillade. Low frequency scattering from fish schools: A comparison of two models. In *Proc. Meetings Acoust.*, volume 20, pages 1–7, 2014. 005001.

[139] C. Feuillade and M. P. Raveau. Sound absorption by fish schools: Forward scattering theory and data analysis. *J. Acoust. Soc. Am.*, 134(5):3990–3990, 2013.

[140] E. A. Zabolotskaya and S. I. Soluyan. Emission of harmonic and combination-frequency waves by air bubbles. *Sov. Phys. Acoust*, 18(3):396–398, 1973.

[141] C. S. Clay and H. Medwin. Scattering and absorption by bodies and bubbles. In *Acoustical Oceanography*, pages 178–215. John Wiley & Sons, Inc., 1977.

[142] A. S. Sangani. A pairwise interaction theory for determining the linear acoustic properties of dilute bubbly liquids. *J. Fluid Mech.*, 232:221–284, 1991.

[143] C. Feuillade. The attenuation and dispersion of sounds in water containing multiply interacting air bubbles. *J. Acoust. Soc. Am.*, 99(6):3412 – 3430, 1996.

[144] M. A. Ainslie and T. G. Leighton. Review of scattering and extinction cross-sections, damping factors, and resonance frequencies of a spherical gas bubble. *J. Acoust. Soc. Am.*, 130(5):3184–3208, 2011.

[145] J. Blaxter and R. Batty. The herring swimbladder: loss and gain of gas. *J. Mar. Biol. Ass. U. K.*, 64(2):441–459, 1984.

# Vita

Craig Nealon Dolder was born in Chelmsford, MA. He received a Bachelor of Science degree in Engineering from the University of Hartford in West Hartford, Connecticut in May 2008. He also traveled to Abheypur, India as part of an Engineers Without Borders team for a clean water project in January 2008 and entered the graduate program of The Cockrell School of Engineering at The University of Texas at Austin in September 2008. At UT Austin he studied the quasi-acoustic noise associated with turbulent flow over an array under the supervision of Dr. Charles E. Tinney and was fortunate enough to take classes on acoustic fundamentals with Dr. Mark Hamilton and Dr. David Blackstock. During this time he also gained a fondness for many forms of social dancing, including Casino, Salsa, Swing, Waltz, and Blues. After obtaining a Masters of Science in Mechanical Engineering for his work of turbulent flow noise he continued toward his PhD by focusing on bubble acoustics and fish schools.

Permanent address: Austin, Texas 78758

This dissertation was typeset with LaTeX by the author.

---

LaTeX is a document preparation system developed by Leslie Lamport as a special version of Donald Knuth's TeX Program.